Politecnico di Milano
School of Industrial and Information Engineering
Master of Science in Energy Engineering
Energy Department

CFD Study on Spark Assisted Compression Ignition Combustion for a Natural Gas Powered Heavy Duty Engine

Supervisor: Prof. Tommaso LUCCHINI

Master thesis by:
Federico PESSAH Matr. 883247

Academic Year 2018-2019

Contents

List of Figures

List of Tables

List of acronyms

AHRR Apparent Heat Release Rate

AKR Anti Knocking Regulation

BDC Bottom Dead Centre

BDS Backward Difference Scheme

CAD Crank Angle Degrees

CDS Central Difference Scheme

CFD Computational Fluid Dynamics

CPU Central Processing Unit

DI Direct Injection

DPF Diesel Particulate Filter

ECU Electronic Control Unit

EVO Exhaust Valve Opening

GIW Gross Indicated Work

HCCI Homogeneous Charge Compression Ignition

ICE Internal Combustion Engine

ID Ignition Delay

IVC Intake Valve Closing

LHV Lower Heating Value

MON Motored Octane Number

ODE Ordinary Differential Equation

ON Octane Number

OpenFOAM Open source Field Operation And Manipulation

PCCI Premixed Charge Compression Ignition

PSR Perfect Stirred Reactor

PV Progress Variable

RoHR Rate of Heat Released

RON Research Octane Number

SACI Spark Assisted Compression Ignition

SCR Selective Catalytic Reduction

SI Spark Ignition

SOC Start Of Combustion

SOI Start Of Injection

TDC Top Dead Centre

Sommario

Al giorno d'oggi avere motori puliti e in grado di emettere poca anidride carbonica è di fondamentale importanza per la salvaguardia e la tutela dell'ambiente. In quest'ottica, il gas naturale è una tipologia di carburante molto interessante in quanto, essendo in condizioni atmosferiche allo stato gassoso, non forma alcun tipo di polvere sottile e, in aggiunta, a causa del basso rapporto carbonio-idrogeno (C/H) permette di avere una minor produzione di CO_2 rispetto alla combustione di una pari quantità di benzina o gasolio. A causa dell'elevato numero di ottani di questo tipo di carburante, il ciclo termodinamico scelto come riferimento è il ciclo "Otto", che tradizionalmente comporta l'installazione di una candela necessaria per rilasciare una quantità di energia minima in grado di controllare la combustione vera e propria, creando un fronte di fiamma. Tuttavia, la fiamma del gas naturale non è abbastanza veloce da poter considerare la combustione come istantanea (assunta teoricamente dal ciclo Otto) e per cui, se si considerano motori a carico pesante in cui un singolo cilindro può avere un volume massimo maggiore di 2 litri, velocizzare il processo di combustione del gas risulta fondamentale per lo sviluppo dei motori a combustione interna. Per fare ciò, modalità di combustione alternativa sono state considerate, come la più famosa HCCI (in cui il rapporto di compressione è talmente alto da far accendere spontaneamente tutta la carica all'interno del volume di controllo) o la più moderna combustione SACI (in cui una parte della miscela brucia per propagazione di fiamma e una minore reagisce per compressione). La seconda risulta più fattibile dato che è grazie alla presenza della candela è possibile controllare maggiormente la combustione e avere minore variabilità tra due diversi cicli di funzionamento. Tuttavia anche quest'ultima ipotesi non è di semplice realizzazione, in quanto è possibile che la combustione per compressione generi onde di pressione talmente importanti da diminuire l'efficienza termica del motore e, nel peggiore dei casi, danneggiare la macchina stessa, risultando quindi detonazione. In questo lavoro di tesi viene quindi analizzata la differenza tra il concetto di detonazione e quello di accensione spontanea e, utilizzando le considerazioni raccolte, viene successivamente sviluppato un motore SACI (ad accensione assistita) in grado di sfruttare l'autoaccensione per velocizzare il processo di combustione e quindi migliorare le prestazioni del motore stesso. Nel corso di questo lavoro quindi sono stati ottenuti due diversi criteri di progettazione che permettono di sfruttare l'accensione spontanea al fine di ridurre il consumo di carburante: un primo prende in esame la forma del pistone, un secondo analizza l'eventuale eccesso d'aria presente in camera di combustione. Attraverso simulazioni numeriche fluido-dinamiche, le prestazioni e le emissioni del motore ottenuto sono state confrontate con quelle di uno tradizionale ad accensione comandata, riscontrando apprezzabili vantaggi garantiti da questa

nuova modalità di combustione soprattutto nelle condizioni a basso e medio carico.

Abstract

Nowadays to have clean engines able to reduce both carbon dioxide and pollutants emissions is of fundamental importance for safeguarding and protecting the environment. For this reason, natural gas is a very interesting kind of fuel, since it does not form any particle matter as it is already gaseous in atmospheric conditions, and the low carbon-hydrogen ratio (C/H) leads to a reduced CO_2 production with respect to the combustion performed with the same amount of gasoline or diesel. Due to the high octane number of this kind of fuel, the thermodynamic cycle chosen as a reference is the "Otto cycle", which traditionally considers the installation of a spark-plug needed to release a minimum energy quantity to control the combustion, creating a real flame front. In any case, the natural gas flame front velocity is not high enough to consider the combustion as instantaneous (which is the one theoretically assumed by the Otto cycle) and, if heavy duty engines which can have a displacement per cylinder over than 2 liters are considered, to speed up the combustion process results fundamental for the development of internal combustion engines. To do so, different and innovative combustion modes have been investigated, as the most famous HCCI (where compression ratio adopted is so high to have a complete compression ignition of the whole charge inside the control volume) or the more modern SACI one (where a part of the mixture burns due to flame propagation and the other one gets ignited by compression). The second one results more feasible since, thanks to the presence of the spark-plug, it is possible to have a better control on the combustion and as a consequence cycle-variability is reduced. In any case, even this last one is difficult to realize, as it is possible that compression ignition combustion generates such intense pressure waves to decrease thermal efficiency of the engine and, in the worst of the cases, to damage the mechanical structure of the machine, hence resulting into knock. In this thesis work, the difference between the concept of knock and the one of spontaneous ignition has been analysed and, using collected considerations, a SACI (spark assisted compression ignition) engine has been developed in such a way it can exploit autoignition phenomenon to speed up the whole combustion process and to improve engine performances. During this work, two different design criteria which permits a good exploitation of partial spontaneous ignition have been derived: the first one considers the shape of the piston, while the second one analyses the possible air excess present in the combustion chamber. Through fluid dynamics numerical simulations, performances and emissions of the engine obtained have been compared with the ones of a traditional spark ignition heavy duty machine, highlighting the appreciable advantages of this innovative combustion mode especially in low and half load conditions.

Chapter 1

Internal combustion engines

Internal combustion engine is an energy production technology used especially in transportation sector. Automotive industry is very important for worldwide economy, such that in 2014 89.75 millions of vehicles were globally produced, and over 80 millions with a thermal engine installed. The main conceptual difference between an internal combustion engine and a lot of other energy production devices consists in having compression, combustion and expansion in the very same volume. As a consequence, they can reach very high powers in small volumes, making the technology suitable for both very small applications (chainsaw for instance) and heavy duty ones (tracks, ships or energy production).
Internal combustion engines can be classified in a lot of different ways: number of strokes per thermodynamic cycle, air feeding, fuel injection are just some of the criteria that people can use. In this introduction section, an analysis has been performed starting from the most known thermodynamic cycles and they can be practically realized, then moving more specifically to combustion and ICE possible future development.
Most known thermodynamic cycles describing engine working principle are Otto and Diesel ones.

Otto cycle

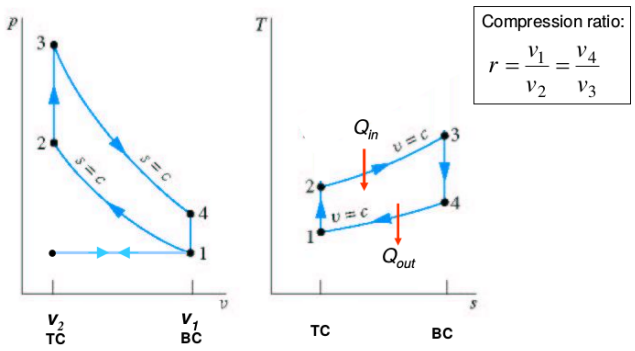

Figure 1.1: Otto thermodynamic cycle

In figure 1, ideal Otto cycle has been illustrated both on pressure-volume and temperature-entropy plane. First phase is adiabatic compression, corresponding to piston rise from bottom dead centre (v_1) to top dead centre (v_2); then an ideally constant volume combustion is performed at top dead centre, rising cylinder temperature to extremely high values. Afterwards, working fluid is expanded, and finally pressure and temperature initial values are restored once cycle is completed. Gas exchange cycle is displayed leftwards to point 1 in pressure-volume plane.
This leads to huge power densities but losses such as thermal ones can become important: ideally, compression and expansion are adiabatic, but since in practice cylinder mixture temperature can reach and overcome 2200 K it is impossible to assume adiabatic walls; also ideal combustion is isochoric (at constant volume), drawn by a vertical line in pressure-volume plane. To assume a constant volume combustion means that fuel heat release is instantaneous; but even if flame velocities are quite high, combustion process needs time to develop, and this time is not negligible if compared to compression/expansion stroke duration: at 1200 rpm, a stroke requires 25 ms to be completed, and combustion duration is in the order of magnitude of 5 ms. These two main kinds of losses are the reason why, when pressure volume curve is actually plotted, chart is quite different with respect to the ideal cycle.

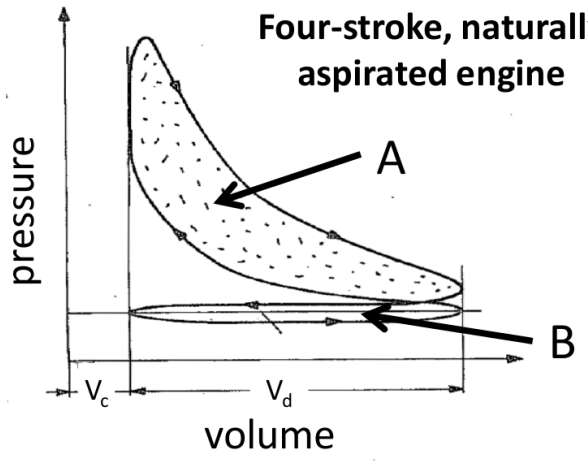

Figure 1.2: Realistic pressure-volume curve

In figure 2, two areas are highlighted: A and B. Area A represents compression, combustion and expansion processes, and it is a more realistic representation of the ideal working cycle illustrated in figure 1: combustion can not be assumed instantaneous, and process representation ends with a rounded pressure maximum. Area B instead represents the gas exchange cycle. As far as engine adopted is a four stroke engine, it needs two shaft rotations to complete a full thermodynamic cycle. With respect to two stroke engines, this design choice aims to maximize thermal efficiency because exiting of burnt mixture from combustion chamber and following engine feeding improves significantly, but as a drawback power reduces because there is just one expansion stroke on

four. Therefore, area A is clockwise oriented, able to represent some useful work; area B can be counterclockwise oriented, requiring energy to be completed.
In modern Otto cycle engines, combustion starts through spark light ignition from a spark plug, a device installed in combustion chamber releasing a small energy quantity to fuel-air compressed mixture. To have a good control of ignition timing, an electronic control unit is used: spark timing is always anticipated with respect to top dead centre (point where cylinder volume is minimum), searching for a compromise between a low compression work and maximizing expansion one, due to combustion non instantaneous lasting.

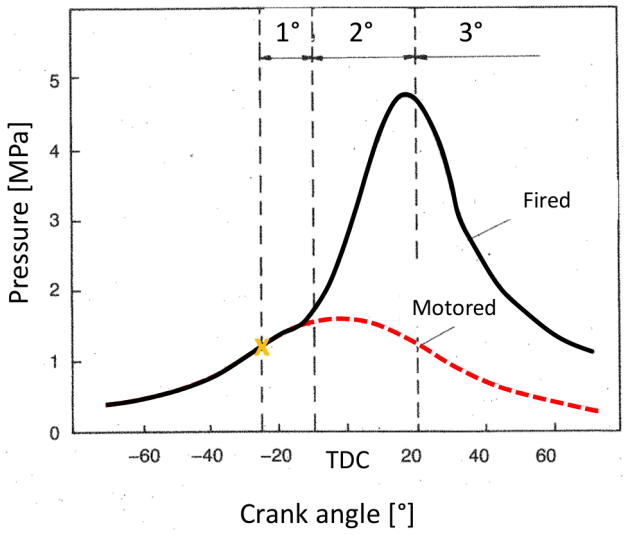

Figure 1.3: Motored and fired pressure curves

In figure 3, motored and fired pressure curves are plotted with respect to the crank angle. This x-axis represents piston position, and it assumes the value of 0° in correspondence of top dead centre, and the value of 180° (positive or negative) at the bottom dead centre. It is also known as engine time, since it can be directly related to physical time once engine rotational speed is known. Motored curve stands for cylinder pressure curve when combustion does not take place: what the engine spends for compression, is given back to expansion and gross indicated work is ideally zero. Fired curve is pressure curve in presence of combustion, which is asymmetrical, otherwise it would be impossible to obtain any useful work. Yellow star stands for spark timing, the exact moment when spark light is igniting the mixture. In this figure it is possible to notice a delay between mixture ignition and effective pressure rise, but this kind of delay is always present. Anticipating spark timing, compression losses rises because there is a pressure increase before top dead centre, decreasing pressure-volume area; also, higher pressures are reached, and rightward (with respect to 0°) pressure curve underlying area increases. Numbers above represent combustion phases, as ignition delay (1°), combustion development (2°) and both combustion completion and expansion (3°). Figure below reports some flame images different combustion moments, to emphasize its not-ideal lasting.

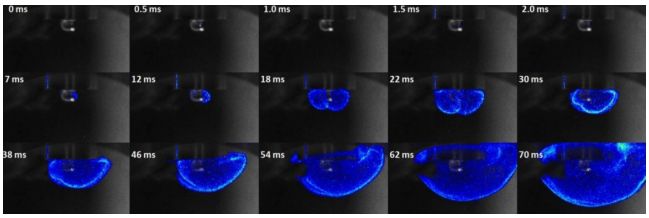

Figure 1.4: Combustion lasting

Efficiency of an ideal Otto cycle depends on compression ratio, defined as the ratio between the minimum and maximum cylinder volumes.

$$compressionRatio = CR = \frac{V_{max}}{V_{min}} \tag{1.1}$$

$$\eta_{th} = 1 - \frac{1}{CR^{\gamma-1}} \tag{1.2}$$

$$\gamma = \frac{c_p}{c_v} \tag{1.3}$$

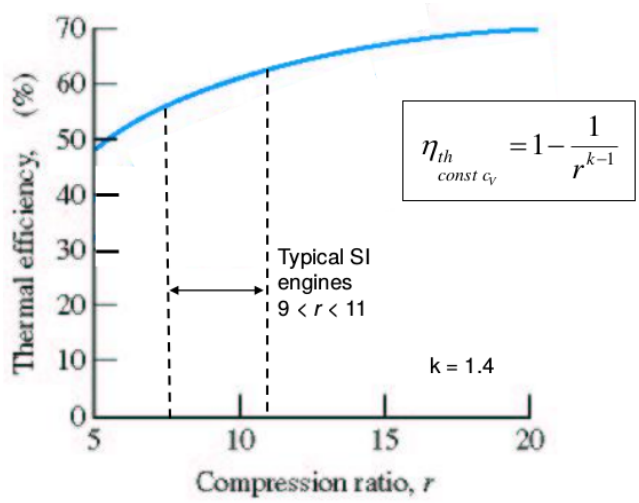

Figure 1.5: Otto cycle efficiency plot with compression ratio

Therefore, ideally thermodynamic efficiency depends just on equations reported above. In practice, spark ignition commercial engines have a compression ratio that can vary between 8 and 11, depending on the fuel they are feeded with, on the kind of injection (port or direct) used and also on the design application. What is limiting compression ratio increase is possible knock presence. Knock is defined as "abnormal combustion", meaning that unburnt fresh mixture reaches such high pressures and temperatures during combustion process that it autoignites. Autoignition in fact is nothing but completing combustion chemical reactions without a real flame propagation, and energy that for flame development is given by spark light, for knock it is given by high pressures and

temperatures. This is why controlling spark timing is so important: by an anticipation, higher cylinder pressures and temperatures are reached, but also it makes more probable autoignition presence.

Diesel cycle

Diesel cycle has been idealized by Rudolf Diesel in 1893.

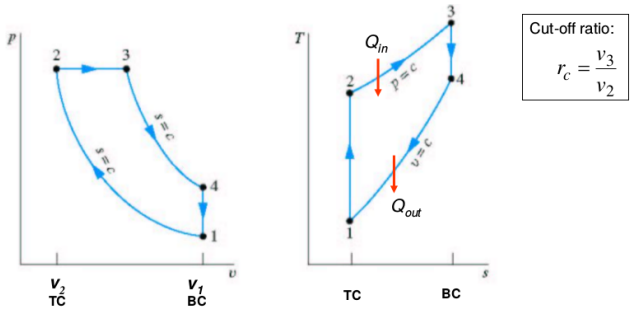

Figure 1.6: Diesel thermodynamic cycle

As illustrated in figure 6, it is very similar to Otto cycle, since both of them are involving an adiabatic compression, an adiabatic expansion and a gas exchange cycle in four strokes engines. The real point of difference is that in the Otto cycle a constant volume combustion is performed, in the Diesel one combustion develops at constant pressure, hence line connecting point 2 to point 3 is horizontal. This difference in combustion process leads to both thermodynamic and engineering differences between the technologies. Starting from thermodynamic ideal efficiency, in equations 4 and 5 η_{th} of both cycles is computed:

$$\eta_{th} = 1 - \frac{1}{CR^{\gamma-1}} \qquad Otto_{cycle} \tag{1.4}$$

$$\eta_{th} = 1 - \frac{1}{CR^{\gamma-1}} \cdot \left[\frac{1}{\gamma}\frac{r_c^{\gamma}-1}{r_c-1}\right] \qquad Diesel_{cycle} \tag{1.5}$$

Expressions illustrated above are very similar, with a multiplicator function of Cut-off ratio present in Diesel cycle thermodynamic efficiency. Cut-off ratio is defined as the ratio of the volume once combustion is completed (v_3) with the top dead centre one (v_2), where combustion is starting.
Expression in the square brackets in equation 5 is always higher than 1, hence Diesel cycle efficiency is lower with respect to Otto cycle one for the same compression ratio. The point of strength of diesel engine is that they can adopt an higher compression ratio with respect to Otto cycle ones: in spark ignition engines, compression ratio is limited to avoid knock presence, assuming values between 8 and 10 in gasoline fuelled passenger cars; in compression ignition diesel engines, this limit is not present and they assume values between 16 and 18 in diesel fuelled passenger cars. Combustion in Diesel cycle engines is spontaneous, meaning there is not a clear flame propagation as happens in spark ignition engines, but as soon as the fuel evaporates and mixes up with air, it ignites by compression.

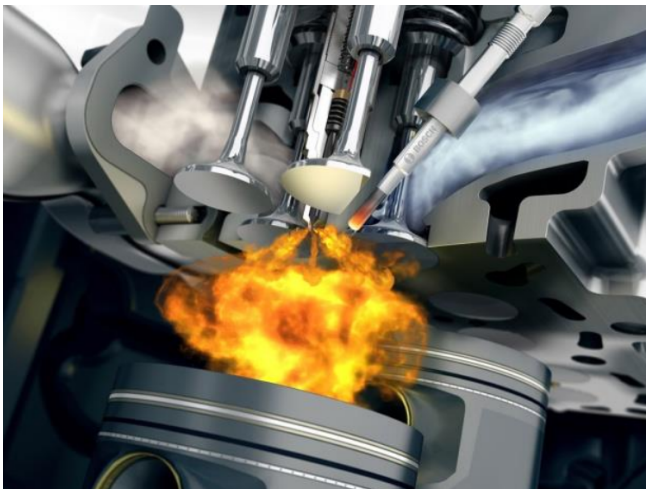

Figure 1.7: Diesel engine combustion

Activation energy necessary for combustion depends on the kind of fuel used. In spark ignition engines, autoignition is something unwanted, hence a suitable fuel must have a high autoignition delay, such as gasoline or natural gas. In Diesel engines, combustion is performed by compression ignition, hence a suitable fuel must have a very low autoignition delay. This is one reason why diesel fuel and gasoline are so different between each other: the first one is quite heavy, but as soon as it is injected in the cylinder it has to ignite due to high pressures and temperatures; the second is more volatile, but much more resistant to compression ignition. In addition, the higher compression ratio in Diesel engines is contributing to reduce diesel fuel ignition delay. Diesel fuel must be injected directly in the cylinder at very high injection pressures (100 MPa as order of magnitude) to have a good spray brake up and an almost instantaneous combustion. As shown in figure 7, in a compression ignition combustion there is not a clear flame front propagating but burnt region volume depends on how fuel spray evaporates and mixes up with air. Since there is not a flame propagation, there is no need to have a stoichiometric (or slightly lean) air-fuel ratio as in spark ignition combustion: compression ignition engines work with high air excess, which is important to reduce heat losses, increasing engine performances. In addition, it is an advantage for the gas exchange cycle too, because there is no need to install a throttle valve, hence pressure losses are reduced.
As a disadvantage, Diesel engines need to be more robust to stand higher stresses due to compression ignition combustion. They are heavier and, to have good spray characteristics, fuel injection system is much more complex with respect to gasoline direct injection ones.
Diesel engines usually run at lower rotational speeds, because the fuel needs time to ignite by compression. As a consequence, a Diesel engine have more torque with respect to an Otto one (at the same power), since it presents maximum torque point at lower rotational speed. Having a high torque improves driveability whenever the engine is installed in a passenger car or in a heavy duty vehicle, since they can rapidly react if resistant forces increase.
As a final consideration, as explained in [2], Diesel engines are more suitable

when power required is high (such as tracks, ships or heavy passenger cars), while spark ignition engines when specific power is lower (light passenger cars).

ICE layout and importance of turbocharging

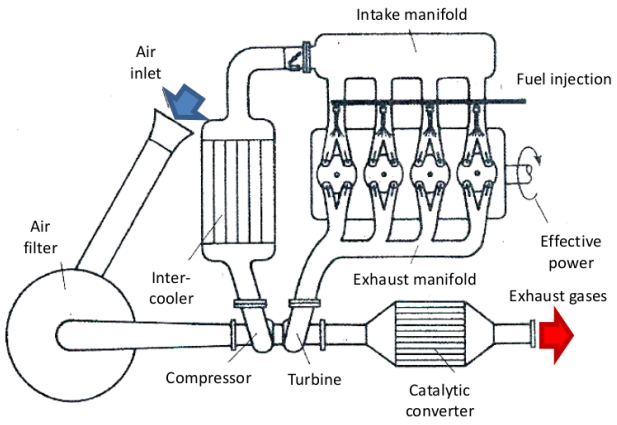

Figure 1.8: Turbocharged spark ignition engine at 4 cylinder scheme

In figure 8, a modern spark ignition engine layout is illustrated. Air mass cylinder feeding is regulated through a throttle valve, drawn exactly at intake manifold inlet. Closer the throttle valve, lower cylinder pressure inlet and hence working fluid mass; fuel injection is electronically controlled by ECU. In a naturally aspirated internal combustion engine (not having both compressor and turbocharger), maximum cylinder intake pressure is the atmospheric one, slightly higher if pressure waves are well exploited. At partial load, breathing pressure is lower with respect to the atmospheric one, leading to the presence of counterclockwise B area illustrated in Figure 2. If throttle valve is further closed, work required for engine breathing increases, penalizing engine fuel consumption. Eliminating throttle valve is a design target for future internal combustion engines.
Torque can be evaluated using following expression:

$$T_b = \eta_b \cdot \lambda_v \frac{\rho_{air} V}{\alpha} \cdot \frac{Q_{HV}}{2\pi\epsilon_{cycle}} \tag{1.6}$$

Two kinds of efficiencies are present: volumetric (λ_v) and global (η_b) efficiency. Volumetric one is representing engine ability to evacuate burnt already exploited gasses to be feeded with fresh charge; global efficiency is related to compression, combustion and expansion processes. Q_{HV} is fuel heating value, while ϵ_{cycle} represents number of rotations needed to complete a full thermodynamic cycle (1 in two stroke engines, 2 in four stroke engines).
$\rho_{air}V/\alpha$ represents fuel mass inside the cylinder, since α is defined as air and fuel mass ratio. For what appears by mathematical formula, increasing air density or cylinder volume leads to no change if losses are not considered. This is the reason why main strategy to have higher naturally aspirated engine power is increasing cylinder displacement, since atmospheric air pressure and density

values can not be overcome. This inevitably leads to design bigger cylinders or adopting more than one.

Figure 1.9: 6 cylinders engine

Implying bigger cylinders, wall surface increases considerably and it is not good for thermal losses. Adopting more than one cylinder (keeping the same displacement) allows both to reduce total heat transfer area and (in spark ignition engines) average flame path in every cylinder, enhancing mixture autoignition resistance. In modern context where reducing pollutant or greenhouse gas emissions is very important, installing higher engine power sacrificing its efficiency is not good both by an environmental and an economical point of view. Therefore, to increase both power and efficiency, a turbocharging system is installed in a lot of modern commercial internal combustion engines: burnt gasses (which have a lot of energy content due to high pressures and temperatures) are further expanded through a Francis turbine that drives a centrifugal compressor. Compressor is placed before intake manifold (as figure 8 shows), such that higher intake valve closing pressures can be reached. By a thermodynamic point of view, this leads to higher thermal inertia due to more mass entered in the cylinder, decreasing losses importance. In addition, if pressure values overcome atmospheric one, difference between breathing pressure and atmospheric one becomes positive, making area B shown in figure 2 clockwise oriented, representing some more useful work. This is the reason why in the context of internal combustion engines the word "downsizing" has been used, to indicate this tendency to build very small engines with high boosting to reduce CO_2 and pollutant emissions. This design choice had some very appreciable results when NEDC (New European Driving Cycle) was reproduced in test bench, but when actual ordinary engine usage and aging were considered, thermal efficiencies had not the predicted benefits. Therefore, at the state of the art it is more common to hear about "rightsizing", a displacement reduction to have good test bench results but not so extreme to compromise engine durability or efficiency stability in different working points.
Common maximum boost pressures reached are in the order of magnitude of 2-2.5 bar in commercial passenger cars or heavy duty vehicles, implying a density increase. Intercoolers (working with ambient air as coolant fluid) are placed after compressor to reduce temperature increasing in compression process, to

have air density benefits and reducing compression work.

Figure 1.10: Downsizing concept

Increasing compression ratio is of key importance for modern internal combustion engine efficiency. In spark ignition context, it is limited to avoid knock presence, that is mechanically dangerous for the engine. In Diesel one, compression ratio has a commercial range of 16-20, also depending on their application. In modern history, different solutions were studied to increase CR, such as direct fuel injection in combustion chamber, which is a more expensive with respect to port fuel one but leading to appreciable efficiency benefits since knock point is delayed. Another interesting solution is Atkinson cycle, a slightly variation of the Otto one.

1.1 Heavy duty spark ignition engines

This thesis work is focused on a natural gas heavy duty engine. In a commercial environment, reduction of fuel consumption is an absolute priority by an economical point of view, and, at the same time, emission standards must be fulfilled. A lot of track application engines are diesel fuelled, in order to adopt high compression ratio and reduce fuel consumption. At the state of the art, engine designers are searching for both new technologies able to improve fuel combustion and different kinds of fuel to reduce pollutant emissions. Natural gas can be a very interesting option for future heavy duty vehicles, as far as it is an already gaseous fuel (no soots are formed) and it is less taxed with respect to other hydrocarbons refinery products. Therefore, a lot of engine models have been converted from a compression ignition diesel design to a spark ignition natural gas one, through spark plug installation and changing of aftertreatment system.

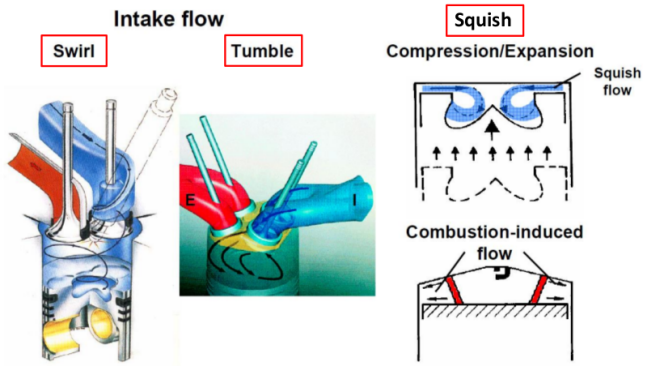

Figure 1.11: Charge motion different kinds

In figure 11 different kinds of charge motions are illustrated. In Diesel engines, swirl is very important to spread diesel fuel inside the combustion chamber. As far as there is not a real flame but just heat release, diesel fuel injection is at high pressure and directly inside the cylinder. Swirl production therefore is determinant for a good fuel combustion. At contrary, spark ignition engines have a flame propagation, and they can be easily assumed as homogeneous charge (especially when port fuel injection is used). Most important charge motion is tumble, since it is able to create turbulences to increase flame velocity. Design criteria can vary a lot between compression ignition engines (where a lot of space is needed to spread fuel along combustion chamber) and spark ignition ones, and shapes can be very different. Another difference consists in cylinder head: diesel engines run lean, hence feeding the cylinder is not the highest priority; otherwise, spark ignition engines run stoichiometric, and a good air feeding can improve both power and efficiency of engine itself.

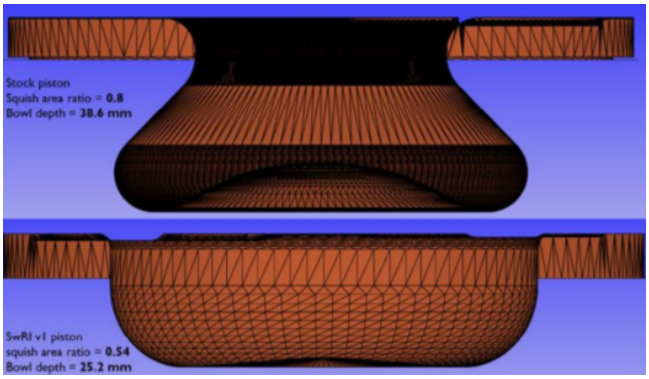

Figure 1.12: Diesel converted to natural gas piston design

In ["Development of a Natural Gas Engine with Diesel Engine-like Efficiency Using Computational Fluid Dynamics" published by Ahmed Abdul Moiz, Zainal Abidin, Robert Mitchell, and Michael Kocsis in the Southwest Research Institute in 2019], conversion of diesel heavy duty engine into a natural gas one is analysed. Main modifications consist in replacing injection system with an

ignition one through a spark plug installation in the combustion chamber; converting common rail into a natural gas injection system; changing piston shape for compression ratio, which is not a gasoline engine one but it can take benefits of higher natural gas octane number. Increasing tumble fluid motion can be a target of intake port modification.
In this study, both an exhaust gas recirculation (EGR) analysis and a computational fluid dynamics (CFD) analysis were carried out for the two piston shape illustrated in figure 12. "Stock piston" geometry has an higher squish area ratio (defined as ratio of area increasing squish fluid motion and the global one, projected on the horizontal plane) that is going to enhance turbulent kinetic energy for a faster flame propagation. "SwR1" piston (the second one) has a lower squish area but also lower wall surface, to contain heat transfer losses. In CFD simulation, RANS $\kappa - \varepsilon$ model has been used.

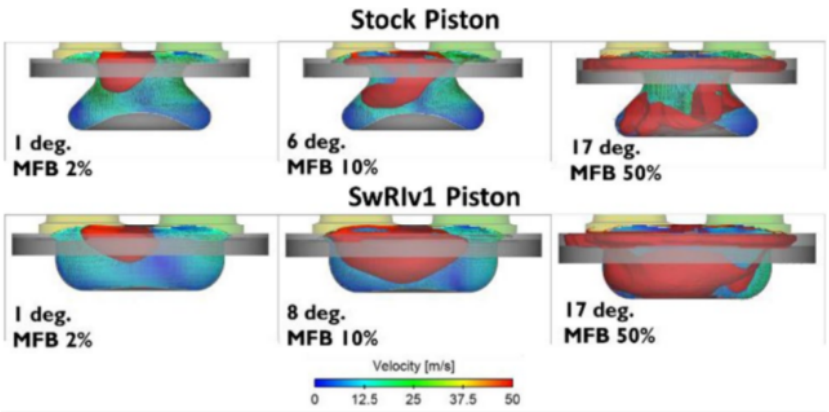

Figure 1.13: Flame developments in the two different combustion chamber compared

As figure 13 illustrates, flame development is very different between the two geometries, with upwards "stock Piston" presenting a faster flame with respect to downward "SwRIv1 Piston". Especially regarding turbulent kinetic energy, "stock piston" top plot is significantly higher with respect to all the others, having more turbulence where the flame is going to start. To match pressure curve, spark timing must be anticipated in the second "SwRIv1" geometry, because of more important ignition delay due to lack of turbulence. If results at close pressure maximum values are compared, second downward geometry "SwRiv1" has a better efficiency with respect of high squish ratio one, because of lower wall heat transfer losses.

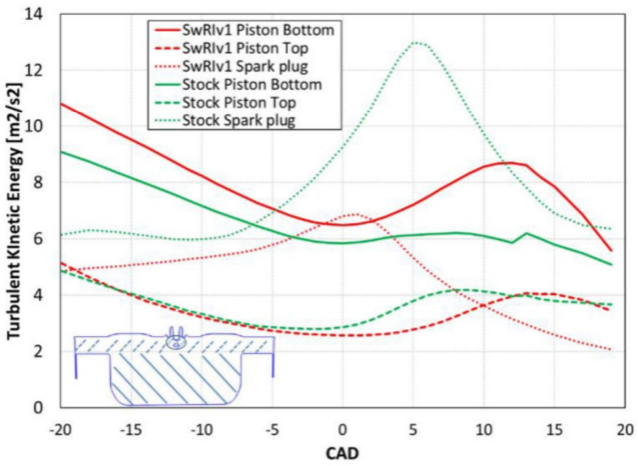

Figure 1.14: Different piston turbulent kinetic energy

In figure 14, turbulent kinetic energy of different piston geometries is plotted. Turbulence intensity can not be well represented as an unique value, as far as it can vary a lot depending on cylinder regions. What is important is having turbulence where flame needs to propagate, to increase flame velocity (which, in presence of turbulence gets quite higher with respect to laminar flame one). Squish area presence play a very important role in it.

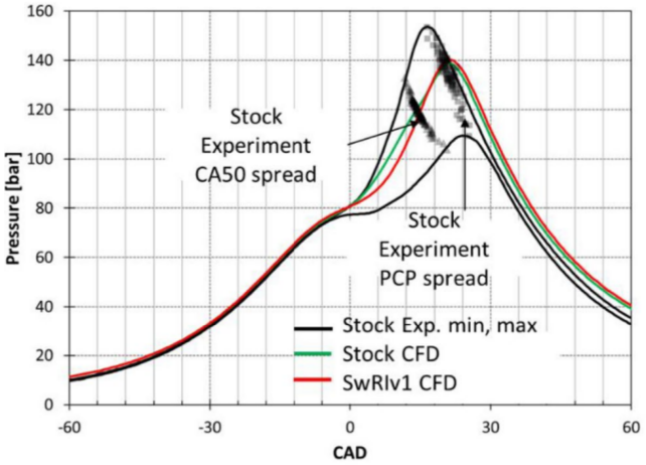

Figure 1.15: Different piston pressure curves

Despite appearances, "SwRiv1" piston shape runs with an anticipated spark timing with respect to "Stock" one, because of higher ignition delay. Pressure maximum values of the two simulated curves are very close, with differences present only in flame propagation instants. Cumulative wall heat transfer in figure 19 is very different, and it is due especially on piston area variations. In the end, second "SwRiv1" geometry presents higher efficiency even if there is a slower flame, since lower heat transfer maximizes useful work once combustion

is completed.

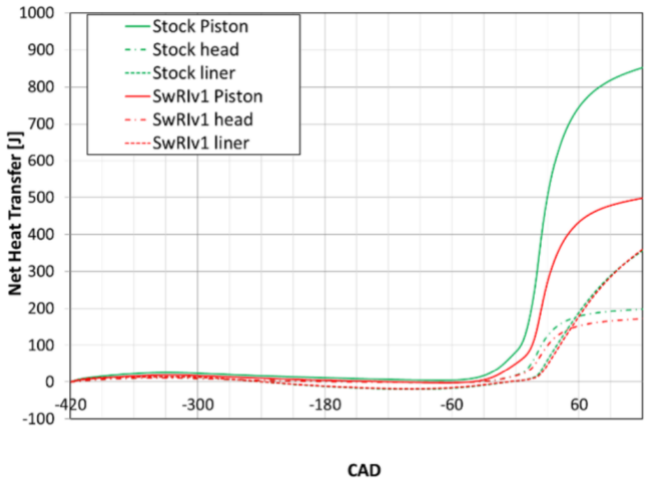

Figure 1.16: Heat transfer development comparison between investigated piston shapes

After such analysis, the paper continues to analyse exhaust gas recirculation rate and effects on combustion, showing an efficiency improvement when EGR is adopted. This section is not reported in this introduction chapter as long as this thesis work does not deal with exhaust gas recirculation. In any case, conversion between diesel engine and natural gas spark ignition one is not trivial, and performances can vary a lot depending on piston geometry adopted.

1.2 Flame propagation combustion

Combustion is both a physical and chemical process through that fuel can oxidise and then release energy. As shown in previous figures, it is characterized by three different phases: ignition delay, turbulent flame propagation and then combustion completes in external cylinder regions. Velocities of these reactions influence engine performances, and they can be measured in different ways:

controlling velocity of reactants consumption

controlling velocity of oxidation products formation

controlling velocity of heat released by reactions

The third criterium is the one most able to summarize the whole combustion process. Since reactions are performing in gas phase, combustion velocity is maximum when fuel-air mixture is homogeneous, since there are not delays correlated to physical fuel evaporation or its mixing with the oxidant. Velocity of these chemical reactions depends on reactants concentration, but especially on temperature. Therefore, it is possible to model reaction velocity w_r through an Arrhenius correlation:

$$w_r = \frac{dc}{dt} = Cp^n exp(\frac{-Ea}{RT}) \tag{1.7}$$

Where C, n and Ea are constants. Ea is representing activation energy needed to overcome the energy barrier and hence to break intermolecular bounds of the fuel, starting combustion process. This activation energy is determined by slowest steps of oxidation chain reaction (the so called rate determining steps) and it varies significantly with the fuel considered. In particular, reaction velocity increases exponentially with temperature. A normal spark ignition combustion is starting from spark plug location and then it propagates to the remaining part of the cylinder, radially to most external regions. Therefore, it is possible to distinguish an area separating combustion products to fresh charge, and flame front is then recognized. The flame front is composed by two different regions: a preheating region, where fresh charge is just heated up but not enough to fully perform combustion reactions; a second one where exothermic chemical reactions associated to combustion are completed. It is possible to define a laminar flame velocity w_{cl} as the attitude of a certain air-fuel mixture to burn more or less in a fast way. Therefore, flame velocity is proportional to reaction velocity w_r, but it will decrease with thermal diffusivity of the mixture itself.

$$w_{cl} \propto \sqrt{\chi w_r} = \sqrt{\frac{\lambda w_r}{c_p \cdot \rho}} \tag{1.8}$$

The higher the thermal diffusivity (χ) of the mixture, the more energy is needed to heat up a mixture portion, hence the slower the flame. In fact, it is possible also to define flame thickness, which is increasing with thermal diffusivity:

$$S_{fl} \propto \frac{\chi}{w_{cl}} \propto \sqrt{\frac{\chi}{w_r}} \tag{1.9}$$

Flame velocity is maximum when mixture is slightly rich. There is a range within flame velocity variations are low (0.1 to 0.2 m/s as order of magnitude), but external to that regions it is possible to have flame extinction because there is not enough fuel or oxidant.

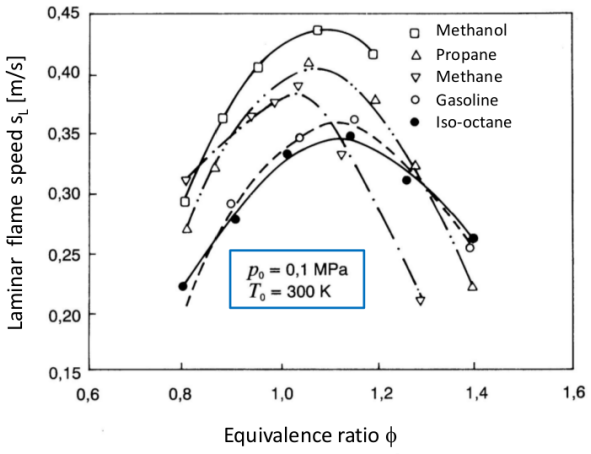

Figure 1.17: Laminar flame velocities of different fuels at different equivalence ratios

In figure 17 some flame velocities of different fuels such as methane or gasoline are plotted. Methane maximum flame velocity value is very close to stoichiometric air-fuel ratio. It is good behaving in lean mixture conditions (with ϕ lower than 1), but bad performing when mixture is rich. Gasoline and isooctane maximum values are more stable, with maximum flame velocity values in rich mixture conditions (ϕ equal to 1.2), but when engine is running lean the flame is significantly slowed down. In particular, flame velocity varies with fresh mixture temperatures and pressures, as explained by equation below:

$$w_{cl} = w_{cl0} \cdot (\frac{T}{T_0})^2 \cdot (\frac{p}{p_0})^{-0.25} \tag{1.10}$$

With w_{cl0} reference flame velocity is indicated, and with T_0 and p_0 reference temperature and pressure conditions corresponding to w_{cl0}. This experimental formula is good to perform a comparison between different thermodynamic conditions: a temperature increase speeds up the flame, since chemical reactions are faster and mixture thermal diffusivity increases also; a pressure increase has a negative effect on flame velocity, since it is not appreciably influencing chemical reactions but energy and mass transport are reduced.
Turbulence contributes to speed up the flame. Defining turbulence intensity u' as mean square value of velocity fluctuations, it is possible to relate turbulent flame velocity w_{ct} to intensity of these fluctuations, through the expression

$$w_{ct} = w_{cl} + a w_{cl} (u'/w_{cl})^b \tag{1.11}$$

From a physic point of view, turbulent micro vortices of a comparable scale with flame front intensify energy and mass transfer, hence increasing w_{ct}. Constants a and b are experimentally determined. A b typical value reported in [2] is 0.7, highlighting the almost linear influence of turbulence intensity on flame velocity.

1.3 Knock and spontaneous combustion

Combustion in spark ignition engines is considered abnormal when it is not caused by flame propagation from spark plug. When high local pressures and temperatures are reached, a portion of fresh charge can autoignite, releasing huge amount of heat. When it happens, two different flame fronts coexist, affecting engine performances.

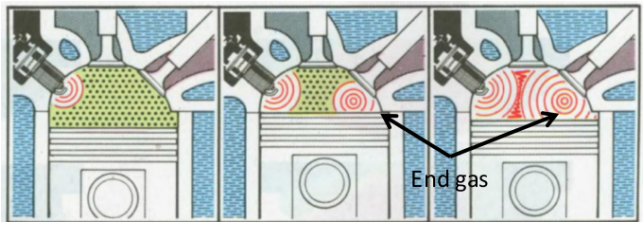

Figure 1.18: Knock illustration

In figure 18 knock is illustrated: some fresh hydrocarbons ignite spontaneously far from burnt gas region. Therefore, two different flame fronts can be

recognized in the cylinder: a first one related to normal combustion, a second one starting from knock origin. This kind of heat release can generate dangerous pressure waves, propagating in the whole combustion chamber. When knock occurs, a metallic noise can be heard, and it is originated by high frequency pressure oscillations. Knock is mechanically dangerous for the engine.
Even autoignition can be modeled through an Arrhenius correlation: it is influenced by cylinder pressure, temperature and mixture fraction, but also by time available for reactions to perform. It is possible to define an autoignition delay τ_a, as the time interval between the moment when mixture reaches certain pressure and temperature conditions and the moment in which an appreciably heat release by autoignition is present.

$$\tau_a = Ap^{-n}exp(\frac{E_a}{RT}) \tag{1.12}$$

Autoignition delay expression and reaction velocity ones are very similar: they present the very same coefficients, but signs of exponential functions are opposites. Introducing autoignition delay concept allows to avoid modelling all chemical reactions associated to combustion, providing a very practical time value. It measures the time duration of the whole intermediate process leading to mixture autoignition.

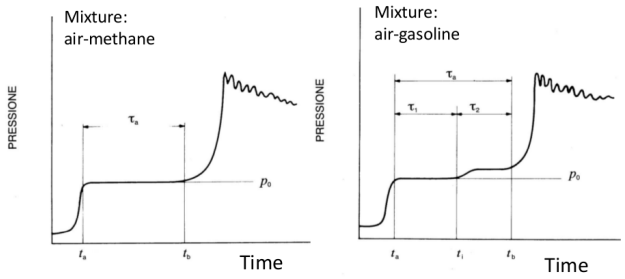

Figure 1.19: Autoignition delay

As displayed in figure 19, after a certain time (τ_a), there is a considerable pressure rise because of heat released by autoignited mixture. In this field, methane and gasoline behave differently. In air-gasoline mixture, the whole autoignition delay is divided in two smaller parts: after a first delay τ_1, a cold flame (with low heat release) appears and cylinder pressure slightly increases; after a second delay τ_2, fuel oxidation performs completely and a huge amount of heat is released. Since this thesis work is focused on natural gas combustion, just an unique autoignition delay τ_a is considered, as in the air-methane mixture case.
Pressure in spark ignition engines is almost homogeneous, hence pressure rise due to flame propagation burnt gases is also involving fresh mixture. For what concerns temperature, it can not be homogeneous because flame front clearly divides burnt mixture region from unburnt one. In burnt mixture region, very high temperatures (over than 2500 K) are reached; in the unburnt mixture region, temperature rise is due to compression and high temperature gradient because of combustion, hence huge temperature differences are present in the

cylinder. Because of a combination of both the effects, unburnt fresh temperature maximum value is reached slightly after top dead centre, before the whole mixture is considerably expanded.
As a generic rule, the more spark timing is anticipated, the more severe thermodynamic conditions are reached, making knock presence more probable.

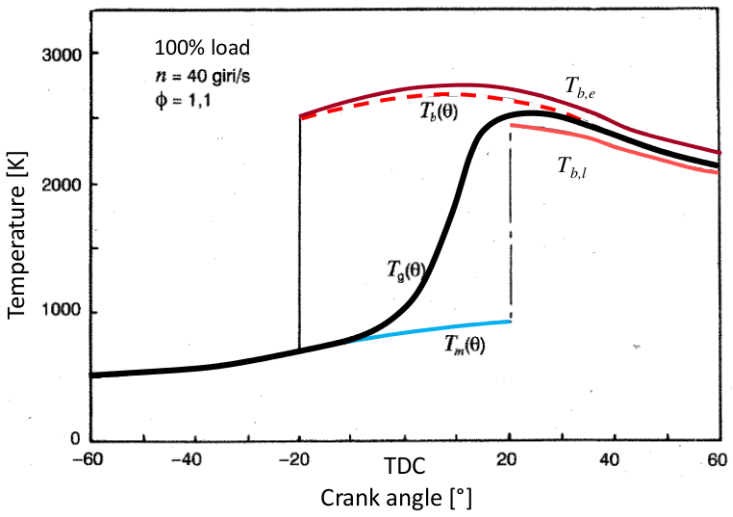

Figure 1.20: Spark ignition combustion temperature chart highlighting differences that can be present in the whole domain considered

Knock is defined as "spontaneous ignition abnormal combustion" because it is very violent causing huge pressure rise. When it appears, pressure waves inside combustion chamber propagates and get reflected by cylinder walls, causing oscillatory pressure rise behavior. In real engine installation it is detected by an accelerometer, and as a corrective action it delays spark timing for the following cycle. There are two kinds of knock: light knock and heavy knock. Light knock can be present in a lot of cycles, leading to not strong pressure rise; heavy knock is something to avoid otherwise engine walls (specially piston) risk to be damaged.
Knock strength and importance are not depending just on pressure and temperature, but also on mixture fraction. In this natural gas powered engine case, fuel-air mixture is homogeneous and once a fresh mixture portion is going to burn spontaneously, it is dropping all the other. If charge is not homogeneous, reaction rate is not uniform inside the combustion chamber and it can enhance or delay knock presence depending on local mixture fraction values.

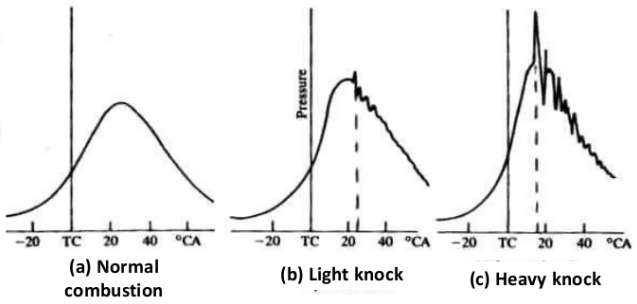

Figure 1.21: Pressure curve in knock presence

In any case, homogeneous charge compression ignition combustion is very fast. If sonic waves are avoided, engine could theoretically take benefits of this combustion kind. This is the main concept behind new and innovative combustion modes, even to have a better exploitation of fuel properties. As it will be defined in section 1.4, octane number is indicating autoignition resistance of the fuel: diesel one is between 15-20 because spontaneous ignition is something wanted when it is used; commercial gasoline one is 95 (or 98 sometimes); natural gas one can vary a lot, but it is in range 120-130. Having a lot knock resistant fuel spontaneously ignited allows to increase compression ratio in an appreciable way, to increase efficiency, but in stoichiometric homogeneous mixture context heat release would be huge, and pressure waves would mechanically destroy the engine itself.
HCCI (homogeneous charge compression ignition) combustion is something that has been investigated a lot for developing future internal combustion engines. High octane number fuel (gasoline or natural gas) is compressed to spontaneously ignite, in similar way of what has been described above.

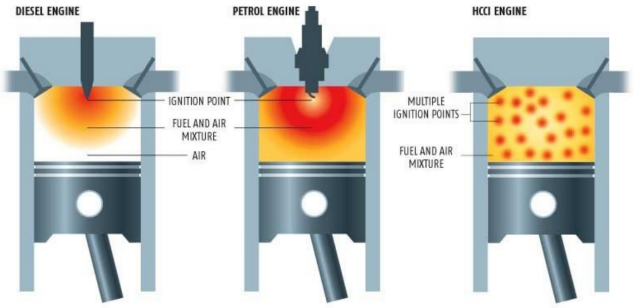

Figure 1.22: HCCI: Homogeneous charge compression ignition combustion

As figure 23 shows, conceptually HCCI is something in between a diesel engine (where no spark plug is needed) and a gasoline engine (since a spark ignition fuel is used), and the result is a compression ignition of fuel air mixture. No flame is present or propagates, but this kind of technology offers a chance to have fast combustion. For a conceptual point of view, it is something similar to knock because it is also causing very high heat release in a very short time, but this kind of heat release is controlled by changing air-fuel mass ratio: HCCI

engine runs lean, meaning inserting more air mass than the reaction would need. Equivalence value ϕ is defined as:

$$\phi = \frac{m_{air,stoichiometric}}{m_{air}} \tag{1.13}$$

meaning that $\phi = 1$ when air mass is exactly stoichiometric one, lower than one if there is any air excess. In this case, HCCI runs lean with ϕ between 0.4-0.5, in order to have a lower heat release spread in the combustion chamber and avoid huge pressure sonic waves. Another great advantage in running in lean condition is that lower maximum cylinder temperatures are reached. As figure 23 illustrates, low equivalence ratio and maximum temperature values can avoid NOx production and oxidise CO formed in combustion process.

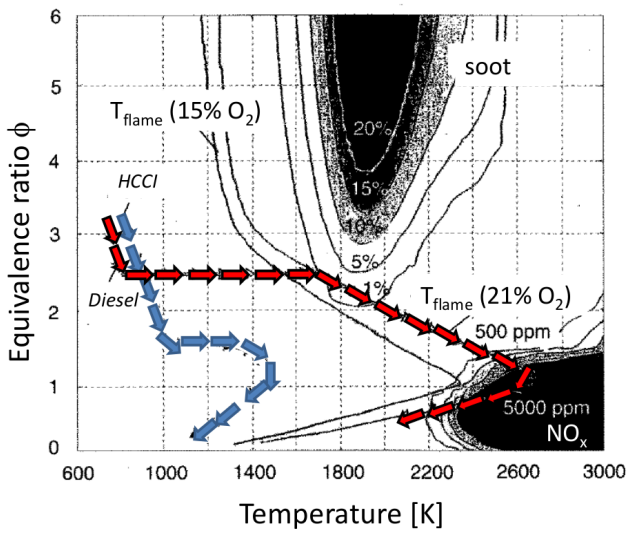

Figure 1.23: HCCI pollution chart, highlighting the advantages of a lean compression ignition combustion and differences with a diesel one

The huge drawback for HCCI engines is combustion control: in a spark ignition engine, combustion can be started by spark plug electronic control; in a diesel compression ignition engine, fuel octane number is so low that as soon as liquid fuel evaporates, it autoignites. In this new combustion concept, it is very hard to predict exactly when combustion is going to take place, making engine control very difficult. To limit these difficulties (and to be sure that no misfire is going to present), compression ratio could be increased, but then mechanical stresses on engine itself would become huge and structurally unbearable.
These are the reasons why innovative combustion concept has been changed, passing from a HCCI engine (where just compression ignition is present) to a controlled autoignition engine, where a spark plug can control autoignition timing.

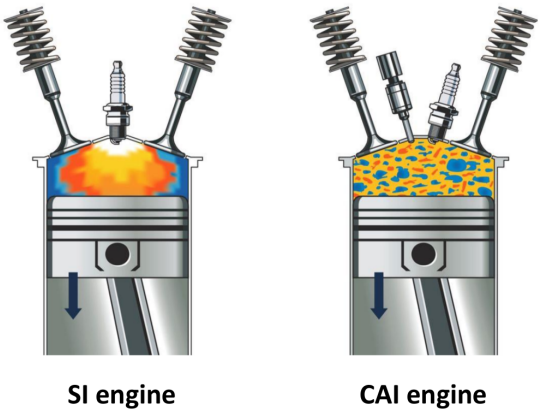

Figure 1.24: CAI: controlled autoignition combustion

Main combustion ignition mode is always compression ignition one, but in this configuration there is a device able to control it and decide when it is taking place. In figure 24, both spark plug and fuel injector are displayed, to illustrate working principle of spark assisted compression ignition (SACI) engine; but it is not the only way to control spontaneous ignition of high octane number fuel, as far as also dual fuel technology is at the state of the art investigated: it consists into injecting few amount of diesel fuel in homogeneous high octane number charge combustion chamber to start autoignition. Once diesel evaporates, combustion is going to begin and then involving the whole charge.
Some both experimental and CFD papers have the purpose to investigate these new combustion modes, as far as they can be promising for increasing combustion efficiency and reducing pollutant emissions at the same time. In [11], a comparison between spark assisted compression ignition technology and a dual fuel diesel-natural gas one is performed. A rapid compression and expansion machine was used to simulate just compression and expansion stroke, in order not to damage the engine if knock occurs. They consider a very high compression ratio (20:1) and very low engine speed (800 rpm) for heavy duty application.

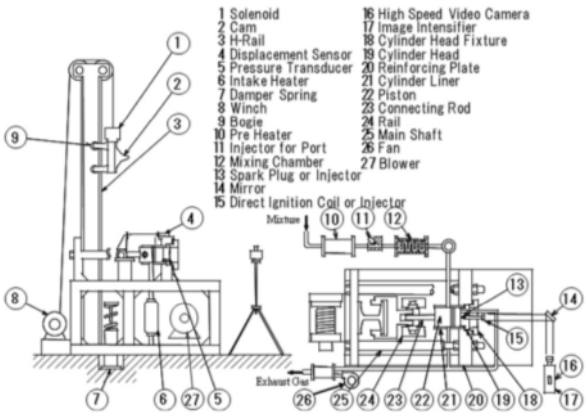

Figure 1.25: Rapid compression and expansion machine

Since just two strokes are experimentally performed and there is not a constant engine rotational speed, swirl motion must be generated though a blower, connected with both intake gasses and exhaust ones.

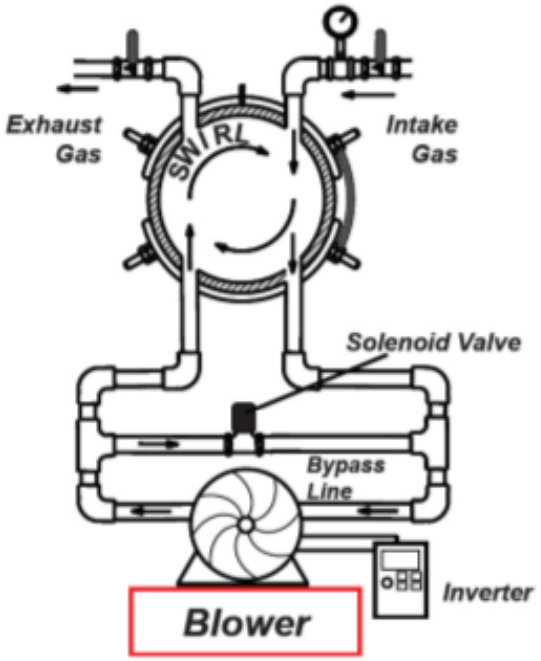

Figure 1.26: RCEM Blower adopted to generate turbulence

The very same rapid compression and expansion machine has been used for spark assisted compression ignition combustion and diesel pilot compression ignition combustion, with diesel pilot fuel mass corresponding to 2% of homogeneous mixture low heating value. Some different investigations are carried, as shown in tables below, where different air excess ratio or piston heads were considered.

Exp. No.	1	2	3	4	5
Initial pressure kPa	111	←	←	←	←
Excess air ratio	1.0	**1.3**	1.0	1.0	1.0
EGR ratio %	0	0	**10**	0	0
Piston head	Flat	Flat	Flat	**Bathtub**	Flat
Swirl ratio	0	0	0	0	**1.5**

Figure 1.27: SACI experimental setups

Exp. No.	1	2	3	4	5	6
Initial pressure kPa	111	111	111	**139**	**139**	111
Inj. pressure MPa	140	**100**	140	140	140	140
Excess air ratio	1.0	1.0	**1.3**	1.0	**1.3**	1.0
EGR ratio %	0	0	0	**20**	**20**	0
Swirl ratio	0	0	0	0	0	**1.5**

Figure 1.28: Diesel pilot injection experimental setups

Therefore, experiments were performed to investigate both pressure rise and efficiency. Since compression ratio is very high (20:1 is commercially unrealistic for high octane number fuel at the state of the art), pressure and heat release curves are not discussed in this introduction chapter, but efficiency plot to understand if these new combustion modes have some future potential.

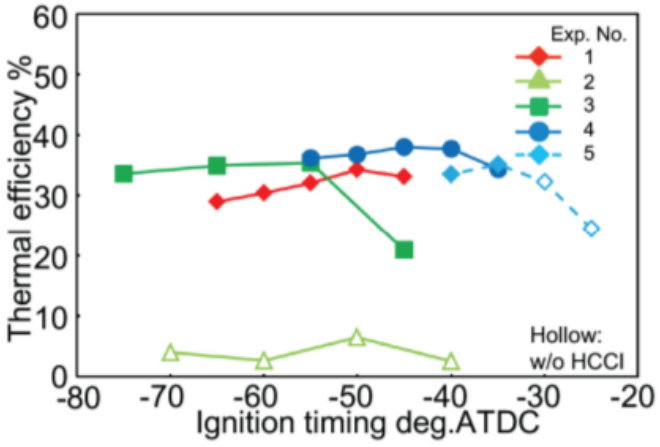

Figure 1.29: Experimental spark assisted efficiency

For what concerns spark assisted, combustion efficiency reaches and overcomes 40% at very low engine speed. Maximum value is reached in presence of stoichiometric air-fuel ratio and 20% of exhaust gas recirculation. When just air excess ($\lambda = 1.3$, defined as ratio of actual fuel air ratio with stoichiometric one) is considered, misfire is present since experimental mixture is too lean to burn, probably also explained by lack of turbulence in experimental machine.

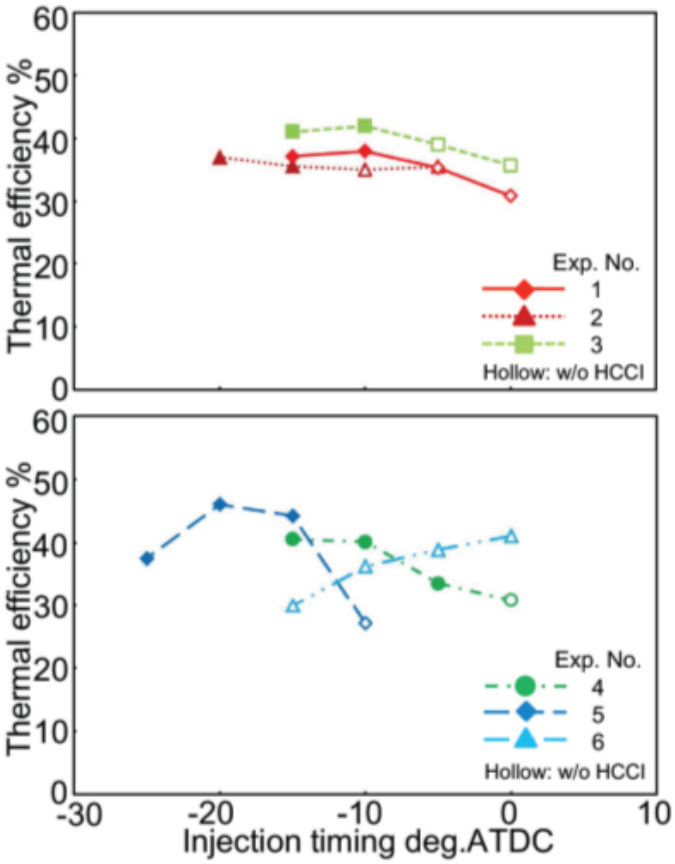

Figure 1.30: Experimental diesel pilot efficiency

When diesel pilot injection is considered, efficiency gets quite higher with respect to spark advance. Diesel pilot injection is very close to top dead centre, enhancing how fast its ignition taking place; in spark assisted efficiencies reported in figure 30, spark advance needed to be anticipated up or even further of -40° (ATDC: after top dead centre), meaning spark assisted fuel air mixture is very difficult to be ignited in experimental engine considered.
This thesis work is focused on spark assisted compression ignition engine, in order to verify its feasibility and efficiency improvements. Engine is a heavy duty diesel converted with a compression ratio of 11.7, similar to the one analysed in [12]. Before starting with engine analysis and investigation, fuel has been discussed, since natural gas has not an octane number or heating value imposed for commercial reasons as gasoline, but its properties can change depending on its composition.

1.4 Fuel and pollution: Natural gas

Hydrocarbon combustion can be described by the following chemical reaction:

$$C_nH_{2n+2} + \frac{3n+1}{2}\mathrm{O_2} -> n\mathrm{CO_2} + (n+1)\mathrm{H_2O} \tag{1.14}$$

This is valid for every hydrocarbon combustion (diesel, gasoline, natural gas) at its completeness. On the rightward member, just combustion products are present but not any pollutants, as far as they are a product of uncomplete reactions. In fact, global chemical reaction associated to combustion is the results of a multiplicity of lower ones having different reaction rate and taking place in different condition. For instance, first methane oxidation step can be summarized by following figure.

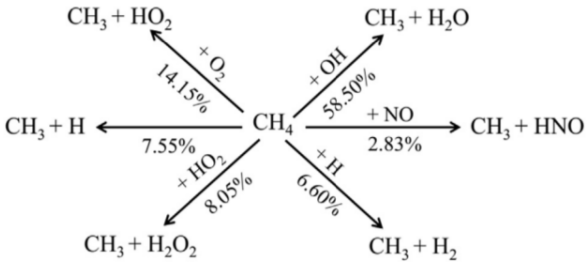

Figure 1.31: Methane first oxidation reaction

Different kinds of products can appear during these processes, as a result of incomplete combustion. Most of them later oxidize once combustion is completed, in order to form just CO_2 and water; but this is not always possible, because of very fast pressure and temperature variation at which an internal combustion engine is exposed to.
Principal internal combustion engine pollutants are:

CO**, formed in stoichiometric or reach combustion due oxygen lack**

soot, present when liquid or solid fuels are used

NOx**, produced at very high temperature in oxygen abundance**

Unburnt hydrocarbons, always present in different percentages

Quantities and kinds of pollutions production strongly depends on thermodynamic cycle and fuel used: diesel engines usually have high soot and high NOx emissions because of difficult fuel evaporation and very high temperature reached, but CO produced in combustion process oxidizes in very lean environment; spark ignition gasoline engine produces all the three kinds of pollutant in different quantities, since it is high volatility fuel but working at stoichiometric charge.
A common strategy to reduce internal combustion engine pollutant emissions in real drive behavior is installing an after-treatment system, therefore something able to recombine the three kinds of pollutants to form N_2, CO_2 and H_2O.

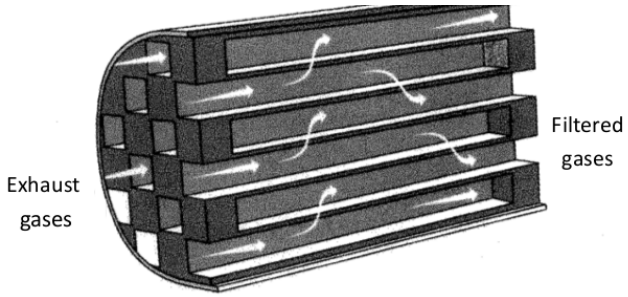

Figure 1.32: Diesel particulate filter

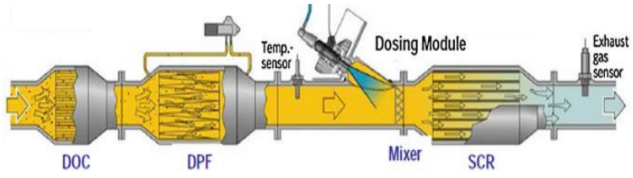

Figure 1.33: Urea injection

In diesel engines usually both a diesel particulate filter (DPF) and urea injection system are installed. The first one aims to filter soot particles, in such a way that they are trapped in the filter itself and not released in atmosphere; the second one makes selective catalytic reaction happen, a chemical reaction that presents ammonia and NOx as reactants and N_2 and water as products. These systems development contributed in reducing diesel engine pollutants, even if they (specially DPF) introduce a pressure loss in correspondence of exhaust pipe.

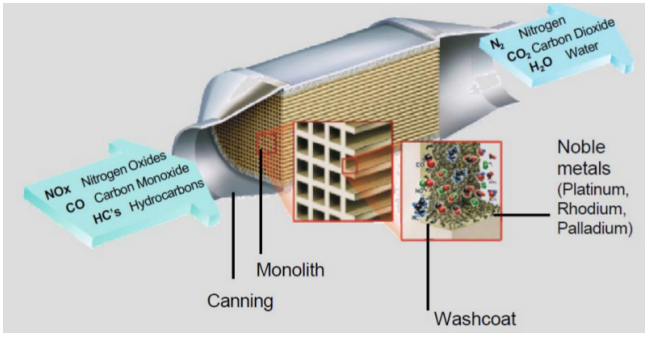

Figure 1.34: Catalytic converter for SI engine

For what concerns spark ignition engine, aftertreatment system is very different. A particulate filter is present again in gasoline fuelled ones, even if it is smaller because generally they produce a lower soot quantity; to make pollutants chemically react, catalytic converter (working with noble materials) is

placed in aftertreatment system. This chemical device needs CO, NOx and unburnt hydrocarbons to work, to recombine as much as possible.

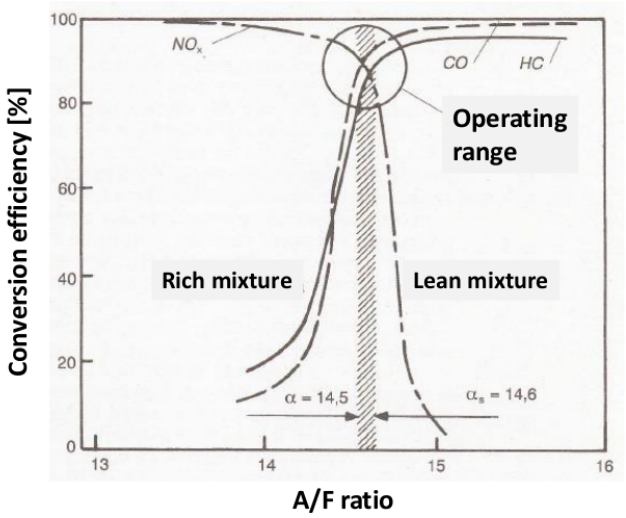

Figure 1.35: Catalytic conversion efficiency

This concept is explained in the conversion efficiency plot, in figure 35: for very rich mixtures, NOx are almost all converted (also because a low quantity is produced) but hydrocarbons and CO conversion efficiency is very low; for very lean mixtures, conversion efficiency of carbon monoxide and hydrocarbons is quite high also because they are oxidizing with the remaining oxygen, but NOx can not be converted. Therefore, SI engines are constrained to run in stoichiometric mixture condition if three way catalyst is installed, to maximize its conversion efficiency. Fuel consumption increases because efficiency is higher when engine is running slightly lean, but pollutant emissions increases significantly.
Natural gas is a very promising fuel for future internal combustion engines, such as it is an already gaseous fuel and no soots are produced in combustion process. In any case, a catalytic converter is installed to convert carbon monoxide and nitrogen oxides, working with unburnt hydrocarbons from combustion chamber. These aftertreatment systems (specially spark ignition ones) introduce a small pressure loss having an effect on cylinder performance, hence target for future internal combustion engine is to perform an always cleaner combustion. In these terms, developing natural gas fuelled spark assisted compression ignition or diesel pilot compression ignition can be a future opportunity for automotive industry.
A natural gas composition analysis has been carried out since it can have a strong influence on fuel properties and octane number. Octane number is an autoignition indicator, assuming the value of 100 if the fuel behaves as isooctane, higher if it is more knock resistant. Natural gas usually has an octane number between 120-130, and it can change between one composition and another.

Hydrocarbon	Ch. formula	MW [g/mol]	LHV [MJ/kg]	Octane number
methane	CH_4	16,04	50,0	130
ethane	C_2H_6	30,07	47,622	108
propane	C_3H_8	44,1	46,35	103
butane	C_4H_{10}	58,12	45,75	91

Table 1.1: Natural gas main hydrocarbons

As showed by the table, in natural gas both "light hydrocarbons" (such as methane and ethane) and "heavy hydrocarbons" (such as propane and butane) are present, and it can be distinguished dry natural gas (poor in heavy hydrocarbons) from wet natural gas (rich in heavy hydrocarbons). Methane is a very knock resistant fuel, but butane and propane are not: as a consequence, their presence can lead the mixture to ignite spontaneously or even knock. Octane number is an experimental indicator (it can even be distinguished between research and motored octane number depending on testing fuel temperature), it can not be arithmetically computed but an experimental or simulation setup is necessary. Especially in homogeneous charge, as soon as a small portion autoignites, it will easily drop all the others, no matter if spontaneous ignition principle is physically given by propane or butane contribution. Hydrocarbons heavier than butane are uncommon in commercial natural gas.
Since it is already in gaseous phase, also nitrogen and carbon dioxide can be present, which are inerts in combustion process, not reacting.

Inert	Chemical formula	Molecular weight [g/mol]	LHV [MJ/kg]
nitrogen	N_2	28	0
carbon dioxide	CO_2	48	0

Table 1.2: Most common inerts present in natural gas

Inerts presence tends to decrease fuel octane number as far as oxygen chemical activity decreases, and they give no heating value contribution. There are not any commercial rules constraining natural gas composition for any application, hence a composition review has been taken.

Compound	Symbol	Percent in Natural Gas
Methane	CH_4	60–90
Ethane	C_2H_6	0–20
Propane	C_3H_8	0–20
Butane	C_4H10	0–20
Carbon dioxide	CO_2	0–8
Oxygen	O_2	0–0.2
Nitrogen	N_2	0–5
Hydrogen sulphide	H_2S	0–5
Rare gases	A, He	0–2

Figure 1.36: Natural gas composition ranges

Composizioni e caratteristiche dei gas naturali distribuiti in Italia

Gas Composizione indicativa	Nazionale (% vol)	Russo (% vol)	Olandese (% vol)	Algerino (% vol)
Metano	99,62	98,07	91,01	83,28
Etano	0,06	0,60	3,70	7,68
Propano	0,02	0,22	0,88	2,05
Butani	0,01	0,09	0,28	0,78
Pentani	–	0,01	0,07	0,21
Esani +	0,01	0,02	0,07	0,11
Anidride carbonica	0,02	0,11	1,11	0,19
Azoto	0,26	0,87	2,84	5,52
Elio	–	0,01	0,04	0,18

Figure 1.37: Consulente energia natural gas compositions

Composizione	CH_4	C_2H_6	altri idrocarb	CO_2	N_2	altri gas	H_s
Italia	99,53	0,06	0,03	0,03	0,35	-	37,7
Russia	97,50	1,06	0,45	0,15	0,83	0,01	38,0
Nord Europa	90,32	4,62	1,33	1,37	2,33	0,03	38,6
Algeria	87,92	6,95	1,77	0,97	2,29	0,10	39,7
Libia	85,28	6,80	2,95	1,44	3,42	0,11	39,9
Rigassificato	90,05	7,82	1,24	-	0,84	0,05	40,4
Matano puro	100,00	-	-	-	-	-	37,7

Figure 1.38: Unirc lecture natural gas compositions

Composizione media del Gas Naturale trasportato in Italia (2008) da SNAM Rete Gas

% mol	Russia	Nord Europa	Algeria	Libia	GNL	Nazionale
Metano	97,532	90,520	88,182	85,511	90,369	98,843
Etano	1,032	4,514	6,993	6,762	7,701	0,415
Propano	0,330	0,916	1,291	1,956	0,973	0,112
Butano+superiori	0,128	0,374	0,418	0,956	0,184	0,041
N2	0,836	2,390	2,151	3,409	0,773	0,508
CO2	0,142	1.286	0,965	1,406	0,000	0,081
PCS (kJ/Sm3)	38005	38543	39689	40,386	40386	37779
WI (kJ/Sm3)	50346	49186	50160	51795	51795	50418

(Fonte: Snam Rete Gas V. Cannizzo Forum Gas Milano 2009).

Figure 1.39: SNAM natural gas compositions

A lot of different natural gas composition sources were considered, and all agree that Italian (sometimes indicated as "Nazionale") natural gas is reacher in methane with respect to the others. Compositions are given in volume or mole percentages, and when converted into mass ones heavier hydrocarbon values rise more than lighter ones. For combustion investigation, natural gas composition must be fixed, and then any variation is addressed to sensitivity analysis. Therefore, composition chosen was Nord European one provided by SNAM source, as far as it is quite rich in heavy hydrocarbons and both propane and butane percentages are provided.
Natural gas composition has been converted into mass percentages, and then following values have been derived.

	Chemical formula	mass percentage
methane	CH_4	81.9%
ethane	C_2H_6	7.65%
propane	C_3H_8	2.27%
butane	C_4H_{10}	1.22%
nitrogen	N_2	3.77%
carbon dioxide	CO_2	3.19%

Table 1.3: SNAM North Europe natural gas composition in mass percentages

As shown in table above, chosen natural gas composition is quite rich in methane, but also propane, ethane and butane mass percentages are important. Taking in consideration a lower octane number fuel for SACI development leads to have a higher compression ignition control, despite flame propagation when compression ignition is not feasible or unwanted. Inerts are something less than 7% of the whole mixture.
In the whole thesis work, a multiplicity of natural gas composition is going to be considered for instance to validate solver used or even to provide an engine performance sensitivity analysis. Target is, as explained before, increasing engine efficiency and at the same time reducing pollutant emissions.
In the end, natural gas can be considered an easy fuel to be stored, for engine conversion from diesel commercial ones and easy for refuelling since fuel station are currently available.

1.5 Numerical simulations

For internal combustion engines design, numerical simulations are very useful since a lot of conditions can be tested with much lower economical efforts and without risking of damaging an experimental engine. CFD, computational fluid dynamics, is used to predict flows behavior in the whole engine, from breathing pipes to exhaust ones, including combustion chamber. In any case, modelling flow ducts is very different with respect to simulating what happens in combustion chamber, hence two different tools are used:

- zero or one dimensional software for flow management

- three dimensional software for combustion chamber design

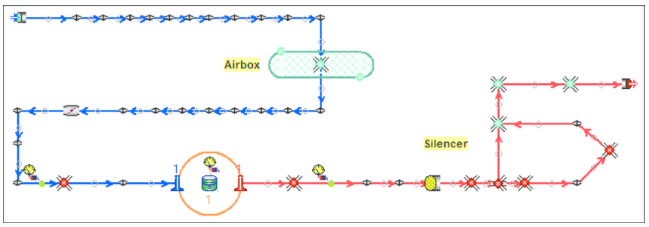

Figure 1.40: Gasdyn interface

Figure 40 reports an example of a mono-dimensional fluid dynamics code. Illustrated interface is from Gasdyn® software, that can describe how inlet and

outlet flows are managed between different pipes or in presence of some devices, such that compressor, turbine or even silencer. It can compute global engine performances, but it can not model the combustion chamber. It is not a stationary fluid dynamics model, considering compressible flows neither adiabatic or isentropic. Mass, momentum and energy conservation equations are written in just one dimension, implying a much lower computational time needed if compared to a 3D CFD software. To model friction forces acting on the fluid is very important, since it can not be properly considered viscous because this assumption would imply a two-dimensional velocity distribution, but tangential friction stress is represented by following equation, function of Reynolds number:

$$\tau_w = f\frac{1}{2}\rho u^2 \qquad with \quad f = \frac{0.25}{[log_{10}(\frac{k}{3.7D} + \frac{5.74}{Re^{0.9}})]^2} \tag{1.15}$$

These kinds of codes are very appropriate to give good fluid pressure and temperature values almost everywhere, but they can not consider properly turbulence or other 2D or 3D phenomena, that in combustion are quite relevant. This is the reason why when designing combustion chamber and engine geometry a 3D fluid dynamics code must be used. Software chosen has been OpenFOAM®, because it is an open source and easy modifiable for author preferences.

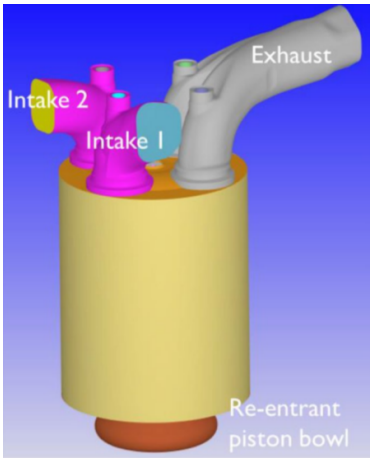

Figure 1.41: 3D simulation example

OpenFOAM is a C++ based open source software. At the state of the art, version 6 is available for free download, but version used is 2.2.x owned by Politecnico di Milano, since it presents some useful modifications. LibICE, developed by Politecnico di Milano in Energy department, has some supplementary codes and utilities used to realize this thesis work.
CFD simulations can require huge computational time, especially if valve motion (opening and closing) and all strokes are both modelled and simulated. To make numerical simulations also suitable for commercial laptops, not the whole cycle is simulated, but just compression, combustion and expansion.

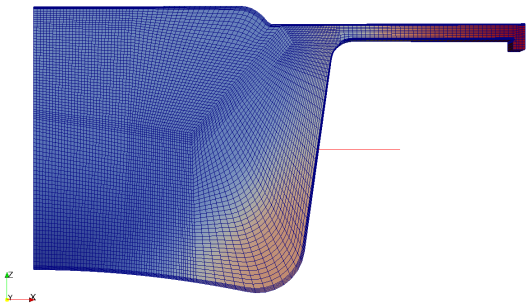

Figure 1.42: OpenFOAM mesh example

Figure 42 illustrates an OpenFOAM case opened in ParaView®interface. Cylinder volume is divided in a lot of smaller ones (over 6000) composing mesh, which has to be numerically suitable for the case studied, not presenting any huge discontinuities, non orthogonalities or some more characteristics compromising mesh quality. Simulations starts from -175° (intake valve closing) ending at 124° (exhaust valve opening), with variable time steps to decrease computational time. Not the whole combustion chamber is modelled: as figure 43 shows from the top view, just 2° of arc of the whole cylinder geometry is meshed, imposing radial symmetry for what concerns the rest of the volume.

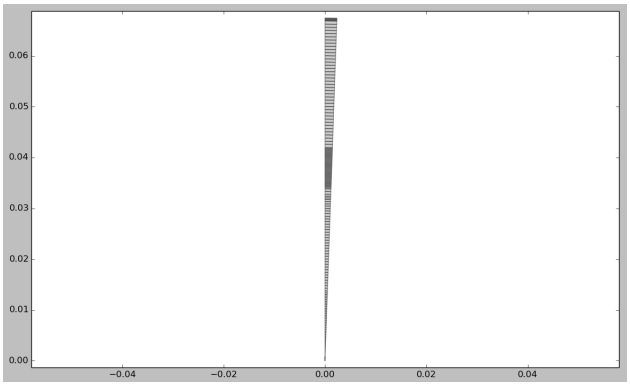

Figure 1.43: OpenFOAM mesh top view

Figure above has been taken from Mesh generator for Diesel Combustion Chamber geometries developed in Politecnico di Milano in the Energy Department, by Professors Augusto Della Torre and Tommaso Lucchini. This has been an useful tool for mesh editing, in order to simulate case in OpenFOAM environment.
Last software used is a CAD (computer aided design) one, Autodesk Inventor® (student license), which has been essential for geometry design.

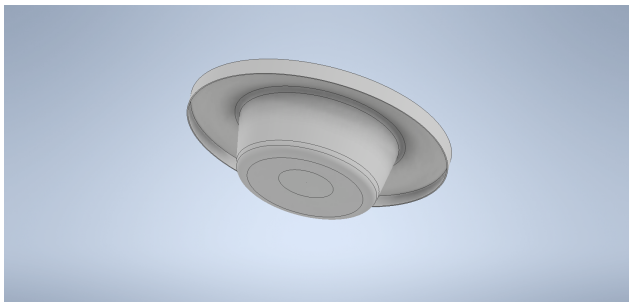

Figure 1.44: Autodesk Inventor interface

Using this approach is possible to design a completely different engine geometry through Autodesk Inventor, editing the mesh using Automatic Mesh Generator and simulating the case in OpenFOAM environment. To begin, a numerical code able to consider both flame propagation and compression ignition combustion needs to be edited.

Chapter 2

Numerical solvers

Computational fluid dynamics (also known with the acronym CFD) can be a very important design tool for fluid machines. Thanks to very powerful computational resources available nowadays, very complex systems can be entirely simulated with excellent results. In this way, it can significantly reduce economical efforts in the design process, especially for internal combustion engines where some extreme conditions have to be investigated. Testing the engine can imply the risk of damaging it, while building a computational simulation no risk to compromise any useful machine is present. Investigating modern combustion modes, heavy knock or too severe pressure rise can occur, leading to concrete risk of damage any experimental setup. Another great benefit of CFD is the possibility to build in-house codes dedicated to different research targets, hence perfectly suitable to investigated application. A physic and engineering knowledge of the flow studied is needed even when writing the code, as far as choosing a wrong turbulence model or numerical scheme can compromise simulation results. For all this reasons, OpenFOAM® has been chosen to build the CFD code, since it is an open-source software with many pre-implemented capabilities.

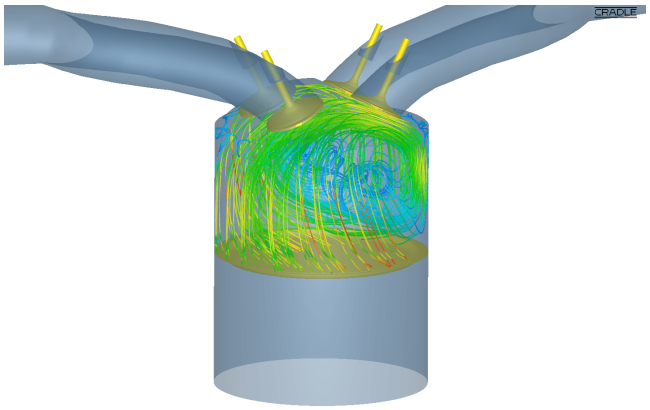

Figure 2.1: CFD gas exchange example

CFD domain is the region being simulated. In this thesis work (just focused

on power cycle), domain of interest is the whole cylinder, divided in different finite volumes by different cells. With the term "mesh" the whole set of cells is indicated. Mesh has already to take into account how the solution should be like, since it needs to be refined in presence of critical areas, while it can be courser elsewhere. Boundaries separate mesh to the surrounding environment, which can actually influence fluid physical quantities if the system can not be considered isolated but just closed: this in internal combustion engine is the case of wall heat transfer, heat losses decreasing engine performances. Therefore, some boundary conditions need to be defined, in order not to model also external regions to determine energy transfer with the investigated system. Especially when complex geometries are composing the domain, mesh represents a first description of the domain itself. In this thesis work some CAD geometries are going to be simulated, hence a different mesh is generated for any interested geometry. As reported in [14], "the main role of the volume mesh is to capture the 3D geometry. Cell should not overlap and completely fill computational domain. A priori knowledge of solution is useful in mesh generation process, in order to locate high resolution zones to capture critical parts, such as shocks, boundary layer".
Mesh grid is considered structured if it is very regular, unstructured if it is identified by irregular connectivity. Mesh used is going to be hybrid, presenting zones where grid is very regular and some others where it is very refined, such that solver is able to consider fuel injection or sonic waves with higher accuracy. Some indicators are commonly used in CFD environment, helping to have a good mesh quality:

Cell equiangular skew :

Cell symmetry is investigated. It is defined taking into account minimum cell angle and maximum one. If cell geometry is equiangular (perfect square for instance), θ_{max} and θ_{min} are equivalent and skewness is 0, as optimal case; if it is not, this indicator will get closer to 1. The lower it is, the better for CFD calculations. Defining θ_e as angle for equiangular cell (60° in case of triangular cell, 90° in case of quadrangular cell and so on), mesh skewness is evaluated as expression below:

$$Skewness = MAX[\frac{\theta_{max} - \theta_e}{180° - \theta_e}, \frac{\theta_e - \theta_{min}}{\theta_e}] \tag{2.1}$$

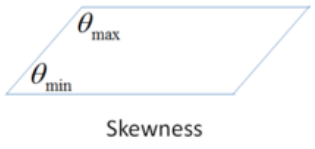

Figure 2.2: Cell equiangular skew

Cell aspect ratio :

Aspect ratio is very similar to equiangular skew, but referred to cell boundaries length. It is defined differently depending if mesh considered is triangular or at least quadrangular, and in second case it is the ratio between

the longest boundary side with the shortest one. Best aspect ratio is 1; the higher it is, the worse for mesh quality. Expressions for aspect ratio computation are the following ones:

$$AR = f\frac{R}{r} \qquad Triangular \tag{2.2}$$

$$AR = \frac{max(Side_{length})}{min(Side_{length})} \qquad others \tag{2.3}$$

In triangular aspect ratio expression, R is circumscribed circumference radius, while r is the inscribed circumference one. In other cell geometries, aspect ratio is defined as the ratio between longest and shortest cell side length.

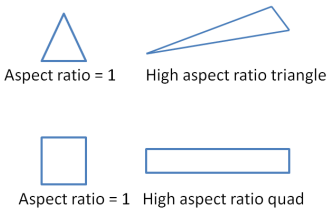

Figure 2.3: Cell aspect ratio

Mesh orthogonal quality :

It is a mesh orientation indicator. If every cell surface normal is pointed to the centre of all the neighboring ones, it assumes the value of 1 as optimal case. If cells are not oriented one to each other, mesh orthogonal quality is decreasing and it can cause some numerical problems during CFD calculations. Hence, defining $\overline{f_i}$ as vector connecting centroid of reference cell and centroid of one of its faces, and $\overline{c_i}$ as vector connecting centroids of two different cells, orthogonal quality is computed as reported by expressions below.

$$OrthogonalQuality = MIN(EQ1; EQ2) \tag{2.4}$$

$$EQ1 = \frac{\overline{A_i} * \overline{f_i}}{|\overline{A_i}| * |\overline{f_i}|} \tag{2.5}$$

$$EQ2 = \frac{\overline{A_i} * \overline{c_i}}{|\overline{A_i}| * |\overline{c_i}|} \tag{2.6}$$

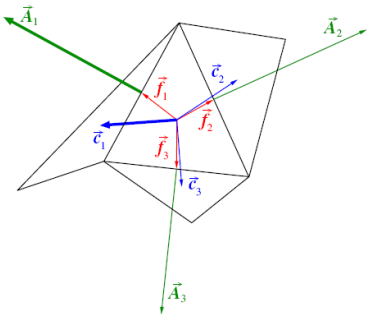

Figure 2.4: Mesh orthogonal quality

Mesh size ratio :

This last mesh indicator is to ensure that every cell side length do not vary in a huge way if compared with neighboring ones. In any case, this is not going to have any important effects in this context where, especially in squish area, flow is oriented mainly to cylinder centre. Defining as Δx_{MAX} and Δx_{MIN} two different cells length in one chosen direction, size ratio is computed as:

$$SR = \frac{\Delta x_{MAX}}{\Delta x_{MIN}} - 1 \tag{2.7}$$

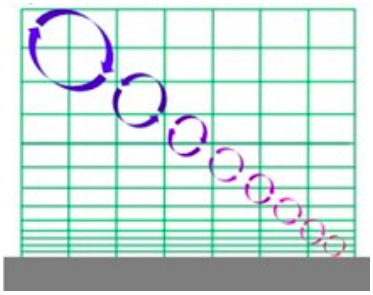

Figure 2.5: Mesh size ratio

First simulations are going to increase fluid flow physic knowledge, especially if it has been just hypothesized a priori when generating the mesh. Therefore, an iterative procedure is commonly applied to improve mesh quality, since after some simulations regions of interest are more clearly defined.

Mesh Motion

There are some applications where domain geometry moves during the calculation. This is the case of internal combustion engines, where the piston is rising from bottom dead centre to top dead centre. Moving deforming mesh algorithm will allow the domain to change its shape during the simulation and preserve its validity, but structure of internal mesh needs to remain unchanged. There

are different ways to adapt the mesh to domain geometry variations. "Shape change" is the most intuitive one, since mesh in boundary layers change their shapes during calculations. This is not very flexible, since it is well performing when changes are very low, but if boundaries deformations are extreme high discretization errors can arise. In internal combustion engines, boundaries are fixed except for the piston which is vertically moving in just one direction; hence, adding or removing computational cells to accommodate boundary deformation is an easier and more suitable mesh motion strategy.

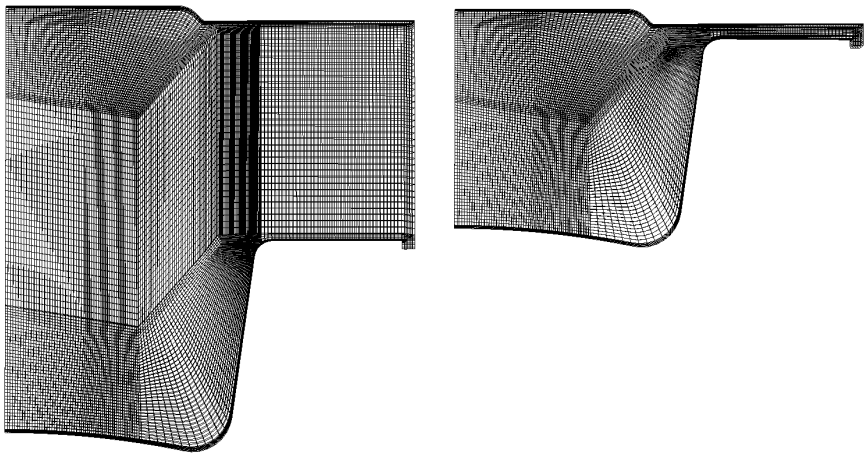

Figure 2.6: Mesh motion layers removal example

As shown in figure 50, mesh structure remains the same, but number of mesh layers change considerably. There are some cases where both kinds of described mesh motion can be used, if for instance also valve opening or closing is modelled. In this thesis work, since it is just focused on power cycle, mesh layers are just added or removed and no valve motion is simulated.
If all these mesh quality indicators are globally analysed, the more the mesh is uniform, the lower numerical issues can arise because of a poor mesh quality. In the context of in-cylinder CFD simulations, a compromise needs to be found between a good mesh suitable for engine geometry and computational time, as far as all equations that will be described are solved for every cell at every time step.

Transport equations

Transport equations of different quantities maintain actually a very similar structure, hence before going deep in every physical detail, a general analysis has been carried with a specific quantity ϕ. This ϕ has not any physical meaning, but it is useful for a numerical analysis that can explain pressure, temperature, density or any other fluid dynamics quantity equation.

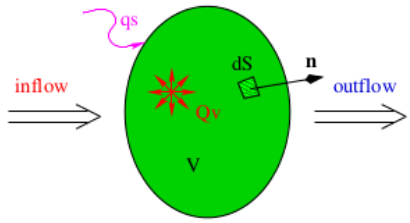

Figure 2.7: Specific quantity flows for each cell

For a generic domain Ω, ϕ can change its value only if fluxes and/or source terms are present:

$$\frac{\partial}{\partial t}\int_{\Omega}\phi d\Omega = -\int_{Surf} Fluxes \;\; dS + \int_{\Omega} SourceTerms \;\; d\Omega \tag{2.8}$$

Fluxes can be two kinds of: convective if interested quantity ϕ is transported by the fluid: $F_c = \phi U$; diffusive if interested quantity ϕ is transported by its gradient: $F_d = -k\nabla\phi$.
For what concerns source terms, they can be surface related such as wall heat transfer, or volumetric such as heat released by combustion in certain cells. Every surface term must be integrated along respective cell face, while volume ones along the whole cell volume. Hence, the previous equation becomes

$$\frac{\partial}{\partial t}\int_{\Omega}\phi d\Omega + \int_{Surf}\phi U dS = \int_{Surf} k\nabla\phi dS + \int_{\Omega} Q_V d\Omega + \int_{Surf} Q_{surf} dS \tag{2.9}$$

Time derivative and convective flux terms are usually reported in the first equation member, while diffusive flux, surface source and volumetric source terms are usually reported on the right side of the equation. Since some of the integrals must be performed in volume domain and some others in surface domain, Gauss divergence theorem has been applied to convert surface integrals into volume ones. Therefore, the following equations are derived, with equation (25) being the integral form of conservation equation and equation (26) the differential (and most known) form of conservation equation.

$$\frac{\partial}{\partial t}\int_{\Omega}\phi d\Omega + \int_{\Omega}\nabla\cdot(\phi U)d\Omega = \int_{\Omega}\nabla\cdot(k\nabla\phi)d\Omega + \int_{\Omega} Q_V d\Omega + \int_{\Omega}\nabla(Q_{surf})d\Omega \tag{2.10}$$

$$\frac{\partial\phi}{\partial t} + \nabla\cdot(\phi U) = \nabla\cdot(k\nabla\phi) + Q_V + \nabla Q_{surf} \tag{2.11}$$

Substituting ϕ with interested physical quantities and defining properly constants and source terms, conservation equations used in CFD are derived.

Discretization

To make equations numerically manageable by a computer, a domain discretization is necessary, hence the mesh. Every cell is recognized by OpenFOAM as a small volume portion, with its well defined faces. For any specific quantity, every cell has a ϕ value ideally located in the cell centre, and it is represented by

different colours when simulation results are displayed; but to evaluate fluxes, surface values are needed for each cell face. Some discretization schemes and criteria need to be introduced, hence every term of transport equation is analysed separately.
Cell interested by equation is indicated as "P", then neighbouring cells such as northwards ("N"), eastwards ("E"), southwards ("S") and westwards ("W") can be easily recognized, as shown in figure 52.

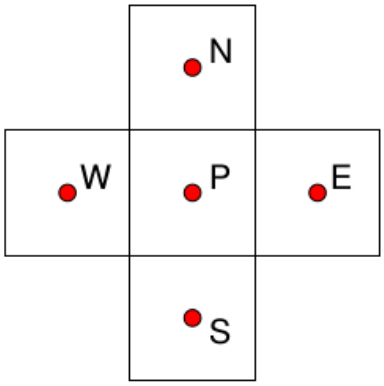

Figure 2.8: Cell references

Time derivative term is referred to central cell value. Euler forward scheme is used to discretize this term, and it is the most intuitive choice since time is just moving forward. Therefore, ϕ_p^t is the value in the cell P of the previous iteration (known), while $\phi_p^{t+\Delta t}$ is the one at the current time step, real unknown of the equation. Time derivative can hence be written as:

$$\int_\Omega \frac{\partial \phi}{\partial t} d\Omega = \frac{\phi_p^{t+\Delta t} - \phi_p^t}{\Delta t} \cdot \Omega_{cell} \tag{2.12}$$

Subscript "p" is referred to cell position, superscripts "t" and "t + Δt" to the different time instants considered.
Volumetric source term si discretized depending on the nature of the source. Assuming for simplicity a constant intensive source term σ, it has just to be multiplied by cell volume.

$$\int_\Omega \sigma d\Omega = \sigma \cdot \Omega_{cell} \tag{2.13}$$

When considering flux terms, just applying an Euler discretization scheme can be not enough. A different flux term must be evaluated for every face of P, hence different ϕ_i (ideally located in each face centre) need to be computed to perform convection term discretization.

$$\oint_{Surf} \phi U dS = \sum_i^{Nfaces} (\phi_i U * S_i) \tag{2.14}$$

A method to compute surface value ϕ_i must be defined. Central difference scheme is a second order method, easy to implement with high precision. If ϕ_N is referred to north cell and ϕ_n corresponds to face shared by cells P and N, applying central difference scheme ϕ_n is computed as in the equation (30)

$$\phi_n = f_x \cdot \phi_P + (1 - f_x) \cdot \phi_N \tag{2.15}$$

Where f_x is a value between 0 and 1 taking into account distances between cells centres and faces.

$$f_x = \frac{\overline{nN}}{\overline{PN}} \tag{2.16}$$

As it can be deduced by equations above, ϕ_n is not influenced by flow direction, hence it assumes the same value if the flow is oriented northward or southward. This can result in a problem when high velocity flows are considered, because the scheme is not able to recognise direction of the flow or even strength of convection relative to diffusion, leading to instability when Peclet number is high.

$$Pe = \frac{\rho u}{k/\delta x} \tag{2.17}$$

As described in the equation above, Peclet number is a measure of the relative strengths of convection and diffusion. To apply central difference scheme, Peclet number must be less than 2, and it is not the case when dealing with in-cylindrical simulations.
Therefore, Gauss linear upwind scheme has been used, since it is a stable second order scheme.

$$\phi_n = \phi_P + \lambda_{P-N}(\phi_S - \phi_P) \qquad if \;\; u \cdot n_n > 0 \tag{2.18}$$

$$\phi_n = \phi_N + \lambda_{N-NN}(\phi_{NN} - \phi_N) \qquad if \;\; u \cdot n_n < 0 \tag{2.19}$$

With "NN" cell northwards to north cell is indicated. λ considers distances between interested cells, so it is defined by faces and cells centroids position.

$$\lambda_{P-N} = \frac{x_n - x_P}{x_S - x_P} \quad or \quad \lambda_{N-NN} = \frac{x_n - x_N}{x_{NN} - x_N} \tag{2.20}$$

Using this approach, ϕ_n can assume different values depending if the flow is oriented to north direction or to south one. Transportiveness property is always guaranteed and scheme is hence stable. Discretization formula of the convection term finally results:

$$if \;\; u \cdot n_n > 0 \qquad \int_{N_{surf}} \phi U dS = (\phi_P + \lambda_{P-N}(\phi_S - \phi_P))(U * S_n) \tag{2.21}$$

$$if \;\; u \cdot n_n < 0 \qquad \int_{N_{surf}} \phi U dS = (\phi_N + \lambda_{N-NN}(\phi_{NN} - \phi_N))(U * S_n) \tag{2.22}$$

These formulae have to be applied for every direction.
Diffusion term is easier to be discretized, since ϕ gradients can be evaluated from different cells centre values.

$$\oint_{Surf} k \nabla \phi \cdot dS = \sum_{i}^{faces} (k \cdot \frac{\phi_i - \phi_P}{d} \cdot S_i) \tag{2.23}$$

With d as the distance between cell centres.
Applying different discretization schemes for every equation term, equations can be handled by a computational machine and then they can be solved.

Solving equations

After writing transport equations for every cell, a linear system is obtained:

$$[A][\phi] = [R] \tag{2.24}$$

Where [A] is the matrix coefficient, $[\phi]$ value of ϕ_p of every cell and [R] is the right hand side. [A] is potentially very big, since it is a square matrix of order NxN, where N is the number of the cells composing the CFD domain. Therefore inverting [A] matrix to solve the equation would be computationally expensive, even occupying a lot of memory, and it is not practically possible to have an exact solution of the system.
At contrary of directs methods, iterative procedures are not so computationally demanding, and they can be managed by a computational machine in a more reasonable time. It works by starting with a guessed solution to be improved during the procedure. Guessed solution is usually the one obtained when solving previous time step, and then a relative tolerance has been imposed to define convergency.

$$RelToll = \frac{\phi_{i,n+1} - \phi_{i,n}}{\phi_{i,n}} \tag{2.25}$$

With lowercase "n" indicating number of iterations performed. If this relative tolerance is less than a pre-chosen value (10^{-9} for pressure equation, 10^{-8} for all the others) equation is considered solved, and a solution very closed to the exact one is obtained.

Courant number

Courant number is a very important indicator for numerical convergence: it is defined as the ratio between fluid velocity and time step as numerator and mesh length as denominator.

$$Co = \frac{u\Delta t}{\Delta x} \tag{2.26}$$

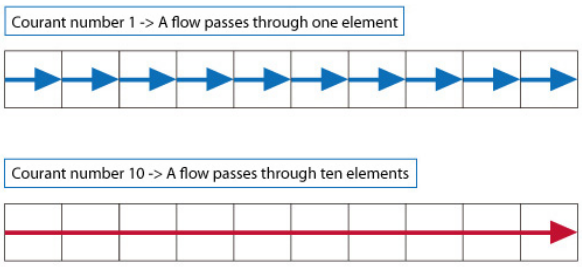

Figure 2.9: Courant number representation

This non-dimensional number is essential to define or correct time step before starting the simulation: on the numerator length covered by the fluid in one time step is represented. By a Lagrangian point of view, a Courant number equal to one means that every fluid particle runs through one mesh size. If Courant number is higher, space covered by a fluid particle is higher than a mesh size. If it happens, a fluid particle can bypass neighbouring cells, causing instability and divergence of the equations when bypassed cell is considered. Fluid velocity u can not be imposed a priori since it can be the result of previous iterations; mesh length Δx and time step Δt can be numerically imposed or modified, matching convergence criteria. The courser the mesh, the larger the time steps can be imposed, both actions decreasing computational time despite result accuracy; finer the mesh, lower time steps need to be imposed and then computational time can increase significantly. This numerical behavior must be considered even in mesh editing process.

Turbulence

Turbulence is a very complex phenomenon to be modelled, as far as it is both random and cahotic. It is made by highly unstable vortexes, called eddies.

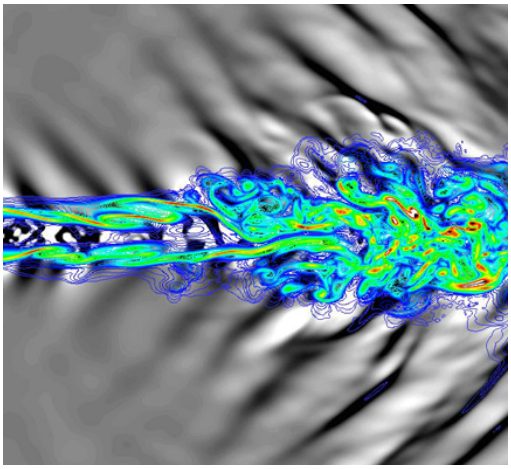

Figure 2.10: Turbulent field with eddies of different size

Eddies of different size have different characteristic velocities and timescales, as far as they tend to dissipate their own kinetic energy. Reynolds number, ratio between fluid inertia forces and viscous ones, is very important in CFD environment and its formulation can be applied also on different eddy sizes:

$$Re = \frac{ul}{\nu} \tag{2.27}$$

When Reynolds is 1 inertial forces are completely dissipated by viscous ones. This happens only if eddy considered is very small, having very few kinetic energy. Kolmogorov scale η is consequently defined, corresponding to smallest eddy present in the fluid, the one that has a Reynolds number equal to unity. For Kolmogorov scale eddies, they dissipate all the kinetic energy they have

with a consequent temperature increase.
Kolmogorov introduced the energy cascade concept, assuming that bigger eddies transfer their kinetic energy to smaller ones. This introduces the energy dissipation rate ε, a rate of energy transfer between different length scale eddies.

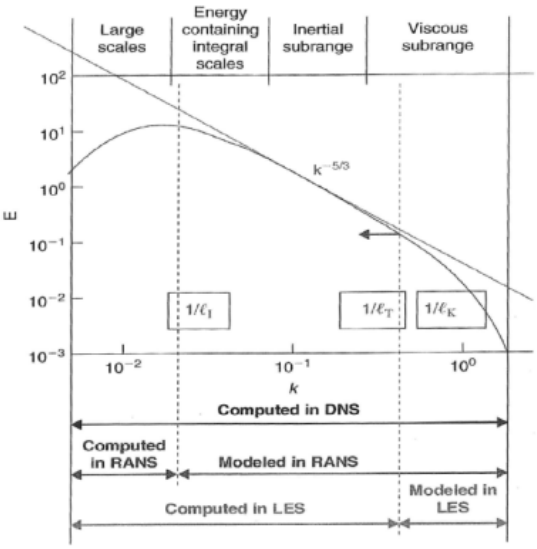

Figure 2.11: Energy cascade

Biggest eddy size is known as integral length, and it depends on environmental geometry. Figure above highlights that energy dissipation rate ε is related to eddy size, and how large scale eddies have much more energy than smaller scale ones. Solving a turbulence problem means solving length, time and velocity scales for each eddy, which is possible but extremely expensive in terms of computational time: DNS (direct numerical simulation) has hence the purpose to compute these scales eddy per eddy, but it is not used for industrial applications because of too huge computational and memory efforts required.
A turbulence model is able to compute turbulent kinetic energy region by region, but not to distinguish different eddies, and then neither their oscillatory behavior, but they present huge computational advantages with respect to direct numerical simulations. RANS approach (Reynolds Average Numerical Simulation) is hence the most used one for engineering design purposes, as far as it is the best compromise between accuracy and computational time available at the state of the art. There are a lot of RANS turbulence models implemented in OpenFOAM or in other CFD programs, but they are all based on defining a turbulent viscosity, function of turbulent kinetic energy and turbulent dissipation rate. Eddies velocity components are not axis per axis computed, then when RANS turbulence intensity is displayed in 3D mesh there is not any vortex representation, but just their kinetic energy predicted. LES (large eddy simulation) can be a very interesting solution for CFD, as far as it solves numerically just large eddies length scales (that have higher kinetic energy), while smaller ones are solved using a RANS approach. At the state of the art, LES is very interesting for fluid physical analysis, but in more complex scenarios such as

internal combustion engine combustion mode design it is prohibitive for commercial purposes.

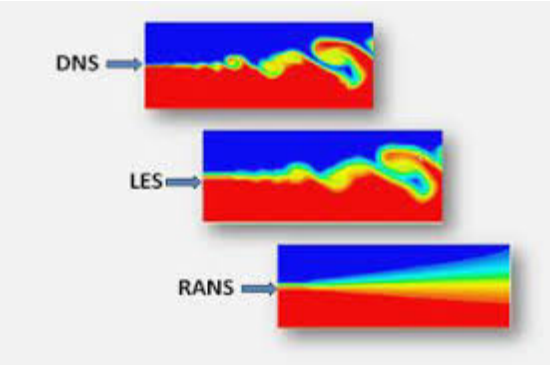

Figure 2.12: Numerical simulation differences

Looking at figure 56 it is possible to appreciate differences between a DNS or a LES simulation and a RANS one: in the two upwards, the vortex is well described, while in the last one just different kinetic energy values are predicted. Reynolds average concept needs hence to be introduced. If velocity over time is plotted, resulting chart is going to be the combination of two different contributions:

a stable velocity given by designed engine operation

a fluctuating term given by turbulence, which varies cycle per cycle

In the figure 57 displayed below, velocity is composed by an average value (0 in the case shown) and some fluctuations caused by turbulence presence. Big, intermediate and small eddies can hence be recognized looking at amplitudes and frequencies of velocity oscillations. In any case, fluctuation behavior is unpredictable because they can change velocity initial condition from cycle to cycle.

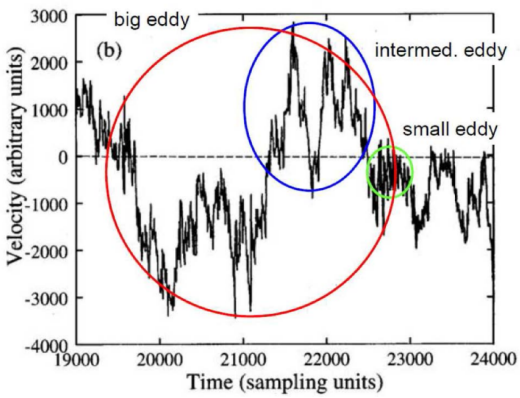

Figure 2.13: Reynolds average

By a mathematical formulation, this kind of analysis is not suitable just for velocities, but also for any specific quantity ϕ.

$$\phi = \overline{\phi} + \phi^{'} \tag{2.28}$$

where $\overline{\phi}$ is the average component and $\phi^{'}$ the fluctuating one. If average of the whole quantity ϕ is performed, what results is:

$$\overline{\phi} = \overline{\overline{\phi} + \phi^{'}} = \overline{\overline{\phi}} + \overline{\phi^{'}} = \overline{\phi} + 0 \tag{2.29}$$

While, as predictable, average quantity ($\overline{\phi}$) and average of its average ($\overline{\overline{\phi}}$) are the same value, $\overline{\phi^{'}}$ is null by a statistical point of view since there is no reason why fluctuations should always increase or decrease ϕ global value. Therefore, all quantities fluctuating average are considered null a priori.
In first appearance, change introduced by Reynolds average is just conceptual, but if two different quantities such as ϕ and ξ are multiplied (as it happens in convective flux term), what results is the following equation:

$$\overline{\phi * \xi} = \overline{(\overline{\phi} + \phi') * (\overline{\xi} + \xi')} = \overline{\overline{\phi} * \overline{\xi}} + \overline{\overline{\phi}\xi'} + \overline{\overline{\xi}\phi'} + \overline{\phi'\xi'} \tag{2.30}$$

$$\overline{\phi * \xi} = \overline{\phi} * \overline{\xi} + \overline{\phi'\xi'} \tag{2.31}$$

While average fluctuation terms are null if considered alone, when two of them are multiplied their influence can not be neglected. By a mathematical point of view, it is easier to understand if $\phi^{'}$ and $\xi^{'}$ had instant per instant the very same fluctuating component: if there is a positive contribution, multiplication result stays positive; if there is a negative contribution, multiplication result becomes positive. Hence there is a term adding in conservation equation, as far as both ϕ and U are composed by an averaged term and a fluctuating one. Conservation equation becomes:

$$\frac{\partial \overline{\phi}}{\partial t} + \nabla \cdot (\overline{\phi U}) = \nabla \cdot (k \nabla \overline{\phi}) + Q_V + \nabla \cdot Q_{surf} - \nabla \cdot (\overline{\phi' U'}) \tag{2.32}$$

Modelling turbulence in RANS approach is determining $\nabla \cdot (\overline{\phi' U'})$ value. From this point ahead, if fluctuated component is considered, apex is reported; if averaged quantity is considered, overline is not reported.

2.1 Solver description

In the first subsection, CFD principles and transport equations have been described, while in this one conservation equations as written in the solver are analysed. Source terms can be defined differently depending on solver engineering purpose, while time derivative, convection and diffusion terms are very similar. Combustion modelling in a CFD code is not as easy as other fluid dynamic quantities, hence it has been dealt in two subsections apart, one dedicated to spark ignition combustion, another one dedicated to spontaneous ignition combustion.

mass conservation equation

$$\frac{\partial \rho}{\partial t} + \nabla \cdot (\rho \vec{u}) = \dot{S}_{evap} \tag{2.33}$$

momentum equation

$$\frac{\partial \rho \vec{u}}{\partial t} + \nabla \cdot (\rho \vec{u} \vec{u}) = \rho g + \mu \Delta \vec{u} + \dot{S}_{turb} + \dot{S}_{U,spray} \tag{2.34}$$

mixture fraction equation

$$\frac{\partial \rho Z}{\partial t} + \nabla \cdot (\rho Z \vec{u}) - \nabla \cdot ((\mu + \frac{\mu_t}{Sc_t}) \cdot \nabla Z) = \dot{S}_Z \tag{2.35}$$

mixture fraction traces equation

$$\frac{\partial \rho Z_t}{\partial t} + \nabla \cdot (\rho Z_t \vec{u}) - \nabla \cdot (\mu + \frac{\mu_t}{Sc_t} \nabla Z_t) = \dot{S}_{Z_t} \tag{2.36}$$

These are the first equations to be solved. By the source term related to fuel evaporation ($\dot{S}_{evap}$) and the one to momentum exchange of liquid droplets ($\dot{S}_{U,spray}$), the solver can consider also spray injection and liquid fuel evaporation. In this case, since the engine is working with an already gaseous fuel and with no direct injection, these two mass and momentum source terms will be null. Since velocity is a vector, momentum equations to be solved in CFD simulation are three, one for each axis.
For what concerns turbulence source term $\dot{S}_{turb}$, the two equations κ-ε turbulence model has been used. It is based on Boussinesq's hypothesis, which assumes an analogy between Reynolds stress tensor (the one related to turbulence) and mean strain one.

$$\dot{S}_{turb,xy} = -\rho \overline{u'_x u'_y} = \mu_t \frac{\partial U}{\partial y} \tag{2.37}$$

Hence a turbulent viscosity μ_t is introduced and by determining this μ_t, momentum source term is derived. Turbulent viscosity is not function of any axial coordinate. Different RANS models use different equations to compute μ_t.
In k-ε one, turbulent viscosity is function of turbulent kinetic energy and turbulent dissipation rate.

$$\mu_t = \rho C_{\mu_t} \frac{k^2}{\varepsilon} \tag{2.38}$$

As reported, μ_t depends on both turbulent kinetic energy (κ) and its dissipation rate (ε). The solver is modelling all kinds of turbulence, from big eddies to small ones, and large eddy simulation (LES) is never applied. Therefore, the solver needs one equation for κ and one equation for ϵ to compute turbulent viscosity:

κ: turbulent kinetic energy equation

$$\frac{\partial \rho k}{\partial t} + \nabla \cdot (\rho \vec{u} k) = \nabla \cdot (\mu + \frac{\mu_t}{\sigma_k} \nabla k) + \rho \varepsilon + 2 \mu_t S_{ij} S_{ij} \tag{2.39}$$

ε: turbulent kinetic energy dissipation rate equation

$$\frac{\partial \rho \varepsilon}{\partial t} + \nabla \cdot (\rho \vec{u} \varepsilon) = \nabla \cdot [(\mu + \frac{\mu_t}{\sigma \varepsilon}) \nabla \varepsilon] + \frac{\varepsilon}{k} (C_{\varepsilon 1} P_k + C_{\varepsilon 2} \rho \varepsilon) \tag{2.40}$$

costants such as $C_{\varepsilon 1}$, $C_{\varepsilon 2}$ and P_k are calibrated on the specific application

About turbulent kinetic energy equation, the last term is equal to laminar kinetic energy destruction term, but opposite in terms of sign; this means that if an increasing of turbulent kinetic energy is wanted, fluid laminar kinetic energy (K) must be destroyed. This is going to have some relevance in the end of this work.
This kind of model is one of the most used in literature because it is both reliable and stable for many kinds of fluid motion, and also not requiring huge computational time with respect to others available at the moment.
After solving combustion equations (which are described in a separated subsection), there is a composition change of species inside the cylinder because of chemical reaction associated to combustion. Hence, two enthalpy equations are solved, one for global enthalpy h, the other one for unburnt gasses enthalpy h_u:

enthalpy conservation equation

$$\frac{\partial \rho h}{\partial t} + \nabla \cdot (\rho \vec{u} h) = \nabla^2 \alpha_{eff} h + \frac{Dp}{Dt} + \dot{S}_{spray} \tag{2.42}$$

unburned enthalpy conservation equation

$$\frac{\partial \rho h_u}{\partial t} + \nabla \cdot \rho(\vec{u} h_u) = \nabla^2 \alpha_{eff} h_u + \frac{\rho}{\rho_u}\frac{Dp}{Dt} + \frac{\rho}{\rho_u}\dot{S}_{h_u,evap} \tag{2.43}$$

From these two equations, bunt and unburnt temperatures are derived. So also energy equilibrium is reached and time step solver algorithm ends here.

2.2 Combustion modelling

As commonly done by CFD researchers, combustion chamber gasses are distinguished into burnt gasses and unburnt gasses, so by a computational point of view there will be the "burnt" and "unburnt" temperature as well as the "burnt" and "unburnt" enthalpy.

burnt gasses: T_b and h_b
unburnt gasses: T_u and h_u
global quantities: T and h

With global quantities as the weighted average of the previous two. Modelling combustion results in a quite difficult computational aspect, since a lot of reactions are involved. Methane combustion can be summarized in the following chemical reaction:

$$CH_4 + 2O_2 -> 2H_2O + CO_2 \tag{2.44}$$

But these reported above are just the global reactants and products of the reaction itself. Considering very low time steps, reactions involved are many (of the order of magnitude of hundreds or thousands), and hence impossible to be modelled in acceptable computational time nowadays.
In the introduction section, a global combustion reaction velocity and an autoignition delay were introduced using Arrhenius correlation, which was a practical value taking into account chemical reaction kinetics without model it. In CFD solver, a progress variable has been introduced, indicating (as suggested by the name) the progress of combustion process. Therefore, a variable c has been defined such that:

if combustion has not already taken place, *c = 0*

if combustion is fully completed, *c = 1*

$$0 \xrightarrow{c} 1$$

It is defined in such a way to have a monotonous trend as reactions proceed. Progress variable must be connected to a physical quantity that is monotonic with combustion progress, assuming a minimum value before combustion starts, and having its maximum when combustion is fully completed. Therefore, choices available are the following:

- species formation enthalpy at a reference temperature of 298 K

- sensible enthalpy of the mixture *h = f(T, t)*

- linear combination of fuel mass fraction

Species formation enthalpy is the chosen one for this thesis work. Enthalpy values are not in the range [0;1] as progress variable has been defined, hence c has been normalized ($c_{normalized}$) in the following way:

$$c_{normalized} = \frac{h - h_{min}}{h_{max} - h_{min}} \tag{2.45}$$

Using equation 60, progress variable becomes both monotonous and in range [0;1].
CFD system is a 5-species system formed by fuel, O_2, CO_2, H_2O and N_2: the increasing of the progress variable is associated to an increasing of combustion products, so CO_2 and H_2O.
In the end, progress variable c has both a chemical and a fluid dynamic meaning, because it is an indicator of reaction progress and of heat released by combustion itself at the same time (once enthalpy balance has been performed), and it is also a way to impose consistency between these two aspects.
Since two kinds of combustion are present, the solver needs two different progress variables to establish the ongoing of both processes. Therefore, the solver defines a priori:

c as an indicator of spark-ignition combustion

c_{fresh} as an indicator of compression ignition combustion

This solver algorithm gives the possibility to model them in a completely different way without generating inconsistencies or superpositions between the two.

2.3 Spark ignition combustion

Spark ignition combustion is modelled through the 2-equations Weller combustion model.

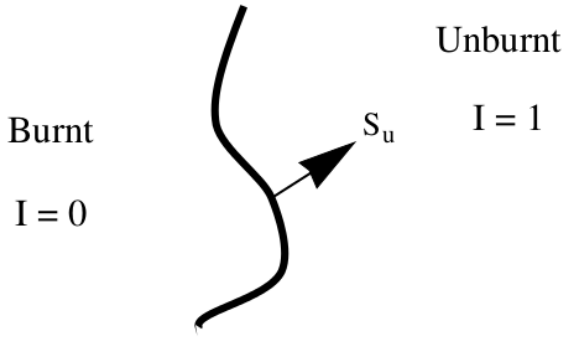

Figure 2.14: Flame interface

As described by the image above, there is a clear flame interface dividing burnt gas region and unburnt one: in the burnt gas region the progress variable is equal to 1; in the unburnt gas region the progress variable is equal to 0. In the end, the flame represents chemical reactions associated to combustion, but in this way it is just the flame to be modelled, not chemical reactions themselves. To have numerical and computational advantages, equations are written respect to a regress variable b:

$$b = 1 - c_{Normalized} \tag{2.46}$$

$$\nabla b = -\nabla c_{Normalized} \tag{2.47}$$

Another quantity to be introduced is the wrinkle factor Ξ, which in Weller's work has been derived by the ratio of the flame area per unit volume (A_f) and the flame area per unit volume projected into the mean propagation direction (A_s). Starting with this first definition, the wrinkle factor can be reconducted to the ratio of turbulent (S_{turb}) and laminar ($S_{laminar}$) flame velocities, as it has been shown in ["The Development of a New Flame Area Combustion Model Using Conditional Averaging", published by H.G. Weller in 1993]:

$$\Xi = \frac{A_f}{A_s} = \frac{S_{turbulent}}{S_{laminar}} \tag{2.48}$$

Indicating with S the corresponding flame velocity.
In flame propagation combustion, turbulent flame velocity is much higher with respect to laminar one, meaning having high Ξ values is something improving combustion process.
Through mathematical analysis, two equations are derived:

$$\frac{\partial \rho b}{\partial t} + \nabla \cdot (\rho \vec{u} b) - \nabla \cdot (\mu_t \nabla b) = \rho \vec{u} S_u \Xi |\nabla b| \tag{2.49}$$

$$\frac{\partial \Xi}{\partial t} + U_s \nabla \Xi + D_\Xi = G + \Xi \hat{n} \nabla U_t \hat{n} - \frac{1}{\Xi} \hat{n} \nabla U_t \hat{n} + \Xi (U_t - U_s) \frac{\nabla |\nabla b|}{|\nabla b|} \tag{2.50}$$

In this two equation model, two important things must be highlighted: first, the source term of the regress variable is proportional to flame velocity $\overline{S_I}\Xi$, meaning that the flame propagation is the source of the chemical reaction and heat released associated to combustion; second, the flame velocity is computed

in every iteration and in every cell, hence varying region by region.
This way spark ignition combustion is fully modeled, and solver *betaFlameletXiEngineDyMFoam* is entirely described. To consider mixture autoignition, chemical reaction model must be added to the solver, having hence the *betaFlameletSACIXiEngineDyMFoam* solver.

2.4 Spontaneous combustion

To model autoignition, no flame must be considered. While spark ignition progress variable c is fully depending on flame propagation, the introduced progress variable c_{fresh} is representing chemical oxidation of fuel particles. In homogenous mixture context, this kind of combustion is going to be very rough and violent, since chemical activity of the fresh mixture is almost homogenous. As before, the progress variable c_{fresh} is the formation enthalpy of the chemical species at reference temperature of 298 K; but this kind of progress variable acts only on fresh mixture, so regions not already reached by the flame (not burnt regions). The fresh progress variable equation is the following one:

$$\frac{\partial \rho c_{fresh}}{\partial t} + \nabla \cdot (\rho \vec{u} c_{fresh}) + \mu \nabla c_{fresh} = \rho \dot{c}_{fresh} \cdot b \tag{2.51}$$

This kind of equation presents on the left side time-derivative, convection and diffusion term as every conservation equation; on the right side the source term related of progress variable increasing, composed by:

a term proportional to chemical reactions velocity ($\dot{c}_{fresh}$)

a term connecting spark ignition combustion to spontaneous one (b)

Term b is added to c_{fresh} source term equation because burnt mixture (having b = 0) has already reacted, and it can not give any further heat release contribution.
The solver needs to have velocity of chemical reactions of the fuel-air mixture. This chemical reaction is depending on both fluid dynamics quantities such as pressure, temperature and mixture fraction of every cell, but also on chemical reaction mechanism of the fuel itself. As anticipated, even considering a fuel composed just by one kind of hydrocarbon (methane for instance) to solve the whole chain reaction is too heavy in computational terms. This is the reason why for this equation, another open-source software has been used: Cantera®. This software allows to build a pre-made chemical kinetics table before the simulation, which, once pressures, temperatures and mixture fractions are given as inputs, it can return source term $\dot{c}_{fresh}$ as an output.

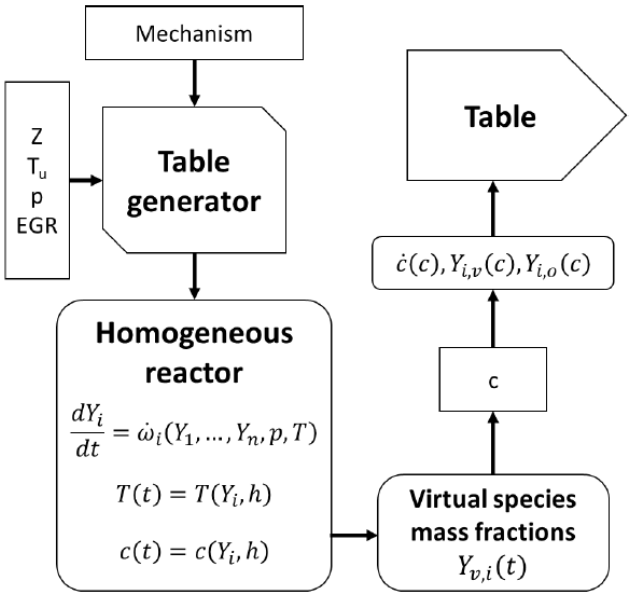

Figure 2.15: Chemical table algorithm description

As shown by figure 59, a set of multiple pressures, temperatures, mixture fractions and EGR are considered in table generation phase.

$$N_{PSRtable} = n_{EGR} * n_p * n_{T_u} * n_Z \tag{2.52}$$

Of course meaningful ranges need to be defined. Equation (67) shows how considering very wide ranges of pressures or temperatures can affect size of the table, hence time needed for generation. PSR stands for perfectly stirred reactor, as far as homogeneous mixture is considered. What is important is defining correctly mixture fraction, pressures and temperature ranges, while EGR are not considered in this analysis.
Pressures are going to assume a very wide range since flame propagation combustion is going to give a significant contribution before spontaneous ignition can occur. Therefore, pressure maximum considered is 180 bar, as it has been assumed maximum engine pressure. Unburnt fresh temperature range is also going to be wide since temperature gradient caused by spark ignition combustion is going to influence unburnt fresh temperature, and so 1400 K is considered as maximum temperature. It is almost unrealistic to assume presence of such high temperature values in volumes not already reached by combustion but applying a very wide range is just compromising table generation computational time, while choosing a too small range can compromise quality of results obtained. In the end, mixture fraction considered goes from very lean ones (Z = 0.1) to stoichiometric one (Z = 1), and no rich mixture condition is tabulated.
System is composed by five different species by a numerical point of view: CO_2, H_2O, N_2, O_2 and fuel. To compute molar fractions, atoms conservation equation

and absolute mixture enthalpy equations are imposed.

$$\begin{cases} \sum_{i=1}^{nvs} x_{v,i} n_{C,i} = \sum_{i=1}^{ns} x_i n_{C,i} \\ \sum_{i=1}^{nvs} x_{v,i} n_{H,i} = \sum_{i=1}^{ns} x_i n_{H,i} \\ \sum_{i=1}^{nvs} x_{v,i} n_{O,i} = \sum_{i=1}^{ns} x_i n_{O,i} \\ \sum_{i=1}^{nvs} x_{v,i} n_{N,i} = \sum_{i=1}^{ns} x_i n_{N,i} \\ \sum_{i=1}^{nvs} x_{v,i} w_i H_i(T,p) = \sum_{i=1}^{ns} x_i w_i H_i(T,p) \end{cases} \tag{2.53}$$

Adopting virtual species composition is an approach able to significantly reduce memory demanded for table generation. Code organization is well described by the following flow diagram.

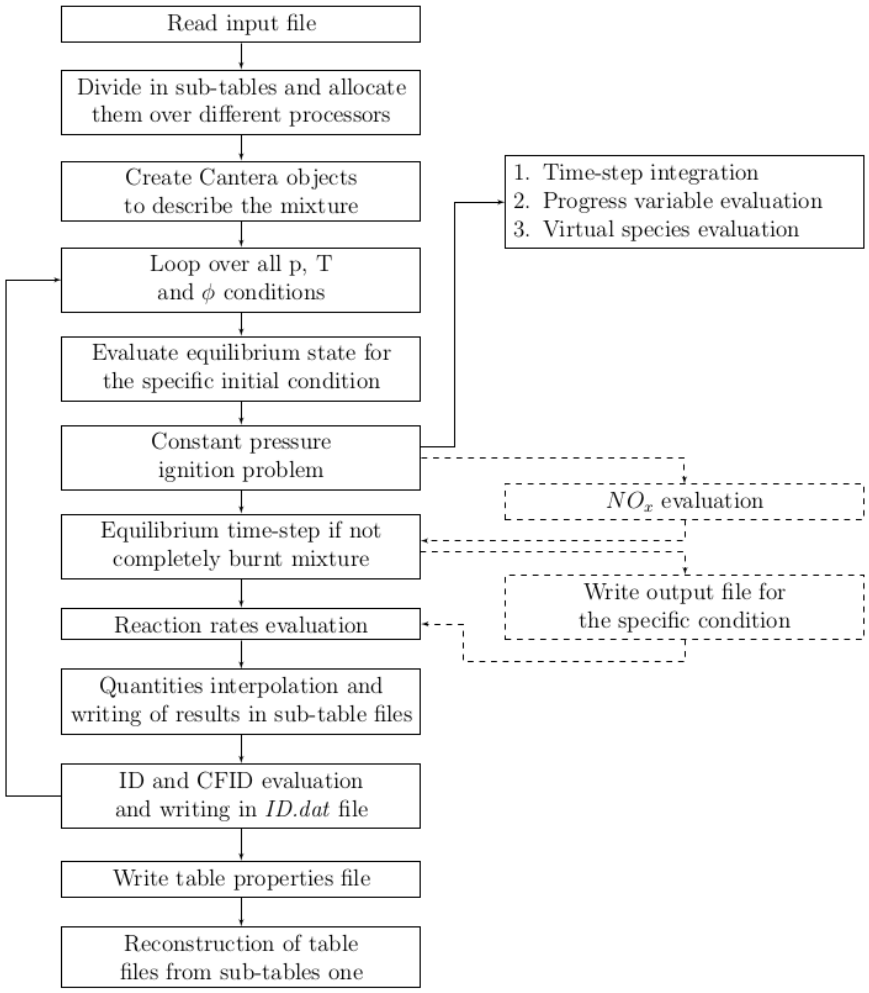

Figure 2.16: Table generation code organization

As figure 60 shows, in code implementation there is also the possibility to evaluate nitrogen oxides emission, but they are not included as far as NOx

transport equation is not available. End time values is a vector providing time at which integration is stopped, in case combustion does not complete for considered pressure, temperature and mixture fraction values, and it presents when chemical reaction reaches asymptotical equilibrium.
When dealing with CFD simulation integration, what is important is $\dot{c_{fresh}}$ resulting by fluid dynamics cell conditions and what kind of species (combination of C, N, O and H) are generated by combustion presence. In this case, pressure, temperature and mixture fractions are input, and what has solver as an output is pvS, the progress variable rise.

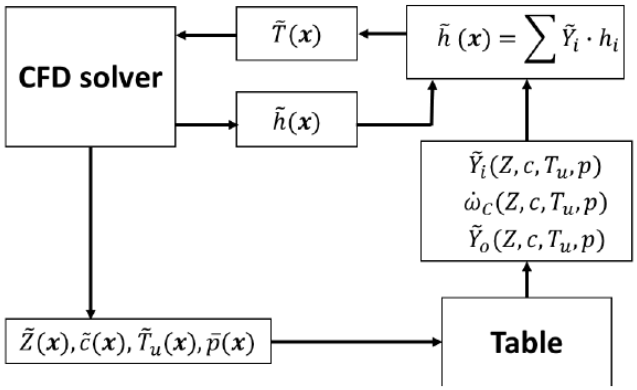

Figure 2.17: Table-solver interaction

$$pvS = f(p, Tu_{fresh}, Z) = \dot{c}_{fresh} \tag{2.54}$$

Figure 62 shows how table and code interact between each other. In this compression ignition analysis, a multiplicity of fuels is considered, hence a different kinetics table is generated for every fuel. If equivalence values range is correctly defined, tables do not need to be changed if lean and stoichiometric mixture engines (running with the same fuel) are compared.

Chapter 3

Spark ignition combustion

In this section, a compressed natural gas fuelled engine for heavy duty application (CNG-heavy duty) is analysed. Geometry of combustion chamber is entirely known, and mesh is already generated. Some real engine working points are known in terms of pressure, gross indicated work, heat release and wall heat transfer, hence what is performed is a solver parameters tuning so that solver itself can represent experimental working point as precisely as possible, then an optimization of these working points in the engine map has been performed.

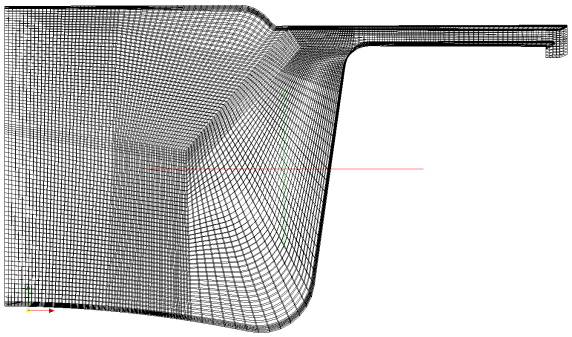

Figure 3.1: CNG-heavy duty engine at top dead centre

In figure 62 the given mesh is displayed: it is a hybrid grid, made up by blocks of structured mesh in the whole combustion chamber. Just one cylinder of the whole engine is simulated, and no valve motion is both modeled or considered. Central spark plug is installed, and in the mesh it is represented at the point of intersection between the revolve axis and the cylinder head. Walls represented in the mesh are three: head (at the top of the mesh), piston (at the bottom of the mesh) and liner (lateral part of the cylinder, drawn rightwards). Cylinder walls are also characterized by a higher mesh density with respect to the rest of the volume, to represent correctly boundary layers, which have a very important part in determining heat transfer losses. Leftwards, cylinder axis with respect to symmetry is imposed. The whole volume at cylinder top dead centre is represented by Figure 64.

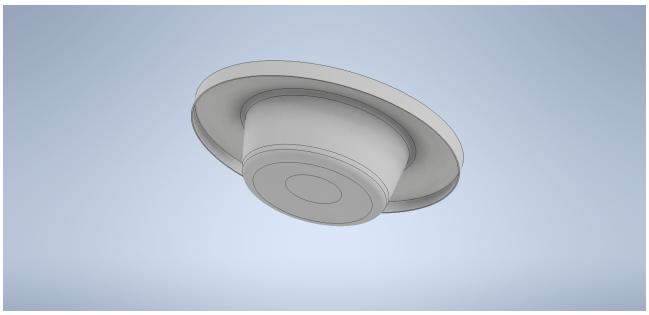

Figure 3.2: Whole cylinder volume

stroke	0.135 m	swirlRPMratio	1.5
bore	0.15 m	swirlAxis	(0 0 1)
conRodLength	0.230	swirlProfile	10^{-5}
IVC	-175°	uprimeUpRatio	0.7
EVO	124°	lintBoreRatio	0.017

Table 3.1: CNG-heavy duty main geometrical parameters

Mesh motion is performed by adding or removing mesh layers depending on piston position, hence number of cells varies hugely between top dead centre (TDC) and bottom dead centre (BDC). At top dead centre (where number of mesh cells is minimum), cells are 8659, almost all of them hexahedral. OpenFOAM is a 3D simulation solver, so cells must be defined in all three axial directions: to not solve equations on y-axis, just 1 cell is present along that direction, in order to have no specific quantity flow along that axis. Mesh has been generated to take into account fuel injection, and this is the reason why there is such a different orientation of some cells in proximity of revolve axis; average orthogonal quality is 15.08, which is not compromising simulation results. In internal combustion engines flow preferential direction can change a lot because off turbulence and/or pressure gradients introduced by combustion. Maximum aspect ratio is 14.0, and maximum skewness is 3.3897.
The whole domain is not big, as far as it is just a cylinder with 0.135 m of bore; cell areas are hence very small (minimum one is $2.0 \cdot 10^{-10}$) and solving conservation equations does not require a lot of iterations to reach tolerance imposed. Time steps are defined in engine time (crank angle) and three different values are used:

$\Delta\theta = 0.125°$ between -175° and -30°

$\Delta\theta = 0.005°$ between -30° and 40°

$\Delta\theta = 0.025°$ between 40° and 124°

These $\Delta\theta$ values lead to have 18526 different time steps between intake valve closing (IVC) and exhaust valve opening (EVO), with a lot of computational time demanded; this is necessary to have acceptable Courant numbers, because if wider time steps are imposed, simulation numerically diverges. Simulation

duration is in the order of magnitude of 6 hours per processor, but it can vary significantly on computer used.
Since it is a half cycle computation (including just one compression and expansion stroke), turbulence must be set a priori: swirl axis (0 0 1) coincides with cylinder one, while its intensity can be changed increasing or decreasing swirlRPMratio value. "uprimeUpRatio" and "lintBoreRatio" are there to define turbulence intensity and its dissipation rate, as illustrated in the table at the top of the page.

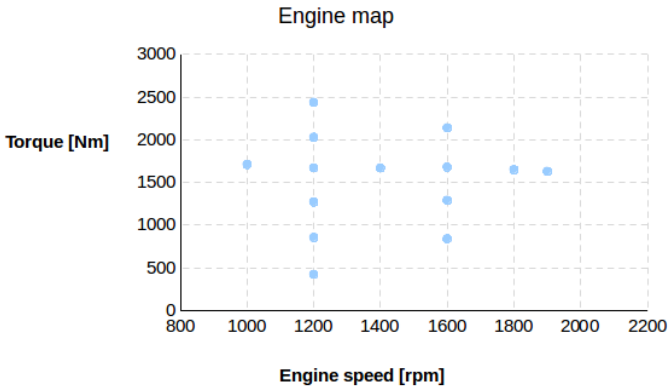

Figure 3.3: Engine map of given experimental points

In figure 64 engine map is showing all different experimental points available. Starting from reliable experimental data is very important to verify CFD solver validity. Cylinder mixture pressure and temperature and cylinder walls temperatures as well are known for each simulation starting point (-175°).
In the engine map, two constant regime sweeps (at 1200 rpm and 1600 rpm) and one constant torque one at 1650 Nm are displayed. Maximum IVC working pressure is 2.44 bar, corresponding to 1200 rpm full load condition, and it is the maximum torque working point experimentally available. Most known regime is 1200 rpm, where six distributed points from 17% load (0.58 bar at IVC) to 100% load (2.44 bar at IVC) are given. Constant torque sweep is also composed by six different points from 1000 rpm to 1900 rpm.
The very first target is to reproduce this experimental working points in a CFD context, so simulations are set with the parameters illustrated in the tables below.

	1200-421	1200-855	1200-1270	1200-2030	1200-2440
Spark time	-24°	-20°	-14°	-9°	-6°
IVC pressure	0.587 bar	0.958 bar	1.32 bar	2.02 bar	2.46 bar
IVC temperature	363 K	360 K	361 K	362 K	362 K
T_{wall} head	447 K	480 K	499 K	523 K	532 K
T_{wall} liner	393 K	405 K	413 K	428 K	435 K
T_{wall} piston	483 K	527 K	551 K	581 K	591 K

	1000-1710	1200-1670	1400-1670	1600-1680	1800-1650
Spark time	-9.75°	-11°	-12°	-13°	-14°
IVC pressure	1.72 bar	1.72 bar	1.73 bar	1.77 bar	1.77 bar
IVC temperature	358 K	362 K	364 K	368 K	372 K
T_{wall} head	508 K	510 K	523 K	533 K	540 K
T_{wall} liner	420 K	420 K	424 K	427 K	430 K
T_{wall} piston	570 K	563 K	572 K	578 K	580 K

	1600-839	1600-1290	1600-2140	1900-1630
Spark time	-16	-14	-11	-15
IVC pressure	0.982 bar	1.37 bar	2.21 bar	1.75 bar
IVC temperature	371 K	368 K	369 K	375 K
T_{wall} head	481 K	513 K	555 K	550 K
T_{wall} liner	407 K	418 K	437 K	432 K
T_{wall} piston	518 K	556 K	602 K	589 K

Table 3.2: Initial available pressure, temperatures and spark timing for every experimental working point represented in CFD map

Working points name is derived by the combination of engine speed and torque: for instance, 1000-1710 means 1710 Nm of torque at 1000 rpm.
A spark ignition solver validation needs to be performed, in order to verify that it is able to reproduce correctly flame propagation combustion, both in terms of flame velocity and heat release. Spark plug strength is kept constant (value of 3), while its energy release duration is kept fixed at 1.25 ms, but changing in terms of engine time. To control spark ignition combustion flame velocity, Ξ_{coeff} equilibrium coefficient has been modified.

$$\Xi = 1 + \Xi_{coeff}\sqrt{\frac{u'}{S_u}}R_\eta \tag{3.1}$$

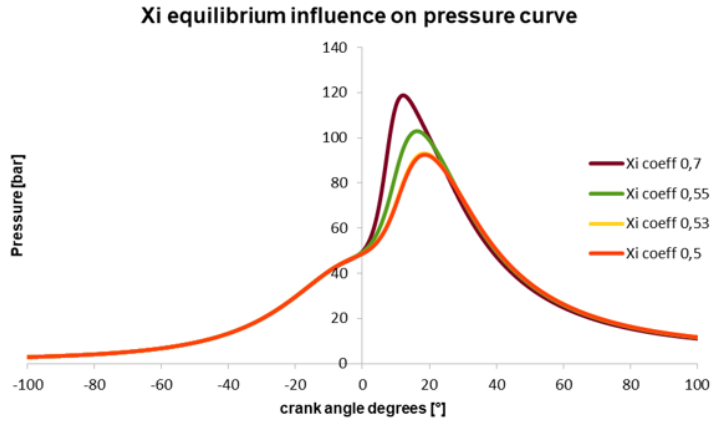

Figure 3.4: Xi equilibrium sweep

The higher Ξ_{coeff}, the higher flame velocity is going to be. By the expression above, it is possible to appreciate also turbulence influence in increasing flame combustion velocity. In figure 65 reported below pressure curves in function of Ξ_{coeff} are represented: with no spark plug energy release modification, both pressure maximum values and pressure underlying areas change a lot, having important effects on gross indicated work. Defining the correct coefficient is essential for having a good solver accuracy result. In figure 65, range considered for Ξ_{coeff} is 0.5 to 0.7. Lowest regime point (1000-1710) has been chosen for a first Ξ_{coeff} validation, resulting that value of 0.5 is the one best fitting experimental results, as shown by both figures 66 and 69. To perform this kind of analysis, fuel chosen is a natural gas composed by 100% of methane. Varying natural gas used as a fuel can lead to significant changes for what regards autoignition, but flame properties are very similar.

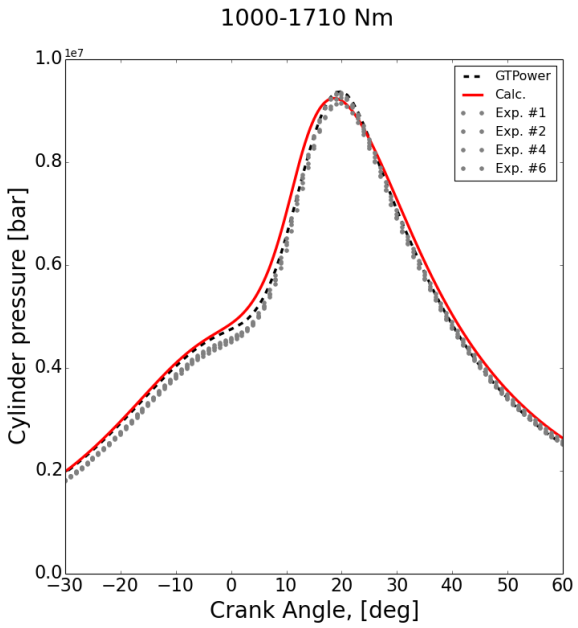

Figure 3.5: 1000-1710 validation: pressure curve comparison

Two pressure curves plotted in figure 66 are very close and similar between each other. If focus is pointed on differences, simulated pressure curve has a lower ignition delay with respect to experimental one, detaching a little bit too early from motored curve behavior. Combustion velocity is well represented since in combustion development phase the curves are almost parallel. Pressure maximum values are very similar, but in computed curve it is slightly anticipated. In the second part of expansion phase (once combustion is completed) simulated curve is slightly above the experimental one.

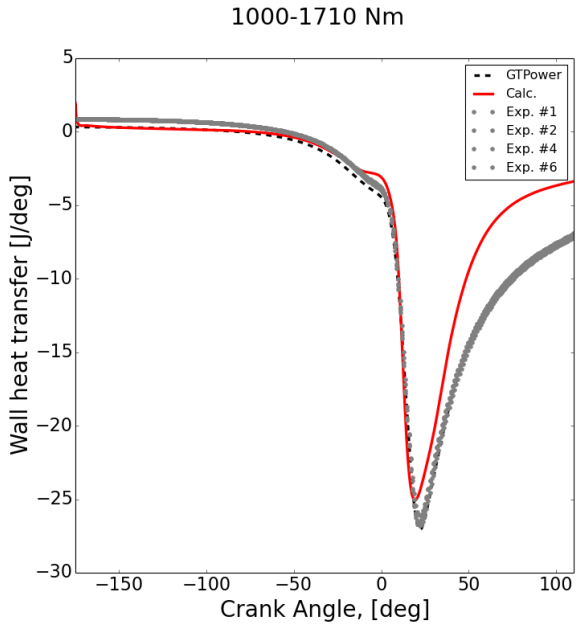

Figure 3.6: 1000-1710 validation: wall heat transfer comparison

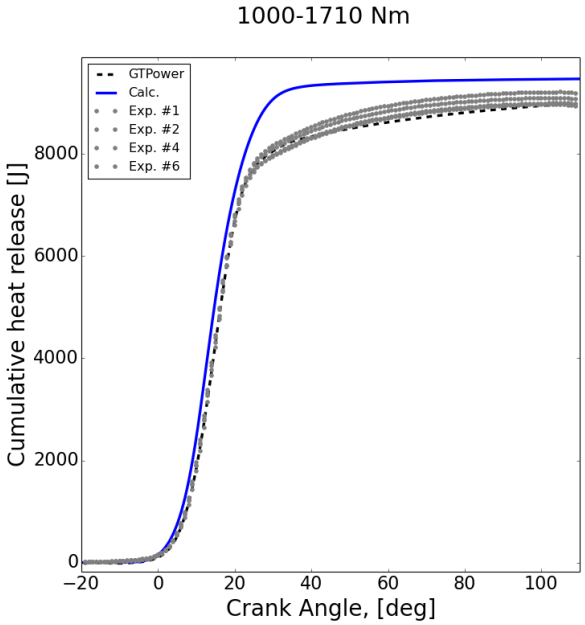

Figure 3.7: 1000-1710 validation: cumulative heat release comparison between simulated and experimental data

As shown in figure 67, wall heat transfer curve is not as well reproduced as the pressure one. In compression stroke, wall heat transfer has very low values, hence also absolute errors are low. When combustion is taking place, wall heat transfer increases in an appreciable way since curves get closer. Minimum of curves are comparable, with simulated one slightly anticipated and higher in terms of magnitude, but when combustion is completed and burnt mixture is expanded, computed values are highly overestimated with respect to experimental ones, contributing in the slight pressure overestimation of the final part of expansion stroke.

In figure 68 cumulative heat release curves are compared. X-axis scale is different with respect to previous figures, since there is no reason to plot heat release curve where combustion is not occurring. The lower ignition delay can be detected also in this chart, as far as simulated cumulative heat release curve detaches earlier from 0 value with respect to experimental one. During combustion process, slopes of the two plotted curves are very similar, indicating that combustion velocity is well represented in CFD environment; in any case, maximum values are different, and at the end of the half cycle fuel-air mixture heat release is overestimated.

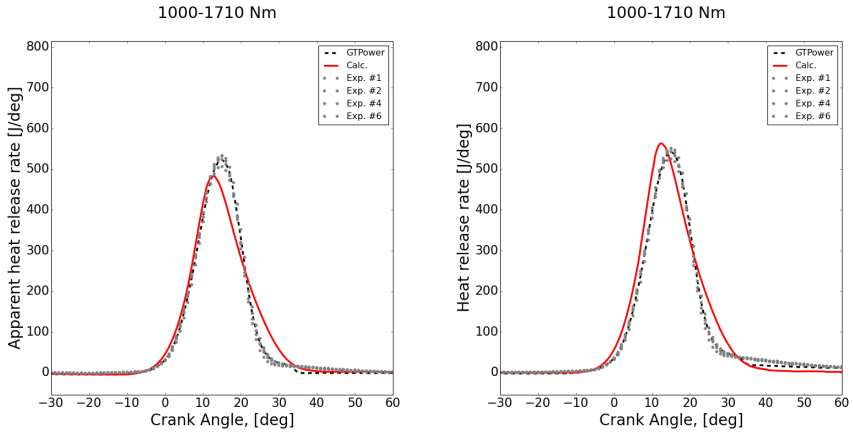

Figure 3.8: 1000-1710 validation: apparent and rate of heat release comparison between simulated and experimental data

From figure 69 it is possible to perform a comparison of both apparent and rate of heat release, plotted over engine time. In both cases, curves rise from 0 value is anticipated because of a lower ignition delay, but then behaviors are very similar up to curves maximum values. In apparent heat release rate, maximum is underestimated, while in rate of heat release maximum is slightly overestimated, but in both cases they are anticipated with respect to experimental ones. After the maximum values are reached, simulated curves are less inclined with respect to experimental values, increasing curves underlying area, hence cumulative heat release.
Using a python post-processing script, main differences between simulated engine case and experimental data have been summarized in the table below. As suggested by already illustrated figures, main differences are about cumulative wall heat transfer values, which is overestimated of more than 25%. More im-

portant data such as gross indicated work, pressure maximum value and its engine time location are very similar. In table 3.3 main computed parameters such as gross indicated work (giw) and maximum pressure timing are compared to the experimental data available.

	giw	heat released	heat transfer	P_{max}	θ @ P_{max}
computed	3512 J	9471 J	-1141 J	92.38 bar	19°
experimental	3333 J	8994 J	-1567 J	97.7 bar	20°
error	5.38%	5.03%	-27.2%	-1.41%	-1.0°

Table 3.3: Comparison between computed and experimental data

This procedure has been repeated also for all other engine experimental working points available. To report all pressure, wall heat transfer and the three heat release curves comparison would be too repetitive, so two different critical points have been chosen: 1200-855 because of the low load, and 1800-1650 because of the high regime.

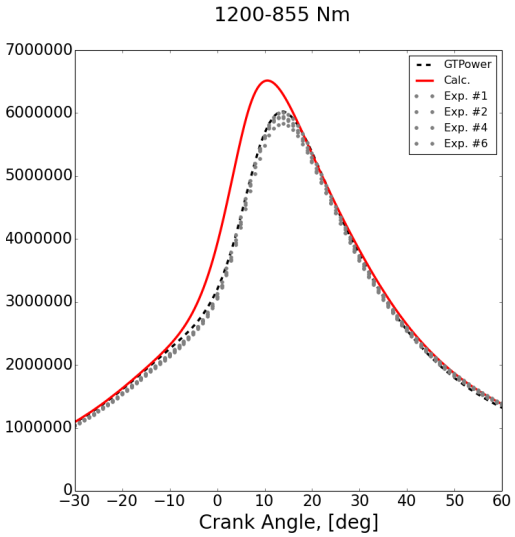

Figure 3.9: 1200-855 validation: pressure curve comparison

Figure 70 displays pressure curve comparison at low load (35%) and 1200 rpm engine speed. With respect to previous pressure curve comparison in figure 66, here differences between values are more evident. Spark timing of this engine working point is -20° (as illustrated by the table), much more anticipated with respect to previous case; hence here ignition delay reduction is having more influence, and simulated pressure curve reaches a higher maximum value and it is also anticipated of few degrees. In any case, shape of both simulated and experimental curves are very similar between each others, suggesting that delaying spark plug energy release more similar curves can be obtained.

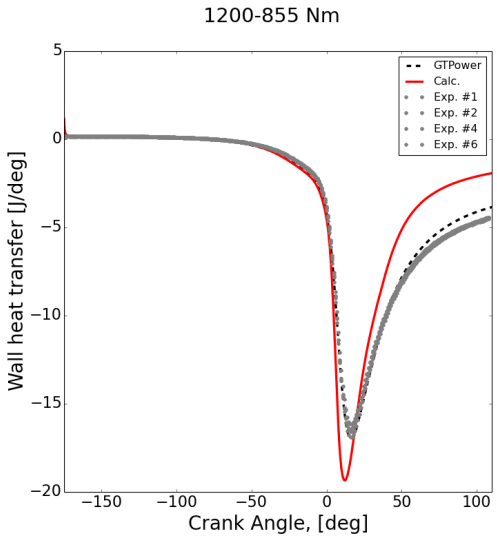

Figure 3.10: 1000x1710 validation: wall heat transfer comparison

In figure 71 wall heat transfer curves are compared. In this case, simulated and experimental values get more similar with respect to 1000-1710 working point case, as far as curves are coincident during combustion development, but after global minimum simulated wall heat transfer behavior is consistent with the previous working point. In this case, wall heat transfer minimum is underestimated, and its timing is getting closer with respect to experimental one. When combustion is almost completed, computed curve returns to be overestimated, but if compared with previous working point cumulative wall heat transfer difference decreases, especially in relative terms.

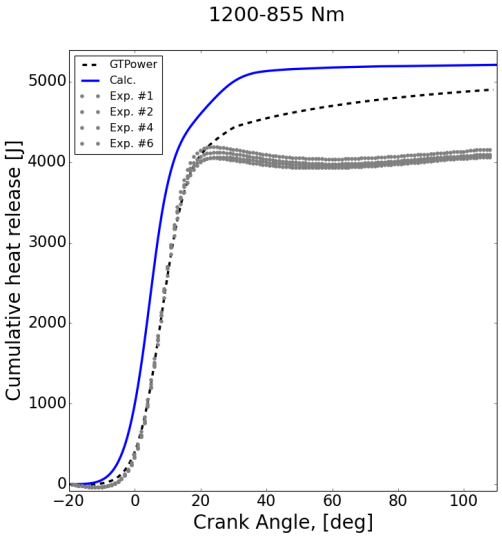

Figure 3.11: 1200-855 validation: cumulative heat release comparison

As figure 72 illustrates, differences when cumulative heat release are compared gets huge. Ignition delay underestimation plays a very important role, as far as simulated and experimental curves are clearly detached. Maximum cumulative heat release is overestimated. Cumulative heat release slopes in combustion development are very similar, suggesting once again to delay mixture ignition to get a better matching.

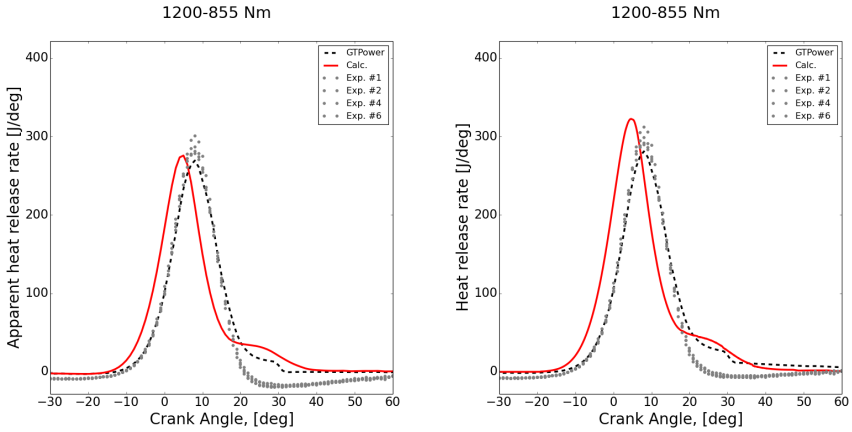

Figure 3.12: 1200-855 validation: apparent and rate of heat release comparison

In the end, figure 73 confirms what has already been described. Shape of both heat release curves are very close, with both computed and experimental curves presenting a similar rate of heat release maximum value. Their timing is significantly anticipated, resulting in a too early combustion with respect to what results from experiments.

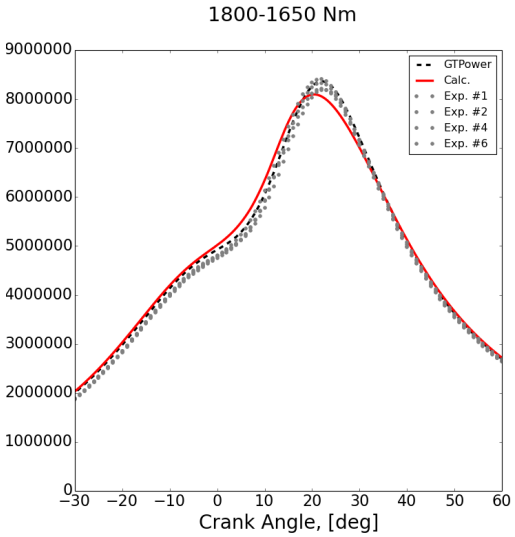

Figure 3.13: 1800-1650 validation: pressure curve comparison

Considering both figure 74 and figure 66, 1000-1710 and 1800-1650 working point validation can be compared. In this high regime working point, pressure curves are very similar. There is also in this case an ignition delay reduction but having no significant effect in combustion developing phase. Simulated pressure curve maximum value is slightly both lower and anticipated, suggesting to delay mixture ignition for correcting maximum timing, but this kind of action would reduce its absolute value. In any case, curve underlying areas are very similar, since pressure gain present in computed curve in ignition phase is balanced by a lower pressure maximum value reached.

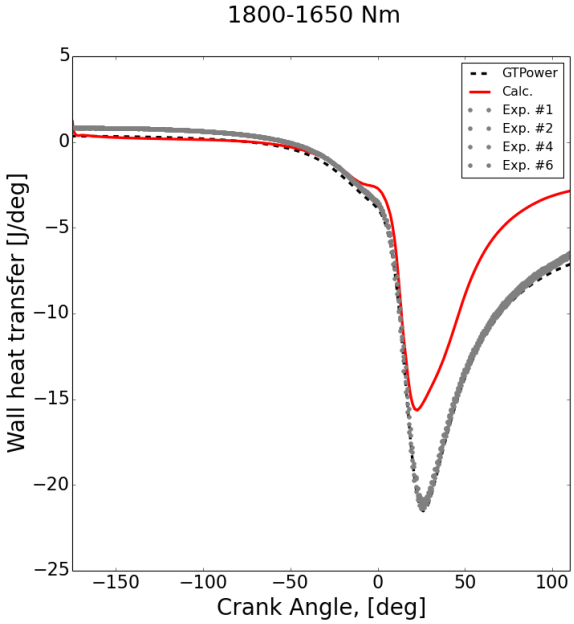

Figure 3.14: 1800-1650 validation: wall heat transfer comparison

In this case, as shown in figure 75, wall heat transfer values are very different between the plotted curves. From top dead centre ahead, wall heat transfer curve is underestimated in every crank angle value, resulting in a cumulative wall heat transfer much higher with respect to experimental one. Also, wall heat transfer minimum timing is underestimated.

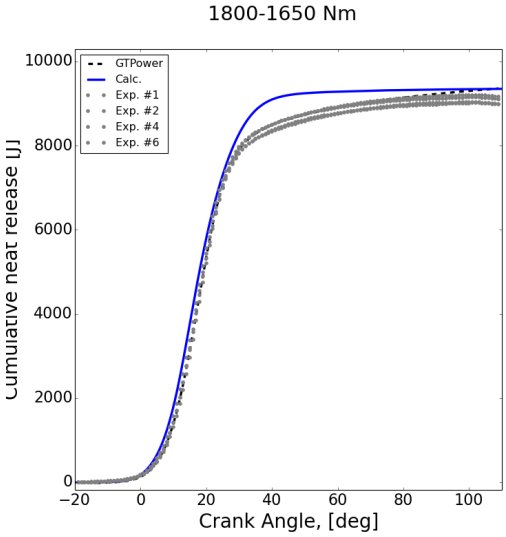

Figure 3.15: 1800-1650 validation: cumulative heat release comparison

In figure 76 cumulative heat released comparison between computed and experimental data is performed. Curves in this case are coincident for almost all the cycle, leading to a good simulation of combustion process, both in terms of shape of the curves and cumulative heat release final values. Differences arise between 20° and 40° crank angle, in last combustion phase, but they are not compromising cumulative value reached at the end of expansion stroke.

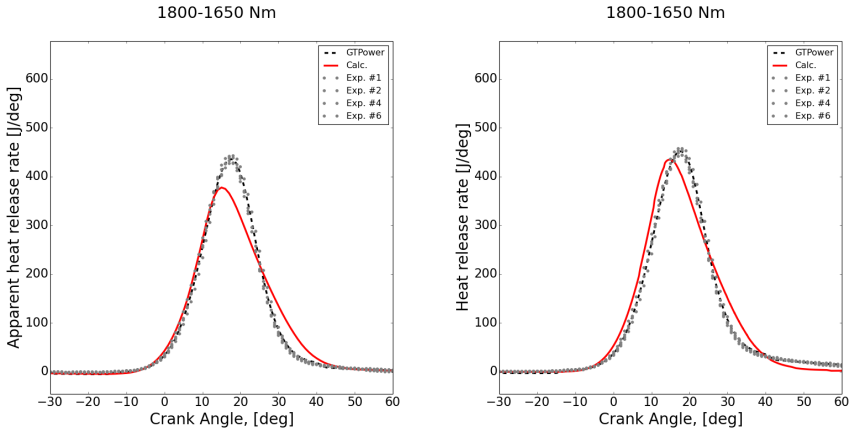

Figure 3.16: 1800-1650 validation: apparent and rate of heat release comparison between simulated and experimental data

To conclude this engine validation process, also rates of heat released are shown in figure 77. Curves are again consistent between each other, presenting similar shapes but with different maximum values and timing. Regarding rate of heat release, maximum value is comparable with simulated one, which is slightly

anticipated; regarding apparent rate of heat release, maximum value is both anticipated and highly underestimated. In combustion final phase, both heat release curves are less vertical with respect to experimental ones, in consistency with previous cases.
What can be concluded by this analysis is that solver is very good in pressure curve representation, that can be adjusted anticipating or delaying spark timing if needed. At high load and engine velocities, heat release is well reproduced, and ignition delay is less influencing solver results. Wall heat transfer computation is the point of weakness of the solver: for every simulation performed, it is overestimated, especially when low loads are considered.
To conclude this validation sub-section, Gross indicated work error is analysed, and an error indicator must be defined:

$$Error_{GIW} = \frac{GIW_{computed} - GIW_{experimental}}{GIW_{experimental}} \tag{3.2}$$

Therefore, an error analysis of the constant torque sweep and of the constant engine velocity sweep has been performed.

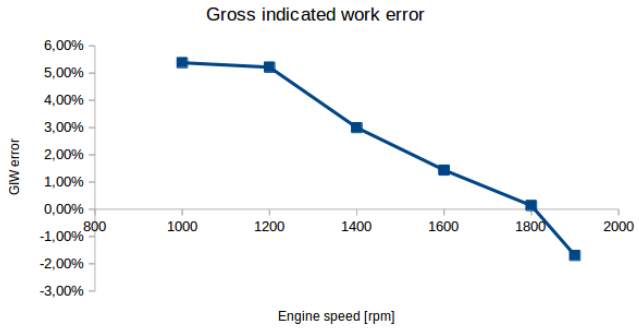

Figure 3.17: Gross indicated work error in constant torque sweep

As shown by figure 78, error in the worst condition slightly overcomes 5%, getting lower at higher engine velocities.

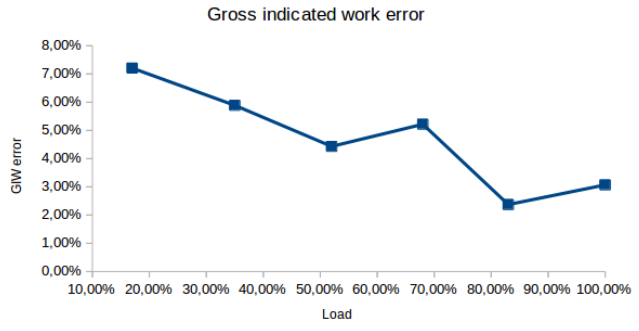

Figure 3.18: Gross indicated work error in 1200 rpm sweep

While in figure 79 error in constant engine velocity has a more varied behavior. As discussed in 1200-855 validation point, fast increasing of the fired

pressure curve is influencing simulation results. To have more accurate computed data and reducing gross indicated work errors, for low load points it is enough to delay spark timing of few crank angle degrees, to have a better matching of the pressure curve.
In the end, the solver is reproducing almost all the cases in a good way, especially when engine is running between 1200 Nm to 1800 Nm of torque. When very low load is simulated, computed curves are anticipated with respect to experimental ones, but shapes are not too much different. When very high regimes (1900 rpm) are simulated, pressure and heat release maximum timings are very similar to experimental ones, but their magnitude values are quite lower; even in the worst case, the difference between CFD and experimental pressure maximum value is -8.33%. It is possible to conclude that the solver is can reproduce empirical data with an acceptable error for every engine working point given. The choice of a proper χ_{coeff} value has been fundamental for this validation.

3.1 Spark advance sweep for engine optimization

Given experimental points are good to validate the solver and calibrate its settings, but they are not very representative of engine performance: a correct spark advance timing is crucial to improve gross indicated work and reduce fuel consumption. In addition, spark timing variation is an easy and reliable control strategy for the engine itself, such that a spark advance delay is important to avoid knock whenever it occurs. At the same time, turbulence or natural gas composition are not that easy to be controlled, hence these kinds of solver input variation are considered a good sensitivity analysis as cycle variability.
Efficiency is the main parameter for thermal engines. It is defined as the ratio between gross indicated work and heat released by the fuel.

$$\eta = \frac{grossIndicatedWork}{cumulativeHeatReleased} = \frac{GIW}{cumRoHR} \tag{3.3}$$

$$GIW = Work_{expansion} - Work_{compression} \tag{3.4}$$

$$cumRoHR = \dot{m}_{fuel} \cdot LHV_{fuel} \tag{3.5}$$

In order to understand how spark timing can be so relevant, the working point 1200-421 has been taken as example; then a constant regime analysis and constant torque analysis are performed.
1200-421 is the lowest torque point available in the whole engine map: it corresponds to 17% of load, with 421 Nm of torque. The engine is running in stoichiometric air-fuel ratio and natural gas considered is composed just by methane, meaning knock can not be present (since a compression ratio of 11.7 is adopted).

lowest spark advance: -11° → -26° highest spark advance

Range imposed is very wide, in order to consider both maximum values but also maximum efficiency working point stability.

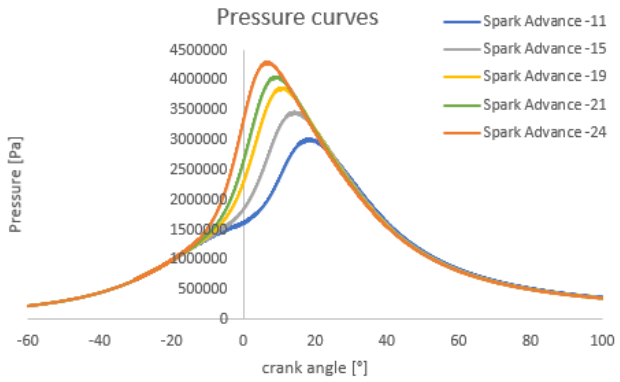

Figure 3.19: spark timing sweep for 1200-421 working point

Pressure curve underlying area is considerably wider when spark timing is anticipated, and also pressure maximum value increases considerably, from 30 bar to over 40 bar. Not all the underlying area is corresponding to useful work: from -175° (intake valve closing, IVC) to 0° (top dead centre, TDC) piston is compressing air-fuel mixture, which is a "cost" in terms of performance, as in all others thermal machines. From 0° to 124° (exhaust valve opening, EVO) expansion stroke is plotted, and that area region needs to be maximized. In any case, p-θ curve is good to analyze pressure behavior with respect to the time, but it is not strictly representing work done by power cycle; pressure-volume curve is more connected to real work done by cylinder itself, and comparisons with the ideal Otto cycle are easier to be discussed.

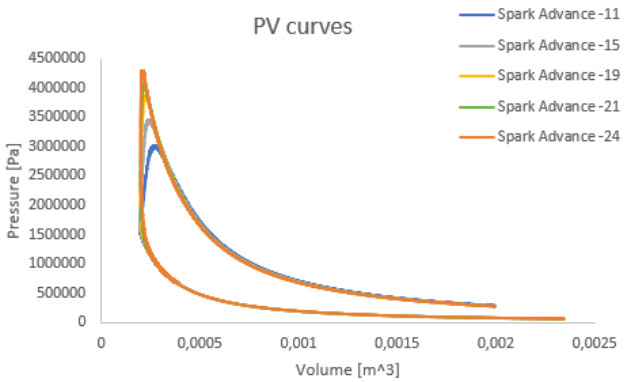

Figure 3.20: PV curve for 1200-421 working point

Otto theoretical combustion is a constant volume combustion, ideally a vertical line in correspondence of top dead centre. The earlier the spark advance, the more ideal the combustion process reaching also higher pressure and temperature values. But also, compression work and heat transfer losses increase anticipating spark timing, so the best compromise between higher combustion ideality and minimization of compression and thermal losses is needed.

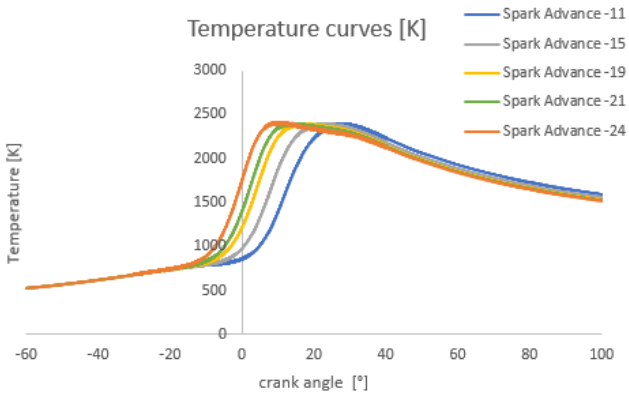

Figure 3.21: Spark advance sweep: cylinder temperatures

In figure 82, cylinder temperatures are plotted. Advancing spark timing, temperature maximum values do not change considerably. High cylinder temperatures increase wall heat transfer losses, hence the curves crosses during the expansion stroke. At the end of the expansion stroke, most advanced condition is the one presenting lower temperature values at exhaust valve opening because of the higher cumulative wall heat transfer, even if maximum value is slightly higher.

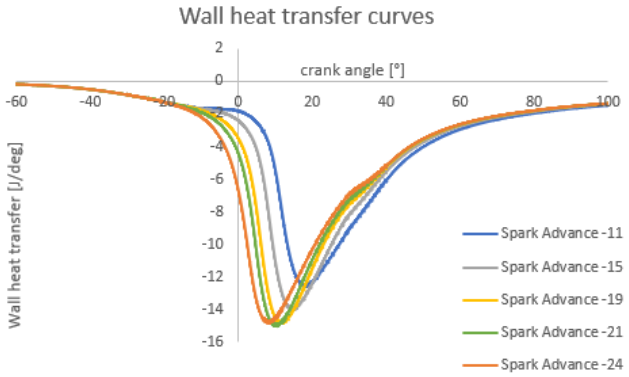

Figure 3.22: Spark advance sweep: wall heat transfer

Figure 83 illustrates how heat losses are conditioned by spark timing, both in terms of heat transfer minimum and cumulative values. Plotted curves are very similar, suggesting that a delayed spark timing can reduce heat losses, which contribute to decrease temperatures. Heat losses are quite important for internal combustion engines because that temperature reduction decreases work done especially in the second part of expansion stroke, when combustion can be considered completed (around 40°).

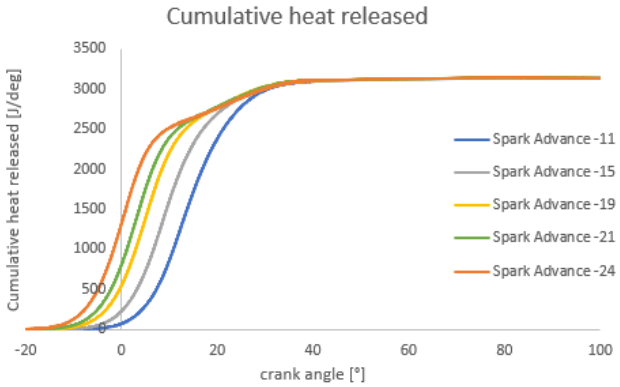

Figure 3.23: Spark advance sweep: cumulative heat release

Heat release curves (plotted in figure 84) have the same maximum value, since it is determined on the quantity of fuel present in the cylinder at intake valve closing. Load can be changed by modifying initial cylinder pressure but, as far as it is a constant load analysis, cumulative heat release curves are very similar between each other. Differences start to arise just when flame interface reaches squish area: there combustion proceeds slowly because of the low space available. Normalized c can reach and overcome 99.98%, meaning that combustion is considered completed.

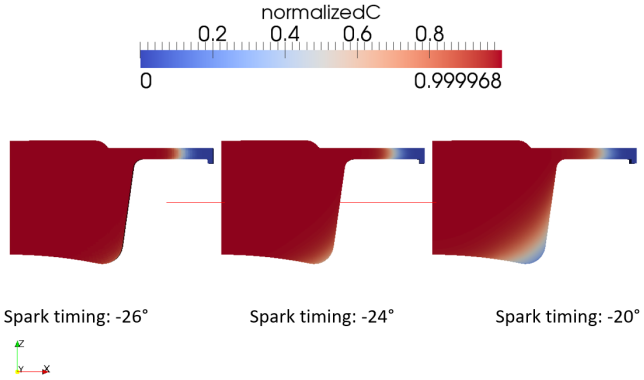

Figure 3.24: Flame interface of low load engine at (from left to right) 26, 24 and 20 of spark advance

In figure 85, flame interface of different spark timing cases is compared at 10° after top dead centre to explain cumulative heat release behavior illustrated in figure 84: most delayed spark timing ignition has an higher flame surface available, hence the higher heat release rise in that piston position.
Combustion efficiency and gross indicated work are influenced by all these thermodynamic quantities. Spark timing able to maximize efficiency is -19°. This thesis work is just focused on power cycle, hence any other considerations such as having a good turbine pressure-temperature inlet for turbocharging or valve timing variations are considered out of this work.

Returning to combustion analysis, maximum efficiency point is very stable, with few variations per few degrees of spark timing changing, leading to a good flexibility of the engine itself.

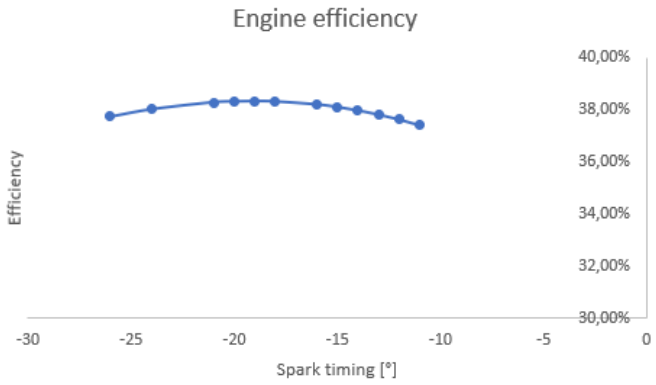

Figure 3.25: 1200-421 efficiency curve with respect to spark timing variations

In figure 86 efficiency curve with respect to spark timing is plotted. Maximum efficiency for this working point is 38.34%, but it is very stable since advancing and delaying of 1° spark timing leads respectively to 38.33% and 38.32% efficiency values, so very low variations.

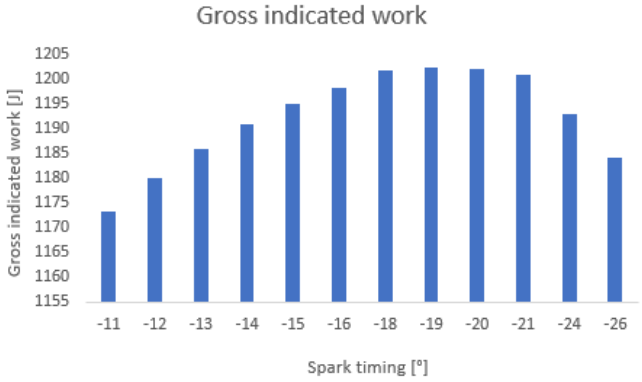

Figure 3.26: Gross indicated work with respect to spark timing variations

While in figure 87 gross indicated work is represented. As far as cumulative heat release does not change, gross indicated work curve has the very same shape of efficiency one if plotted with respect to spark timing axis. GIW varies from 1200 J to 1170 J in the worst case, proving again the high efficiency stability.

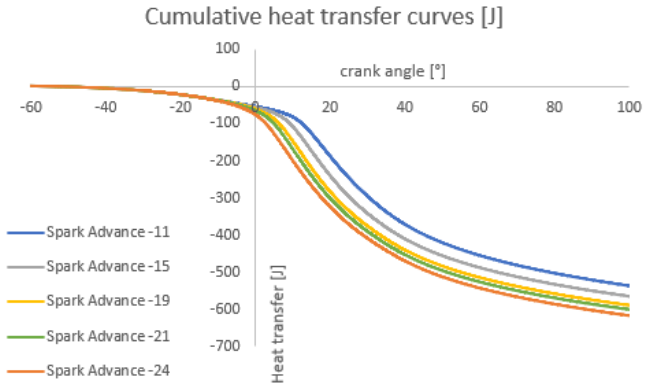

Figure 3.27: Spark timing sweep cumulative wall heat transfer curve

In figure 88 cumulative heat transfer to the wall is shown. It is the only solver quantity having a strictly monotone trend, also meaning that advancing spark timing heat losses will always increase.

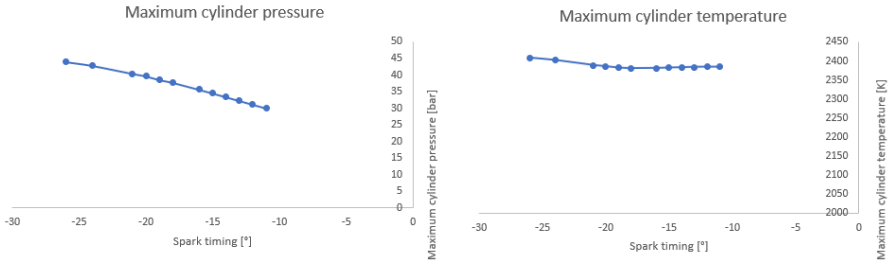

Figure 3.28: 1200-421 spark timing sweep: pressure and temperature maxima

In conclusion of this analysis, figure 89 reports cylinder pressure and temperature maximum values. They both have an almost linear behavior, with more maximum pressure relative variation with respect to maximum temperature one. Pressure maximum values can vary from 30 bar at very delayed spark timing to 45 bar at very anticipated spark timing, meaning the 50% of relative variation is present. At the same time, temperature (weighted averaged) maximum values are almost constant, with a very few increasing when early ignition is adopted.

3.2 Constant torque sweep

By the engine map, it is possible to recognize a constant torque sweep at almost 1700 Nm. Engine has a minimum rotational speed of 1000 rpm and a maximum one of 1900 rpm.

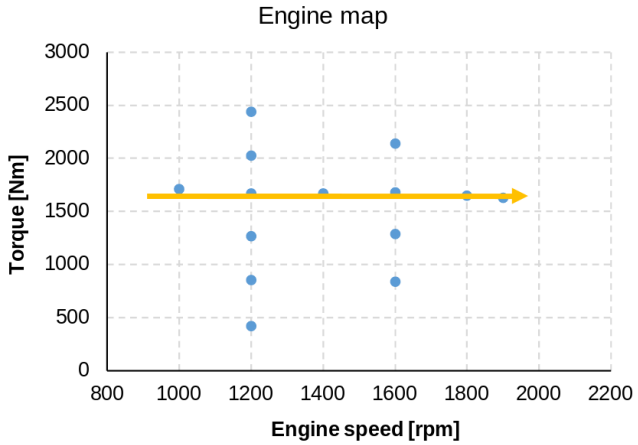

Figure 3.29: Constant torque sweep

Engine time is referred to piston position in compression and expansion stroke, but if rotational speed doubles, stroke duration gets halved. As a consequence, what is expected is no flame velocity variations in terms of time (in seconds), but determinant variations in terms of engine time (in crank angle). Also, electric spark light delay, fixed at the value 0.001 s, is going to be more influencing at high engine speed with respect to lower ones. In this sub-section, all points have already been optimized with respect to spark timing, as previously described. No turbulence or other numerical parameter has been changed.

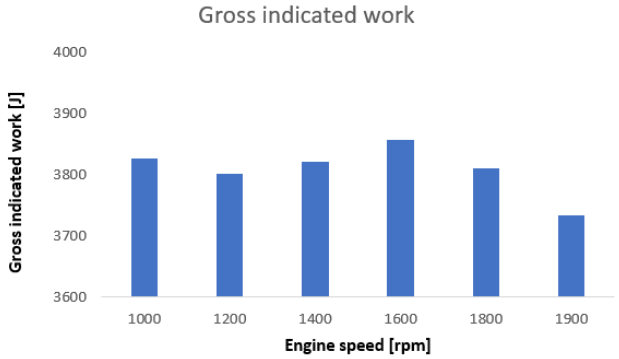

Figure 3.30: Gross indicated work at constant torque

As described in engine presentation, for this analysis (and mainly in the rest of this thesis work) load is determined by fixing cylinder pressure at IVC. Since it is a constant torque analysis, gross indicated work (shown in figure 91)

is more a constrain than a parameter to be post processed, in fact values are almost coincident. Once optimization is performed, gross indicated work from power cycle varies depending on which working point was closer to optimization in original settings.

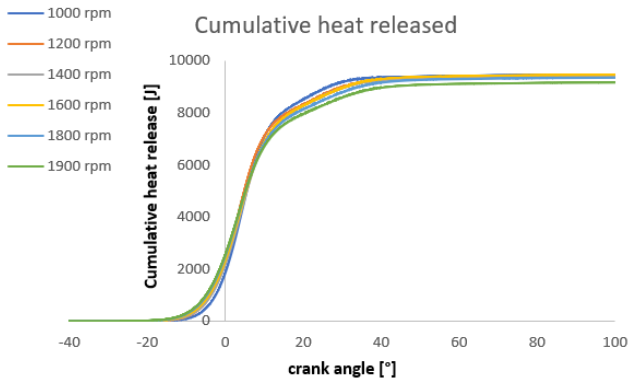

Figure 3.31: Cumulative heat released curves at constant torque

By heat release curves illustrated in figure 92, low engine speeds need a delayed spark timing to reach the optimum, and it can be seen by a delayed appearing of low regime curves; but combustion needs less crank angle degrees to be completed, and a curves intertwinement around 10° after top dead centre is present. Even if in terms of seconds combustion is requiring almost the same time, in terms of engine time (crank angle) combustion is slower, leading to a less ideal one.

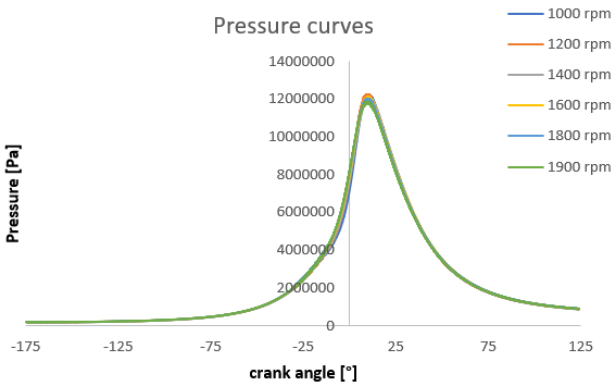

Figure 3.32: Optimized pressure curves at constant torque

Pressure curves displayed in figure 93 are very similar, even if engine rotational speed changes. Mixture ignition needs to be anticipated when engine is rotating faster, and pressure maximum values are getting lower, but changes in optimized pressure curves are not very important.

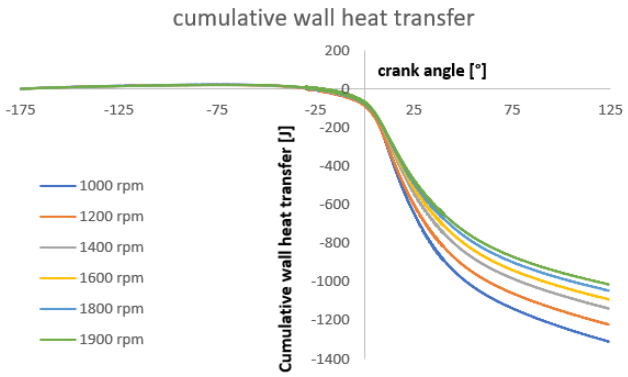

Figure 3.33: Cumulative heat transfer curves at constant torque

In cumulative wall heat transfer curves reported in figure 94, it is possible to understand the real advantage of having higher engine speeds: heat losses reduction. If engine is rotating faster, exhaust gasses have less time available to exchange heat with cylinder wall, resulting in a more ideal compression and expansion. This is possible to be observed also in temperature curves, where temperature maximum values are almost the same, but at the end of expansion stroke burnt gasses are hotter in higher engine speed cases.

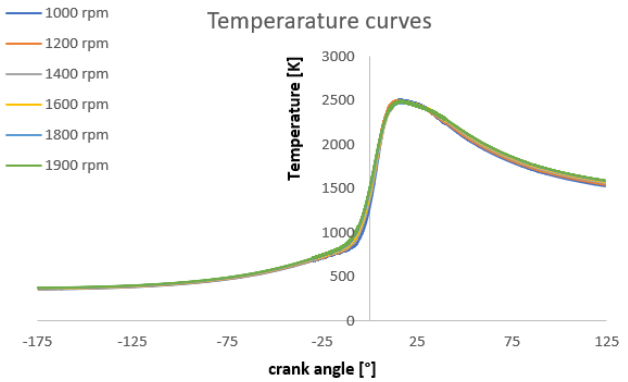

Figure 3.34: Temperature curves in constant torque sweep

Figure 95 reports temperature curves in this constant torque sweep. Curves are almost coincident, but there are two areas where some important differences can be detected: when mixture starts to ignite due to different spark timings imposed and temperature final values, due to lower wall heat transfer at high engine rotational speeds. Even if temperature maximum values are very close, end ones can change of more than 60 K between slowest engine rotation (1000 rpm) and fastest available one (1900 rpm).

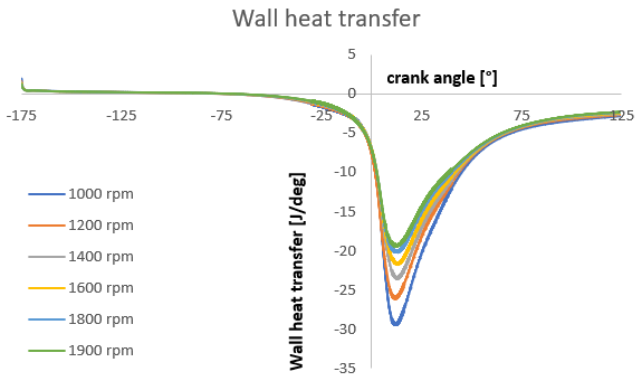

Figure 3.35: Wall heat transfer curves in constant torque sweep

Figure 96 can show how wall heat transfer curves have a very similar shape, enhancing how faster rotational speed configurations have lower heat losses along the whole cycle.
Another huge difference between load and regime variation is the fluid turbulent kinetic energy. Swirl is initialized by imposing a "Swirl-RPM ratio", meaning that keeping constant this ratio, fluid motion becomes more important at high engine speeds. Turbulent kinetic energy curves in this analysis almost uniformly increase to higher values.

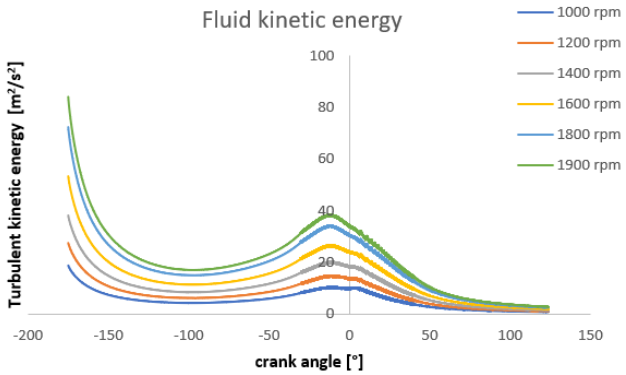

Figure 3.36: turbulent kinetic energy in constant torque sweep

Therefore, turbulent kinetic energy of different working points is reported in figure 97, evidencing both how turbulence increases with rotational speeds, but also how they dissipate during compression stroke. At the end of high engine speed curve, some vibrations are present. This kind of vibrations are the results of a combination of multiple factors such as combustion behavior, pressure and temperature condition but mainly piston geometry. In any case, they are going to be discussed later in this thesis work. In this section, what is important is to evidence that the more turbulence is present in the engine, the faster the combustion (which is also explained in solver section, were b-Ξ equations are discussed).

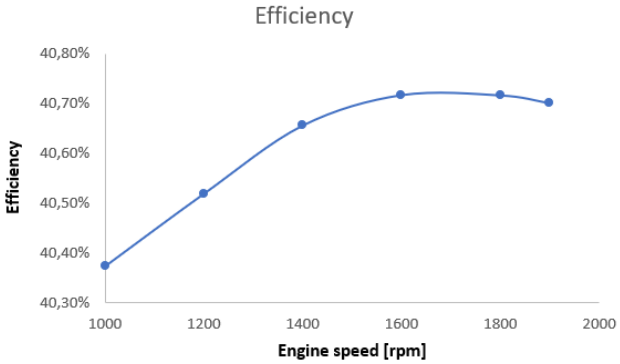

Figure 3.37: Efficiencies in constant torque sweep

In efficiency terms, as shown in figure 98, a maximum value is present at 1600 rpm, which represents the best trade off between a faster combustion and lower heat losses. In any case, figure displaying efficiency is very zoomed, since the whole vertical axis varies from 40.3% to 40.8%.

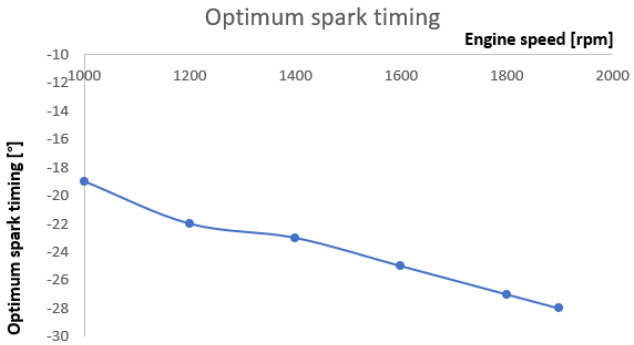

Figure 3.38: Optimum spark timing in constant torque sweep

Even if η curve is quite flat, spark timing needs to be changed considerably inside this sweep, as shown in figure 99. In this way it is possible to get the already represented pressure curves to optimize different power cycles.

3.3 Constant speed sweep

In this subsection, engine speed is kept constant and different loads are simulated. Chosen regime is 1200 rpm, since there are six experimental points available for that condition, and a spark timing optimization for all the loads has been performed with criteria described in subsection 3.1. Other parameters such as turbulence are not changed.

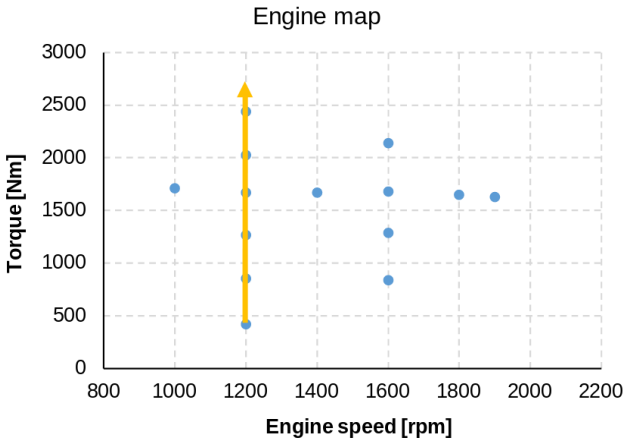

Figure 3.39: Load sweep illustration

In a stoichiometric mixture engine, having higher load means rising intake valve closing pressure, hence quantity of fuel inside the cylinder. In consistency, what is expected is a graphical curve enlargement of pressure, GIW, and heat released.

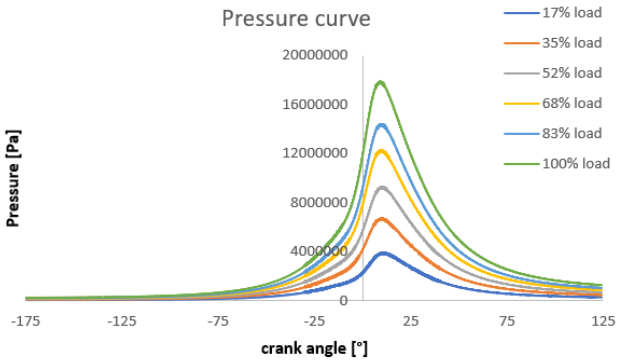

Figure 3.40: Load sweep pressure curves

Figure 101 illustrates different pressure curves when different loads are computed. Shape of the curves is very similar, with an almost coincident maximum value timing.

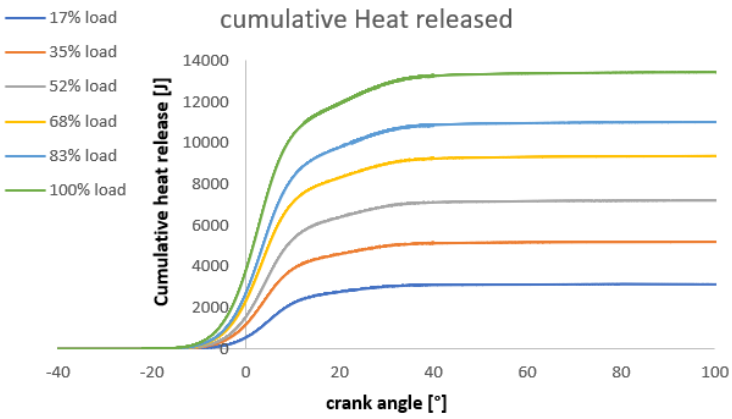

Figure 3.41: Load sweep cumulative heat release curves

The same behavior of pressures curves can be seen in cumulative heat release ones, displayed in figure 102. They move to always higher values, accordingly to the higher mass of fuel inside the cylinder.

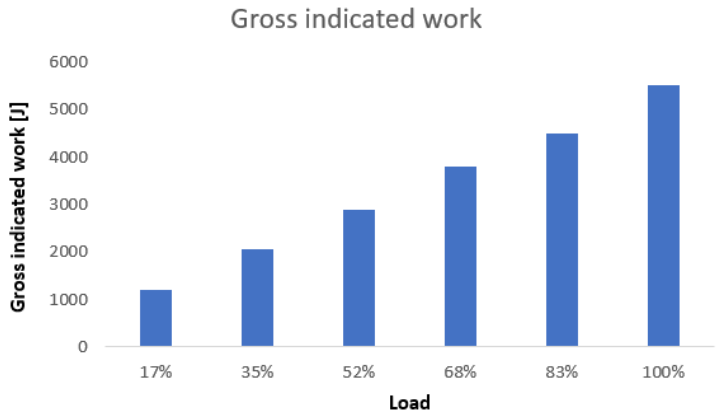

Figure 3.42: Gross indicated work histogram

As expected, in figure 103 gross indicated work increasing when higher loads are required to the engine is shown. Maximum intake valve closing pressure is 2.4 bar, value taken from experimental data.
What can be interesting of this analysis is verifying the existence of an optimum spark timing or efficiency variation and what it is due to. In terms of temperature, load doesn't influence so much maximum values since engine is running stoichiometric, but temperature reduction once combustion is completed.

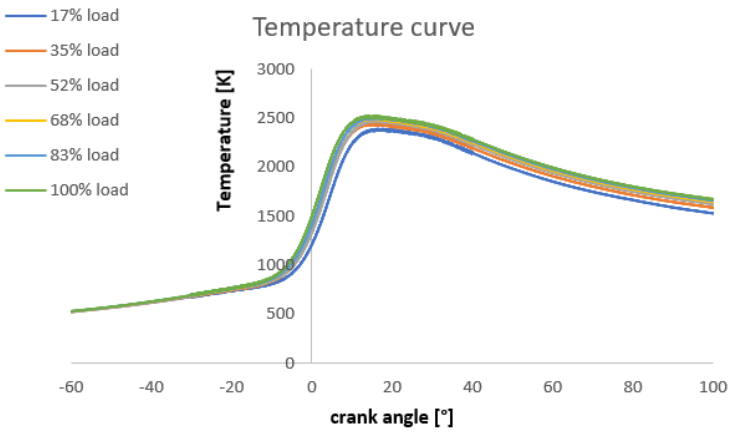

Figure 3.43: Constant regime temperature curves

Figure 104 illustrates the behavior described above: shape of the curves is very similar, with very close maximum values because engine is running stoichiometric. Air-fuel mixture mass inside the cylinder is not the same, and hence neither thermal inertia: at low load, heat losses are relatively more important, and it can explain temperature differences starting to arise even before combustion and increasing once combustion is completed.

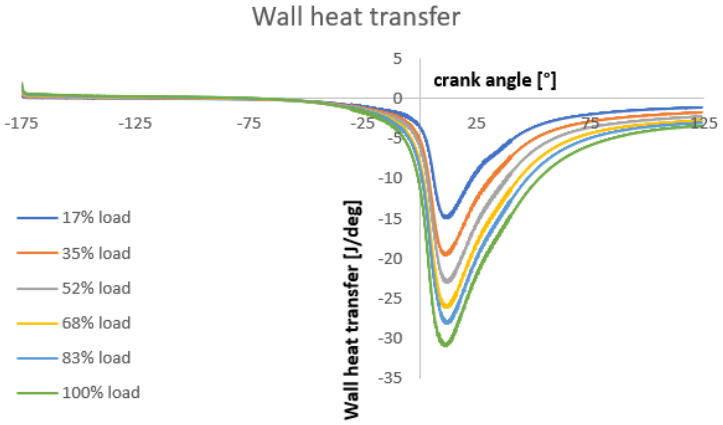

Figure 3.44: Constant regime wall heat transfer curves

Wall heat transfer curves displayed in figure 105 confirm behavior described. They are not proportional to air-fuel mixture mass, and proportionally heat losses are more important when load is lower.

Figure 3.45: Efficiency at constant regime

What finally results, as illustrated in figure 106, is a high load efficiency higher with respect to low load one. Efficiency variations are huge if compared to constant torque case, from 38.5% in lowest load case to 41.0% in highest load one, over than 6% of relative variation. Since heat losses play a very important role in that, this behavior explains also why turbocharging is so important for modern internal combustion engines, since higher load can be reached without increasing cylinder surface, hence reducing heat losses.

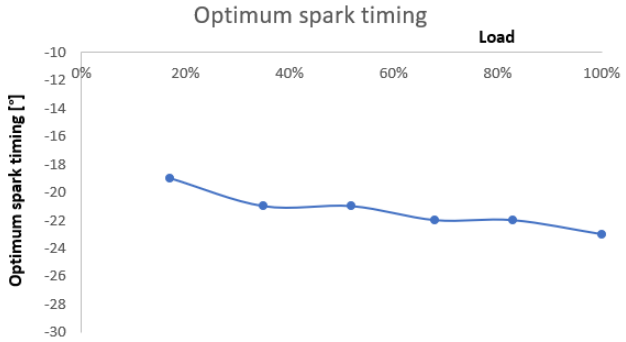

Figure 3.46: Optimum spark timing at constant regime

This efficiency-load monotonic behavior stands also because there is no knocking issue since compression ratio is not that high and fuel considered is fully methane. The reduction of wall heat transfer importance is reflected in optimum spark timing ongoing, represented in figure 107: since at high load cylinder gasses have more thermal inertia, pressure curves can be raised up with lower drawbacks; optimum spark advance passes from -19° in lowest load condition to -23° in highest load condition.

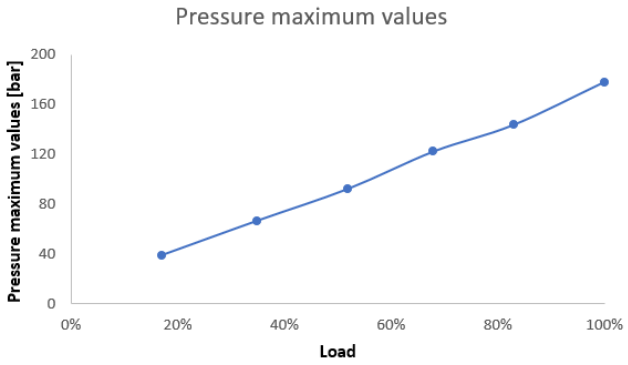

Figure 3.47: Pressure maximum values at constant regime

In the end, maximum pressure reached is a little bit lower than 180 bar, as shown by figure 108. Full load at 1200 rpm is the only working point available to reach such a high pressure, hence this is going to be considered in spark assisted compression ignition engine development, as this pressure maximum values is very closed to supposed mechanical limit.

3.4 Engine map

Finally, with no change to engine geometry or any fluid dynamics settings, engine map efficiency is significantly growing, evidencing the importance of spark timing control.

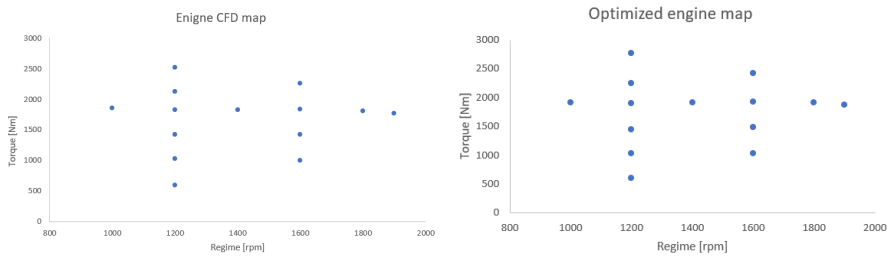

Figure 3.48: CFD and optimized engine map comparison

Engine points location do not change very much, in fact at first sight the two maps showed above very similar. Once also torque and efficiency numerical values are observed, it is possible to notice some significant improvements to the work done by the cylinder.

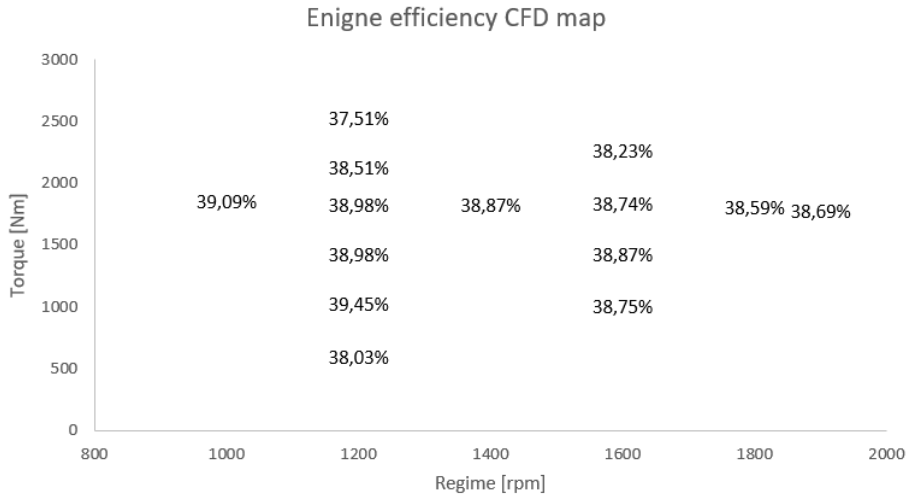

Figure 3.49: CFD working points efficiency engine map

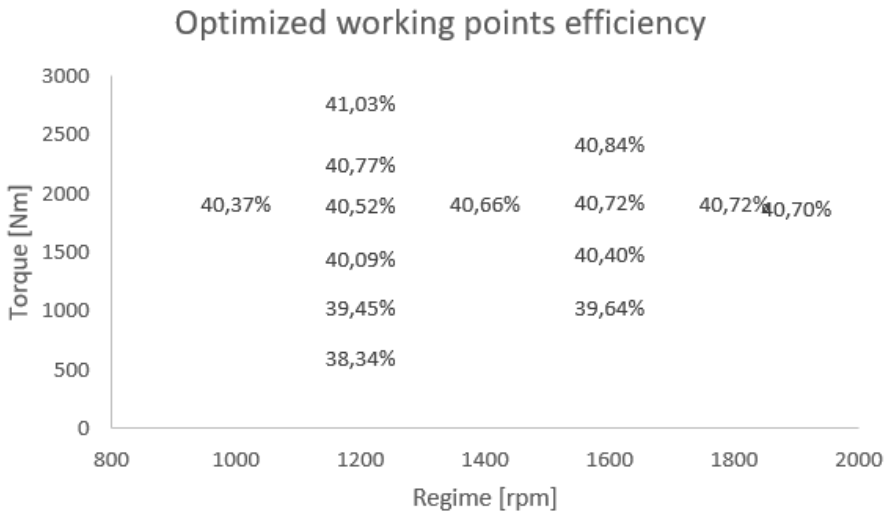

Figure 3.50: CFD efficiency engine map after optimization

As shown in figure 111, most significant improvements are at high load where experimental spark timing is very delayed, while it needs to be anticipated to improve performances. At this low compression ratio (in natural gas engine), knock or maximum pressure values do not correspond to a real issue to be managed. Regarding to engine efficiency values, spark ignition engine is better behaving at high load with respect to low load working points. Therefore, at low load efficiency must be improved in order to have a significant reduction of fuel consumption.

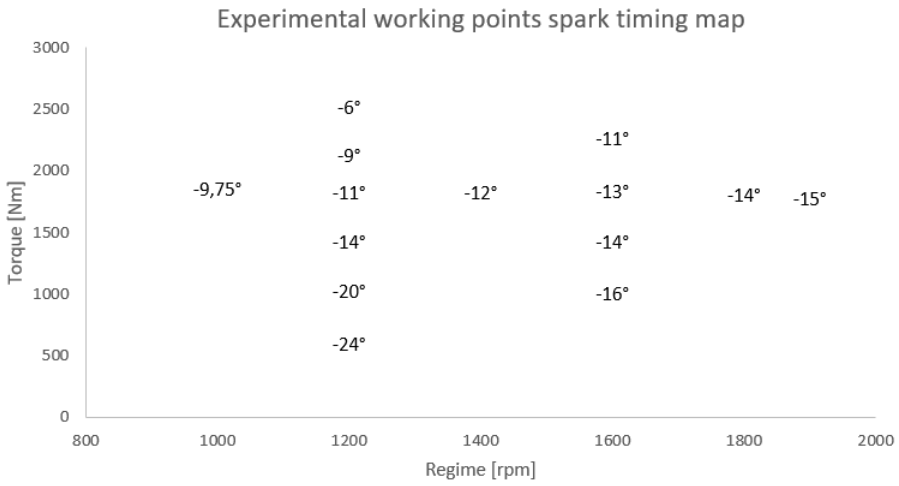

Figure 3.51: Experimental working points spark timing map

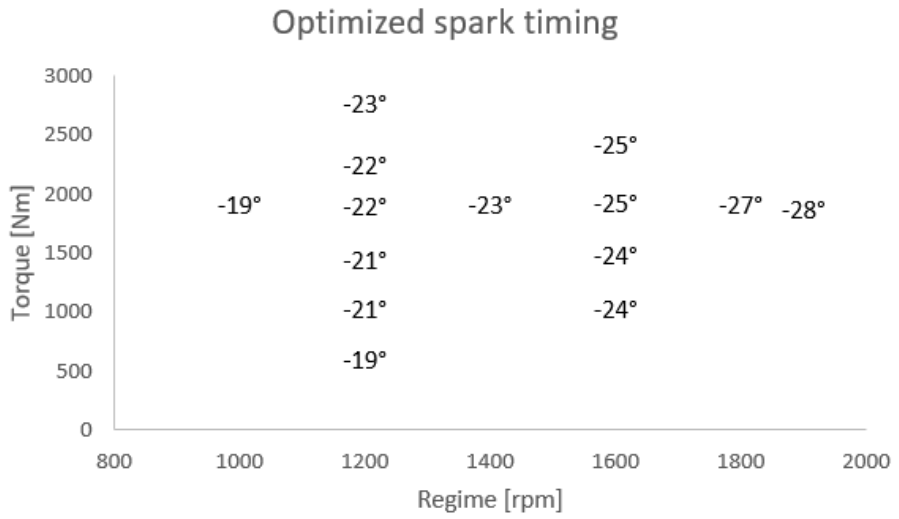

Figure 3.52: CFD optimized spark timing engine map

In figures illustrated above it is possible to compare the experimentally given spark timings (in figure 112) and the optimized CFD derived ones (in figure 113). Differences get higher at high load, corresponding also to condition where efficiency improvement is maximum. At low load spark timings are very similar, hence there is no significant efficiency improvement. Fuel used in CFD simulation is composed by 100% of methane, hence knock can limit spark timing anticipation in no way.

Chapter 4

Knock prediction

In spark ignition engine context, knock is an abnormal combustion occurring when some cylinder regions are exposed to such high pressures and temperatures that fresh air-fuel mixture burns spontaneously. It is very violent and dangerous for the engine, and it is strongly unwanted. In this section solver behavior in knock presence is analyzed, also to understand peculiarities of this phenomenon. Spontaneous ignition combustion is strongly influenced by the kind of fuel used: octane number is a knock tendency indicator, defined such that the higher it is, the more resistant the fuel will be to knock. In the solver algorithm, determining reaction velocities in function of local pressures, temperatures and mixture fraction is left to Cantera table generation, hence a different table for every kind of natural gas composition must be created. In order to let the engine knock, just for a part of this section fuel used is isooctane, which has an octane number of 100 by definition. Natural gas one can vary within a range of 120-130, so in this simulation set very violent knocks should take place.

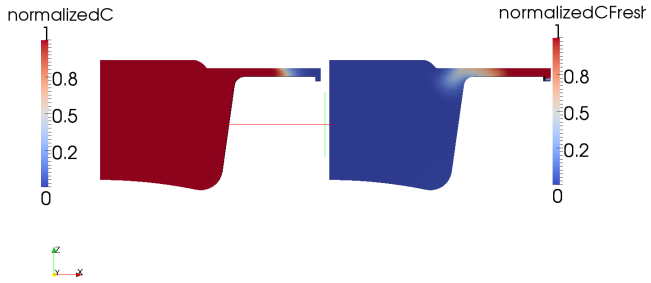

Figure 4.1: Engine flame front and spontaneous ignition visualization

Combustion chamber used is the one described in validation process; no change has been made. Therefore, compression ratio is fixed at 11.7 and working point chosen for this analysis is the full load one at 1000 rpm (1000-1710), which should be the one presenting the highest knock intensity because of the

low rotational speed. In natural gas port fuel injection engines, mixture can easily be assumed homogeneous, and the same assumption has been made also for these isooctane fuelled cases. Imposing a homogeneous mixture fraction means having no differences in Z values, hence once a part of engine knocks, also all the remaining unburnt ones are supposed to. In figure 4.1, it is possible to notice that flame is propagating from spark plug location, while knock starts from cylinder extremities. Once the very first fresh mixture region ignites spontaneously, in 2-3° combustion is going to be fully completed.

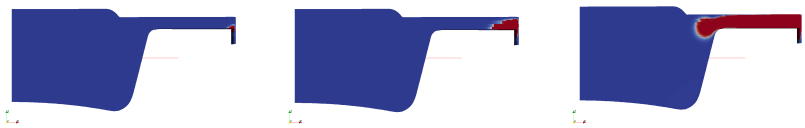

Figure 4.2: Autoignition propagation in 2 crank angle degrees

Figure 4.2 is displaying what has been textually described. Engine time difference between most anticipated cylinder image (leftward) and most delayed one (rightward) is exactly 2° of crank angle. In such a short time, all the unburnt fresh mixture is supposed to release heat, with a consequent pressure rise and sonic wave propagation.

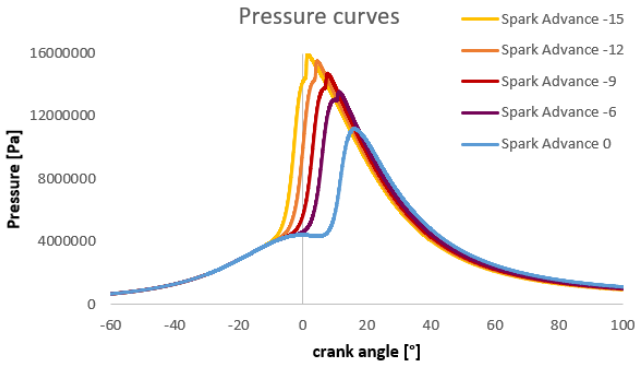

Figure 4.3: Pressure curves when engine is powered with isooctane as fuel

To make a deep analysis on how knock presents and how it can be controlled, a spark advance sweep as illustrated in figure 4.3 has been performed. In displayed pressure curves it is easily possible to detect knock: there is an almost vertical pressure rise when it takes place, causing even some vibrations afterward. Magnitude of this increase can vary a lot, depending on quantity of autoignited air-fuel mixture and when (in terms of engine time) it is occurring. Theoretically, pressure curves in knocking cycles should present two different maximum values: a "rounded" one because of flame propagation combustion and a more vertical one because of compression ignition combustion. This second one moves depending on where autoignition takes place: if it happens after flame propagation pressure maximum value, the two both can be distinguished;

if knock is very anticipated, there is just compression ignition maximum visible. Another very important thing to be remarked is the importance of spark timing for knock control: always regarding figure 4.3, it is possible to notice how maximum values increase anticipating spark timing. Spontaneous ignition in fact is enhanced when severe pressure and temperature conditions inside the cylinder are present. Even if delaying spark timing logically air-fuel mixture should have more time available to react, reaching high cylinder temperature values is definitely more influencing, meaning that the more spark is advanced, the more knock is enhanced.
By previous sections, two mechanical engine limits regarding pressure values were supposed: an absolute maximum of 180 bar and a pressure rise one of 15-18 bar/deg. Pressure rise in post-processing CFD context has been defined as:

$$pressureRise = \frac{\partial p}{\partial \theta} = \frac{p^{\theta+\Delta\theta} - p^{\theta}}{\Delta\theta} \tag{4.1}$$

Due to high heat release presence (and consequent violent fluid dynamics quantities increase) time step in combustion range needs to be reduced: in previous section, $\Delta\theta$ chosen between -30° and 40° was 0.005°, while in this one it has been reduced up to 0.0025° (the halved value), otherwise Courant number becomes huge and divergence when equations are solved arises.

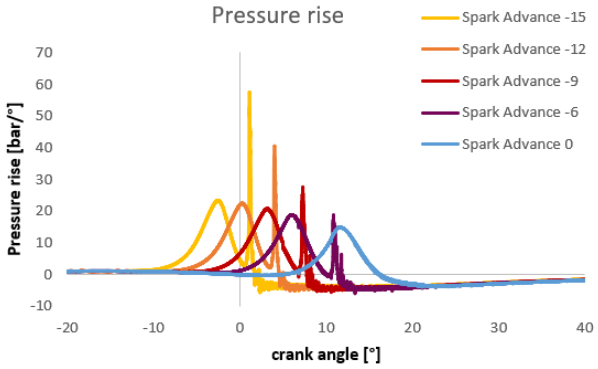

Figure 4.4: Pressure rise curves when engine is powered with isooctane as fuel

In figure 4.4 pressure rise curves have been displayed. In every knocking cycle, they report two maximum values: a rounded (and so smoother) one because of flame propagation combustion, and a very vertical one due to compression ignition combustion consistently with what shown in figure 4.3. This second one can become really huge with values of even 60-70 bar/deg depending on quantity of autoignited air-fuel mixture mass. After this maximum, some pressure rise vibrations are present due to sonic waves propagating and rebounding in the whole cylinder, mechanically heavy for the engine resistance. The solver is not able to reproduce these waves in a proper way, because of the high time step used and the turbulence model chosen. For a more physical description of them, a LES could be more appropriate but, as written in introduction section, it is at the state of the art too expensive in computational terms to be used for this thesis work targets.

The only not knocking case can be easily recognized because it has just one pressure rise maximum, occurring when spark timing is very delayed since engine is designed to work with natural gas.

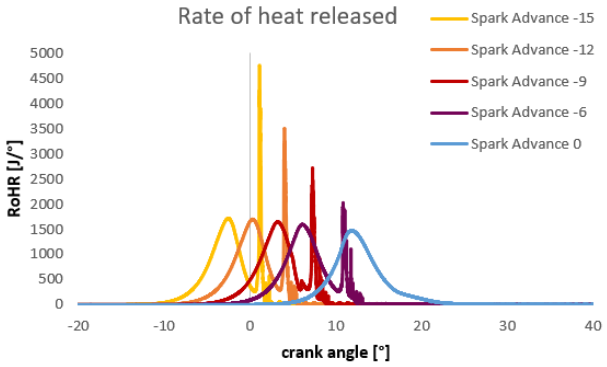

Figure 4.5: Heat release curves when engine is powered with isooctane as fuel

As shown in figure 4.5, also apparent heat release has a similar behavior with respect to pressure rise: it presents two maximum values, one from spark ignition combustion (hence function of flame properties such as front velocity and surface), the other from compression ignition combustion. Even in this plot, autoignition maximum value can be much higher with respect to flame propagation one, and close to that region curves are as inclined as pressure rise ones, highlighting the direct relation between heat released by air-fuel mixture and pressure increase. Some negative values (low in terms of magnitude) can arise in apparent heat release CFD data, but these are small numerical issues with no physical meaning due to very violent heat release rise. Even in this time, the only not knocking cycle has just one heat release maximum value since knock is not present.

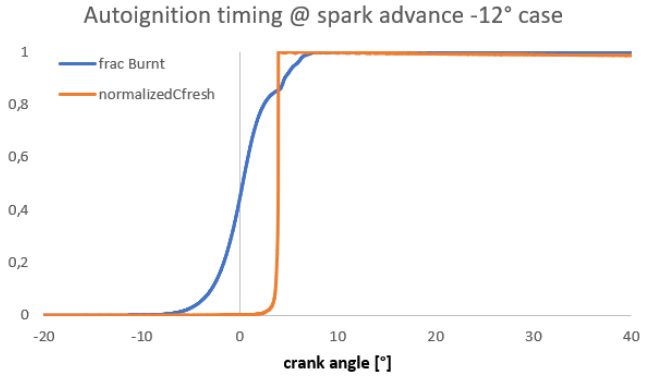

Figure 4.6: Autoignition timing when engine is powered with isooctane as fuel, -12 spark timing case

In figure 4.6 a comparison between fraction burnt and maximum c fresh ongoing has been performed. Spontaneous combustion starts when normalized

c_{fresh} reaches the value of 1; afterwards, it involves the whole unburnt fresh mixture remaining. In solver code, even if spontaneous ignition arises, flame continues to propagate with a different velocity because of higher local pressures, temperatures and even turbulent kinetic energy caused by compression ignition; but mixture can not release any further heat because it has already reacted in c_{fresh} equation, and combustion products are computed in "Updating composition" script. Normalized c_{fresh} graph is very similar to a Heaviside function, from 2% to 100% in less than 1° crank angle.
PvS is the source term for c_{fresh} equation, and its behavior can explain such a vertical progress variable increase.

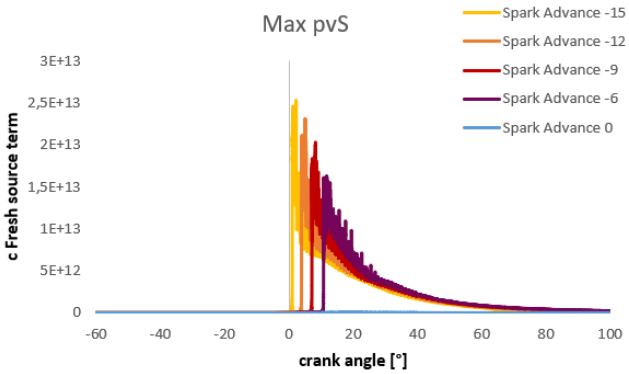

Figure 4.7: Cfresh source term when engine is powered with isooctane as fuel

In figure 4.7 source term of c_{fresh} equation is plotted. Velocity of homogeneous mixture compression ignition combustion can be easily seen also by pvS values: when knock occurs, maximum pvS increases from 4 to 5 orders of magnitude with respect to a not knocking case. This is numerically explaining why progress variable and heat release have this ongoing once knock occurs, and why spontaneous ignition combustion is so fast.

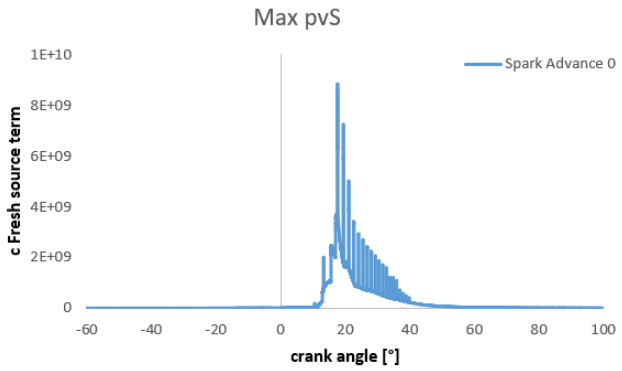

Figure 4.8: Cfresh source term in a not knocking CFD simulation

If figures 4.7 and 4.8 are compared, before knock occurrence pvS are very similar between the different charts. Once knock presents, c_{fresh} source term

increases vertically, homogeneously in almost all the unburnt regions. This behavior can change if mixture can not be considered homogeneous anymore, but since in this thesis work just natural gas port fuel injection has been taken into account, Z values have no differences inside the whole CFD domain.

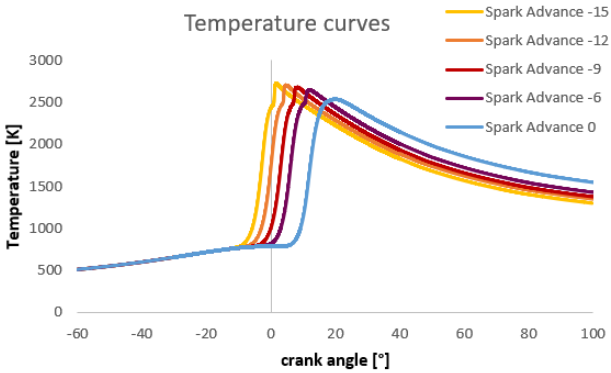

Figure 4.9: Temperature curves when engine is powered with isooctane as fuel

For what concerns temperatures, as shown in figure 4.9, autoignition is contributing to rise up weighted average values considerably: maximum reached is around 2700 K while, when knock is not occurring, it is from 200 to 300 K lower. For what regards heat transfer to the walls, it is certainly influenced by cylinder temperatures, but there is a more important contribution for its rise.

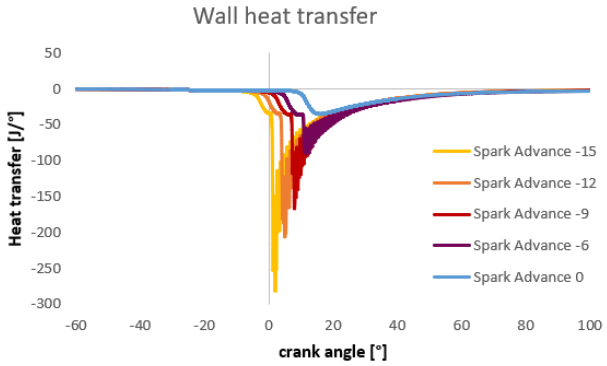

Figure 4.10: Wall heat transfer when engine is powered with isooctane as fuel

As figure 4.10 illustrates, wall heat transfer curves minimum values have too huge changes to be explained with just a temperature increase; as it will be discussed in section 5, pressure waves and fluid kinetic energy release plays a very important role in determining heat losses. Of course, this heat transfer behavior is influenced by knock presence, but specific quantities interested are going to be analyzed when engine is fuelled with natural gas to provide a more complete explanation. In this case, autoignition is so violent that in previous figure it is difficult to distinguish heat losses increase due to flame propagation combustion from the contribution given by knock.

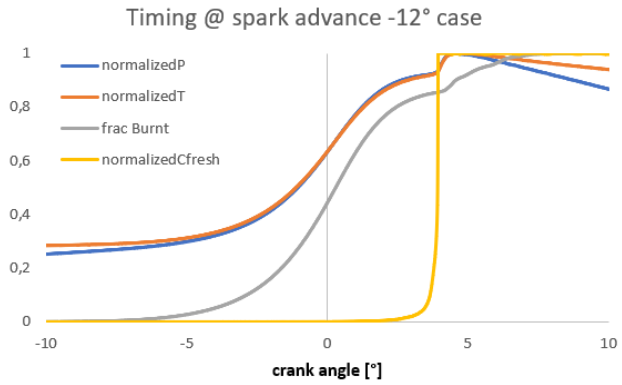

Figure 4.11: Main specific quantities normalized

Figure 4.11 provides an idea of autoignition effects on pressures and temperatures, focusing on rise speed. It is possible to appreciate how in much less than 1° from the first autoignition appearance pressure and temperature increase of almost 8%, resulting in the huge pressure rise previously displayed. Crank angle distance between first autoignited mixture particle and pressure/temperature maximum values can depend on fuel used and even on the piston shape.
Even if the focus in this subsection has been pointed on spark advance, engine speed is actually playing a very important role for autoignition: the faster the engine, the lower the time available for the mixture to react. This sub-section has been useful to introduce heavy knock and to explain how it can be detected; from this point ahead, natural gas has been used again to provide a deeper and more meaningful knock and autoignition description.

4.1 Knock experimental validation

In this particular study, it is not enough to validate just spark ignition combustion since it is not the only heat release source available. Compression ignition combustion is considered by the solver as something detached, included in a separated equation. In addition, natural gas can be an extremely octane number variable fuel, depending on which kinds of hydrocarbons are present. To be sure that the proposed solver is suitable for spark assisted combustion, also a knock validation is necessary, and to have some reliable data an experimental study is needed. This subsection is fully dedicated to comparison between solver results and a paper published in 2012 by Jiri Vavra, Michal Takats, Vojtech Klir and Marcel Skarohlid of the Czech Technical University, named "*Influence of Natural Gas Composition on Turbocharged Stoichiometric SI Engine Performance* [10].
In this experimental study, knock tendency of a compressed natural gas engine has been analyzed by including some additives to a reference fuel composition. Engine has hence been tested with a multiplicity of different fuels, in order to detect if knock is occurring or not. If the solver *betaFlameletSACIXiEngineDyMFoam* can reproduce results comparable with experimental values, validation can be considered completed and the solver able to be used for design purposes. What has been looked for is a result consistency between CFD

simulation and researcher's experimental paper: a perfect spontaneous ignition representation can not be reached. In this paper, Czech Technical University researchers wanted to investigate knock presence and performance sensitivity of an experimental engine to the fuel. Layout of the turbocharged compressed natural gas spark ignition engine is shown in figure 4.12.

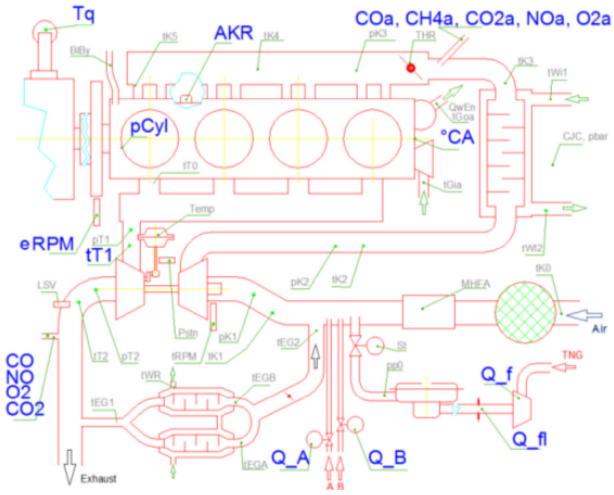

Figure 4.12: Paper experimental engine setup

Air fuel ratio is stoichiometric ($\phi = 1$) and compression ratio is 12:1, very similar to the CNG-heavy duty one (11.7:1). Other geometrical parameters such as bore or stroke are given, and in the following table a comparison between the two is presented. What is not described in the publication is engine piston geometry, which has a very important role in enhancing or avoiding autoignition.

	paper engine	CNG-heavy duty
compression ratio	12:1	11.7:1
max boost pressure	2.4 bar	2.44 bar
bore	102 mm	135 mm
stroke	120 mm	150 mm
IVC	-125°	-175°
EVO	123°	124°
ϕ	1	1

Table 4.1: Comparison between paper engine and CNG-heavy duty one

Boost pressure and exhaust valve opening are very similar between the two engines. CNG-heavy duty is definitely bigger, since both bore and stroke values are higher. Adopting a bigger engine is also a knock-promoting factor: if flame velocity between the two cases is going to be very similar, flame path is predicted to be higher in a bigger engine, hence more time available for the fresh mixture to autoignite. As written before, experimental combustion chamber geometry is not known and this is a source of results discrepancy, since parameters like

squish area ratio or piston and head shapes can influence knock presence.
To have a major data consistency, CFD compression ratio of CNG-heavy duty engine has been increased up to 12:1 and turbulence has been reduced. This numerical change is just for having more similar pressure curves between the two engines, using ones provided by experimental paper. Compression ratio changing procedure adopted is described in the following section.

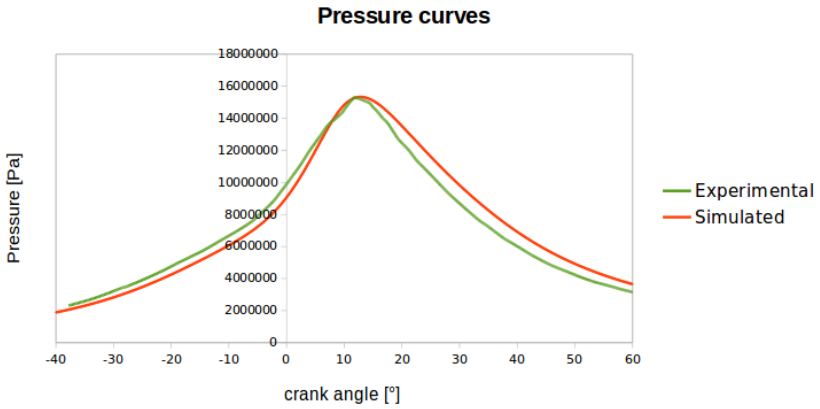

Figure 4.13: Experimental and simulated engine tuning

Figure 4.13 illustrates a comparison between experimental and simulated engines pressure curves. As one can see, they are not coincident and there are considerable differences in both compression and expansion stokes. In any case, pressure maximum value and its timing (illustrated in crank angles) are very similar, and no further change has been imposed to the CNG-heavy duty one. Spark timing in CFD simulations is set at -21°, the same declared in the paper. Experimental engine can not reach very high knock pressures to preserve mechanical integrability of the engine itself: this is why it is equipped with an electronic control unit (ECU) able to delay spark timing whenever spontaneous ignition presents. To determine not just knock presence but also its intensity, a Bosh AKR sensor (knock recognition system) is installed in the engine: this sensor through a Fourier transform can convert knock intensity (in terms of pressure increasing) into a voltage output. As anticipated in the introduction section, knock can be easily detected by the presence of pressure waves, which have a much higher frequency than rotational engine one; through the Fourier transform, the sensor can distinguish knock caused pressure rise from the flame propagation one. An AKR 2V threshold is imposed to distinguish heavy from light knock, hence if sensor voltage output is higher than 2 V it is considered heavy, otherwise it is light.
To perform a fuel sensitivity analysis, a reference natural gas composition must be fixed.

Fuel Composition (%vol) yearly average		stdev (%vol)
CH_4	98.39	0.323
N_2	0.84	0.015
C_2H_6	0.44	0.179
C_3H_8	0.16	0.068
C_4H_{10}	0.1	0.012
CO_2	0.07	0.045
Main Fuel Properties		stdev
HCV_{Vol} [MJ/m^3]	37.94	0.101
Density [kg/m^3]	0.728	0.002

Figure 4.14: Reference natural gas composition

Figure 4.14 describes the fuel that has been taken as reference, provided by Czech grid operator data and reported in the experimental paper. Numbers in the table represent hydrocarbons and inerts volume percentages, so when converted into mass ones they need to be multiplied with the respective molecular weight. In order to let the engine knock, some heavy hydrocarbons are added to the fuel, and then a multiplicity of natural gas composition of different octane numbers is obtained.

Component	Volumetric fraction range
C_2H_6	0 – 0.12
C_3H_8	0 – 0.06
C_4H_{10}	0 – 0.03
H_2	0 – 0.25

Figure 4.15: Added hydrocarbons ranges

In figure 4.15 ethane (C_2H_6), propane (C_3H_8), butane (C_4H_{10}) and hydrogen (H_2) additions to reference natural gas composition are shown. Data as in the figure before are reported in volumetric fractions.
In order to summarize all kinds of fuel used in this investigation, figures below display composition of all kinds of natural gas used, converted into mass percentages. Standard deviations of reference natural gas composition have not been considered.

	Reference NG	Adding 5.5%vol ethane	Adding 12%vol ethane
methane	96,73%	87,76%	79,08%
ethane	0,82%	10,02%	18,92%
propane	0,44%	0,40%	0,36%
buthane	0,38%	0,34%	0,31%
N2	1,44%	1,31%	1,18%
CO2	0,19%	0,17%	0,16%

Figure 4.16: Natural gas composition with ethane addition

Figure 4.16 illustrates fuel composition in mass percentages when 5.5% and 12% in volumetric fraction of ethane is added to reference natural gas.

	Reference NG	Adding 1%vol propane	Adding 3%vol propane
methane	96,73%	*94,14%*	89,35%
ethane	0,82%	*0,80%*	0,76%
propane	0,44%	*3,11%*	8,05%
buthane	0,38%	*0,37%*	0,35%
N2	1,44%	*1,40%*	1,33%
CO2	0,19%	*0,19%*	0,18%

Figure 4.17: Natural gas composition with propane addition

Figure 4.17 illustrates fuel composition in mass percentages when 1% and 3% in volumetric fraction of propane is added to reference natural gas. Additions are considered separately, hence first column reporting reference fuel composition is the same in all the three illustrated tables.

	Reference NG	Adding 1%vol buthane	Adding 3%vol buthane
methane	96,73%	*94,14%*	89,35%
ethane	0,82%	*0,80%*	0,76%
propane	0,44%	*3,11%*	8,05%
buthane	0,38%	*0,37%*	0,35%
N2	1,44%	*1,40%*	1,33%
CO2	0,19%	*0,19%*	0,18%

Figure 4.18: Natural gas composition with butane addition

Finally, figure 4.18 illustrates fuel composition in mass percentages when 1% and 2% in volumetric fraction of butane is added to reference natural gas.
Equivalence between AKR knock voltage output and pressure increasing just due to compression ignition has been determined, exploiting pressure curves reported in the paper. The sensor is not having as output all kinds of pressure variation, but just the high frequency ones caused by pressure waves inside the cylinder and consequent values oscillation. Result obtained is 2.16 "knocking bar" per volt.

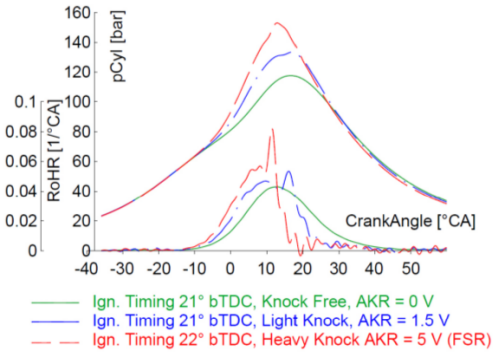

Figure 4.19: Pressure curves used for sensor signal conversion

In figure 4.19 different pressure curves are represented and AKR sensor voltage output is reported. Associating pressure rise due to spontaneous ignition (recognizable from the almost instantaneous heat release) to the reported voltage outputs, it is possible to derive the previously described 2.16 bar/V value. Distinction between flame propagation and compression ignition pressure rise in solver results has been made in the same way hence, applying the conversion value, a simulated sensor output can be obtained.
What results by this analysis is a very good knock representation when a considerable amount of ethane, propane or butane is added to reference fuel composition. In the other cases, CFD represented knock is quite heavy with respect to experimental one, probably because of the higher average flame path due to the bigger engine adopted. In any case, even when few amounts of hydrocarbons are added, simulated AKR voltage output does not overcome the value of 2 V, which is the threshold between light and heavy knock.
This accordance of results can lead to a good solver behavior, but it can be considered also a confirmation that the two combustion equations (c and c_{fresh} transport ones) involved in the solver do not interfere between each others in an undesired way.

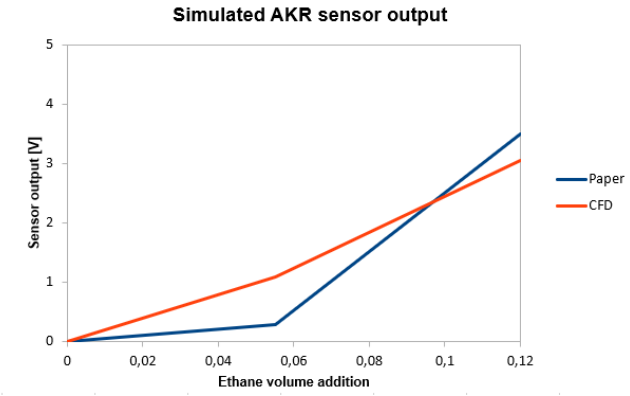

Figure 4.20: CFD simulation of voltage output sensor with ethane addition

As shown in figure 4.20, simulated and paper values are similar. Light knock

is presenting when 5.5% in volume of ethane is added to the reference fuel, and results are getting similar once higher quantity of ethane is added.

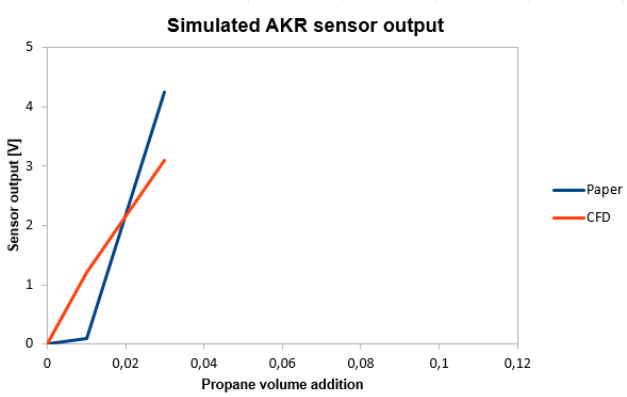

Figure 4.21: CFD simulation of voltage output sensor with propane addition

And when propane is added, as shown in figure 4.21, solver results are consistent if compared to ethane addition. In any case, if just 1% in volume of propane is added, light knock occurs; if the addition increases up to 3%, knock turns to be heavy.

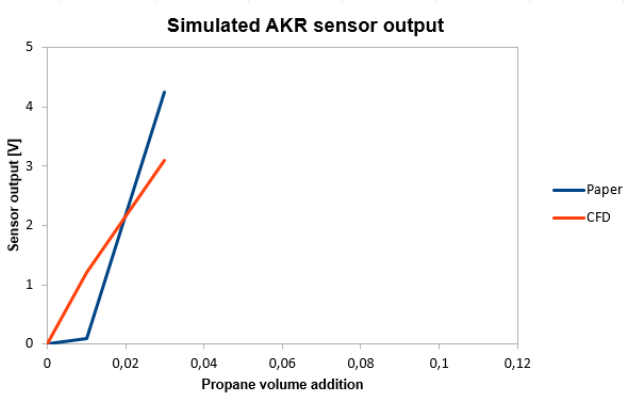

Figure 4.22: CFD simulation of voltage output sensor with butane addition

And results when butane has been added to natural gas are consistent with previous two already discussed cases. As figure 4.22 confirms, CFD and experimental paper knock results are similar when few amounts of hydrocarbons are added, while they get more different as fuel becomes heavier. As previously written, experimental engine combustion chamber geometry is not known, but also bore and stroke of the two are different; this can be a cause of inconsistency between CFD simulation and experimental reported results. What has to be highlighted is that whenever knock is described as light in the paper, also the one predicted in CFD simulation is; if knock detected by AKR sensor is heavy, also the computed one is.

4.2 Natural gas knock

In the introduction section, some physical flame and chemical behaviors have been discussed, focusing on the importance of flame development and how autoignition can be modeled defining a chemical reaction delay time. Passing from an isooctane to a natural gas knock study, two main things must be highlighted: isooctane flame is very fast and, because of the high temperatures reached for its octane number, autoignition is going to be heavy and to considerably speed up the final part of combustion.

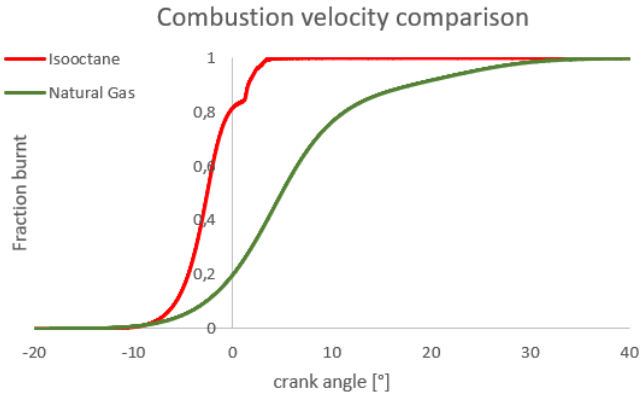

Figure 4.23: Combustion velocity fuel comparison

Adopting a compression ratio of 11.7 is prohibitive of an isooctane fuelled engine running with stoichiometric homogeneous charge, as knock intensity showed in the first subsection. From now on, the focus is pointed on natural gas and how its composition can influence engine knocking tendency.
Natural gas is not an easy manageable fuel for internal combustion engines because, as explained in introduction section, its composition can vary significantly region by region, influencing its chemical properties. Always in the introduction section, a reference natural gas derived from North Europe data composition has been chosen (displayed further on in table 4.2), presenting almost 7% of inert gases. If compared to methane as it can be see by figures below (4.24 and 4.25), when knock is not occurring, pressure and heat release curves of two different natural gas are very similar. Spark timings used in this section are the ones displayed in figure 3.52, as they maximize working points efficiency.

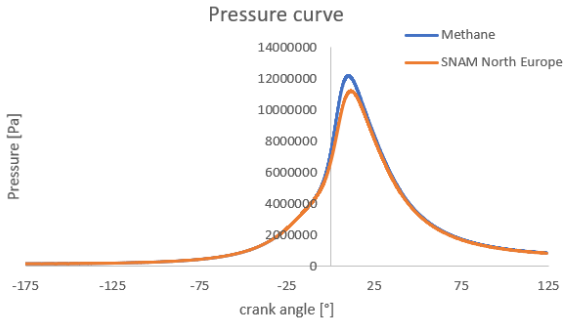

Figure 4.24: Pressure curve comparison between different natural gas composition

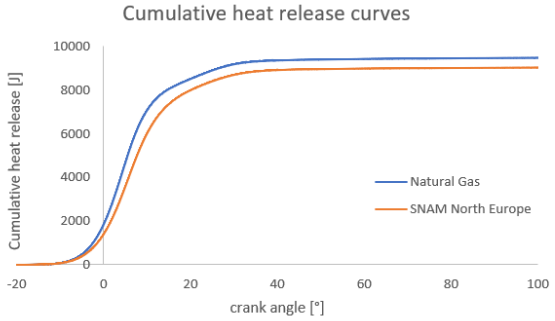

Figure 4.25: Cumulative heat release comparison between different natural gas composition

Lower heating values of the hydrocarbons present in natural gas are very similar, hence they do not lead to any appreciable difference in pressure or heat release curves: if two natural gas with both no inerts and no knock presence are compared, resulting curves will be coincident. This is not entirely valid if some inerts are present in the gas composition: fuel lower heating value decrease as figure 4.25, hence maximum pressure in figure 4.24 is affected. But as it can be deduced by heat release curves, the flame propagation phases (ignition delay, combustion development and its completing) do not vary appreciably, and no visible difference is present in specific flame propagation quantities.
Another very important characteristic of SNAM North Europe natural gas fuelled case is the complete absence of spontaneous ignition: no rough increase in both heat release and pressure curves occurs. In consistency, if normalized c_{fresh} value is plotted (as in figure 4.26), it does not overcome the value of 0.5%, leading to a negligible heat release.

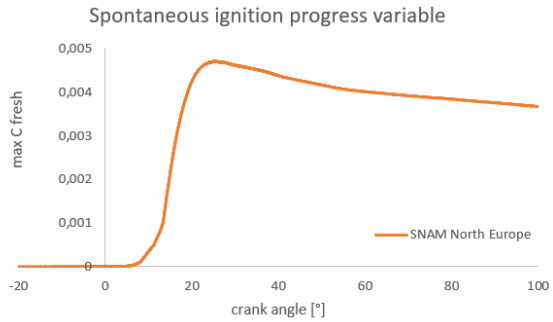

Figure 4.26: Compression ignition progress variable of natural gas considered

This kind of consideration is numerically important, because it is showing that there is no interaction between c and c_{fresh} equation implemented in the solver, meaning that flame propagation and its heat release are not affected by the addition of a different progress variable. To have some autoignited mixture fraction, fuel composition needs to be changed in a heavier one, with no inerts to enhance knock presence hence richer in propane and butane. Therefore, a very heavy natural gas composition is introduced, as illustrated in the table below.

	SNAM	heavy Natural Gas
Methane	81.88 %	84 %
Ethane	7.65%	8%
Propane	2.28%	6%
Butane	1.23%	2%
Nitrogen	3.77%	
Carbon Dioxide	3.19%	

Table 4.2: Natural gas composition in mass percentages

In table 4.2, also reference "SNAM" natural gas is reported in order to perform a comparison between the two. In the introduction section, time influence on compression ignition occurring has been emphasized, as one of the main phenomenon parameters. To verify its influence, a constant torque sweep has been performed with the "heavy Natural Gas" just edited, in order to understand how knock behaves in a natural gas fuelled engine and how it is influenced by combustion duration.

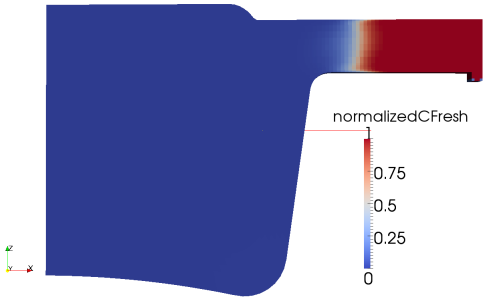

Figure 4.27: Natural gas knock region

As shown by figure 4.27 that catches the 1200 rpm case at 20° after top dead centre, knocking region is not changed since it is always interesting the most external cylinder region not already reached by the flame front. Natural gas compression ignition is very violent, with an almost instantaneous pressure rise as happened for isooctane. All the cases considered (from 1000 to 1900 rpm) are simulated in correspondence of spark timing optimization point, as derived in section 3.1 and illustrated in figure 3.52 of section 3.4. The slower natural gas flame velocity is of course a parameter increasing spontaneous ignition occurring probability, even if pressure and temperature rises are going to be smoother. At contrary, engine cooling and heat transfer to the wall are decreasing combustion chemical reaction velocity, but in this study engine cooling system is not investigated.

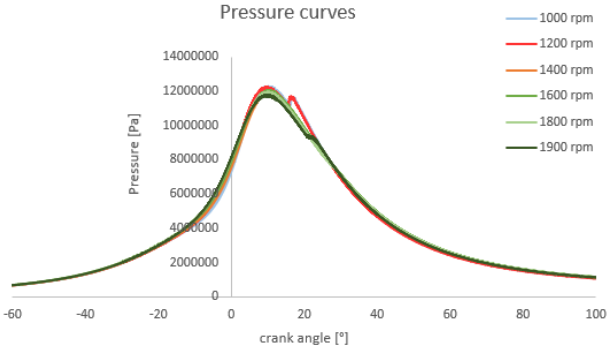

Figure 4.28: Pressure curves of knocking natural gas fuelled engine

As it can be seen by figure 4.28, even if a heavy fuel is used, spontaneous ignition is very delayed: both rounded (due to flame propagation) and vertical (due to compression ignition combustion) pressure maximum values are clearly visible, with the first one higher than the second in all the computed cases. Low engine speeds present a more severe knock with respect to the higher ones; 1000 and 1200 rpm pressure curves are almost coincident, while from 1400 to 1900 rpm compression ignition pressure increase is slightly visible. With such a delayed knock, pressure underlying area gain because of a faster combustion

is very small, and this is a very important consideration for spark assisted compression ignition engine development.

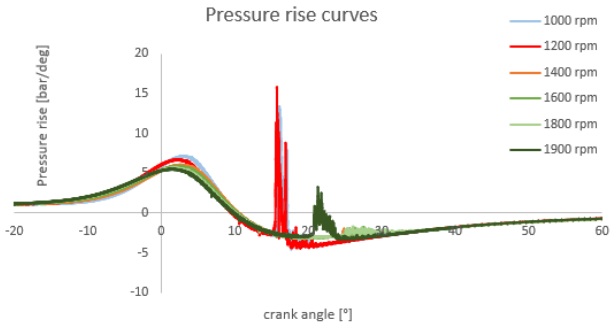

Figure 4.29: Pressure rise curves of knocking natural gas fuelled engine

Pressure rise curves displayed in figure 4.29 are very consistent with what happened when isooctane was used as fuel. Even if absolute pressure increase is not that evident, pressure rise maximum value in 1000 and 1200 rpm cases is comparable with supposed engine limit. When rotational speed gets higher, knock still occurs but its magnitude is very low: at 1400, 1600 and 1800 rpm it is present but it is so delayed to be hardly recognized, while at 1900 rpm it is more visible having a pressure rise maximum value of 2 bar/deg. Then time has a strong influence on autoignition presence and strength, but also temperature is a very important parameter to be considered.

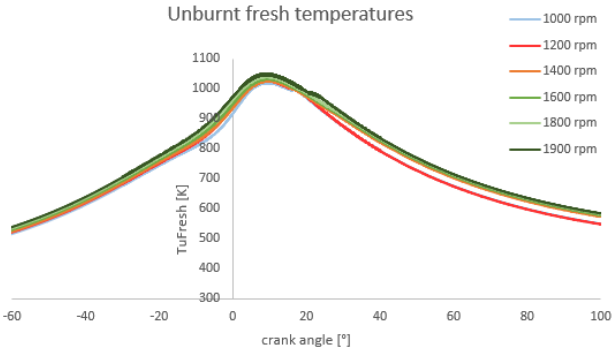

Figure 4.30: Unburnt fresh temperature curves of knocking natural gas fuelled engine

Unburnt fresh gases are that portion of the air-fuel mixture which is not already reached by the flame front, hence not any chemical reaction has been performed. Other unburnt gases such as nitrogen are homogeneously distributed in the whole combustion chamber, but they have not the possibility to perform any wanted combustion reaction. Fuel air mixture located in the external region have the potentiality to autoignite before flame propagation, hence this unburnt fresh temperature chart is referred to the most external part of the cylinder.

"TuFresh" is also the input necessary to obtain corresponding pvS, source term of spontaneous ignition progress variable. Fresh unburnt mixture temperature increases because of compression and of the gradient originated from the flame, but its values are far from the over 2200 K of the burnt gas region. Because of the lower time available for heat transfer, when rotational speed increases unburnt gas temperature gets always higher, and cylinder conditions become more severe for knock.

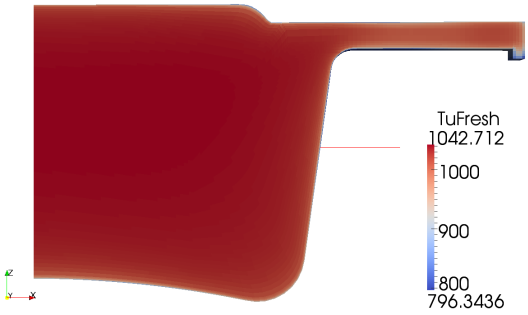

Figure 4.31: Unburnt fresh temperature values in the whole cylinder

In addition, by figure 4.31 displayed above, TuFresh (as "unburnt mixture fresh temperature") values are almost uniform in the whole cylinder, with the only exception for regions very close to cylinder walls, strongly influenced by heat losses. In the introduction section it has been reported that combustion reaction velocity and autoignition delay have a square dependency on temperature, as in equation 1.10. This behavior seems to confirm that experimental correlation, since 1900 rpm case presents an appreciable pressure rise if compared to some lower engine speed cases, and at the same time it is the one with the highest TuFresh values.
Therefore, the histogram reported below shows how autoignition strength varies between the different rotational speeds, as it has been defined as the portion of volume interested by compression ignition combustion.

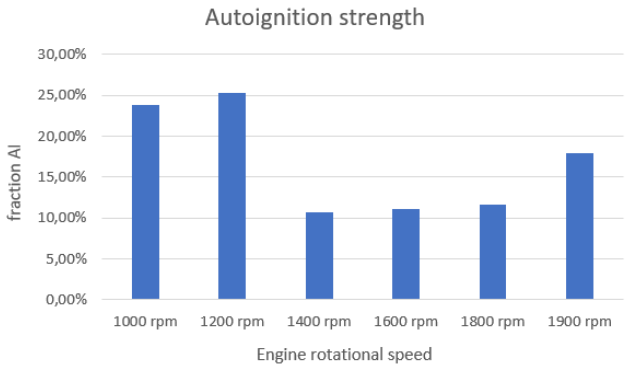

Figure 4.32: Autoignition strength in constant torque sweep

This not continuous knock behavior with engine speed is obtained because 1° of $\Delta\theta$ in spark timing optimization phase has been set. Rate of heat release (figure 4.33) is another good indicator for compression ignition; as happened for isooctane knock, it presents two maximum values, in perfect consistency with autoignition strength histogram and pressure rise curves.

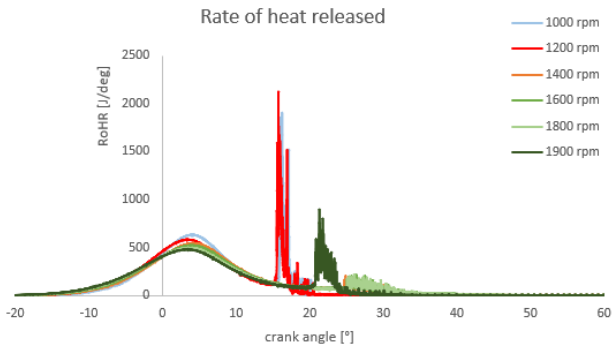

Figure 4.33: Rate of heat release of knocking natural gas fuelled engine

If a further focus is pointed in unburnt fresh temperature curves of figure 4.30, one can see a little detach between heavier knock occurring curves and the others just after autoignition. Because of the geometry of engine simulated, knock takes place in squish area region, which is distant for the flame to be reached, hence compression ignition should contribute in an increasing of both kinds of temperatures values (weighted averaged and unburnt fresh one). But wall heat transfer is hugely affected by knock presence, as shown in figure 4.34 displayed below.

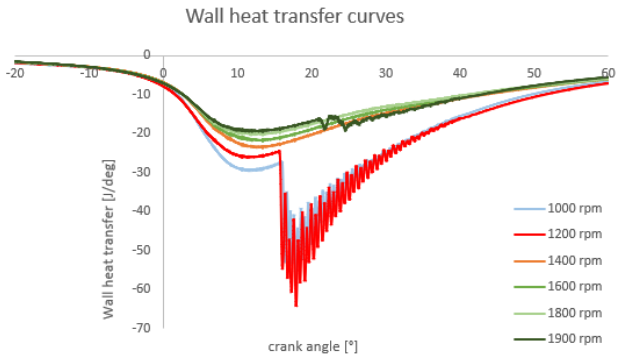

Figure 4.34: Wall heat transfer of knocking natural gas fuelled engine

Especially in 1000 and 1200 rpm heat transfer curve, a very vertical heat loss increasing is present. This is actually the result of the pressure waves generated: they propagate in the whole combustion chamber and rebound in correspondence of cylinder walls, and both these phenomena increase fluid kinetic energy of the already burnt mixture inside the cylinder.

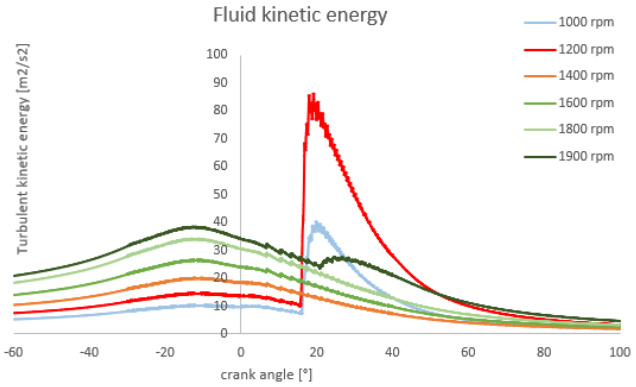

Figure 4.35: Turbulent kinetic energy of knocking natural gas fuelled engine

As predicted, turbulent kinetic energy has a very similar behavior to wall heat transfer in knock correspondence, providing a reliable explanation of such a temperature behavior.
Solver in the end can represent all main knock characteristics, from rapid pressure and temperature increase to the presence of waves inside the CFD domain. To complete this knock study, fuel composition has been changed in order to consider a wide multiplicity of fuels; according to what has been described in section dedicated to natural gas, huge variations of ethane, propane and butane mass percentages were considered. Therefore, the figure below highlights a "knocking area" (fuel composition such that knock occurs) and a "not knocking area" (knock safe natural gas composition) for the engine considered at 1000 rpm, in optimal efficiency case. on x axis, mass percentage of propane; on y axis, mass percentage of ethane. Therefore, methane composition of natural gas

simulated is:

$$\%methane = 1 - \%ethane - \%propane - \%butane \tag{4.2}$$

with butane amount fixed per plane and no inerts considered. If the natural gas is richer in heavy hydrocarbon composition it is much more knock inclined fuel; otherwise, it is a good octane number fuel if methane composition gets higher.

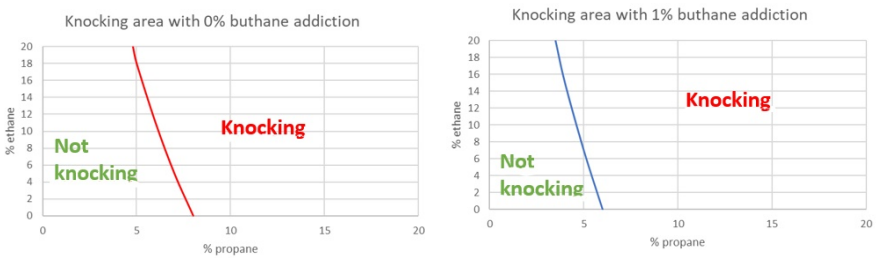

Figure 4.36: Natural gas knocking areas

From figures above, it is possible to notice how engine is knocking only if very heavy fuels are used. Inerts were not considered in this section, and their presence is surely increasing fuel octane number. In any case, natural gas composition used for this knock analysis is very unlikely, as the brief research in different fuel composition shows. If a spark assisted compression ignition is wanted, engine designers must increase the compression ratio in order to have more spontaneous ignition strength and stability. Even by figures illustrated in this section engine performances and their spark timing optimization are influenced considerably by the composition of natural gas used, hence another good target of this study is to perform a sensitivity analysis addressed to natural gas composition, to quantify its influence on engine performances.

4.3 Boundary conditions and temperature wall function analysis

As introduced in section 2, modeling heat transfer to the walls of an internal combustion engine is not trivial, hence boundary conditions and wall functions must be imposed in order not to include in the CFD domain regions external to the combustion chamber. As illustrated in table 3.2 of section 3, a different wall temperature is known for each wall and working point, while cylinder ones are a result of conservation equations solution. A first focus is pointed on kinds of boundary conditions chosen for each wall, while in the second part of this subsection a comparison between Angelberger and Huh Chang wall functions has been performed.

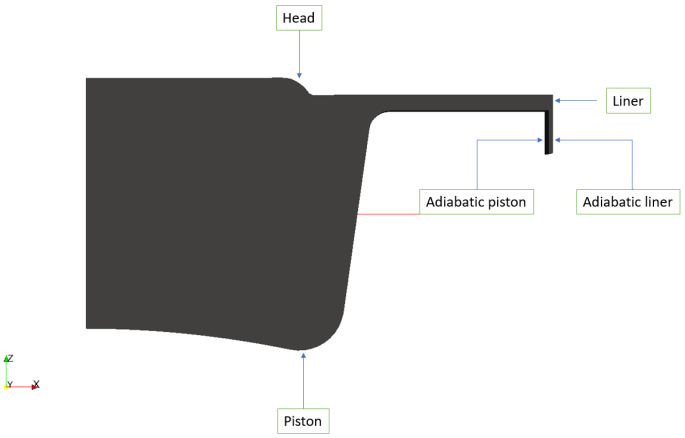

Figure 4.37: Cylinder walls names

In figure 4.37 different cylinder walls are illustrated, as well as how they are called. Head, piston and liner are the main ones most conditioning heat transfer values, while "adiabatic piston" and "adiabatic liner" are closing crevice region. While head and piston areas are fixed within power cycle, liner surface changes, presenting a maximum value in correspondence of bottom dead centre and a minimum one at the top dead centre. Adiabatic walls are so called because it is possible to assume no heat transfer in a complete spark ignition combustion, but this could be a considerable mistake when knock is considered. Two different walls boundary condition can be imposed to the solver:

- zeroGradient which assumes the selected wall adiabatic

- fixedValue which keeps the selected wall temperature constant in the cycle

For head, piston and liner the "fixed value" boundary condition has been applied, selecting temperature values illustrated in table 3.2. As the name suggests, for adiabatic walls "zero gradient" boundary condition can be chosen, but a comparison between the two has been performed to verify if it influences knock presence. As previously discussed, when these kinds of walls are considered adiabatic, knock begins very close to crevice region, as illustrated in figure 4.38.

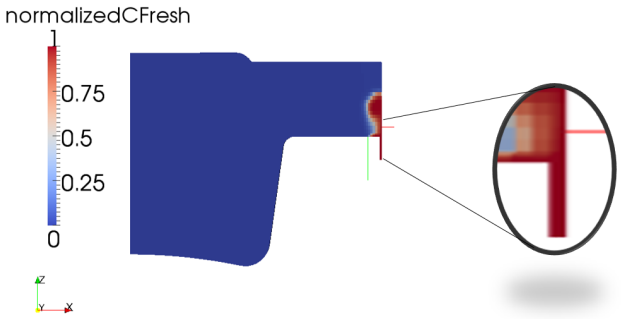

Figure 4.38: Autoignition principle if crevice walls are considered adiabatic

Spontaneous ignition hence starts between adiabatic piston and adiabatic liner, to then propagate inside the combustion chamber. If these two walls can exchange heat (then a "fixedValue" boundary condition is imposed to the solver), heat losses in correspondence of that region is very low, if compared to minimum heat transfer values.

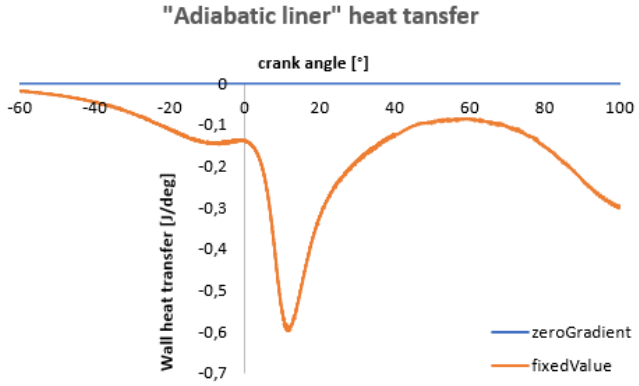

Figure 4.39: "Adiabatic liner" wall heat transfer comparison

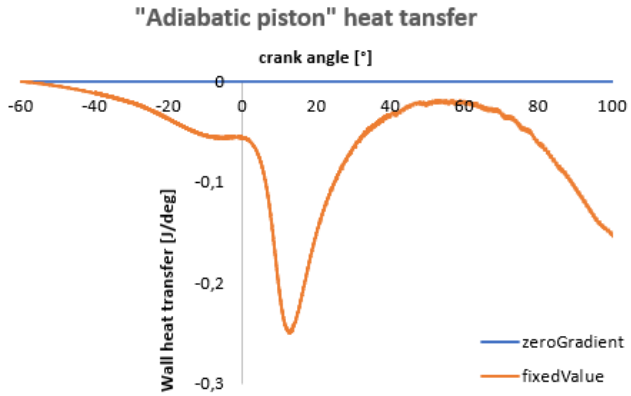

Figure 4.40: "Adiabatic piston" wall heat transfer comparison

Figures 4.39 and 4.40 display heat losses values through these walls, applying to both adiabatic walls a "fixedValue" boundary condition, imposing the liner temperature (around 440 K) to "adiabatic liner", and the piston temperature (around 530 K) to "adiabatic piston". Minimum of global heat transfer value was in the order of magnitude of -30 J/deg, and values reported in both figure 4.39 and 4.40 are very low. When zeroGradient boundary condition has been set, no heat transfer can occur a priori; when a fixedValue boundary condition is chosen, wall temperatures are constant and heat transfer coefficient α_t is determined through selected wall function.

Figure 4.41: Same case of before but crevice wall are not considered adiabatic

In any case, this very low heat values difference lead to a very important consideration: when zeroGradient boundary condition has been applied, knock occurs as shown in figure 4.38; when fixedValue boundary condition has been imposed, no knock presence is detected as figure 4.41. This result entirely depends on heat transferred occurring in these walls: if also head, piston and liner ones are compared, curves are perfectly coincident but in knock presence.

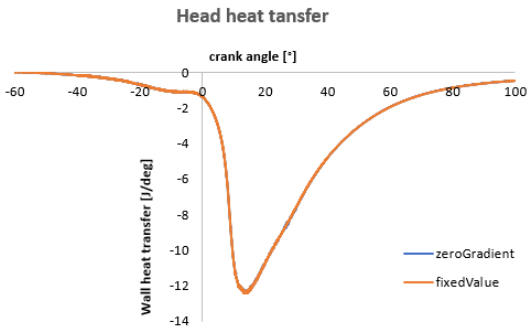

Figure 4.42: Head heat transfer in adiabatic walls boundary condition comparison

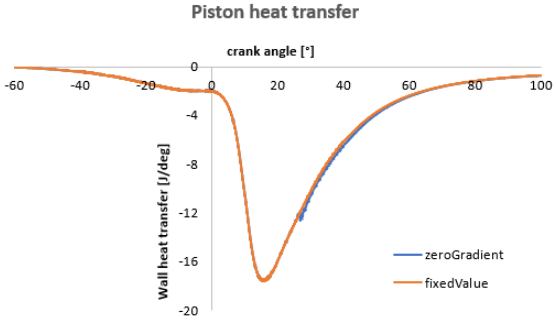

Figure 4.43: Piston heat transfer in adiabatic walls boundary condition comparison

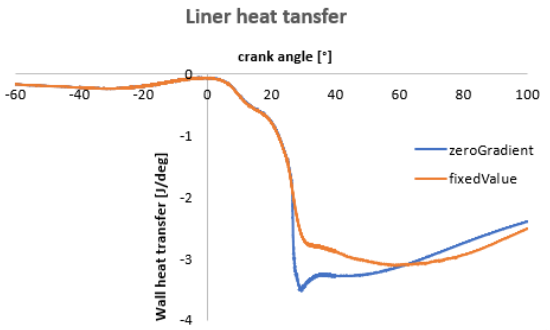

Figure 4.44: Liner heat transfer in adiabatic walls boundary condition comparison

As shown by figure 4.42, 4.43 and 4.44, curves are perfectly coincident with just a liner heat transfer detach because knock occurs very close to that region. Surely even in knock absence using fixedValue boundary condition contributes to increase heat transfer computed, but not in such a way to compensate experimental and simulated value difference detected when validation has been performed.

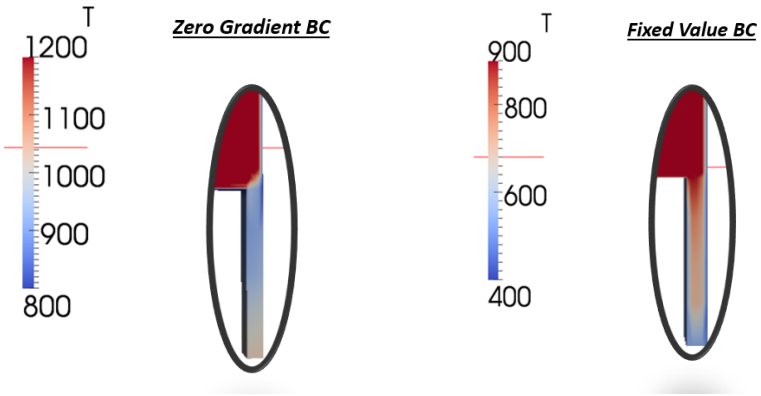

Figure 4.45: Crevice temperatures when different boundary conditions are applied

In figure 4.45 there is a CFD visual representation of that heat losses effects. Both "adiabatic walls" heat transfer minimum values summed together are between -0.8 J/deg and -0.9 J/deg, but if focus is pointed on local temperatures it is possible to see how different they are: when zeroGradient boundary condition is applied, temperatures are in a range of 950 - 1100 K, while in fixedValue BC case they are few hundreds of kelvin lower. Hence in leftwards case knock starts at the very bottom of the region illustrated, which in more realistic representations it is cooled down by walls presence. In conclusion, if zeroGradient boundary condition is applied, simulated knock is very delayed (over 30° after top dead centre) because that region is very difficult to be reached by flame front, but it is very unlikely because it is actually cooled by walls presence.

"FixedValue" boundary condition offers a much more realistic simulation, and it is the only one applied from section 5 on.
As anticipated at the beginning of this subsection, also a wall function comparison has been performed. Angelberger WF is the one used so far. Huh Chang wall function has been developed to have a more realistic representation of heat transfer in HCCI combustion, where influence of pressure waves is huge. Target of different wall functions is computing α_t, heat transfer coefficient used to determine heat losses. Huh Chang wall function is composed by one steady term and a time-dependent transient term, as explained in [18].

$$\dot{q}_{wall,HC} = \frac{k}{l}(T_m - T_l) + k \sum_{n=1}^{N} \Phi_n [(A_n + B_n) cos(n\omega t) - (A_n + B_n) sin(n\omega t)] \quad (4.3)$$

The presence of a time dependent term makes this formula better behaving in correspondence of huge pressure waves inside the cylinder. HCCI combustion is considered too violent and very difficult to control, hence huge pressure waves must be considered in heat transfer formula.
Angelberger expression is much closer to standard wall functions ones:

$$\dot{q}_{wall,AN} = \frac{\rho c_p u_\tau T ln(\frac{T}{T_{Wall}})}{2.075 ln(y^+) + 3.9} \quad (4.4)$$

As already remarked, this last wall function is the one used in section 3 where engine validation has been performed. For a brief remind, almost all computed heat transfer curves were underestimated, especially in cumulative terms. Minimum values were close to the experimental ones when engine regime was not high, and even its timing was almost correct. Curves detached after they reached minimum values, causing cumulative heat transfer differences of more than 25% in the worst cases. With this comparison, the author wants to verify that the used wall function is the best one fitting the experimental data, since, as many case in CFD, there is not an "a-priori" best one to be used.

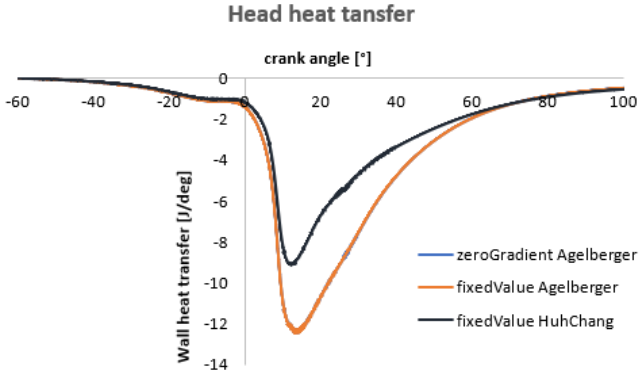

Figure 4.46: Head heat transfer wall functions comparison

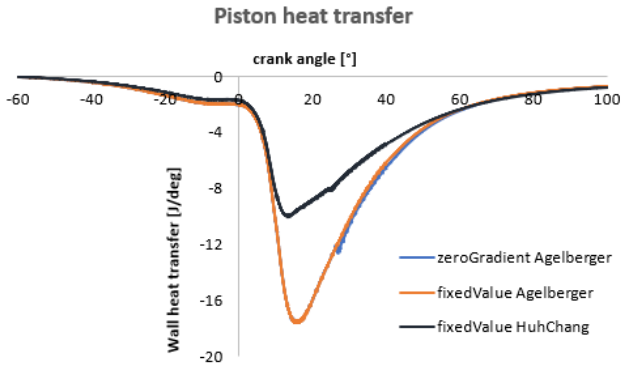

Figure 4.47: Piston heat transfer wall functions comparison

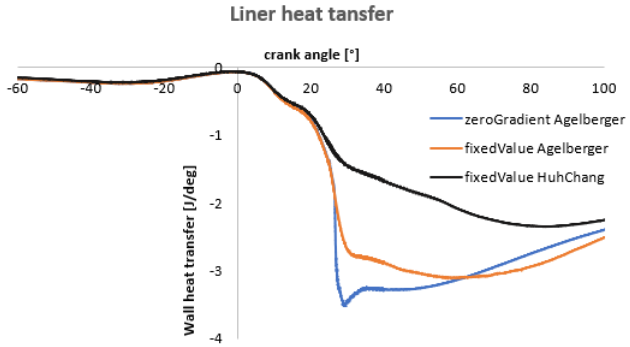

Figure 4.48: Liner heat transfer wall functions comparison

As it can be seen by figures 4.46, 4.47 and 4.48, Huh Chang is further underestimating heat transfer in correspondence of the three main cylinder walls. In compression stroke and in combustion developing phase, all the three derived curves are almost coincident, but after combustion development the detach is clear with an always lower heat losses estimation of the Huh Chang wall function with respect to the Angelberger one.

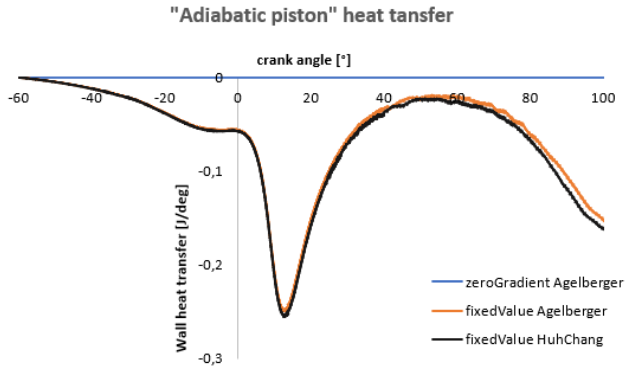

Figure 4.49: "Adiabatic piston" heat transfer wall functions comparison

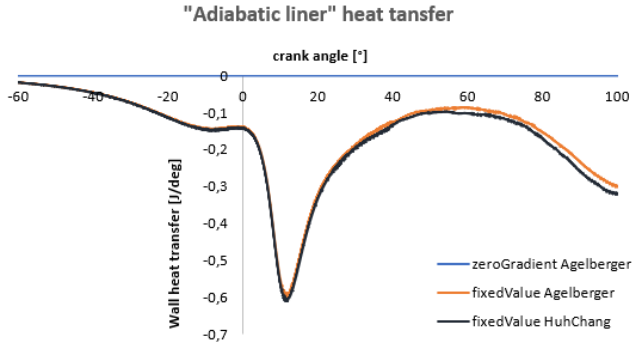

Figure 4.50: "Adiabatic liner" heat transfer wall functions comparison

While main combustion chamber heat losses are hugely underestimated by Huh Chang wall function, figures 4.49 and 4.50 show that heat losses curves of crevice region walls are almost coincident. But in the end this wall function used in HCCI engine simulation is considerably underestimating heat losses. As happened when the two boundary conditions were compared, this heat losses underestimation provokes a knocking region.

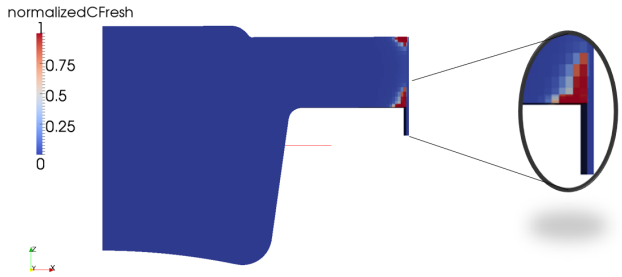

Figure 4.51: Simulated knock when Huh Chang wall function is used

As illustrated by figure 4.51 displayed above, simulated knock occurs when Huh Chang wall function is used, even if "fixedValue" boundary condition is imposed to adiabatic walls. In any case, this kind of knock is different with respect to the one obtained before: in the previous case, it started from crevice region to then propagate inside the combustion chamber, but in this one it is originated in correspondence of both piston and head walls. Mixture in crevice region does not chemically react because it is cooled down by "adiabatic walls", presenting also very low turbulence values. Even if this kind of knock is originated by a heat transfer underestimation, this analysis provides a better idea of where it starts and how it develops: knock obtained in "zeroGradient" boundary condition case is just numerical, starting in a region where spontaneous ignition presence is almost impossible; this kind of knock, even if it is caused by a huge heat losses underestimation, has a much more realistic point of origin to then propagate inside the combustion chamber, as the others did.
In conclusion, from this section several useful results have been obtained: solver including knock has been validated using an experimental publication, knock as

represented in the solver has been analyzed identifying its most important physical and numerical peculiarities, influence of natural gas composition has been investigating and, in the end, importance of wall heat transfer influence of knock has been highlighted. From now on, Angelberger wall function has been used to not have a further heat transfer underestimation with respect to experimental working point data of section 3, and fixedValue boundary condition has been imposed to avoid numerical knock. Figure 4.52 briefly summarizes different wall function heat transfer values obtained in this last subsection analysis.

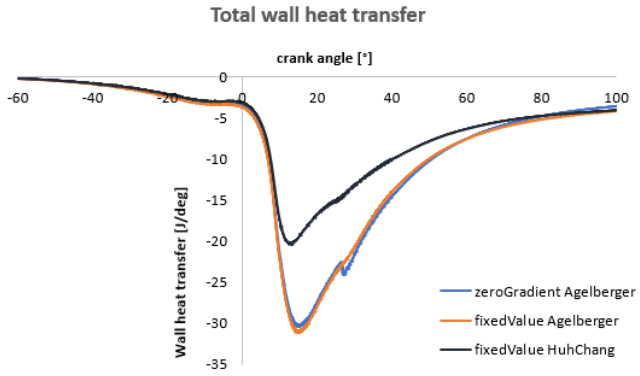

Figure 4.52: Total heat transfer wall functions comparison

For a spark assisted compression ignition (SACI) engine development, a stable spontaneous ignition must be achieved, without sacrificing accuracy of solver results. As a consequence, engine compression ratio must be increased, in order to reach more severe pressure and temperature values and have a stable and reliable natural gas compression ignition, leading to engine performance advantages.

Chapter 5

SACI engine development

In previous section CNG-heavy duty engine could knock only if powered with very heavy natural gas, unlikely to be found in ordinary fuel stations. To develop a SACI (spark assisted compression ignition) combustion, spontaneous ignition must be reliable and under control, not depending on kind of natural gas used. Therefore, compression ratio has been increased to have higher pressures and temperatures and then enhance fresh air-fuel mixture autoignition. This leads to a redesign of the combustion chamber, performed in such a way to increase the compression ratio adopted but to not introduce significant changes on piston shape.

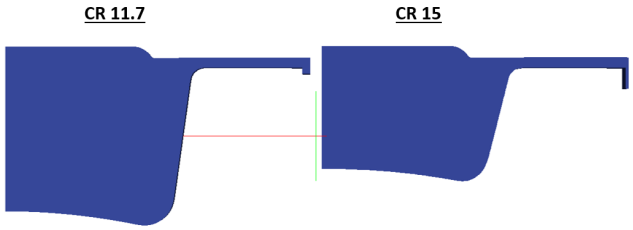

Figure 5.1: Combustion chamber shapes at top dead centre

As it is possible to see in figure 5.1 where original design and the new one are compared, volume at top dead centre of increased compression ratio chamber is far way lower. Parameters such as bore and stroke are not changed, so this kind of modification practically implies just a substitution of the original piston with a new one. As a consequence, even head cylinder shape remains the same, while the size of the crevice region has been kept as similar as possible between edited designs. A multiplicity of engines working with different compression ratios has been investigated, all of them obtained with a volume reduction that maintains constant during the whole cycle, as shown in figure 5.2. By both figures 5.2 and 5.3, considering the same working points (characterized by initial cylinder pressure and temperatures values) a lower mass of fuel is injected inside the cylinder.

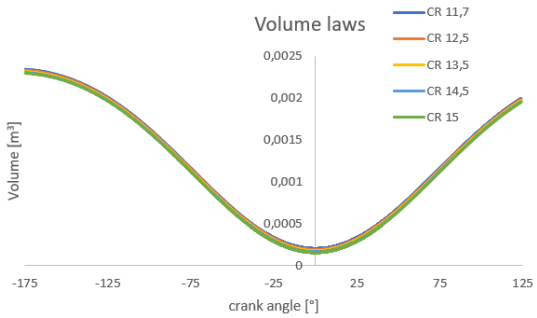

Figure 5.2: Volume variation with compression ratio

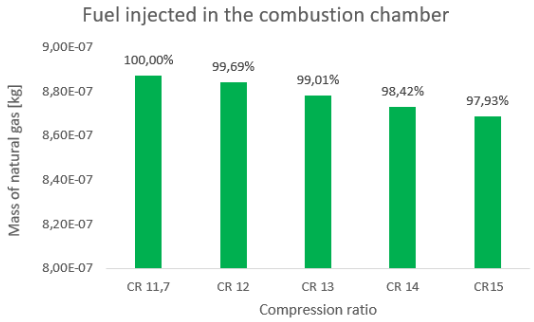

Figure 5.3: Mass of fuel injected in different compression ratio engines

This leads to a first advantage in terms of efficiency: as shown in figure above, for the same initial pressure and temperature values, in the CR 15 case fuel amount is more than 2% lower with respect to the reference one at CR 11.7. In addition, since a better thermal efficiency is predicted, even gross indicated work should increase, leading to another efficiency benefit. Also knock must be taken into account: in a spark assisted engine, it needs to be controlled to be exploited for a more ideal constant volume combustion. At this purpose, two different solvers are used in this section:

- betaFlameletXiEngineDyMFoam: including b equation

- betaFlameletSACIXiEngineDyMFoam: including b and c_{fresh} equations

As briefly described, the just "Xi" solver can not consider autoignition, and as a consequence it is possible to simulate very extreme compression ratio engines without any knock presence. "SACI" solver instead includes both flame propagation combustion and chemical reaction delay time, computing also heat released by a possible mixture autoignition. A comparison between these two solver results is very important to isolate combustion mode influence from all the other parameters that affect the power cycle, and to have clearer advantages and disadvantages concerning just spontaneous ignition.
To conclude this last section introduction, in figure 5.4 a render image of the combustion chamber adopting a compression ratio of 15 designed using the software Autodesk Inventor is illustrated. It is possible to see how important the

squish region is to generate turbulences inside the whole cylinder, as much as combustion volume is far way lower with respect to 11.7 CR one. To have such a small space for combustion leads to a delayed optimum spark timing, because average flame path length is lower and it needs lower time to be covered.

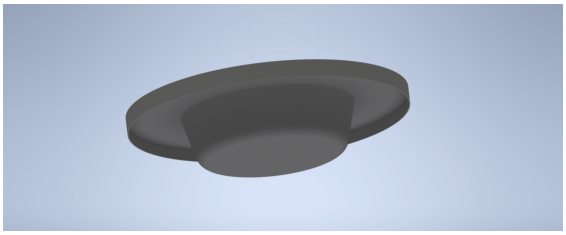

Figure 5.4: Autodesk inventor design render, with 15 as CR

5.1 Spontaneous ignition effects on engine performances

As already proved, spontaneous ignition can be very rough and violent, stressing in a dangerous way mechanical components of the engine. Due to the almost instantaneous heat release, it is possible to reach very high cylinder pressures and, if bad controlled, it can turn into heavy knock. For this reason, not all the working points in the engine map can work using a SACI combustion mode, but to protect engine mechanical structure two different pressure limits are introduced: an absolute maximum value slightly above 180 bar, and a pressure rise not to overcome 18 bar/deg.
Therefore not all the working points in the engine map are suitable for a spark assisted compression ignition combustion, but just the ones at half load or lower. In the figure below engine map is revisited, with SACI combustion target points drawn in green, while entirely flame propagation combustion ones in red. Low load thermal efficiency were the most penalized in the optimization section. In addition, at high loads knock is more likely to occur, hence to be able to perform both kinds of combustion for the same regime (as it happens for 1200 and 1600 rpm) can be complicated. At first analysis, SACI has been developed for 1200 rpm 52% load working point; then feasibility of entirely flame propagation combustion at full load is verified.

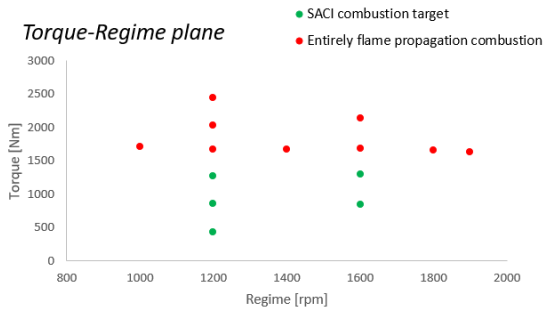

Figure 5.5: Revisited engine map, showing SACI points target

As previously described both solvers have been used, indicating with "Xi" the one considering just flame propagation, while with "SACI" the one considering both flame propagation and autoignition. In this analysis, the focus is pointed on gross indicated work variation between the two combustion modes and the compression ratio of 15 has been chosen for this comparison.

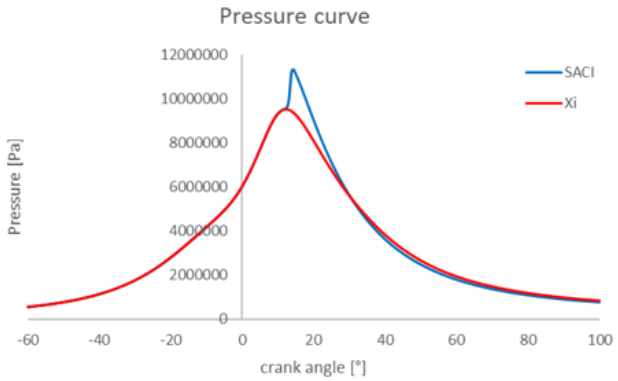

Figure 5.6: Pressure curves obtained by both solvers in the same initial conditions

As illustrated in figure 5.6, spontaneous ignition occurs in correspondence of maximum pressure value, evidently increasing SACI solver curve underlying area. A spark timing of -16° has been imposed to both the cases, as well as SNAM North Europe derived natural gas composition (the same that could not autoignite in section 4) has been used. Because of spontaneous ignition, pressure maximum value increases considerably, over than 20% in relative terms. Especially regarding cumulative heat release curve of figure 5.7, one can appreciate how fast compression ignition combustion is in homogeneous mixture conditions: in the case where it is included in the solver, combustion ends between 13-14° crank angle, almost 20° before entirely flame propagation combustion is completed. This of course leads to a very severe and dangerous pressure rise, that overcomes enormously the already high assumed limit.

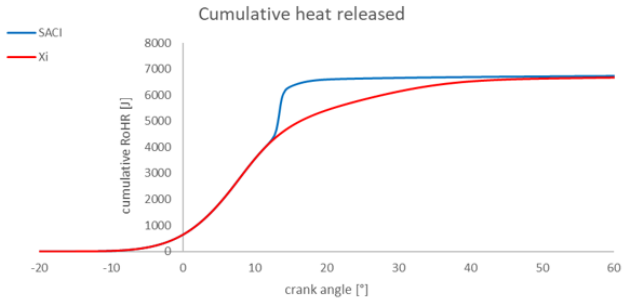

Figure 5.7: Cumulative heat release curves obtained by both solvers in the same initial conditions

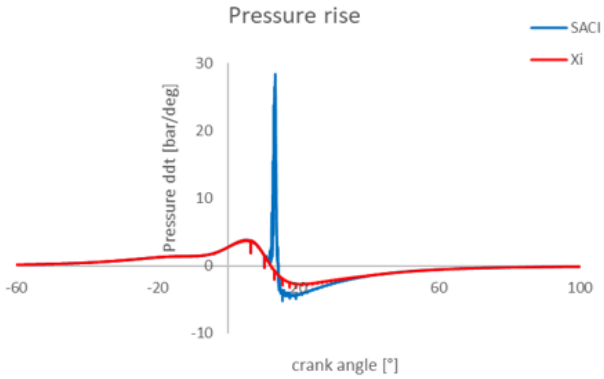

Figure 5.8: Pressure rise curves obtained by both solvers in the same initial conditions

As shown in figure 5.8, pressure rise is close to 30 bar/deg, more than 12 bar/deg over the engine limit but, since this analysis is focused on efficiency variation, this is not the main analysis target at the moment. If cumulative gross indicated works are compared, result obtained seems in contradiction with pressure curves previously illustrated. As shown in figure 5.9, after spontaneous ignition occurs curves intertwine two different times: at the very beginning where SACI one takes benefits of the faster combustion, but in the end of the expansion stroke gross indicated work curve computed by "Xi" solver gets higher, resulting in the end to have a better thermal efficiency.

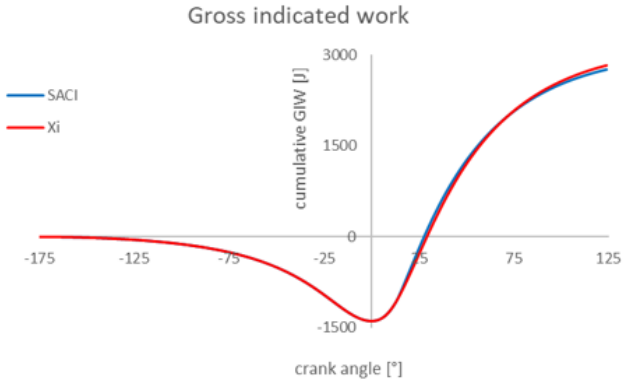

Figure 5.9: Gross indicated work curves obtained by both solvers in the same initial conditions

It is hard to detect differences in curves behaviors of figure 5.9 because they are almost coincident, and it is also hard to recognize by sight which one is presenting higher or lower values. To have a better knowledge of work during the cycle, instantaneous gross indicated work is computed as illustrated in the equation below:

$$GIW_{instantaneous} = \frac{p \cdot \Delta V}{\Delta \theta} = \frac{\frac{p_i + p_{i+1}}{2} \cdot (V_{i+1} - V_i)}{\theta_{i+1} - \theta_i} \tag{5.1}$$

In equation 5.1, "i" stands for time step considered, "p" for cylinder pressures, "V" for combustion chamber volume and, in the end, "$\Delta\theta$ for the time step used computed in crank angles. In this way it is much easier to follow gross indicated work variation during the cycle, as in figure 5.10.

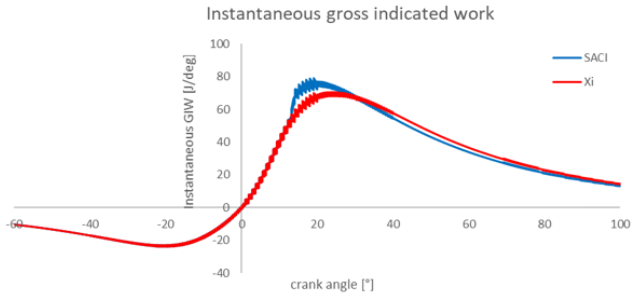

Figure 5.10: Instantaneous gross indicated work curves obtained by both solvers in the same initial conditions

Before top dead centre, instantaneous gross indicated work is negative because piston motion is compressing air fuel mixture. In the expansion stroke, work gets higher because of combustion presence, and cumulative gross indicated work as figure 5.9 is considering both work spent in compression stroke and useful one derived from expansion stroke. Returning to figure 5.10, the two curves are coincident up to spontaneous combustion presence, which increases blue curve pressure values hence instantaneous work made by burnt gases. Even if the detach is clear, in less than 20° the curves crosses, and expansion computed by "Xi" solver is clearly more efficient with respect to the one computed by the "SACI" one whenever combustion process is completed.
As predicted by the theory, knock is characterized by the presence of huge pressure waves increasing the heat transferred to the walls. As figure 5.11 confirms, in knock presence minimum wall heat transfer values become huge, affecting cylinder temperature hence useful work in the expansion stroke.

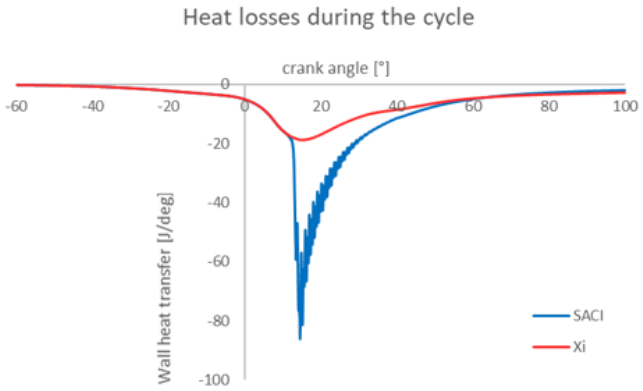

Figure 5.11: Wall heat transfer curves obtained by both solvers in the same initial conditions

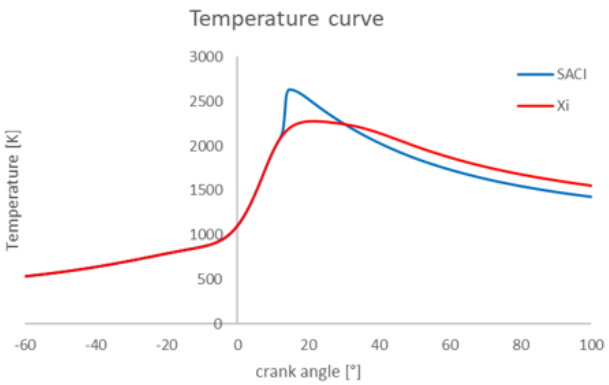

Figure 5.12: Temperature curves obtained by both solvers in the same initial conditions

Wall heat transfer minimum value in knock presence is more than four times lower than the one computed by solver "betaFlameletXiEngineDyMFoam" reported in red. Effects on temperature curves are enormous, since immediately after compression ignition weighted average maximum values are higher of 300 - 400 K, but then burnt mixture cools down in a very fast way and blue curve negative slope after compression ignition is considerable. Burnt mixture has hence less energy to be exploited for almost all the second part of the expansion stroke, and cumulative gross indicated work gets lower at the end of the cycle. This leads to a sort of paradox, because with spark assisted compression ignition a more ideal combustion mode has been reached, but losses are so important to considerably reduce power cycle work and efficiency. As it can be deduced by heat release curve, autoignited mixture fraction is in the order of magnitude of 40%, which is very high in homogeneous mixture condition. Figure 5.14 displayed below shows spontaneous ignition principle timing related to fraction burnt because of flame propagation.

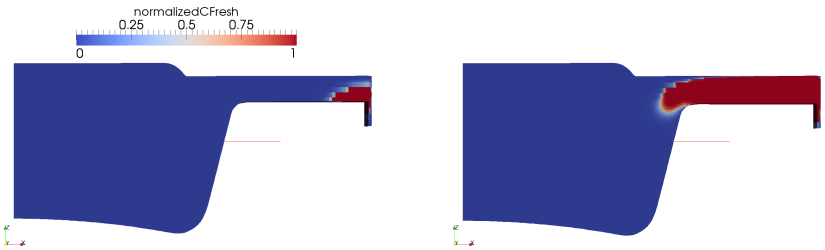

Figure 5.13: Autoignition propagation in CR 15 engine; 13 deg after TDC leftwards, 14 deg after TDC rightwards

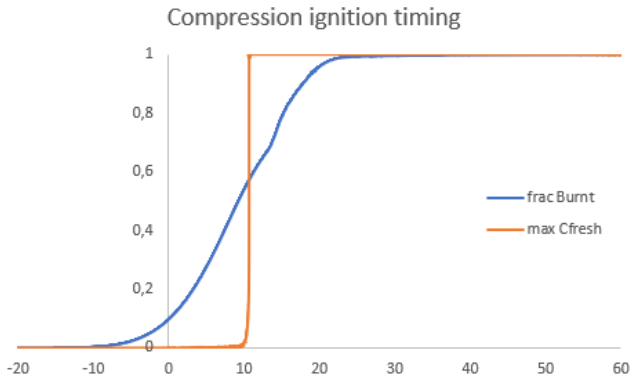

Figure 5.14: Autoignition principle in CR 15 engine

Adopting such a high compression ratio, temperatures reached inside the combustion chamber make spontaneous ignition propagation even faster, resulting in very heavy knock. Values reported in table 5.1 summarize this comparison between different solver results. As evident, pressure and weighted average temperature maximum values increase, but especially cumulative wall heat transfer rise is impressive, of more than 46%. This leads to the apparent contradiction that a more ideal Otto cycle such as the one computed by SACI solver has a lower thermal efficiency with respect to a less ideal one. In figure 5.15 it is evident how spark assisted combustion is faster and closer to a constant volume one, however resulting efficiency is lower because of too huge losses.

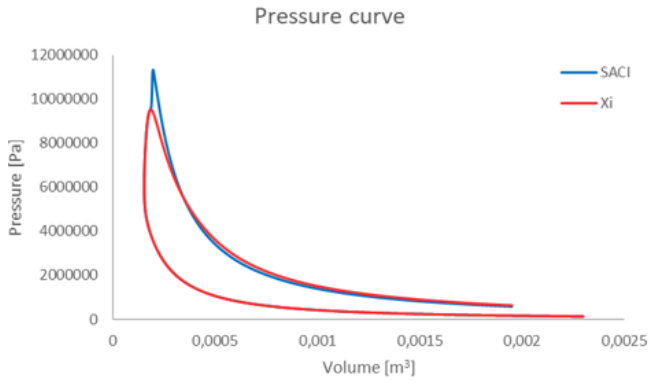

Figure 5.15: Pressure-volume curves obtained by both solvers in the same initial conditions

	η	GIW	cum Heat losses	P_{max}	T_{max}
SACI	40.78%	2759 J	-1359 J/deg	113.2 bar	2633 K
Xi	41.89%	2827 J	-927 J/deg	95.2 bar	2276 K

Table 5.1: SACI and Xi solvers comparison

5.2 Wall temperature, spark timing and load sweeps

Spark assisted compression ignition combustion in previous subsection turned to be more ideal but also less efficient because of huge wall heat transfer presence. In order to reduce heat losses, temperatures imposed to the walls have been increased by 80°C (per wall), in order to verify if a thermal efficiency increase is associated.

	Head	Piston	Liner	Ad. Piston	Ad. Liner
SACI	551 K	499 K	413 K	499 K	413 K
SACI high T	631 K	579 K	493 K	579 K	493 K

Table 5.2: Wall temperature values

To distinguish this configuration with the previous one, the name "SACI high T" has been chosen to indicate the configuration with high wall temperatures imposed; with the label "SACI" instead the previously analysed one is reported. Since cylinder walls are hotter in this case, heat losses should decrease because of lower temperature difference between air-fuel mixture and cylinder walls and, consequently, thermal efficiency is predicted to increase. This is what happens when combustion is totally driven by flame propagation, while if also spontaneous ignition is considered this can turn into an enhanced probability for knock to occur. As it is possible to see in figure 5.16, autoignition is anticipated in "SACI high T" configuration, presenting also an increased pressure maximum value.

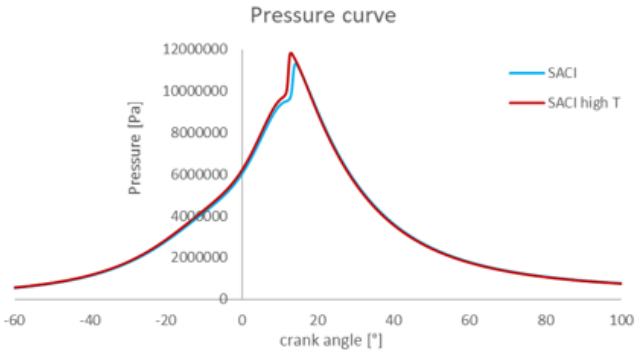

Figure 5.16: Autoignition anticipation when engine walls are at higher temperatures

In cumulative wall heat transfer curves of figure 5.17, the high wall temperature curve is clearly above the "SACI" one before spontaneous ignition occurs, and heat losses are hence contained; but once knock presents, red and light blue curves intertwine, and at the end of the power cycle the configuration that should theoretically contain wall heat transfer is worse behaving because of the heavier knock.

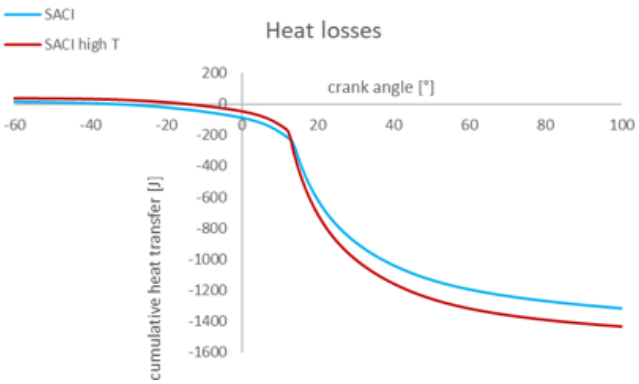

Figure 5.17: Heat losses curves when engine walls are at higher temperatures

From this very brief investigation, increasing walls temperature is not a good strategy to take advantage from homogeneous compression ignition combustion. As it is possible to see in instantaneous gross indicated work curves in figure 5.18, during the expansion stroke the light blue one is always above the dark red one, hence the lower the amount of mixture autoignited the higher the work done by burnt gases. This is also summarized in table 5.3 where thermal efficiency of the engine decreases of about 1% instead of growing up, also introducing higher loads to the mechanical structure of the machine. By a first sight analysis, an increase of autoignited fraction leads to a thermal efficiency decrease.

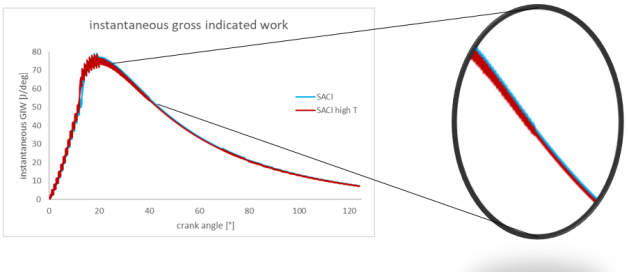

Figure 5.18: Instantaneous gross indicated work curves when engine walls are at higher temperatures

	η	GIW	cumulative Heat losses	P_{max}	T_{max}
SACI	40.78%	2759 J	-1359 J	113.3 bar	2633 K
SACI high T	39.92%	2700 J	-1470 J	118.3 bar	2648 K

Table 5.3: Standard and high wall temperature performance comparison

To verify this behavior and to consider even more extreme conditions, a spark advance sweep has been performed, considering a delayed mixture ignition (corresponding to -14°) and an anticipated one (at -19°). During this analysis, also autoignited mixture fractions are compared between different cases.

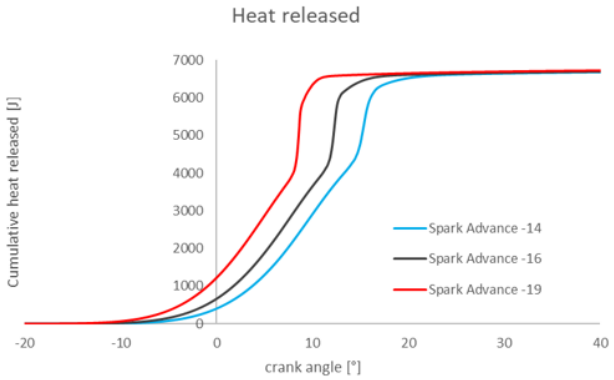

Figure 5.19: Cumulative heat release in high compression ratio spark advance sweep

From heat release curves of figure 5.19, it is possible to see how combustion is further speeded up when spark ignition is anticipated. The more severe pressure and temperature conditions contribute to a more ideal combustion, and it gets even more similar to a constant volume one. While pressure curve underlying area varies evidently, temperature curve behavior is far way more similar: both of them are weighted average values taking into account all the cells in the CFD domain. This means that in presence of compression ignition temperature weighted average maximum values change because of the higher number of cells involved in combustion process, but maximum cell burnt temperatures do not vary considerably.

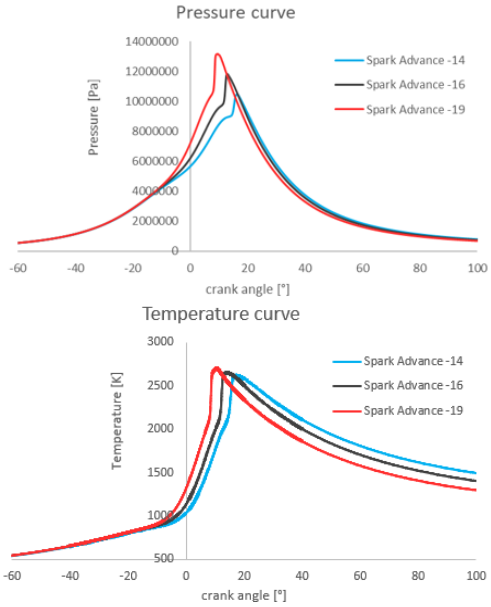

Figure 5.20: Pressure and temperature curves in high compression ratio spark advance sweep

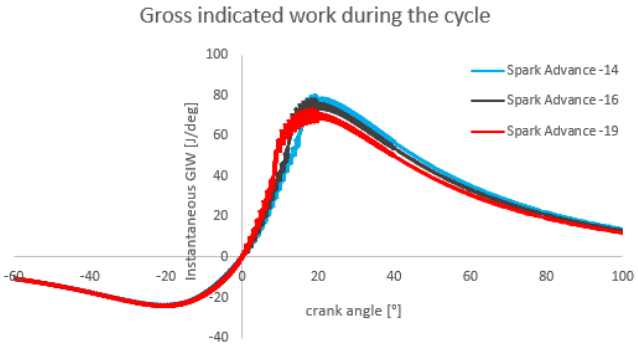

Figure 5.21: Instantaneous gross indicated work in high compression ratio spark advance sweep

As in all the other cases, instantaneous gross indicated work provides very important indications of points of strength and weakness of this combustion mode during the cycle, showing how most delayed spark timing configuration is the best one in this sweep. Once engine performances are considered, a higher underlying pressure - θ curve area is not directly corresponding to higher performances, because energy released by the fuel contributes to increase more heat losses and fluid kinetic energy than useful work done by burnt gases. If a deeper analysis is performed, pressure and turbulent kinetic energy values must be regarded cell by cell during all the different combustion phases. To make this analysis even clearer, the most knock severe case is investigated, hence the one at anticipated spark timing with increased cylinder wall temperatures.

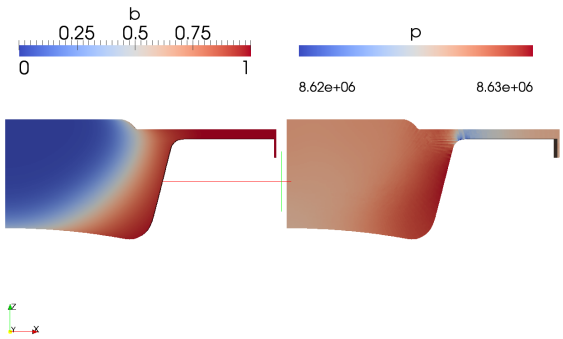

Figure 5.22: Flame front and cylinder pressure in an entire flame propagation combustion

Figure 5.22 shows pressure increasing inside the cylinder in an entire flame propagation environment, before spontaneous ignition occurs. For these representations, it has been chosen the regress variable "b" to indicate flame front and surface positions, and the normalized progress variable "c_{fresh}" to refer to compression ignition combustion. In flame propagation combustion pressure rise is homogeneous inside the cylinder, with very low almost numerical gradients in

regions where mesh orthogonal quality is particularly poor. Temperature values are not as uniform as pressure ones, such that in burnt gas region 2700 - 2800 K are reached, while fresh mixture temperatures are stable between 1000 K and 1100 K. This provokes some density differences between different areas, hence fresh mixture mass concentrates in most external cylinder regions.

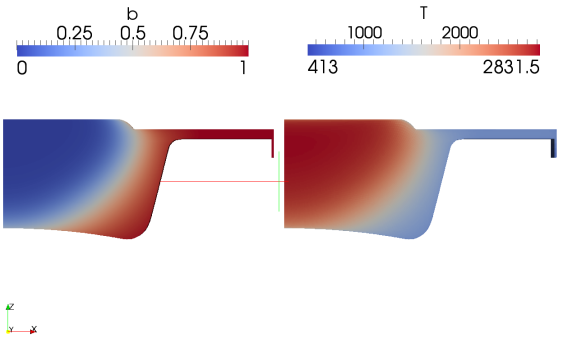

Figure 5.23: Flame front and cylinder temperature in an entire flame propagation combustion

In the very first phases of compression ignition development, because of huge amount of heat released high pressure values appear in the most external region of the cylinder, introducing significant pressure gradients inside the combustion chamber. As a consequence, the working fluid is moving from high density regions towards the more internal one, at very high velocity. Figure 5.24 displayed below captures one of the very first autoignition phases, with the presence of an always higher pressure gradient originated in the most external part of the cylinder. Since heat release is huge and squish transversal area is constant, that high pressure fluid finds a lot of difficulties in expanding, originating the wave and hence derived pressure gradient.

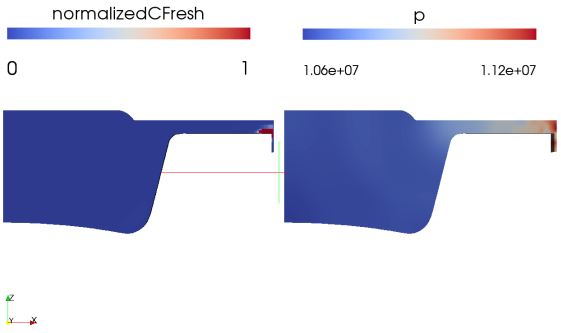

Figure 5.24: Pressure gradient at compression ignition origin, 8 deg after TDC

It has previously discussed in this thesis work how low time step imposed

and considered 2D geometry are a limit of this analysis introduced to optimized computational resources available; but also using these solver settings, pressure gradient after some crank angle degrees is moving from the external part of the cylinder to the internal one, increasing of two orders of magnitude fluid turbulent kinetic energy. This behavior is strongly connected to pressure waves presence, which move from the most external cylinder region to the inner of the combustion chamber to then rebound in correspondence of cylinder walls. Turbulence k value that have been plotted so far are derived performing a weighted averaged considering all mesh cells, hence maximum κ values are far way higher when the whole CFD domain is displayed. This kind of behavior is actually typical of all knock met so far, and it provides a further explanation on performance decrease encountered. Some crank angle degrees after spontaneous ignition is completed, pressure gradient inside the combustion chamber becomes maximum, with pressure differences of over than 30% in most severe knock condition. All of it is contributing into increasing kinetic energy of the working fluid, and as a consequence heat transfer coefficient between the fluid and the wall, explaining also why heat transfer curve and turbulent kinetic energy ones have such a similar behavior.

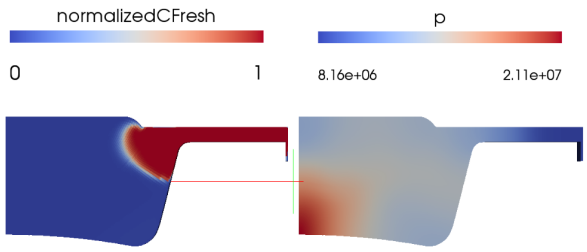

Figure 5.25: Pressure gradient immediately after compression ignition is completed, 9 deg after TDC

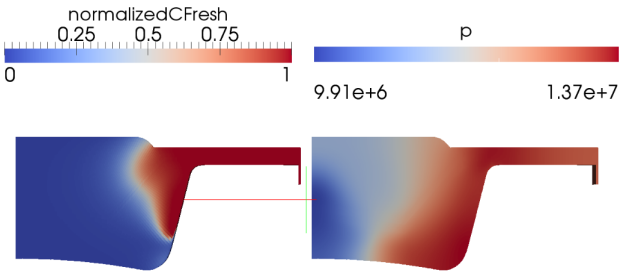

Figure 5.26: Pressure gradient after wave has propagated inside the combustion chamber, 11 deg after TDC

Between figure 5.24, 5.25 and 5.26 there are just three crank angle degrees

of difference, but cell pressure values change completely. All of them are of the same case, but these figures in sequence provides an idea on how wave propagates inside the whole combustion chamber and how difficult is for the fluid to expand in squish region. If in the CFD domain turbulent kinetic energy during flame propagation is compared to the one after compression ignition occurring, behavior described is further verified. Therefore, in figure 5.27 it is possible to see two turbulent kinetic energy time step values of the same case: leftwards, during flame propagation but before autoignition appearance; rightwards once spontaneous ignition is almost completed and huge heat has been released. As evident, maximum κ values differs of more than two orders of magnitude. In an entire spark ignition context, turbulent kinetic energy reaches its maximum values very close to squish area, which is designed to increase fluid turbulence and hence flame velocity; after autoignition occurs, κ reaches its maximum values as soon as the fluid is exiting from the squish area to go towards inner parts of the combustion chamber, as soon as there is more space for the pressure wave to propagate.

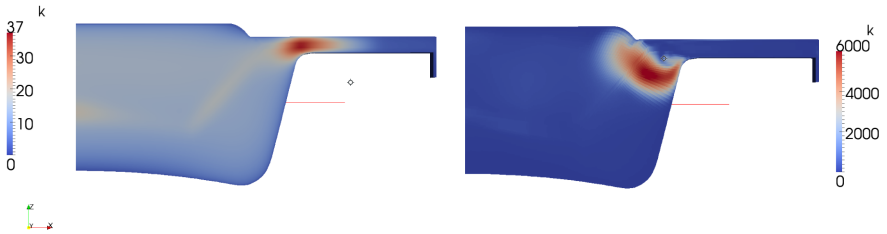

Figure 5.27: Turbulence intensity comparison between before (left) and after (right) autoignition

As a consequence, the higher the quantity of spontaneously ignited mixture fraction the higher the efficiency loss. This is clearly visible by figures 5.28 and 5.29 displayed below, where the best efficiency case corresponds to lower autoignition fraction one.

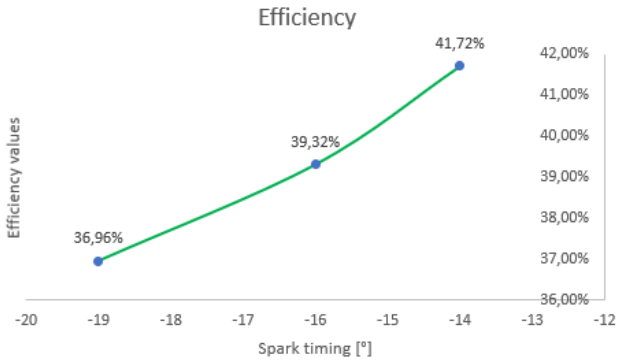

Figure 5.28: Efficiency curve with spark timing in a heavy knock engine

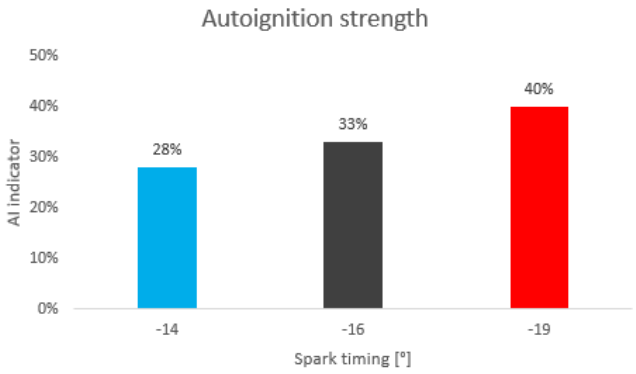

Figure 5.29: Autoignited mixture fraction in spark timing sweep. AI indicator is the ratio between autoignited mixture mass and the whole mixture mass

In chapter 3 where engine has been optimized, it has been discussed how efficiency curve in an entire flame propagation context is stable, varying of some tenths of percentage for each spark timing degree of change. Figure 5.28 illustrated above clearly shows that this is not the case anymore: there is an absolute efficiency variation of more than 4% between most spark delayed case and most spark anticipated one. As summarized by table 5.4 below reported, minimum of wall heat transfer value changes of more than four times between these two cases, conditioning cumulative curves in a huge way. From first to the last case (always referred to table 5.4), heat losses becomes almost the double, with a consequent reduction of gross indicated work. Pressure and temperature maximum values reach very high numbers for a half load condition.
To summarize what has been derived so far:

- Autoignition is originated in squish area, to then propagate into inner region of the combustion chamber

- In squish area, once autoignition occurs the compressed burnt mixture has no space to expand: this is enhancing pressure wave presence and turbulent kinetic energy, hence heat transfer between the working fluid and the walls

- About heat losses, in squish area distance between the piston and the head of the cylinder is very small, hence heat transfer area between the wall and the working fluid is very big. Volume/surface ratio in that region when spontaneous ignition occurs is very low, and the just burnt mixture at very high temperature dissipate almost all of heat released, with very poor thermal inertia.

θ_{Spark}	η	Heat transfer$_{min}$	Heat losses	GIW	P$_{max}$	T$_{max}$
-14°	41.72%	-52.4 J/deg	-1100 J	2818 J	104.7 bar	2618 K
-16°	39.32%	-128.1 J/deg	-1470 J	2700 J	118.3 bar	2648 K
-19°	36.96 %	-219.2 J/deg	-1946 J	2506 J	131.7 bar	2702 K

Table 5.4: Spark timing sweep performance table

In these pages, very heavy knocks have been obtained more than a controlled spontaneous ignition. Before modifying combustion chamber, some other considerations are needed, hence a load sweep has been performed to check what happens if cylinder works at lower pressures. When engine is running at decreased loads, there is a lower quantity of mixture mass inside the cylinder, with a consequent density reduction. Therefore, in one hand, the lower thermal inertia should increase heat losses if related to mixture mass, as it happened in an entire flame propagation context; but in the other one, spontaneous ignition should delay, leading to a lighter knock and, for what has been obtained so far, an increase of useful work from power cycle. Also, full load condition has been taken into account, to check maximum pressure values reached and how knock occurs even at very severe cylinder temperatures.

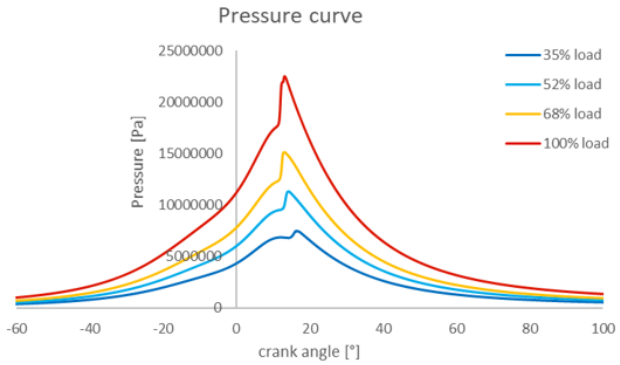

Figure 5.30: Pressure curve in load sweep, in knock presence

As illustrated by pressure curves of figure 5.30, the higher the load, the heavier the knock. Temperature curves are easier to be compared, since engine is working in stoichiometric condition hence adiabatic flame temperature does not change within the sweep. Full load maximum value in figure 5.31 is both the highest one and the most anticipated, but it soon crosses with lower loads temperature curve leading to the presence of more important heat losses.

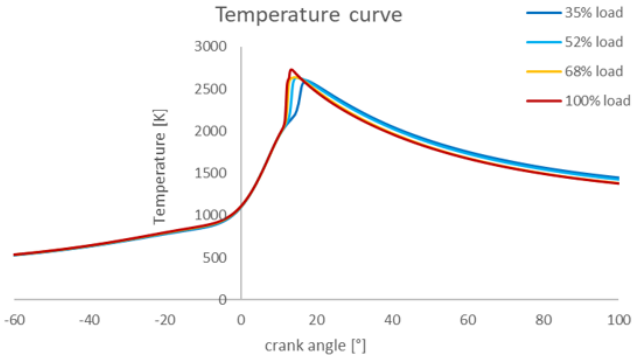

Figure 5.31: Temperature curve in load sweep, in knock presence

Wall heat transfer as shown in figure 5.32 presents very low values, even if

compared with spark timing sweep previously performed. At full load condition, knock is so heavy that wall heat transfer is lower than -300 J/deg.

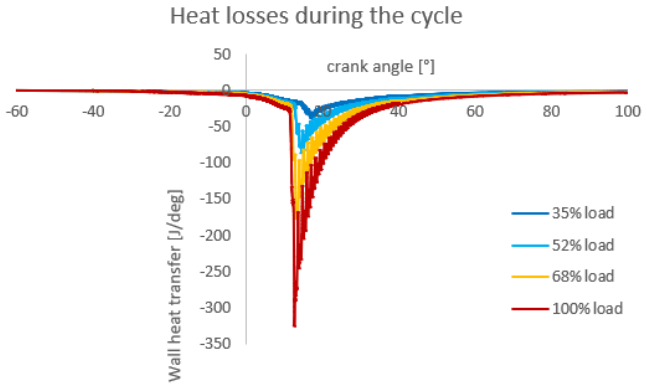

Figure 5.32: Wall heat transfer in load sweep, in knock presence

When a load sweep is performed, it is difficult to compare gross indicated work because of the different fuel amount injected. Instantaneous gross indicated work has been displayed in figure 5.33, presenting curves almost moving on y-axis direction with the different load imposed. The only thing that needs to be remarked is the vibration increase once knock occurs, which can be also detected by wall heat transfer figure above, and it is strongly connected with knock intensity.

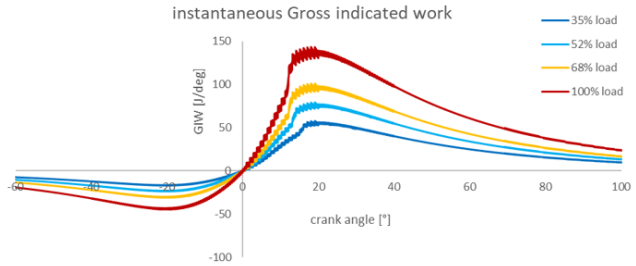

Figure 5.33: Instantaneous gross indicated work in load sweep, in knock presence

Passing to efficiency curve, once again violent autoignition leads to no gross indicated work benefit. At the contrary of what has been obtained in section 3, low load working points present a better efficiency with respect to high load ones, just because spontaneous ignition is weaker. In any case, efficiency curve has not a constant shape or behavior, but it varies between different load conditions: by the first three point, engine efficiency is decreasing in always faster way, even with η difference of 1.5% between half load and 68% load conditions. Between 68% and full load working points, slope of the curve is much higher, hence an efficiency decrease of just 0.35% is present. It has been shown how full load autoignition strength is far way the highest computed in this work, and to provide explanation of this behavior, compression ignition progress variable is displayed in CFD domain, as represented in figure 5.35.

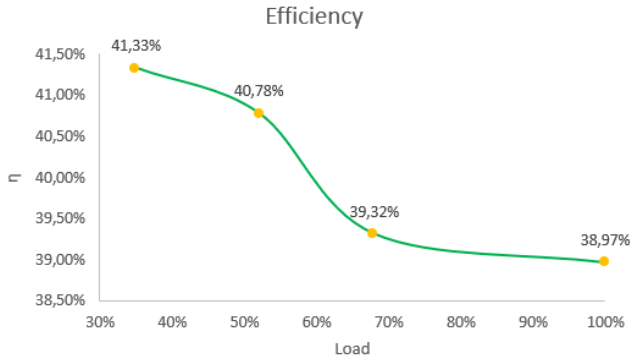

Figure 5.34: Efficiency curve in load sweep, in knock presence

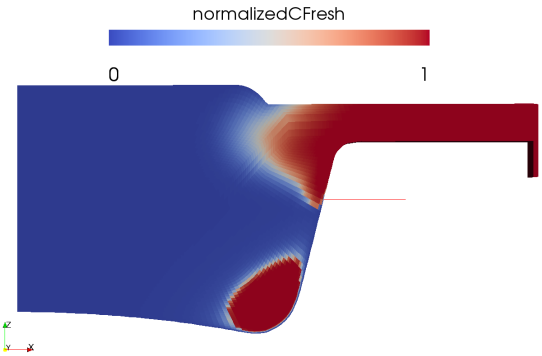

Figure 5.35: Autoignition principles in full load condition

As it is possible to see in figure 5.35, mixture is spontaneously ignited in two different points: one in squish region as in all other simulations, another one in the combustion chamber in correspondence of the piston curvature. Both are very violent causing huge pressure waves, but in squish area burnt gases are transferring heat almost to the walls, while a big portion of the whole second autoignition core surface is facing the mixture already burnt by flame propagation. Therefore, instead of losing that fraction of heat release, energy transfer takes place between both kinds of burnt gases, not wasting fuel energy. Engine is taking some advantages from the faster combustion, and a lower percentage of spontaneous ignition heat release is dissipated through the cylinder walls. Hence, homogeneous mixture compression ignition can be an opportunity to increase efficiency of the engine, but it has to be correctly exploited to not waste that kind of heat release enhancing losses.
This analysis concerning full load condition has been performed just to have a better knowledge of how compression ignition can influence engine performances. As showed by figure 5.5 at the very beginning of this section, full load working point is not of interests of spark assisted compression ignition, because of too high pressure values reached.

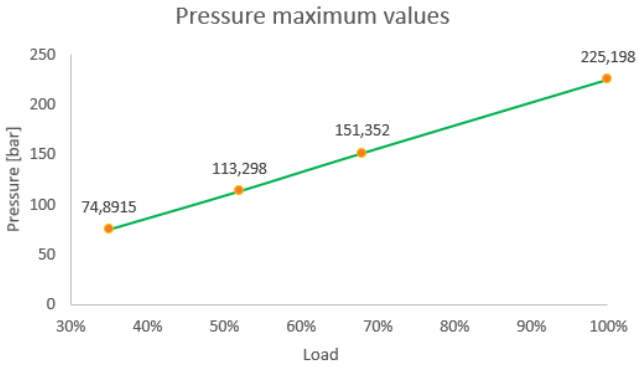

Figure 5.36: Pressure maximum values in load sweep, in knock condition

As shown in figure 5.36, computed maximum pressure in full load condition is 225.2 bar, more than 45 bar over the assumed limit. Such high stresses are unbearable for the engine, hence in spark assisted compression ignition design, high loads and vibrations must be considered.
To conclude this subsection, turbulent kinetic energy in CFD domain is shown in figure 5.37. It is possible to see how second core of heat release is not increasing working fluid turbulent kinetic energy as much as squish region one. Value scale has been edited in order to show that fluid kinetic energy close to the piston is in the range of 100-200 m^2/s^2, while at the inlet of squish region computed values can overcome even 10000 m^2/s^2.

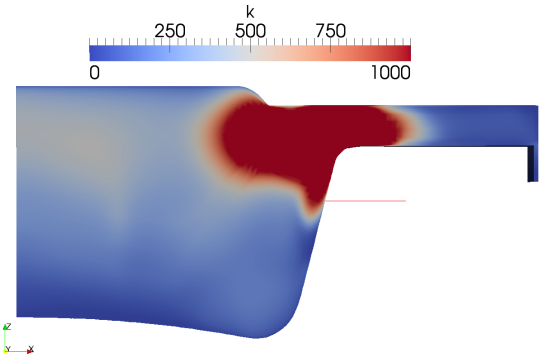

Figure 5.37: Turbulent kinetic energy values in full load condition

In these two first subsections knock phenomenon has been further analysed and an almost complete knowledge of its behavior is provided. Combustion always results into a more ideal one, visible especially in pressure volume plane. To take advantage of it, two different strategies are investigated: piston shape changes and leaner air fuel ratio. The first one can be explained by these last considerations, showing that pressure waves are enhance by squish region; the second aims to have both a far way less violent compression ignition and to have more thermal inertia of gases inside the cylinder, in order to reduce heat losses.

5.3 Piston geometry influence

It has been demonstrated how squish region is important for flame properties but also detrimental for a good exploitation of compression ignition. Heat released from homogeneous charge autoignition is far way faster than the one coming from flame propagation; hence combustion chamber has been redesigned in the external region with the aim of taking benefits of this combustion mode, keeping the same compression ratio. Most important geometrical parameters such as stroke, bore or cylinder head shape have not been changed to not impose huge modifications to the engine: once again piston shape is investigated, focusing on most external regions.

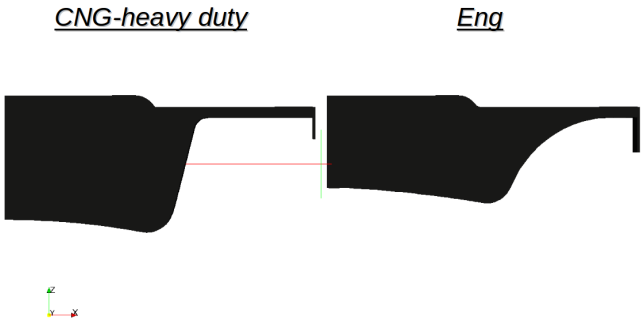

Figure 5.38: Piston geometry comparison at top dead centre with respective names

In figure 5.38 geometry changes are illustrated, with both images taken in correspondence of top dead centre piston position. Some more space has been added in correspondence of squish area, in such a way to expand the pressure wave originated by compression ignition. The extension of this region forces the designer to reduce the distance between cylinder head and piston in the central part of the combustion chamber (in correspondence of the axis of symmetry), and for flame propagation this is a huge disadvantage because flame front surface will be lower and combustion is predicted slower than before. Taking in consideration these assumptions, also a third piston geometry has been simulated, called "Turb". Just this last combustion chamber design has a slightly lower compression ratio (14.8), and it has been edited to find a good exploitation of flame surface properties.

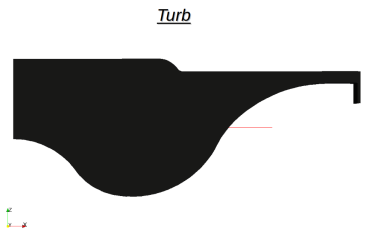

Figure 5.39: "Turb" piston geometry at top dead centre

In both of these two last edited geometries, importance and influence of squish area have been remarkably sacrificed to exploit homogeneous charge compression ignition, which in CNG-heavy duty geometry was too violent. In figure 5.40 displayed below, an "Eng" geometry render has been showed, evidencing how squish area influence has been considerably decreased.

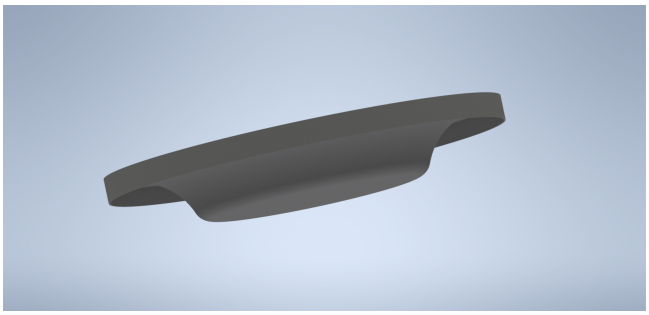

Figure 5.40: 3D render of "Eng" combustion chamber

Therefore, a first set of simulations has been performed, keeping the same working point parameters such as initial pressure, temperatures, stoichiometric air-fuel mixture ratio and turbulence, with a spark timing of -16° imposed for all the different geometries.

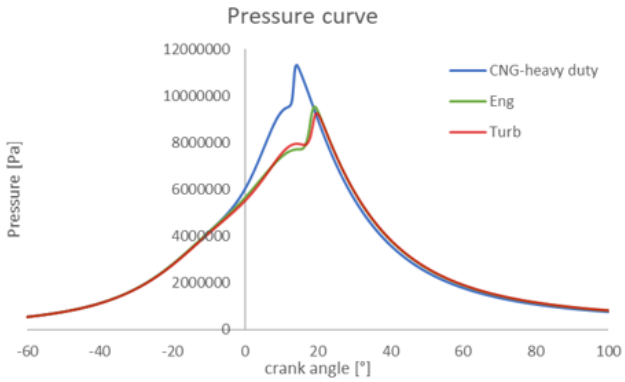

Figure 5.41: Pressure curves associated to different piston geometries

From figure 5.41 displayed above, it is evident how combustion is far way slower in "Eng" and "Turb" geometries, which have almost coincident pressure curves. Spark ignition combustion in CNG-heavy duty engine is considerably faster but pressure rises due to autoignition of the three cases are comparable. As predicted, combustion velocity is reduced because of the lower flame front surface but also to the lower turbulence intensity presence, as shown in the figure below.

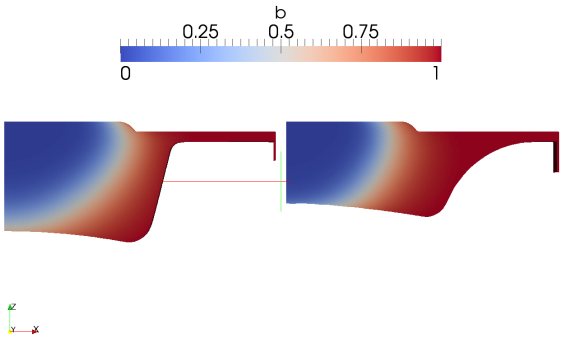

Figure 5.42: Flame front visualization in CFD domain associated to different piston geometries

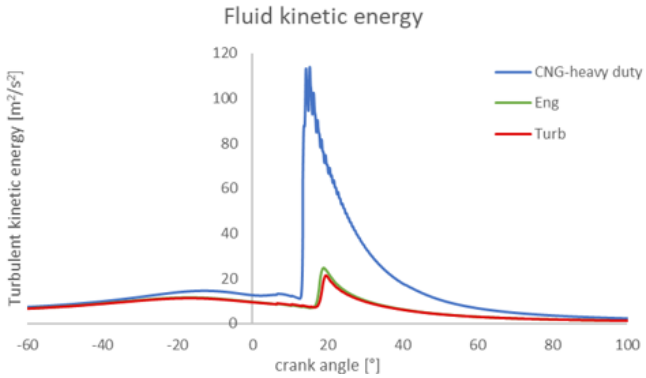

Figure 5.43: Turbulence intensity associated to different piston geometries

Figure 5.42 reported above illustrates in a good way behavior previously described: CNG-heavy duty geometry presents a flame front with a higher surface, leading to considerable advantages for combustion. If the two flame front distances along piston head are compared, it is evident how CNG-heavy duty flame is also faster, leading to a better spark ignition combustion under every aspect. These CFD domains shown are in correspondence of 4° after top dead centre.
Even if combustion development has been slowed down, power cycle efficiency values between the three different cases are comparable:

	solver	η	GIW	Heat Losses
CNG-heavy duty	SACI	40.78%	2759 J	- 1359 J
Eng	SACI	41.69%	2831 J	- 1169 J
Turb	SACI	42.01%	2869 J	- 1080 J
CNG-heavy duty	Xi	41.89%	2827 J	- 927 J

Table 5.5: Efficiencies comparison of different piston geometries, with the same initial conditions and spark timing

In table 5.5, efficiency values are reported in such a way they can be compared. When "SACI" solver is chosen compression ignition always occurs, but both "Eng" and "Turb" efficiency values are higher with respect to CNG-heavy duty one. In the previous subsection, a comparison between "SACI" and "Xi" solver results has been performed, to verify efficiency gain just due to new combustion mode; by the very same table, Eng and Turb geometry efficiency values are very close to the target of 41.89%, even overtaken of one tens by Turb piston geometry. This results have been obtained in a non-optimized condition as the one displayed in figure 5.42, demonstrating that in these two edited geometries combustion can take advantages from a partial compression ignition even when air-fuel mixture is stoichiometric. Therefore, a spark time sweep has been performed, not just to find an optimized value for these two engines, but also to understand how compression ignition behaves and if there are differences between these geometries and CNG-heavy duty one.
The spark advance sweep has been performed for both the geometries, but just "Turb" one is illustrated since they lead to very similar considerations.

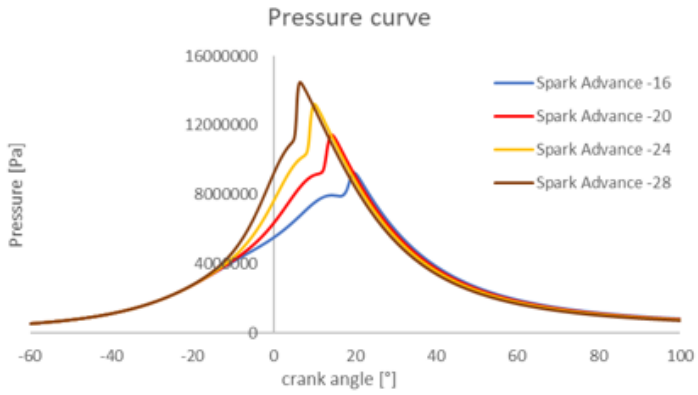

Figure 5.44: "Turb" pressure curves in spark timing sweep

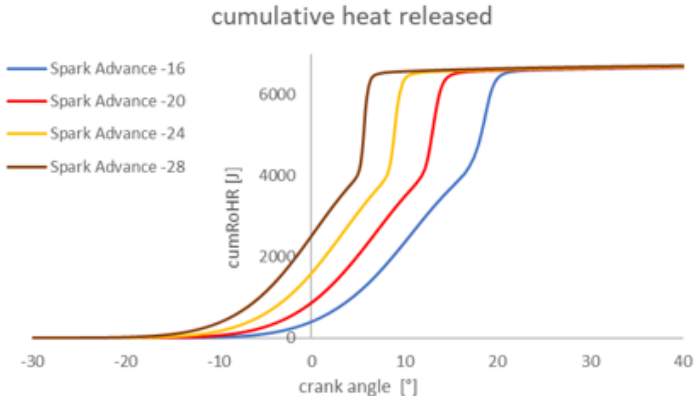

Figure 5.45: "Turb" heat release curves in spark timing sweep

Pressure curves behavior (shown in figure 5.44) is consistent with the one previously analysed. Compression ignition is occurring in every cycle, with an increasing intensity as spark timing is anticipated. By cumulative heat release curves of figure 5.45 it is possible to see how autoignition strength is important in all cases. When spark timing is very delayed for that geometry (16° before top dead centre), autoignition occurs in correspondence of 18°, which is very delayed if compared to previous cases.
It has been discussed how flame propagation has been sacrificed to favor compression ignition. Especially, geometry aims to slow spontaneous ignition down of even some tens of degree, in order to have a smoother pressure rise hence lower pressure wave intensity. In figure 5.46 it is shown autoignition development from its origin (11°) to its ending (14°). Changing in squish area is also important to give a shape or compression ignition development, as happens with flames. When squish area was adopted, as soon as autoignited mixture has more space, it developed in a messy way, originating pressure waves. With this geometry, c_{fresh} has a more defined shape very similar to the one of a flame coming from most external regions, hence wave generated is far way lower leading to heat losses reduction. In figure 5.47 also "Eng" geometry compression ignition is reported, to verify that this smoother kind of compression ignition is due just to the redesign of the most external cylinder region, not properly a squish area anymore.

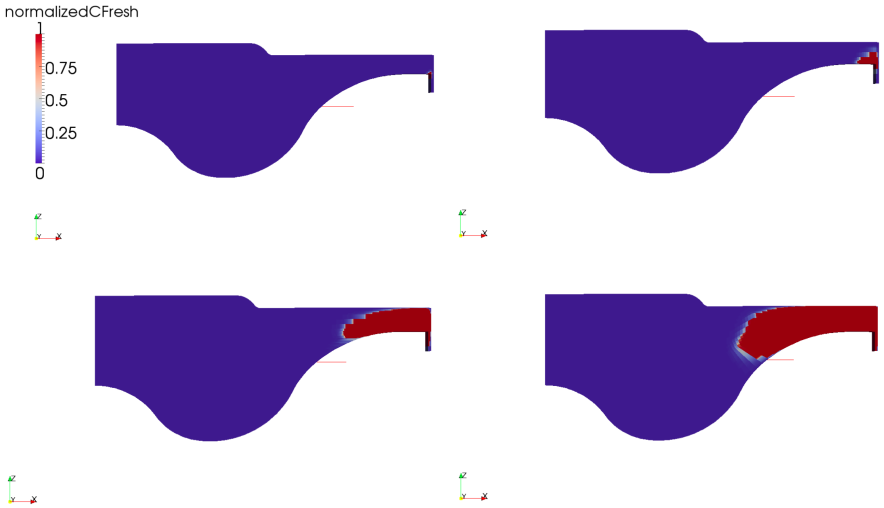

Figure 5.46: Compression ignition evolution between 11 deg and 14 deg in "Turb" geometry

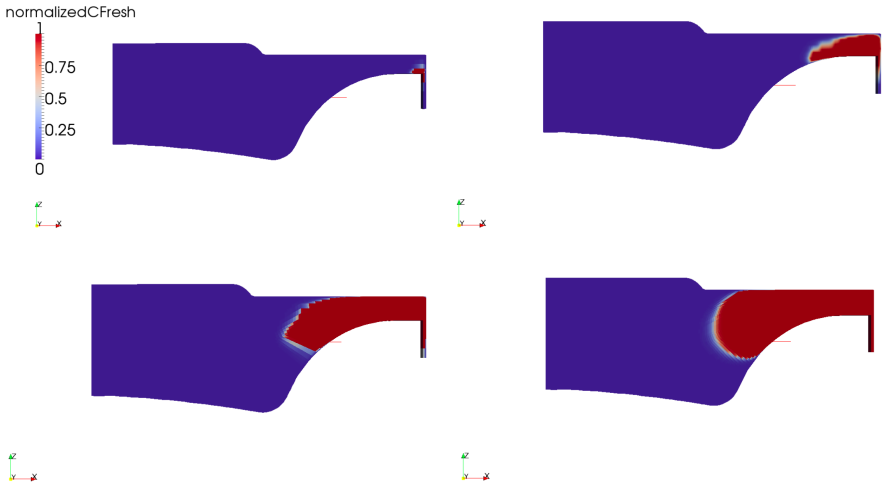

Figure 5.47: Compression ignition evolution between 11 deg and 14 deg in "Eng" geometry

Spark timing influences spontaneous ignition strength, as cylinder fresh mixture can reach different temperature values. As previously described, weighted average turbulent kinetic energy can provide an indication of pressure wave intensity, but maximum mesh values can be very different from weighted averaged ones. Figure 5.48 presents a sort of hyperbolic relation between turbulent kinetic energy peaks, leading to absolutely not stable cumulative heat transfer curves.

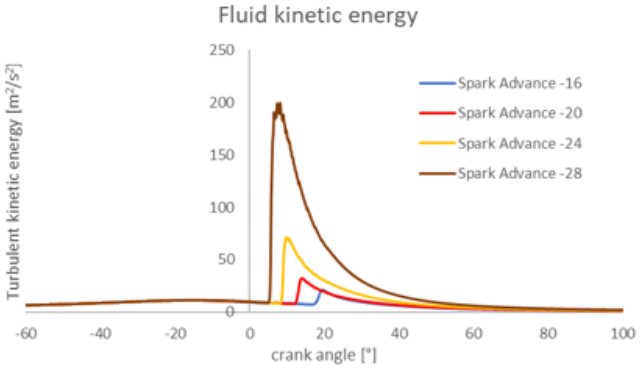

Figure 5.48: "Turb" turbulent kinetic energy curves in spark timing sweep

In previous section relation between heat transfer and kinetic energy has been described, emphasizing how fluid motion originated by spontaneous ignition is increasing heat transfer coefficient. This simulation set provides another confirm of that behavior, with contained heat transfer minimum values when high intensity pressure waves are not present, to then fall down as soon as compression ignition gets stronger.

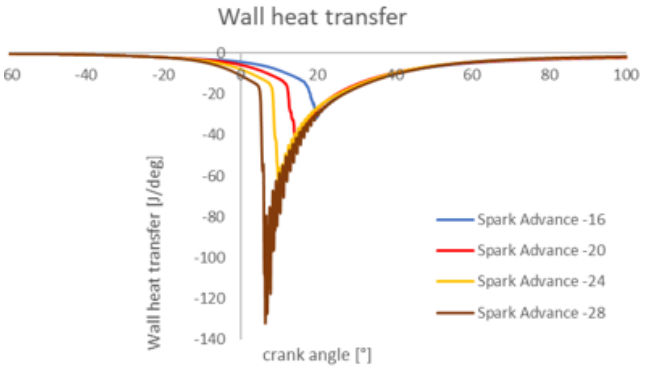

Figure 5.49: "Turb" wall heat transfer curves in spark timing sweep

In figure 5.49, wall heat transfer curves are shown. Minimum values of "Spark Advance -16" and "Spark Advance -20" curves are contained in the interval between -20 and -40 J/deg, far way higher with respect to the one seen in CNG-heavy duty when autoignition was occurring. With such a behavior, engine can take advantage of a faster spark assisted compression ignition combustion even in stoichiometric homogeneous charge, since heat losses are considerably contained. When cumulative curves are compared, this behavior is even more evident: as illustrated in figure 5.50 reported below, end stroke cumulative heat transfer values decrease more than linearly with spark timing, leading to a heat losses increase and a huge performance reduction in the second part of the expansion stroke, once combustion is completed.

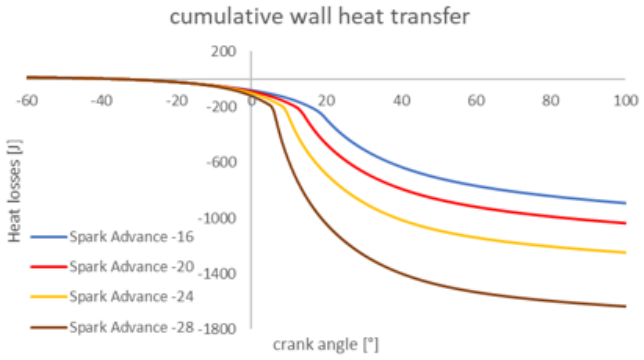

Figure 5.50: "Turb" cumulative wall heat transfer curves in spark timing sweep

But this effect is not as detrimental as for CNG-heavy duty geometry, where efficiency was always higher with the decreasing of autoignition strength, hence spark timing delaying. When both "Eng" and "Turb" geometries are adopted, efficiency reaches its maximum value when a spark timing of -20° is imposed.

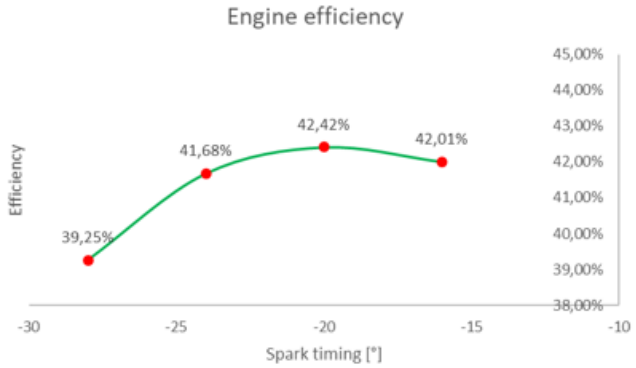

Figure 5.51: "Turb" efficiency curve in spark timing sweep

From figure 5.51, several very important considerations can be derived: first of all, efficiency curve is not monotonous with autoignition strength as happened for CNG-heavy duty engine; second, efficiency target of 41.8%, imposed by "Xi" solver simulation of very high compression ratio spark ignition engine, is definitely overtaken. These geometries edited can work with very high compression ratio engines in a spark assisted context without penalizing their performances, but taking advantage of a faster combustion completing phase. All the flame propagation phases are hugely penalized by lower turbulence presence in the engine, as it leads to a slower flame and to a more anticipated spark timing optimum value. As declared at the beginning of this section, not in the whole engine map it is possible to perform a spark assisted combustion because of the high loads transmitted to the engine. Working point analysed up to this subsection is 52% load working point, which can be a realistic threshold dividing the two combustion modes. By looking at curves in figure 5.52, pressure rise in the optimum condition is slightly above the already high assumed limit of 18 bar/deg. Therefore, it is difficult to develop entirely spark assisted compression ignition engines at the state of the art, but they must be designed to be able to work also in normal spark ignition mode.

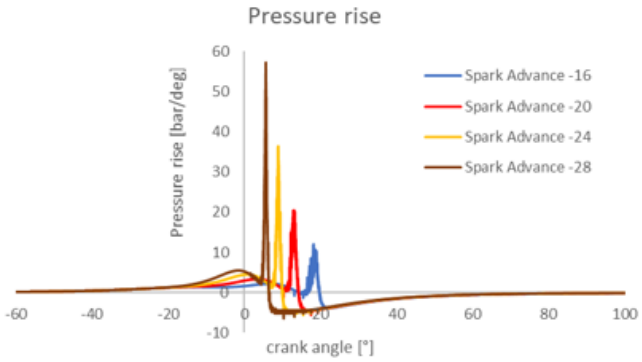

Figure 5.52: "Turb" pressure rise curves in spark timing sweep

In tables 5.6 and 5.7 results of the two spark timing sweep are displayed to be

compared. Both efficiency increases are appreciable, with the "Turb" geometry better performing with respect to "Eng" one not just in efficiency terms, but also in maximum pressure and pressure rise ones. In the whole sweep, $dp/d\theta$ changes massively: in 2° of spark time difference, it rises of almost 9 bar/deg leading to much higher loads on the engine. It is far way more controlled with respect to the one previously obtained, but spark control must be performed in a precise way. At contrary of what has been expected, best efficiency point is stable for very low spark timing variation, to have then a massive decrease if it is further anticipated; a delayed spark timing leads to not huge efficiency differences. As pressure rise, also pressure maximum value is strongly influenced by autoignition strength, reaching 114.5 bar at half load.

θ_{spark}	η	GIW	Heat losses	P_{max}	T_{max}	$dp/d\theta_{max}$
-16°	42.01%	2839 J	-938.5 J	92.6 bar	2622 K	12.04 bar/deg
-20°	42.42%	2868 J	-1080 J	114.5 bar	2695 K	20.4 bar/deg
-24°	41.68%	2821 J	-1285 J	132.2 bar	2754 K	36.4 bar/deg
-28°	39.25%	2662 J	-1669 J	144.8 bar	2798 K	57.2 bar/deg

Table 5.6: Simulation summary for "Turb" spark timing sweep

θ_{spark}	η	GIW	Heat losses	P_{max}	T_{max}	$dp/d\theta_{max}$
-16°	41.69%	2815 J	-999 J	95.4 bar	2622 K	13.76 bar/deg
-20°	41.89%	2831 J	-1169 J	117.6 bar	2683 K	24.4 bar/deg
-22°	41.87%	2831 J	-1229 J	126.9 bar	2719 K	33.2 bar/deg

Table 5.7: Simulation summary for "Eng" spark timing sweep

These two tables previously illustrated confirm that a very precise spark time control is needed, and that both pressure values must be reduced to preserve the mechanical integrability of the engine. But a change of the piston geometry is needed to exploit compression ignition, and to have a further analysis the three are compared together. For CNG-heavy duty one, a spark timing of -16° has been chosen since it is the one taken as reference so far; for "Eng" and "Turb" ones, spark timing chosen is -20° as it is the best efficiency one.

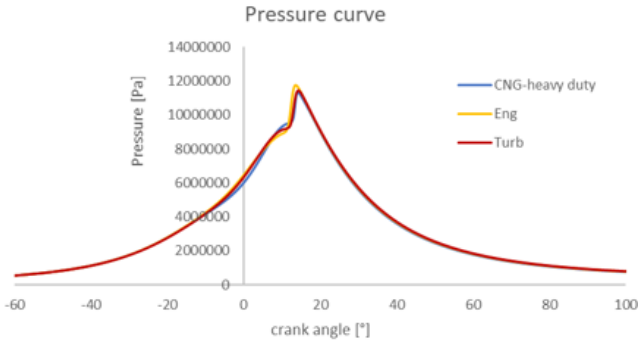

Figure 5.53: Geometry comparison pressure curves

Figure 5.53 illustrates the three pressure curves, showing that they are almost coincident and hence the comparison between the three geometries can be considered fair. While CNG-heavy duty engine efficiency is penalized by compression ignition because it takes place in the squish area, in the two edited geometries there is not a proper squish region, and also turbulent kinetic energy is influenced. As it can be seen in figure 5.54, turbulence maximum value for CNG-heavy duty engine is almost four times "Eng" and "Turb" geometries one. Piston shape hence plays a very important role in compression ignition development and leaving space to the most external cylinder regions can be a good criterion to have very fast combustion exploitation.

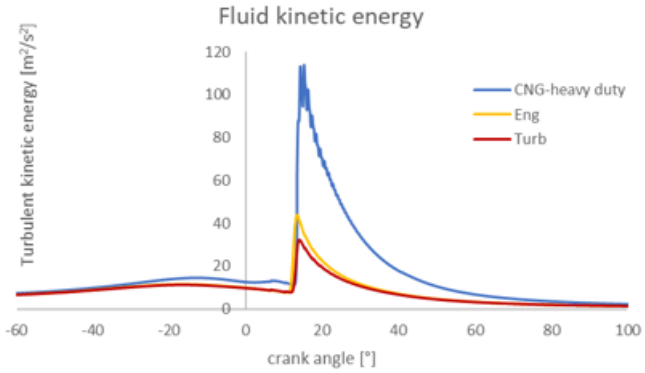

Figure 5.54: Geometry comparison turbulent kinetic energy curves

This leads also to a sort of contradiction in engine design phase, since flame propagation combustion needs to be speeded up, while spontaneous ignition combustion propagation needs to be slowed down. As shown in figure 5.55, CNG-heavy duty flame velocity gain is considerable, leading to lower compression work and a better engine behaving where spontaneous ignition is unwanted. Developing a SACI engine means hence finding the best compromise between a fast flame propagation and a good compression ignition, but it can lead to appreciable efficiency advantages: In section 3, for 1200 rpm half load working point, efficiency obtained was 40.09% while, in this one, best value is 2.33% higher with lower natural gas injected in the combustion chamber because of the volume reduction.

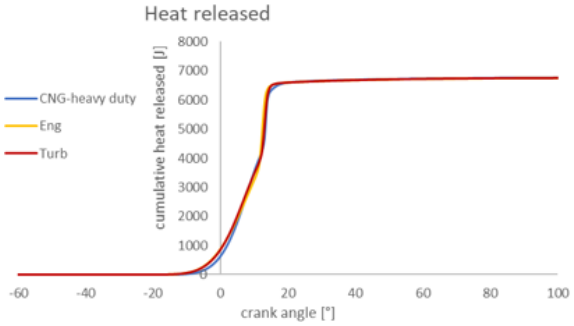

Figure 5.55: Geometry comparison cumulative heat release curves

Another important thing focusing on autoignition analysis is to distinguish knock from a well exploited compression ignition. Knock is defined by theory as an abnormal combustion in a spark ignition Otto cycle engine that can be recognized by the presence of metallic noise coming from the engine. It origins pressure waves which, propagating in the combustion chamber and rebounding in correspondence of cylinder walls, reduce power cycle efficiency and hence gross indicated work, even if the whole combustion process needs less time to be completed. In this thesis work, knock caused performance loss is associated to a wall heat transfer increase due to turbulence generated by the wave itself. As a consequence, to decrease that performance loss, piston geometry can be changed to have a smoother and organized spontaneous ignition flame front. Heat losses, detrimental for engine performances, are hence strongly reduced as figure 5.56 shows, keeping very similar pressure-crank angle curves.

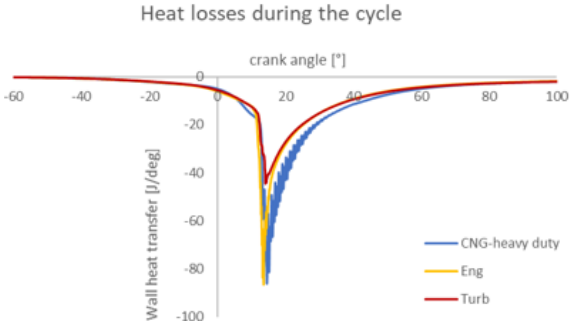

Figure 5.56: Geometry comparison wall heat transfer curves

This wall heat transfer difference between the geometries remain consistent even considering wall per wall values, with just a small discrepancy in the liner minimum value of the "Eng" combustion chamber. In figure 5.56, "Eng" and "CNG-heavy duty" have such a similar minimum value because "adiabatic walls" in "Eng" geometry are bigger with respect to other cases, leading to a huge instantaneous loss. But this loss does not have a considerable overlying area, meaning that in cumulative terms it is not as important as reference geometry one. Another phenomenon easier to be detected in curves of figure 5.57 is the difference in vibration intensity between the geometries. These vibration

propagation of almost all specific quantities considered by the solver are the one caused by pressure waves, typical of knock. For all these reasons merged together, autoignition occurring in "CNG-heavy duty" geometry is considered knock, while the one presented by "Eng" and "Turb" ones can be considered a controlled spark assisted compression ignition.

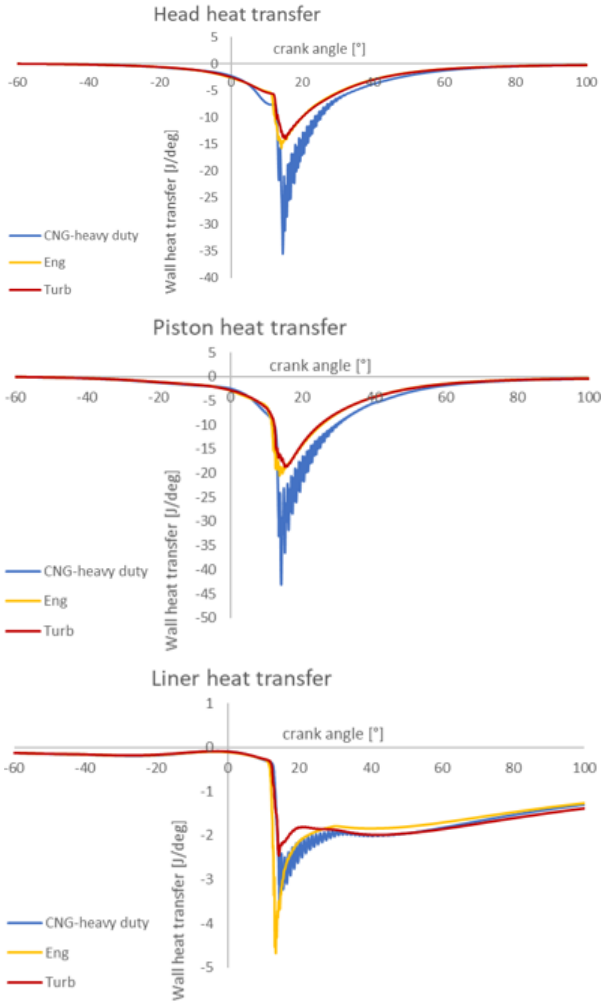

Figure 5.57: Wall per wall heat transfer geometry comparison

In addition, differences in gross indicated work due to this phenomenon are considerable, since between best performing piston configuration and worst one GIW variation is about 100 J, corresponding to 50 Nm of torque. This result has been obtained with no variation in amount of fuel injected, meaning that this efficiency variation can be addressed in a decreased amount of fuel consumed by the engine.

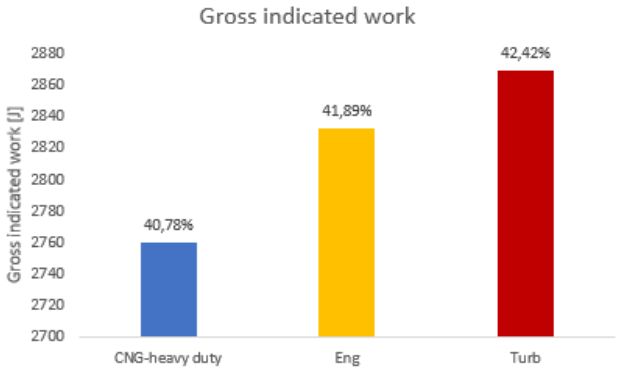

Figure 5.58: Gross indicated work geometry comparison, with corresponding thermal efficiency values reported in percentage

In this subsection piston influence has been investigated, and very good efficiency have been reached in half load condition. While pressure maximum constrain has been fulfilled, pressure rise one has not, since a value of 20 bar/deg has been reported for the best efficiency condition. To further slow compression ignition down, in the next subsection lean air-fuel ratios are considered, in order to compare obtained results with stoichiometric mixture ones.

5.4 Lean SACI combustion

To chose a lean air-fuel ratio instead of a stoichiometric one can lead to considerable advantages, such as a reduction of cylinder maximum temperature or having higher gas thermal inertia. Best efficiency point of Otto cycle engine is in slightly lean condition, in order not to compromise too much flame velocity but also to have a better exploitation of the fuel injected in the cylinder. In previous subsection, it has been discussed how geometrical criteria for a good spark assisted compression ignition and the ones for a fast flame propagation are somehow opposite. Therefore, to make autoignition useful even for the "CNG-heavy duty" geometry can lead to several advantages, especially in working points where SACI combustion is unwanted. Equivalence ratio, as introduced in previous sections, represents the ratio of mass of air in stoichiometric condition and mass of air present in the engine. Therefore, the lower the ϕ, the higher the air excess imposed, while rich mixtures are not considered because even theoretically efficiency predicted decreases.
Equivalence ratio imposed in this subsection is 0.8, so the engine is evidently lean, but no flame extinguish risk is present. As working points initial conditions are well defined, there are two ways to obtained such a lean ϕ: to keep constant initial cylinder pressure hence reducing quantity of natural gas used, or to keep constant amount of fuel injected and increasing cylinder pressure at the intake valve closing.

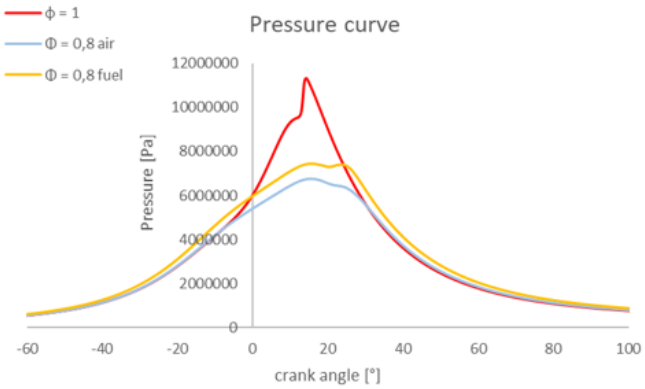

Figure 5.59: Pressure curves when engine is running in lean conditions

In the legend of figure 5.59, "Φ air " indicates that inlet cylinder pressure has been kept fixed, while "Φ fuel" denotes that amount of fuel has been kept constant. In both lean cases, it is evident even from pressure curves how combustion is far way slower than before. Piston geometry considered in the figure above is the "CNG-heavy duty" one, and the same spark timing of -16° has been imposed for all the three cases. Therefore, a spark timing sweep is needed since lean pressure curves maximum value is too low, and one of the two must be chosen. "Φ fuel" is the selected one, because engine efficiency variation with the same amount of fuel injected is the objective of this investigation. As fuel quantity is kept fixed, combustion chamber needs to be fed with more air, and derived intake valve closing pressure rises from 1.32 bar to 1.46 bar.

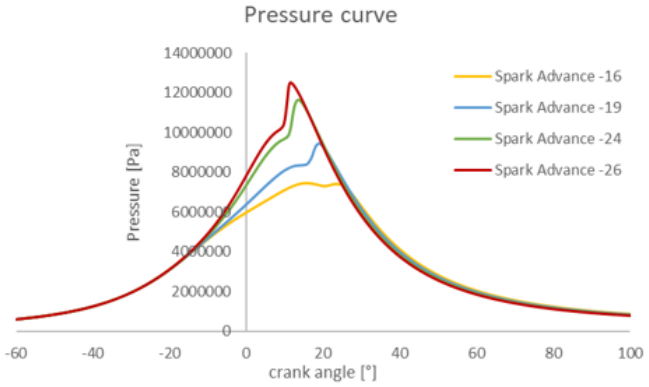

Figure 5.60: Pressure curves spark timing sweep in lean conditions

In figure 5.60 a very wide spark timing range needs to be considered: flame propagation is slower in all its phases and especially ignition delay is affected. By anticipating spark timing up to -24°, a similar pressure curve with the stoichiometric mixture one can be obtained, hence also different computed results can be compared.

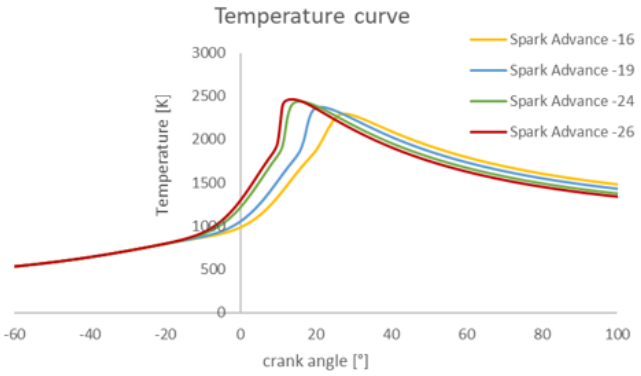

Figure 5.61: Temperature curves spark timing sweep in lean conditions

By both figures 5.60 and 5.61, it is possible to note that compression ignition is occurring in all the simulations performed. Since geometry used presents an important squish area, flame velocity is not that much compromised, and just a 8° of spark timing further anticipation is needed to obtain comparable pressure curves. Temperature ones of figure 5.61 present a lower maximum value, as the ones obtained in all the previous simulations were over 2600 K. This is a result of the lower adiabatic flame temperature due to air excess, leading to an important contribution in heat losses reduction. Slopes of the temperature curves once combustion is completed is not as low as before, both due to lower temperatures in the combustion chamber but also to the higher thermal inertia since there is more air mass inside the cylinder. From a pollutants point of view, an oxygen excess can enhance NOx production in the combustion process, even if weighted averaged cylinder temperatures reached are lower. In any case, a subsection regarding combustion pollutants formation has been reported, considering CO and unburnt fuel hydrocarbons.

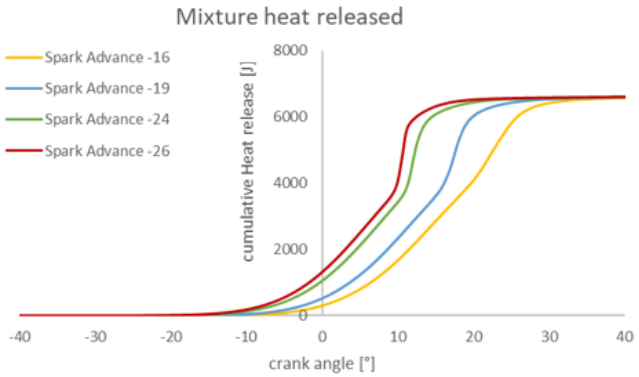

Figure 5.62: Cumulative heat release curves spark timing sweep in lean conditions

In figure 5.62 cumulative heat transfer curves are illustrated. Even from this chart, it is possible to see how combustion is slower especially in first phases and it takes more time to develop, with autoignition occurring in every curve

(even if slightly visible in the most ignition delayed one). Also, autoignition appears to be slower as some slopes even in cumulative heat release curves can be seen. Therefore, the pressure wave originated inside the combustion chamber is weaker and, consequently, heat losses during the power cycle are far way lower.

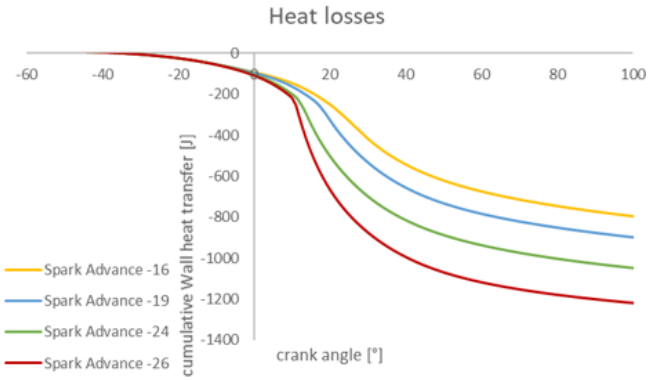

Figure 5.63: Cumulative wall heat transfer curves spark timing sweep in lean conditions

In the reference -16° spark timing stoichiometric mixture case, wall heat transfer assumed a cumulative value of -1470 J while, in figure 5.63 displayed above, all the illustrated curves do not cross the horizontal line corresponding to -1200 J. Containing heat losses can lead to several advantages in the expansion stroke, as instantaneous gross indicated work shown in figure 5.64 shows.

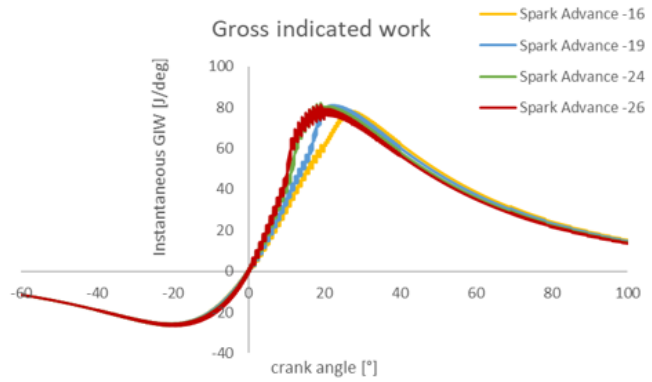

Figure 5.64: Instantaneous gross indicated work curves spark timing sweep in lean conditions

When engine was running stoichiometric, there was a huge difference between high and low autoignition intensity curves, especially once compression ignition occurred and combustion is considered completed. In figure 5.64 instead, after 40° all the four curves are almost coincident, not wasting the whole heat released by compression ignition. Cumulative gross indicated work hence benefits of spontaneous ignition even if it occurs in squish area, and the engine is not knocking.

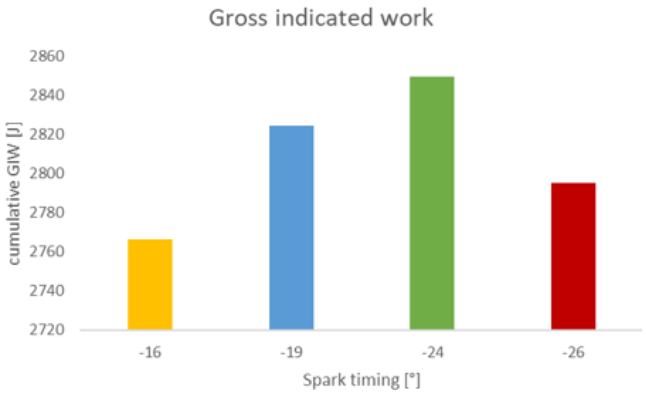

Figure 5.65: Gross indicated work curves spark timing sweep in lean conditions

Even if geometry is presenting the squish area, fresh mixture autoignition is not something to be avoided anymore, as far as gross indicated work is maximized in correspondence of -24° of spark timing. This behavior is reflected also once pressure values are displayed in CFD domain, as in figure 5.66: pressure gradient is very smooth, and difference between maximum and minimum local values is just the 5% of the maximum one. When heavy stoichiometric mixture knock occurred (as in figure 5.26), this difference could even overcome the 30% in extreme wall temperature condition. Therefore, an important result has been obtained, since making the engine work in lean condition could be an opportunity especially for low load working point, where the reduced thermal inertia compromises the cumulative gross indicated work.

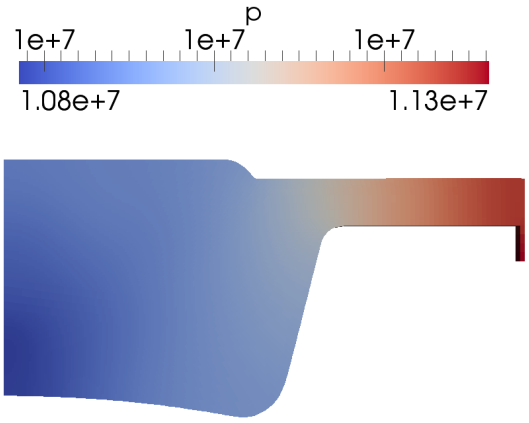

Figure 5.66: Pressure gradient in the CFD domain after lean compression ignition occurred

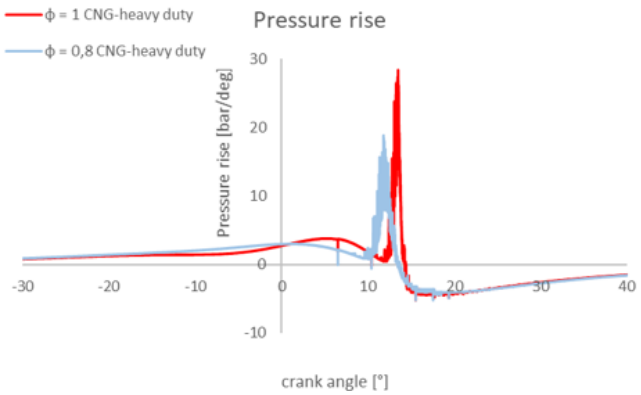

Figure 5.67: Pressure rise comparison between stoichiometric and lean mixtures conditions

In the whole lean spark timing sweep, engine reaches the highest efficiency when ignition starts at 24° before top dead centre, as illustrated in figure 5.65. If a comparison between stoichiometric and optimized lean charges is performed, it is evident how autoignition is smoother when cylinder works with some air excess, leading to an opportunity to reduce pressure rise without compromising useful work. As in figure 5.67, one can see how maximum pressure time derivative has been considerably reduced, decreasing also mechanical stresses induced to the engine. In all the previous simulations (even when piston geometry has been changed), all the pressure rise maximum values were higher than the assumed limit. In a spark assisted compression ignition engine, a lot of not predictable variables can condition fuel-air chemical reaction velocity, such as turbulence variations due to cycle variability or even a change in natural gas composition. Therefore, adopting a lean air-fuel ratio can be a wise choice to have a slowed down homogeneous charge compression ignition, easy applicable to all the possible combustion chamber geometries. Rate of heat release curves (displayed in figure 5.68) provides another confirm of this behavior.

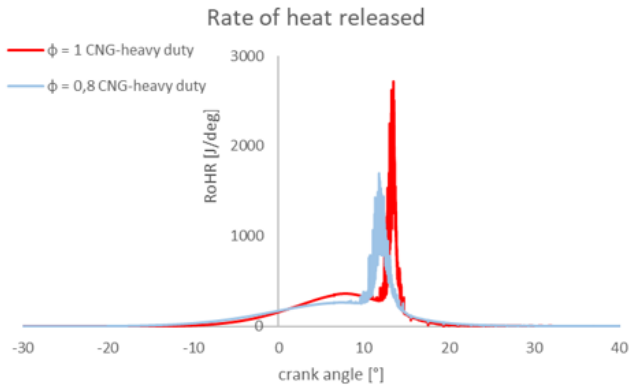

Figure 5.68: Rate of heat release comparison between stoichiometric and lean mixtures conditions

Since fuel quantity has been kept fixed, cumulative heat release values are the same for both the cases. The two shown in figure above have similar amount of autoignited mixture fraction, but combustion behavior is very different: in the first phases, the flame velocity reduction due to the air excess is evident, since lean flame propagation rate of heat released maximum value is definitely lower than stoichiometric one, even if its ignition is anticipated. Comparing the two autoignition regions, it is possible to recognize that in lean conditions compression ignition is slightly anticipated, even if cylinder temperature values are lower if compared to the stoichiometric charge case. But second and more important thing, for almost the same underlying area, compression ignition in lean engine needs more time to be completed, leading to lower rate of heat released and hence being a less violent combustion mode. Duration differences are important, since lean engine autoignition last almost two times the stoichiometric one, and from this behavior the weaker the pressure wave displayed in figure 5.66, the lower the heat losses, represented in figure 5.63.
Therefore, it has been proved that lean charge can take several benefits to engine efficiency, even leading to a good exploitation of spontaneous ignition at high compression ratio. If efficiency curve of figure 5.69 is observed, one can note that the 42.42% efficiency value of "Turb" piston shape has been not just reached but also overtaken. The low difference between -19° and -24° spark timing efficiency values presumes a good curve stability, which is essential to have a flexible load control with spark timing.

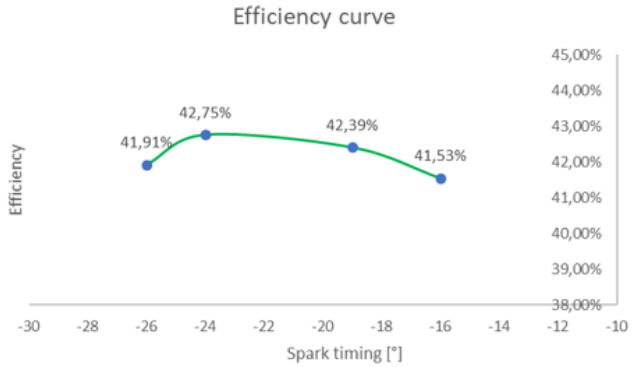

Figure 5.69: Engine efficiency of lean CNG-heavy duty piston shape in spark timing sweep

Since lean air-fuel mixture can improve significantly SACI combustion efficiency and control, also the other piston shapes have been tested. In these cases, both air excess and combustion chamber shape slow the flame down, hence a wide spark timing range must be considered. In this brief spark sweep range, ignition has been anticipated up to 30° before top dead centre. Load is constant at 52%, and no other change has been imposed. For the same reason of subsection 5.3, just "Turb" geometry related curves are displayed, because behavior of the two edited combustion chamber is very similar. In any case, a spark advance sweep has been performed even for "Eng" one, and it is reported at the end of this analysis.

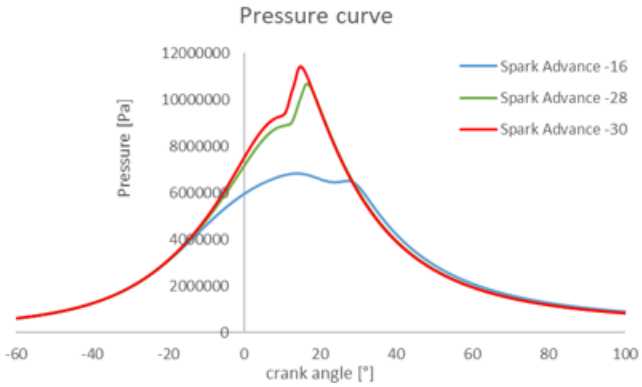

Figure 5.70: Pressure curves of lean "Turb" piston shape in spark timing sweep

In pressure curves of figure 5.70, just the most advanced one is comparable with the previous cases. Flame propagation is very slow especially in the first phases, and even when compression ignition occurs a pressure curve slope can be recognized at sight. Dealing with efficiencies, very high values can be reached: as figure 5.71 reports, maximum value is about 43.34%, a very high one for this kind of thermal engines.

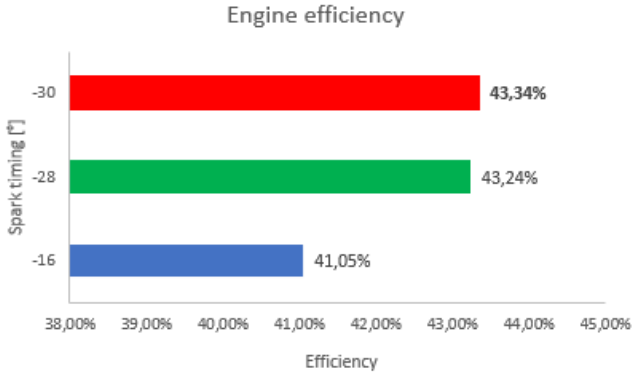

Figure 5.71: Efficiency curves of lean "Turb" piston shape in spark timing sweep

This is the result of adopting high compression ratio and air excess inside the combustion chamber. As previously specified, cumulative heat released does not vary within this analysis, and the whole efficiency gain is due to an increase of the gross indicated work. The strength of these kinds of configurations are definitely the heat losses reduction: from the -1400 J of the stoichiometric mixture CNG-heavy duty geometry to the over -1000 J obtained in this spark advance sweep, even with a very anticipated mixture ignition. In figure 5.72 heat losses of the whole sweep are reported: more than the low values reached, what is even more important is the very low distance between the -28° and -30° ignition timing curves, meaning that pressure wave generated by this compression ignition combustion is almost negligible.

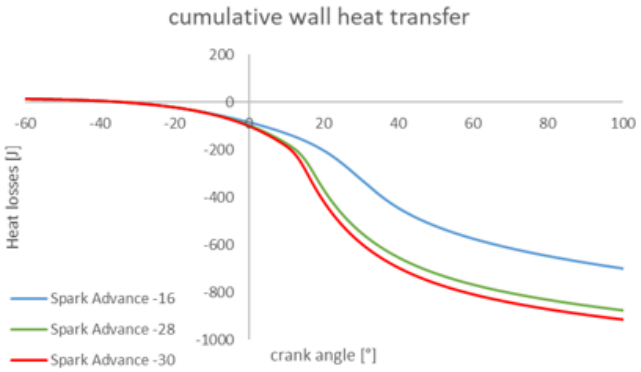

Figure 5.72: Heat Losses curves of lean "Turb" piston shape in spark timing sweep

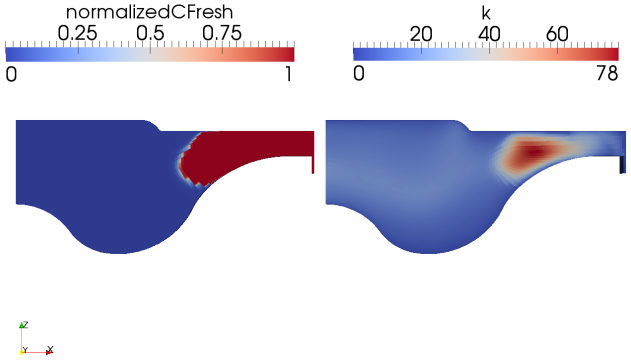

Figure 5.73: Turbulent kinetic energy of lean "Turb" piston shape in CFD domain

As predictable, even turbulent kinetic energy in the whole CFD domain assumes very low values, as an indicator of how compression ignition has been slowed down. Maximum fluid kinetic energy region is always in correspondence of spontaneous combustion reactions, but values reported in figure 5.73 are not comparable with all the ones previously obtained in this thesis work.
In the tables 5.8 and 5.9, both spark timing sweeps main results are illustrated.

θ_{spark}	η	GIW	Heat losses	P_{max}	T_{max}	$dp/d\theta_{max}$
-19°	41.05%	2735 J	-748 J	68.3 bar	2298 K	1.82 bar/deg
-28°	43.24%	2882 J	-915 J	106.7 bar	2474 K	8 bar/deg
-30°	43.34%	2889 J	-953 J	114.2 bar	2500 K	10.4 bar/deg

Table 5.8: "Turb" piston shape lean spark timing sweep

θ_{spark}	η	GIW	Heat losses	P_{max}	T_{max}	$dp/d\theta_{max}$
-19°	41.09%	2736 J	-746 J	71.4 bar	2338 K	3.44 bar/deg
-28°	42.90%	2858 J	-1005 J	112.7 bar	2481 K	11.2 bar/deg

Table 5.9: "Eng" piston shape lean spark timing sweep

Efficiency values in both cases are very high: 42.9% for "Eng" geometry and 43.34% obtained by "Turb" one are an appreciable increasing with respect to the starting target of 41.8% obtained by the solver "betaFlameletXiEngineDyMFoam", hence not considering spontaneous ignition. In addition, these best efficiency values are obtained reducing stresses induced to the engine at the same time. In figure 5.74 reported below, a comparison of maximum rate of heat released between the most important simulations have been reported. Since in all the illustrated cases compression ignition is occurring, heat release rate maximum value is going to be the one caused by spontaneous ignition as this combustion mode is faster than flame propagation one. This can be considered a measure of autoignition strength: as it is possible to notice, between "CNG-heavy duty" geometry and "Turb" lean one, heat release rate has been more than halved, with a consequent reduction of autoignition strength. This decrease does not involve amount of mixture autoignited (since in all cases it is pretty similar) but the velocity of compression ignition, leading to a definitely better exploitation of it. This behavior influences almost all specific quantities considered in the solver, including pressure gradient, turbulent kinetic energy and, because of these two, heat transfer.

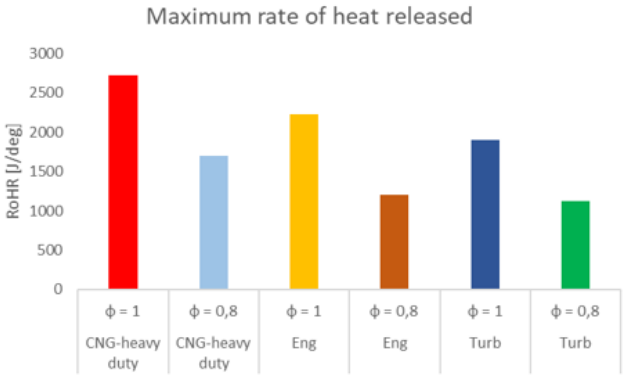

Figure 5.74: Main piston shape and equivalence ratio comparison in heat release maximum values

And figure 5.75 is a direct consequence of this. Pressure rise intensity and pressure waves generated by compression ignition are strongly connected, as it has been discussed. Previously, "CNG-heavy duty" lean engine was good behaving even with spark assisted combustion mode, but pressure rise obtained was higher the assumed engine limit. Adopting both "Eng" and "Turb" geometries, an increase of gross indicated work and a reduction of stresses induced to the engine are obtained at the same time: pressure rise maximum value in best efficiency condition is 10.4 bar/deg, but if it is needed to be further reduced, by delaying spark timing it is possible to get 8 bar/deg losing just a tenth of the

whole thermal efficiency.

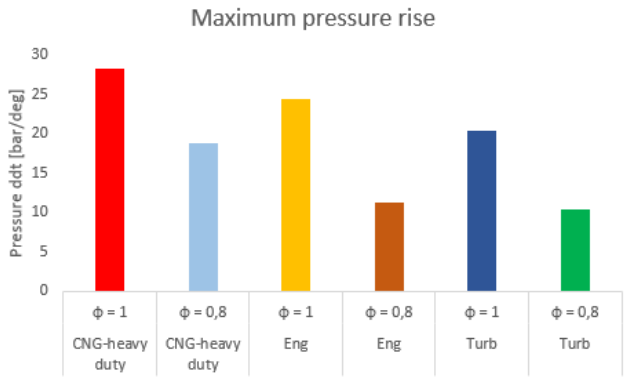

Figure 5.75: Main piston shape and equivalence ratio comparison in pressure rise maximum values

52% load working point has been chosen as the design reference for spark assisted compression ignition engines, but also all the other points of the whole engine map needs to be considered; in particular, 1000 and 1200 rpm full load once are tricky, since for the same or lower engine speed both kinds of combustion mode should be possible to be performed. Piston shapes analysed in this section so far have a compression ratio of 15, too high for an entire spark ignition engine: at full load, 1200 rpm spark timing must be delayed in order not to have any knock. If for medium-low loads working points a huge efficiency gain is predicted, for high load ones (especially at low regimes) ignition timing needs to be such delayed that thermal efficiency is not going to increase that much with respect to optimized values shown in section 3.
Fixing 1200 rpm full load working point as a reference for entirely flame propagation combustion, adopting a compression ratio of 15 means having knock even at -8° of spark timing when "CNG-heavy duty" geometry is used, and that would lead to very low thermal efficiency values; when "Eng" or "Turb" geometry are used, spark timing must be delayed up to -10°, but flame propagation is slower and thermal efficiency is getting even worse. To develop an entire engine map, "CNG-heavy duty" geometry with a slightly reduced compression ratio of 14.5 has been chosen: the presence of squish area should increase flame velocity when combustion is performed entirely through spark ignition, while autoignition strength is controlled via air excess resulting in a more ideal Otto cycle.
In this section, an equivalence ratio of 0.8 is considered, since it is enough lean to take several benefits but not that much to have flame extinguish. When an equivalence ratio of 0.7 is considered, flame can propagate through combustion chamber, but as illustrated in figure 5.76 the regress variable b has a minimum value of 0.038, hence the fuel is not predicted to release all of its energy in flame propagation combustion process. Adopting a different spark light able to release higher quantities of energy can be a solution of this problem for this equivalence ratio, but it is not an object of study of this thesis work as no huge thermal efficiency gains are predicted.

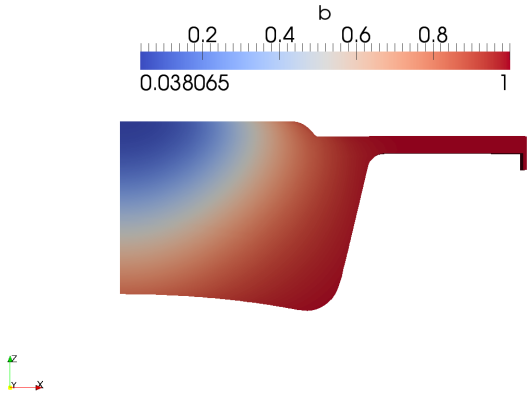

Figure 5.76: Flame propagation when an equivalence ratio of 0.7 is adopted, showing that the minimum b value can not be considered 0

When engine is running even leaner, flame extinction occurs. As illustrated in figure 5.77, near the spark plug b assumes low values, meaning a small volume of fuel-air mixture is igniting. Heat released by these small volumes is not enough to generate a real flame front and then a good spark ignition combustion, and after some time the flame extinguish and both kind of combustions are not possible anymore. Three CFD domains of the figure below represent (from left to right) the regress variable at -25°, -20° and -15°, and hence combustion can not take place.

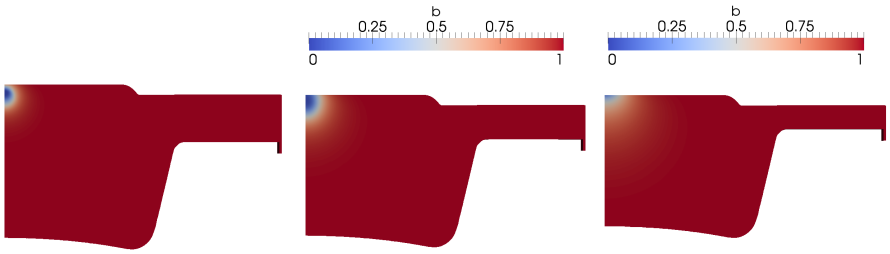

Figure 5.77: Flame extinction when an equivalence ratio of 0.6 is adopted

Therefore, to conclude this lean engine analysis, adopting an equivalence ratio of 0.8 can be an interesting opportunity to reduce autoignition velocity hence to take advantage of spontaneous ignition combustion. Leaner fuel-air mixtures can not ensure a reliable control on flame propagation development, since not the whole heat can be released by the mixture itself. This characteristic can also depend on the kind of natural gas used, since in SNAM North Europe derived composition one almost 7% of inerts are present in the fuel itself, further reducing flame propagation velocity.

5.5 SACI engine map

As explained in previous pages, for the development of a spark assisted compression ignition combustion engine map has been chosen the "CNG-heavy duty"

piston geometry with a compression ratio of 14.5. In high load or high regime working points, an entire flame propagation combustion is wanted, while in low load working points a spark assisted compression ignition combustion has been performed. Each working point illustrated in the figure 5.5 has been optimized, considering the same criteria of section 3.

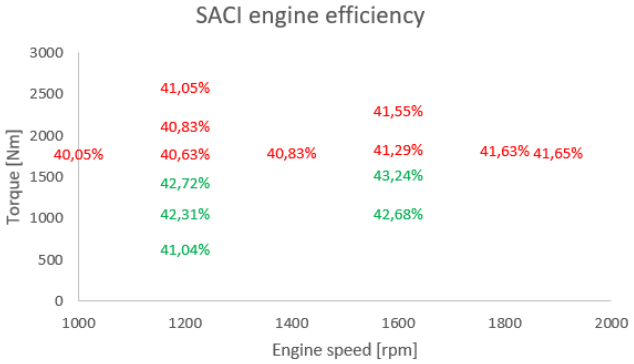

Figure 5.78: Efficiency SACI engine map

In figure 5.78, in green thermal efficiencies of SACI combustion are reported, while corresponding to red written number no spontaneous ignition occurs. Maximum efficiency points has been reached at 1600 rpm in half load condition, with the very high value of 43.24%. The higher the regime, the lower the heat transfer and it can be considered important when compression ignition occurs, since the increased turbulence in combustion chamber is enhancing engine heat losses. If this efficiency map is compared to the one derived in section 3, one can note that in figure 5.78 maximum efficiency points are low load ones, while in the other one the higher the load, the higher the thermal efficiency. This can be an important consideration when dealing with real life operation, since engine is not predicted to run in all working points with the same probability, and a well chosen design reference can further decrease fuel consumption. In fact, if thermal efficiencies are plotted within a spark timing sweep, it is possible to note how values are decreased once the engine passes from a SACI combustion to a flame propagation one.

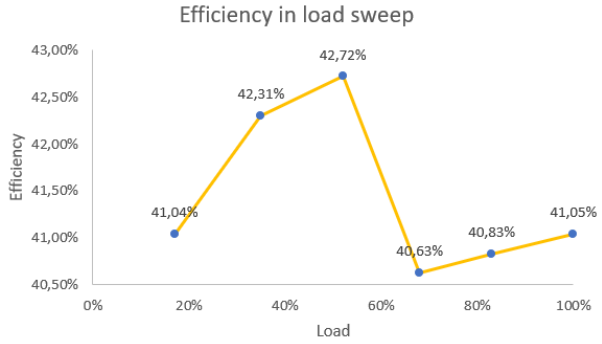

Figure 5.79: Efficiency curve for a SACI engine in load sweep

Load sweep of figure 5.79 is performed at 1200 rpm, as the presence of six different working points suggests. Spark timing and its controlling are essential to perform a good combustion mode: at high load, engine risks to knock in the whole map, leading to a problem especially when engine rotational speeds are low. For this reason, squish area is important for flame propagation development, since in these point a very fast flame is needed. Adopting a "Turb" or an "Eng" geometry is a more risky choice, since they would present higher efficiency values in low load SACI working points, but a definitely lower in entire flame propagation ones.

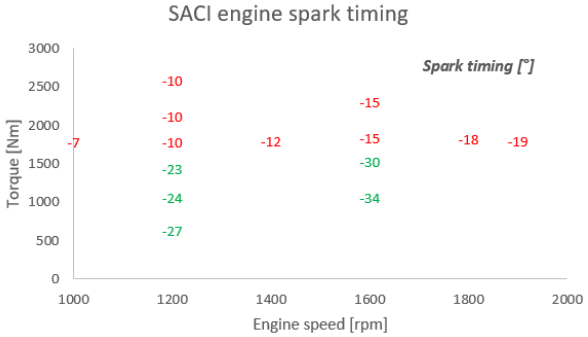

Figure 5.80: Spark timing SACI engine map

In figure 5.80, spark advance chosen in the whole engine map are reported. Both in 1200 and in 1600 rpm sweep, spark advance is imposed by knock presence, which does not vary that much between considered working points. While, in low load ignition must be very advance, and even a -34° spark timing is set at 1600 low load engines. Mixture fraction autoignited is very important within the load sweep range, since it aims to be controlled through ignition timing. For a brief remind, green SACI points works with lean air-fuel ratio, while flame propagation ones with stoichiometric ϕ. Transition between the two different conditions can be an object of study for future works. As figure 5.81 highlights, as soon as transition in entire flame propagation is completed, optimum spark timing is constant with the load. Between minimum and full loads, huge optimum ignition timing variations are present.

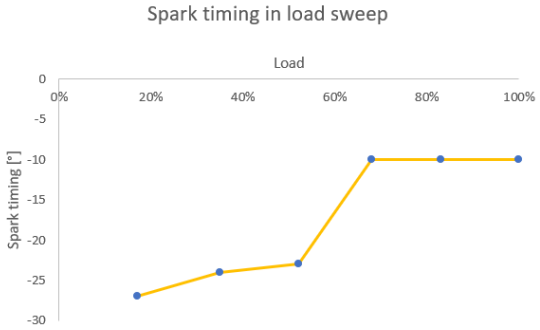

Figure 5.81: Spark timing in load sweep at 1200 rpm

In points displayed in greed, a spark assisted compression ignition combustion of a lean mixture is performed, adopting an equivalence ratio of 0.8. Due to the high compression ratio, the entirely flame propagation combustion is compromised, in order to avoid knock presence. As anticipated in the first section, load (defined by fuel mass injected at the intake valve closing) has been kept fixed to develop this combustion mode; in table 5.10, gross indicated works are reported, always keeping 1200 rpm as fixed engine speed.

	entirely Flame propagation	SACI mode	$\Delta\eta$
CR	11.7	14.5	
17% load	1202 J	1245 J	+ 2.71%
35% load	2054 J	2116 J	+ 2.86%
52% load	2894 J	2953 J	+ 2.68%
68% load	3800 J	3567 J	+ 0.11%
85% load	4500 J	4216 J	+ 0.06%
100% load	5522 J	5164 J	+ 0.02%

Table 5.10: Differences in gross indicated work between starting flame propagation combustion and obtained spark assisted one, with differences of thermal efficiencies reported rightwards

$$\Delta\eta = \eta_{SACI} - \eta_{entFlamePropagation} \tag{5.2}$$

Entirely flame propagation combustion in table 5.10 has been obtained using methane as a fuel (hence higher heat released with respect to SNAM North Europe one due to no inerts presence) and since a higher compression ratio is adopted, for the same initial pressure fuel mass injected is slightly higher, as illustrated in figure 5.3 at the beginning of this chapter.
In conclusion of this brief subsection, focus is pointed on pressure rise. It has been discussed how it is important to have a limited value of it in order to not induce too high mechanical stresses to the engine; as figure 5.82 shows, there is just 1200 rpm half load condition when pressure time derivative reaches dangerous values. In all others working points, because of a load reduction or a faster engine speeds, values assumed by pressure rise are considerably lower, not too much severe for a heavy duty engine.

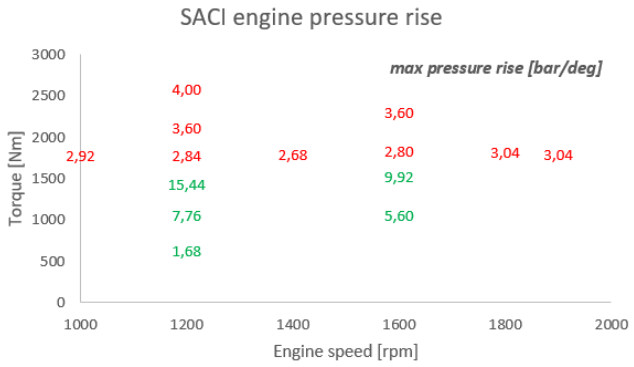

Figure 5.82: Pressure rise SACI engine map

The importance of having a good control of spontaneous ignition needs once more to be highlighted, since a different natural gas composition can move optimized spark timing or vary maximum pressure rise. Since at low load compression ignition is something wanted, a more reacting fuel should lead to an efficiency increase in low load points, but managing high load ones could be an issue. In any case, an almost versatile natural gas composition has been taken as a reference. In Italy, a lot of sources reports a natural gas reached in methane and poorer in heavy hydrocarbons, as illustrated in section 1. This kind of change in practice should not lead to huge thermal efficiency variations, but maximum pressure rise values are predicted to decrease because of the lower chemical reactivity of the fuel itself.

5.6 Pollutants analysis

Running the engine lean could be a problem for the three-phase catalyst since, as explained in the introduction section, conversion efficiency is optimized in stoichiometric air-fuel mixture condition, where it can overtake even 95% and consequently decrease pollutant emissions of the whole engine. Since in this CFD solver after-treatment systems are not considered, focus is pointed first on the carbon-monoxide formation during the combustion process and then on the amount of unburnt hydrocarbons at the end of the power cycle, in such a way to have some values to be compared with possible future works. However, NOx transport equation has not been implemented in the solver, hence it is possible just to give general considerations but not to quantify nitrogen-oxides production in the combustion process.
Working with some air excess in a homogeneous mixture flame propagation engine implies that adiabatic flame temperatures are going to be lower and some oxygen, able to react with reaction products, is remaining even after the combustion is completed. As previously described, air excess is present just in SACI combustion mode working points, hence as point of interest the half load one at 1200 rpm has been chosen. Piston shape chosen is the CNG-heavy duty one with a compression ratio of 14.5, and its pollutants emission have been compared with the optimized one in section 3 (the entirely flame propagation engine adopting 11.7 as compression ratio).

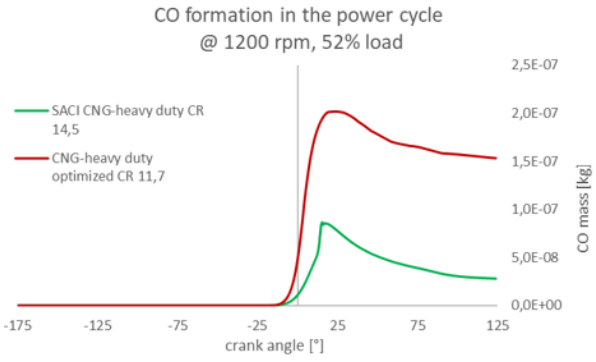

Figure 5.83: CO production in 1200-half load working point comparison. $\phi = 0.8$ SACI reported in green, while stoichiometric flame propagation in red

First pollutants to be analysed is the carbon monoxide. As evident by the figure 5.83, air excess enhances carbon oxidation both during and after the combustion process. Reducing the equivalence ratio from 1 to 0.8, less than the 25% of the CO is globally formed at the exhaust valve opening, and this quantity is even predicted to decrease once exhaust gases cross the catalyst. Carbon oxidation proceeds with an appreciable velocity until to the end of the expansion stroke (with a slowdown at around 90° crank angle because of gases temperature reduction) and the pollutants is homogeneously distributed within the whole combustion chamber.

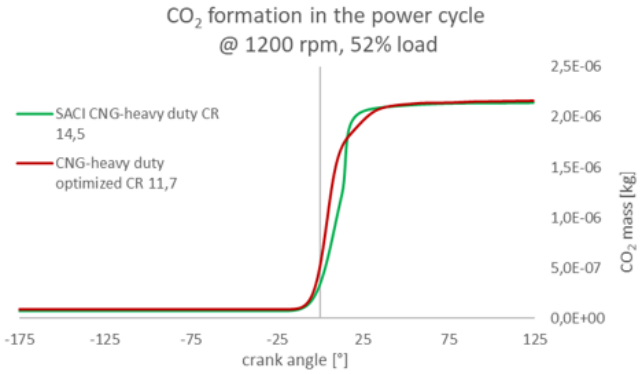

Figure 5.84: CO_2 production in 1200-half load working point comparison. $\phi = 0.8$ SACI reported in green, while stoichiometric flame propagation in red

Passing to CO_2 as shown in figure 5.84, it is considered a complete reaction product connected to the amount of fuel used, detached by quality of combustion process. Therefore, the only way to decrease carbon dioxide emission of an internal combustion engine is to increase its thermal efficiency, in such a way to use a lower fuel mass to satisfy every demanded torque.

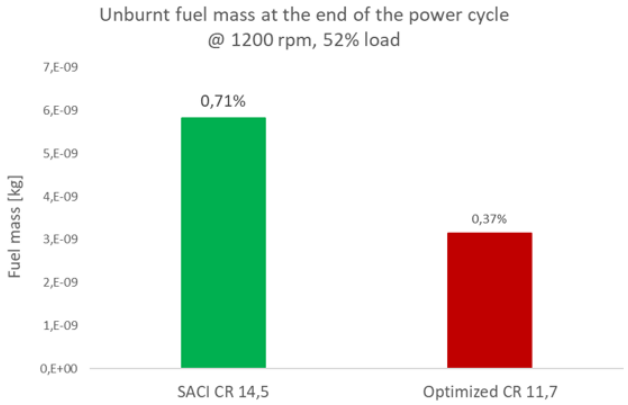

Figure 5.85: unburnt hydrocarbons after the whole combustion process in 1200-half load working point comparison. $\phi = 0.8$ SACI reported in green, while stoichiometric flame propagation in red

However, not all the fuel particles can burn and then release heat: as shown by figure 5.85, even if at higher compression ratios a lower fuel quantity is injected in the engine (for the same initial pressure), unburnt natural gas quantity increases, probably due to a wider flame extinguish region near to cylinder walls. Always in the same figure, respective percentages representing the ratio of unburnt hydrocarbons with respect to mass of fuel injected are reported. In the lean SACI engine, the 0.7% of the fuel is not taking part to the combustion process, and to decrease this amount can be a target for future combustion chamber designs.
For what regards nitrogen-oxides emission, however the solver can not predict NOx formation. For sure, the oxygen excess is enhancing their production, but adopting a leaner mixture permits to have a lower adiabatic flame temperature hence decrease NOx production.

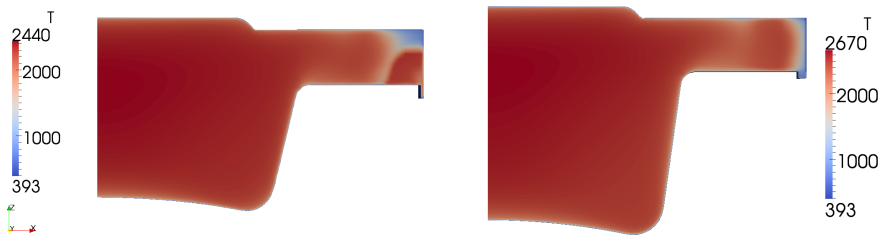

Figure 5.86: Cell temperatures in 1200-half load working point comparison, at the same engine time. $\phi = 0.8$ SACI reported leftwards, while stoichiometric flame propagation rightwards

Figure 5.86 previously reported compares cell by cell temperatures reached in a SACI at high compression ratio with the ones of an entirely flame propagation combustion. Temperature weighted average values are higher when spontaneous combustion takes place, but this increase is given by the presence of two different combustion modes, which speed up fuel oxidation reactions. Since cell temperature maximum values in lean conditions are almost 200 K lower with respect to the stoichiometric case, these effects combined should limit the overall NOx production during the power cycle.
As already written, these calculations were performed ignoring the presence of any after-treatment system at the turbine outlet. In any case, three-phase catalyst conversion efficiency is function of NOx, CO and hydrocarbons inlet mass, and this can be an interesting study case for future works. Figures displayed so far permits to compare lean SACI pollutants emission with a stoichiometric flame propagation reference case. These considerations are consistent even if higher regimes are analysed: as reported by figures 5.87, 5.88 and 5.89, at 1600 rpm pollutants formation behavior is consistent with what has been discussed so far.

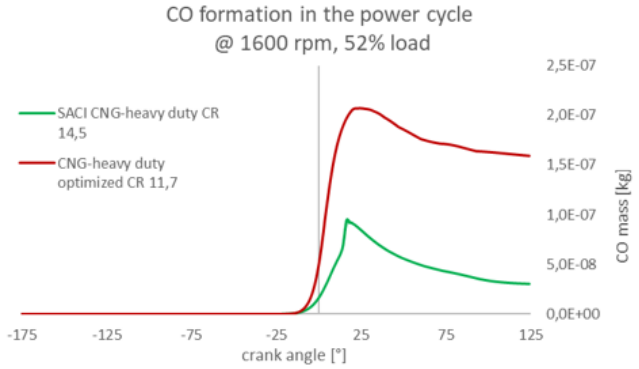

Figure 5.87: CO production in 1600-half load working point comparison. $\phi = 0.8$ SACI reported in green, while stoichiometric flame propagation in red

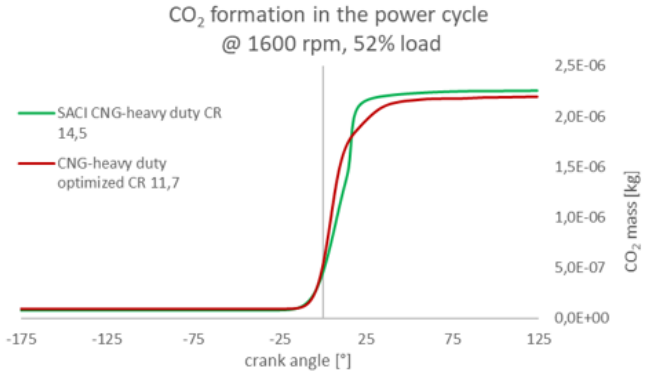

Figure 5.88: CO_2 production in 1600-half load working point comparison. $\phi = 0.8$ SACI reported in green, while stoichiometric flame propagation in red

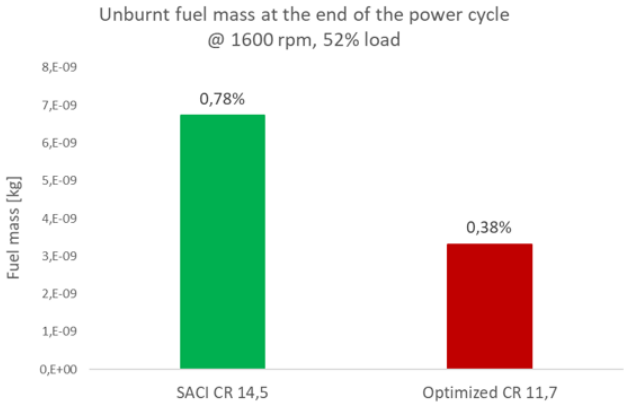

Figure 5.89: Unburnt hydrocarbons after the whole combustion process in 1600-half load working point comparison. $\phi = 0.8$ SACI reported in green, while stoichiometric flame propagation in red

In this kind of engines designed to exploit homogeneous charge compression ignition, even high load working points where autoignition is unwanted must be taken into account. As a consequence, downwards a flame propagation engine running with a compression ratio of 11.7 (adopting -23° as spark timing) and the one derived so far at 14.5 as compression ratio (which, as presented in subsection before, has a very delayed spark timing corresponding to -10°) are compared.

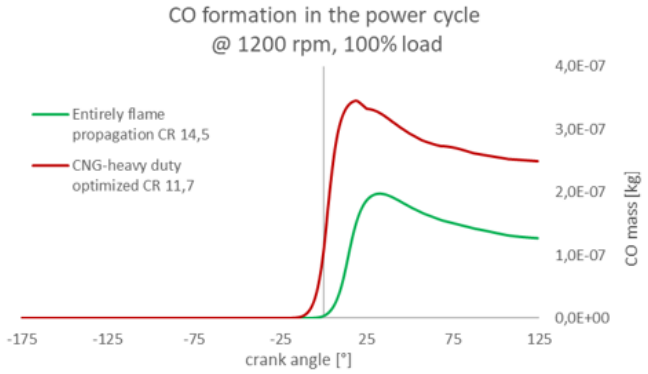

Figure 5.90: CO production in 1200-full load working point comparison. Both power cycles performed through entire flame propagation

The ongoing of these charts is very similar: as shown in figure 5.90, the two curves have a much more rounded peak and a lower decreasing afterwards, because of a lower oxygen partial pressure and then CO_2 formation results more complex and slower. The lower fuel amount used and the lower temperatures reached (due to more delayed spark timing) allow to have a carbon monoxide production far way lower such that, even if both cases run in stoichiometric conditions, at high compression ratio CO outlet mass is almost halved.

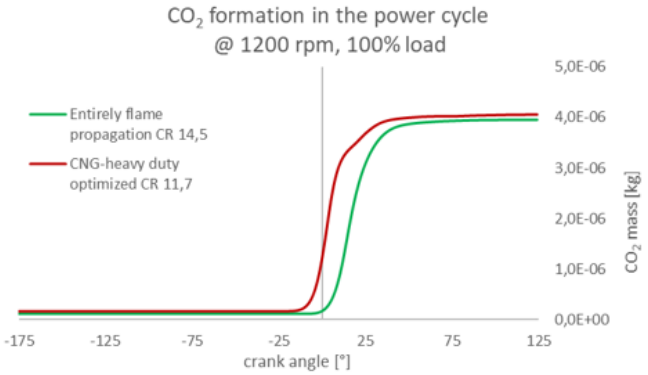

Figure 5.91: CO_2 production in 1200-full load working point comparison. Both power cycles performed through entire flame propagation

As previously written, CO_2 is a complete combustion product and its mass is directly related to the amount of natural gas used. For sure, to have a fuel composed by heavier hydrocarbons enhances carbon dioxide production, but

when different commercial natural gas compositions are compared, differences are not so evident. Therefore, the whole CO_2 reduction is totally connected to the lower amount of fuel used.

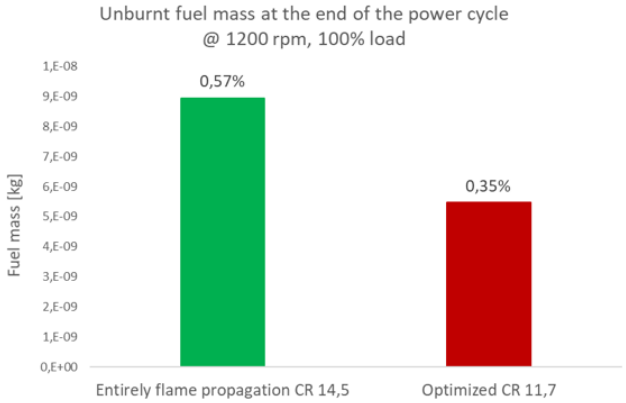

Figure 5.92: Unburnt hydrocarbons after the whole combustion process in 1200-full load working point comparison. Both power cycles performed through entire flame propagation

For what regards unburnt hydrocarbons mass, as illustrated in figure 5.92 stoichiometric air-fuel mixture ratio helps to have lower unburnt fuel released after the exhaust valve opening: while previously mass of unburnt natural gas were over the 0.7% of the whole fuel injected, in this case this percentage decreases up to 0.5%. Since at full load mixture results stoichiometric, three-way catalyst is predicted to work at maximum conversion efficiency to drastically reduce the whole engine pollutants emissions.

Conclusions

Purpose of this thesis was the prediction of knock and combustion under the so-called spark-assisted mode in a heavy duty engine operating with natural gas. Onset of knock limits the spark-advance and compression ratio and its correct estimation makes possible to identify the maximum engine performance and define suitable modifications to the combustion chamber layout to avoid it. Engine operation under the spark-assisted mode is similar to knock, but with a reduced pressure rise rate. Understanding the difference between knock and spark-assisted combustion is one of the main objectives of this thesis work: both of them can considerably speed up the combustion process, but in case of knock pressure gradients are so extreme to dissipate a huge part of energy released in heat losses. Therefore, if pressure gradient inside the combustion chamber is low and controlled, engine performances can take advantage of this faster combustion mode. Two different strategies to reduce pressure gradients have been analysed: the design based one (which acts on piston shape in correspondence of the squish area) and the mixture based one (which instead changes air-fuel stoichiometric ratio into a leaner one). In any case, not the whole engine map is suitable for a spark assisted compression ignition combustion: it induces very high stresses to the mechanical structure of the engine. For this reason, the whole map has been divided in two regions:

- from zero to half load where spark assisted compression ignition combustion is used to improve engine performances;

- form half to full load where spontaneous ignition of any nature is undesired to not have too high pressure values in the combustion chamber.

To further preserve the mechanical integrability of the engine, two more limits have been added: a maximum pressure of 180 bar and a pressure-rise not to overtake the value of 18 bar/deg. If piston design is investigated, region of interest it the furthest one from spark plug, where spontaneous ignition usually starts. In this region, squish area is located in such a way to have higher turbulence intensity for a faster flame propagation; but when autoignition takes place, a non negligible part of the heat released is lost to the walls. To avoid this effect which compromises the efficiency, extreme cylinder regions must have a wider compression ignition flame front surface in order to exchange more energy with flame propagation burnt gases and at the same time reduce the pressure wave intensity. Adopting this strategy, efficiency can overcome the value of 42% at half load exploiting spark assisted compression ignition combustion but turbulences generated inside the combustion chamber are far way lower and flame propagation results slower. In SACI combustion working points, this undesired

effect can be counterbalanced anticipating the spark timing of almost 4° to have similar pressure curve maximum values; but in high-load working points where spark assisted compression ignition combustion is not wanted, the lower flame velocity reduces the engine efficiency, even if compression ratio adopted is higher. Then the second strategy has been investigated: the possible presence of air excess in the engine can be easily regulated by the throttle valve installed before the intake port, in such a way to have a lean mixture when spontaneous ignition is wanted and a stoichiometric mixture in entirely flame propagation working points at high loads. Equivalence ratio chosen for lean working points is 0.8 to avoid the possibility of the flame to be extinguished. Thermal efficiency improvements obtained are significant, with values even overcoming 43% at 1600 rpm half-load working point. However, no performance improvement is predicted at high load: compression ratio adopted (14.5) is very high for such a big engine (having 2.15 liters as displacement) and spark timing must be delayed to avoid knock. Therefore, maximum efficiency point (which in common Otto cycle engine is the full load one) moves to the half load condition because of the different combustion mode used and fuel consumption of the overall map has been appreciably reduced. The main drawback of adopting leaner engine is represented by the three-way catalyst, as its conversion efficiency is maximum when air-fuel mixture used is stoichiometric. But if pollutants formations just by combustion are analysed comparing the derived SACI combustion with the entirely flame propagation one, when engine is running lean carbon monoxide emissions are reduced up to the 75% and maximum temperature reached are more than 150 °C lower, which should theoretically discourage NOx formation. However, no nitrogen oxides transport equation is implemented in the solver, hence no quantification has been performed.

Bibliography

[1] H. Versteeg and W. Malalasekra, *An Introduction to Computational Fluid Dynamics*, 2, Pearson India Education Services (2009)

[2] Giancarlo Ferrari, *Motori a combustione interna*, 1, Socierà editrice Esculapio (2016)

[3] Nicolò Bachschmid, Stefano Bruni, Andrea Collina, Bruno Pizzigoni, Ferruccio Resta, Alberto Zasso, *Fondamenti di meccanica teorica e applicata*, Graw Hill, 2015

[4] D.S. Malik, *Introduction to C++ Programming*, 1, Apogeo Education (2009)

[5] Tommaso Lucchini, Angelo Onorati, Gianluca D'Errico, Alessandro Stagni and Alessio Frassoldati, *Modeling non-premixed combustion using tabulated kinetics and different flame structure assumptions*, Dipartimento di Energia, Politecnico di Milano (2017)

[6] H.G. Weller, *The Development of a New Flame Area Combustion Model Using Conditional Averaging*, Imperial College Mechanical Engineering Department (1993)

[7] H.G. Weller, S. Uslu, A.D. Gosman, R.R. Maly, R. Herweg, B. Heel, *Prediction of Combustion in Homogeneous-Charge Spark-Ignition Engines*, Imperial College Mechanical Engineering Department (1994)

[8] Maurizio Mastropasqua, *Modellazione del processo di combustione in motori Diesel mediante modelli di combustione basati su cinetica chimica tabulata*, Dipartimento di Energia, Politecnico di Milano (2016)

[9] Alberto Comolli, *CFD Modeling of Diesel Combustion with Tabulated Kinetics Based on Homogeneous Reactor Assumption*, Dipartimento di Energia, Politecnico di Milano (2018)

[10] Jiri Vavra, Michal Takats, Vojtech Klir and Marcel Skarohlid, *Influence of Natural Gas Composition on Turbocharged Stoichiometric SI Engine Performances*, Czech Technical Univ. (2012)

[11] Akira Kikusato, Hiroyuki Fukasawa, Kazutoshi Nomura, Jin Kusaka and Yasuhiro Daisho, *A Study on the Characteristics of Natural Gas Combustion at a High Compression Ratio by Using a Rapid Compression and Expansion Machine*, Waseda Univ. (2012)

[12] Ahmed Abdul Moiz, Zainal Abidin, Robert Mitchell, and Michael Kocsis, *Development of a Natural Gas Engine with Diesel Engine-like Efficiency Using Computational Fluid Dynamics*, Southwest Research Institute (2019)

[13] Yalan Liu, Xuexiang Zhang, Junxia Ding, *Chemical effect of NO on CH_4 oxidation during combustion in O_2/NO environments*, University of Chinese Academy of Sciences (2019)

[14] Hrvoje Jasak, *Numerical Solution Algorithms for Compressible Flows*, University of Zagreb, Croatia (2006)

[15] Jinlong Liu and Cosmin Dumitrescu, *CFD Simulation of Metal and Optical Configuration of a Heavy-Duty CI Engine Converted to SI Natural Gas. Part 2: In-Cylinder Flow and Emissions*, West Virginia University (2019)

[16] Fubai Li, Changpeng Liu, Heping Song, and Zhi Wang, *Improving Combustion and Emission Characteristics in Heavy-Duty Natural-Gas Engine by Using Pistons Enhancing Turbulence*, Tsinghua University (2019)

[17] William P. Attard, Elisa Toulson, Harry Watson and Ferenc Hamori, *Abnormal Combustion including Mega Knock in a 60% Downsized Highly Turbocharged PFI Engine*, The University of Melbourne, Australia (2010)

[18] G. Brecq, A. Ramesh, M. Tazerout and O. Le Corre, *An Experimental Study of Knock in a Natural Gas Fuelled Spark Ignition Engine*, Ecole Des Mines De Nantes,(2001)

[19] Junseok Chang, Orgun Güralp, Zoran Filipi, and Dennis Assanis, *New Heat Transfer Correlation for an HCCI Engine Derived from Measurements of Instantaneous Surface Heat Flux*, University of Michigan (2004)

[20] Jeremie Dernotte, John Dec, and Chunsheng Ji, *Investigation of the Sources of Combustion Noise in HCCI Engines*, Sandia National Labs (2014)

[21] Magnus Sjöberg and John E. Dec, Nicholas P. Cernansky, *Potential of Thermal Stratification and Combustion Retard for Reducing Pressure-Rise Rates in HCCI Engines, Based on Multi-Zone Modeling and Experiments*, Sandia National Labs and Mechanical Engineering Department, Drexel University (2005)

[22] Patrick Pertl, Alexander Trattner, Andrea Abis , Stephan Schmidt and Roland Kirchberger, Takaaki Sato *Expansion to Higher Efficiency - Investigations of the Atkinson Cycle in Small Combustion Engines*, Graz University of Technology and DENSO Automotive Deutschland GmbH (2012)

[23] Laura Manofsky, Jiri Vavra, Dennis Assanis and Aristotelis Babajimopoulos *Bridging the Gap between HCCI and SI: Spark-Assisted Compression Ignition*, Univ. of Michigan and Czech Technical Univ (2011)

[24] William P. Attard and Hugh Blaxill, Eric K. Anderson, Paul Litke, *Knock Limit Extension with a Gasoline Fueled Pre-Chamber Jet Igniter in a Modern Vehicle Powertrain*, MAHLE Powertrain, National Research Council and US Air Force Research Laboratory (2012)

[25] Anne Prieur and Richard Tilagone, *A Detailed Well to Wheel Analysis of CNG Compared to Diesel Oil and Gasoline for the French and the European Markets*, IFP (2007)

[26] Chang, J., Kim, M. And Min, K., *Detection of misfire and knock in spark ignition engines by wavelet transform of engine block vibration signals*, Measurement Science and Technology, 2002.

[27] Ohtubo, H., Yamane, K., Kawasaki, K., Nakazono, T. and Shirouzu, T., *PCCI Combustion for Multi Cylinder Natural Gas Engine (Second Report) - Leading Auto-ignition Reduction of Cylinder-to cylinder Variations by using Spark Ignition* JSAE Proceeding Paper, 2007

[28] Roberts, C.E., Snyder, J.C., Stovell, C., Dodge, L.G. et al., *The Heavy-Duty Gasoline Engine-An Alternative to Meet Emissions Standards of Tomorrow* SAE Technical Paper, 2004

[29] Liu, J. and Dumitrescu, C.E., *Combustion Visualization in a Single-Cylinder Heavy-Duty CI Engine Converted to Natural Gas SI Operation*, State College USA, 2018

[30] Yu, X., Liu, Z., Wang, Z., and Dou, H., *Optimize Combustion of Compressed Natural Gas Engine by Improving In-Cylinder Flows* International Journal of Automotive Technology, 2013

[31] Wang, Z., Wang, J., Shuai, S., Tian, G., An, X., and Ma, Q., *Study of the effect of spark ignition on gasoline HCCI combustion*, Journal of Automobile Engineering, 2006.